MAY 10 1949

THE PHYSICAL REVIEW

VOLUME 75 Second Series NUMBER 9

MAY 1, 1949

Published for the

AMERICAN PHYSICAL SOCIETY

by the

AMERICAN INSTITUTE OF PHYSICS

Incorporated

LANCASTER, PA., AND NEW YORK, N. Y.

THE PHYSICAL REVIEW

A journal of experimental and theoretical physics established by E. L. Nichols in 1893

Published by the American Institute of Physics for the

AMERICAN PHYSICAL SOCIETY

Officers

President

F. W. Loomis
University of Illinois
Urbana, Illinois

Vice-President

I. I. Rabi
Columbia University
New York, New York

Secretary

K. K. Darrow
Bell Telephone Laboratories
Office:
Columbia University
New York 27, New York

Treasurer

G. B. Pegram
Columbia University
New York 27, New York

Local Secretary for the Pacific Coast

J. Kaplan
University of California at Los Angeles
Los Angeles, California

Managing Editor

John T. Tate
University of Minnesota
Minneapolis, Minnesota

BOARD OF EDITORS

Editor

John T. Tate

Assistant Editor

J. W. Buchta

Associate Editors

H. A. Bethe — S. A. Goudsmit — W. E. Lamb, Jr.
L. A. Ellenbogen — E. M. Purcell — R. G. Herb
W. H. Zachariasen — V. F. Weisskopf — J. Bardeen

Manuscripts for publication should be submitted to John T. Tate, University of Minnesota, Minneapolis, Minnesota. The authors' institutions are requested to pay a publication charge of $4 per page which, if honored, entitles them to 100 free reprints. Instructions will be sent with galley proofs.

Proof and all correspondence concerning papers in the process of publication should be addressed to the Publication Manager, American Institute of Physics, 57 East 55 Street, New York 22, New York.

Subscription Price

United States and Canada $15.00
Elsewhere $16.50

Back Numbers[1]

Yearly back number rate when complete year is available: $20.00.
Single copies: $2.00 each, prior to July, 1929;
$1.00 each, July, 1929–December, 1941;
$2.00 each, January, 1942–December, 1946.
Current issues: $1.00 each.
General index, 1893–1920: $4.00.

Subscriptions and orders for back numbers should be addressed to Prince and Lemon Streets, Lancaster, Pennsylvania, or to the American Institute of Physics, 57 East 55 Street, New York 22, New York.

Changes of address in the case of members of the American Physical Society should be addressed to the Treasurer; in the case of other subscribers to the Business Manager, American Institute of Physics.

[1] For Series I inquire of Physics Department, Cornell University, Ithaca, New York.

The Physical Review is published semi-monthly at Prince and Lemon Streets, Lancaster, Pennsylvania.

Entered as second-class matter March 6, 1917, at the Post Office at Lancaster, Pennsylvania, under the Act of March 3, 1879.

Acceptance for mailing at special rate of postage provided for in paragraph 4, section 538, P. L. & R., authorized January 27, 1925.

THE
PHYSICAL REVIEW

A journal of experimental and theoretical physics established by E. L. Nichols in 1893

SECOND SERIES, VOL. 75, NO. 9 MAY 1, 1949

Alpha-Particles from Fission as Recorded by Photographic Emulsions

L. MARSHALL
Argonne National Laboratory and University of Chicago, Chicago, Illinois
(Received January 10, 1949)*

Eighty long range alpha-particles coincident with U^{235} fission have been observed in photographic plates. There is a tendency for the alpha-particles to emerge with greatest energy at an angle slightly greater than 90° from the heavy fragment. In accordance with previous observers, it is found that most alpha-particles emerge approximately perpendicular. It is also found that the majority form an angle slightly obtuse to the heavy fragment. The energy of the alpha-particles is found to be derived largely from the kinetic energy of the fission fragments. The alpha-emitting fissions have approximately the same mass ratio as do normal fissions.

I. INTRODUCTION

THE alpha-particles coincident with fission were first observed during the war by L. W. Alvarez (see first paragraph of reference 3). Independently the same particles were observed in photographic plates by Green and Livesey who reported them at the Physical Society Conference at Cambridge in July 1946, and by San-Tsiang, Zah-Wei, Chastel and Vigneron,[1] who were apparently the first to publish it in the open literature.

At approximately the same time, Demers,[2] knowing of Alvarez' discovery, published an analysis of fissions observed in photographic plates. In an examination of 1500 fissions he found 6 fissions emitting alpha-particles, a frequency of 1 in 250 fissions. Using a special emulsion consisting of a thin layer of a uranium salt sandwiched between two layers of emulsion, he was able to observe a gap in the fission track corresponding to the point at which the fission occurred. From the coincidence of the gap with the point of emission of the alpha-track he calculated that the alpha-particle was emitted less than 2×10^{-14} second after fission. The maximum energy observed for the alpha-particles was about 19 Mev.

Farwell, Segrè, and Wiegand,[3] in a publication of work done during the war, give the frequency of alpha-emission in U^{235} as 1 in 250, a figure based on good statistics. By bombarding a film of U^{235} in an ion chamber with neutrons they were able to measure the bias and absorption curves for the alpha-particles so produced and thus to identify them positively. The resolving time of their electrical circuits allowed them to ascertain that the alpha coincided with fission within 5×10^{-6} second. The maximum energy observed was about 16 Mev.

A study of alpha-particles from fission observed in photographic plates was made by Wollan, Moak, and Sawyer[4] on twenty individual events. These particles were found to emerge at approximately right angles to the fission tracks. From this fact the authors conclude that the alpha-particle is released at the instant of fission and not from either fission fragment. The maximum energy observed was 22.1 Mev.

A more extensive investigation using photographic plates was made by Green and Livesey.[5] In an examination of 25,000 fission tracks, they found 1 light particle emitted in every 80 fissions. Most of these were of short range and many emerge at angles less than 70° to the fission track. In view of the criterion to be discussed below it would seem probable that a large number of these light particles are protons of the emulsion knocked on by the fission fragments, even though such a possi-

* Date of manuscript July 8, 1948 AECD 2382.
[1] San-Tsiang, Zah-Wei, Chastel, and Vigneron, Comptes Rendus 223, 986 (1946).
[2] Pierre Demers, Phys. Rev. 70, 974 (1946).
[3] Farwell, Segrè, and Wiegand, Phys. Rev. 71, 327 (1947).
[4] Wollan, Moak, and Sawyer, Phys. Rev. 72, 447 (1947).
[5] L. L. Green and D. L. Livesey, Nature 159, 332 (1947).

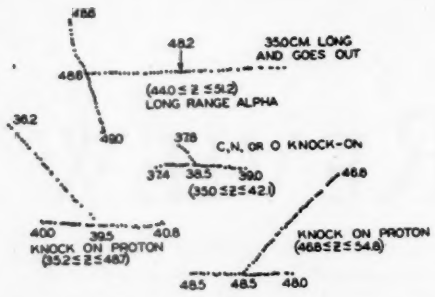

FIG. 1. Tracings of tracks of fission fragments from which branch tracks of light weight particles. These tracks have been projected from photographic emulsions, traced at 1950× magnification, and reproduced here at 540× magnification.

bility has apparently been discarded by the authors.

II. EXPERIMENTAL DATA

In the present research, an examination of approximately 18,500 fissions has been made in Eastman Kodak emulsion NTB. Among these, 80 fissions were found which emitted long range alpha-particles. Approximately 150 fissions were found from which emerged tracks of protons of the emulsion knocked on by the fission particles. A criterion has been found by which to distinguish the knock-on protons from the true long range alpha-particles emitted in fission. An analysis has been made of the energies, and angles of emission of the observed alpha-particles and of the total length and of the separate lengths of the fission fragments of the alpha-emitting fissions. Comparison has been made with the corresponding quantities of normal fission.

Eastman Kodak Nuclear Research Emulsion NTB, 50 microns thick, was soaked in uranium acetate for 5 minutes and while wet, exposed for a few seconds to a flux of thermal neutrons from the Argonne heavy water pile. The emulsion was developed for 20 minutes in full strength D-19 and fixed. Control plates were made, both with uranium acetate, unexposed to neutrons, and without uranium acetate, exposed to neutrons.

The plates were scanned at about 1000× magnification, using a microscope projection table. When a fission track coincident with a light fragment track was found, the image of the event was traced at 1950× magnification. The different parts of the track were brought successively into focus and the height of the objective above the emulsion at each significant point was noted. The thickness of the emulsion was measured by finding the heights of the objective when the top and bottom grains of the emulsion were in focus. This last datum measures the amount by which the emulsion has shrunk during development.

From the tracing, and the data on the depth of the track at various places, the true geometry of the event as it occurred in the emulsion at its original thickness has been calculated. Examples of such tracings are reproduced in Fig. 1.

III. EXPERIMENTAL RESULTS

Approximately 18,500 fissions were examined. Of these about 230 fission tracks had light particle tracks emerging from them. Since it is easy to confuse tracks due to knock-on protons with those due to alpha-particles emitted at the instant of fission, some criterion is necessary by which this distinction can be made.

In order that the long range alphas might be sorted out, the following method was used. From the range-energy relation as determined by Lattes, Fowler, and Cuer for protons in emulsion of the same high silver bromide content, the velocity of each light particle, assuming that it was a proton, was calculated for its measured range. Since the mass of a proton may be neglected in comparison with the mass of a fission fragment, the approximate

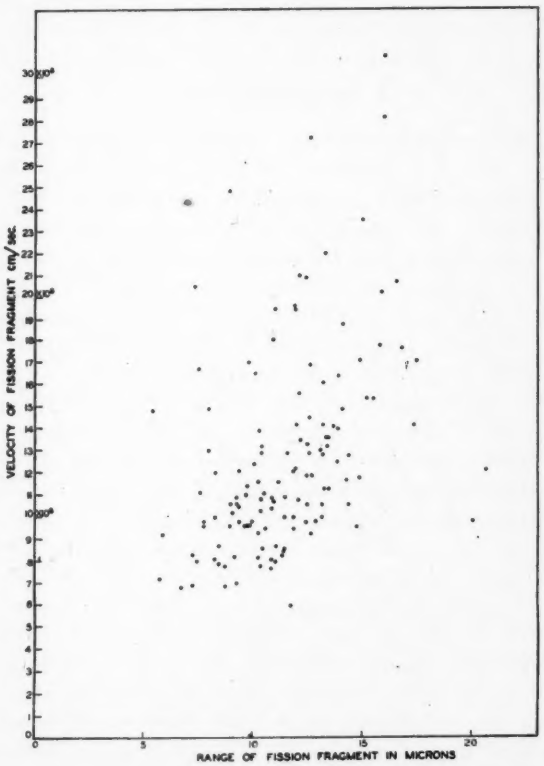

FIG. 2A. Velocity of fission fragments *versus* range of fission fragments as determined from events in which tracks of light weight particles branch from tracks of fission fragments. Each point is determined from a single event. If the light weight particle of such an event, when treated as a knocked-on C, N, O, or H nucleus of the emulsion, gives a point compatible with the range energy relation for fission fragments, it is considered to be such a knock-on fragment. If the resulting point lies far from the range-energy curve, the particle is considered to be an α-particle emitted in fission.

relation is valid:

$$V_p = 2V_F \cos\theta, \qquad (1)$$

where V_p and V_F are the velocities of proton and of fission fragment, and where θ is the angle between their trajectories.

From this relation the velocity of the fission fragment was calculated and plotted against the range of the fission fragment measured from its end to the point where the light particle emerged at an acute angle. The range-velocity plot of the points so obtained is given as Fig. 2A, except for a considerable number of points, corresponding to particles of long range, which lie off the top of the figure (see Fig. 2B). A large fraction of the points below 18×10^8 cm/sec. cluster in a region compatible with a range-velocity relation for fission fragments.

It has been found experimentally by various investigators[6–8] that the range of fission is proportional to the velocity, in accordance with the Bohr relation. The constant of proportionality can be calculated for the emulsion used here from the average length of normal fission in the emulsion together with the average masses and energies of the fission fragments. The average light fragment, with a mass of 93 and an energy of 96 Mev has a velocity of 14×10^8 cm/sec. The heavy fragment of mass 141 and energy 64 has a velocity of 9.3×10^8 cm/sec. The average total range for normal fissions in this emulsion (see Fig. 5) is 27.0 microns.

$$27.0 \text{ microns} = K(14+9.3)\times10^8 \text{ cm/sec.},$$
$$K = 1.160\times10^{-8} \text{ micron sec./cm.}$$

It may be seen that this line lies well in the cluster of those points of Fig. 2A which lie below 18×10^8 cm/sec.

The possibility that the light particle tracks were carbon, nitrogen, or oxygen recoils was also considered. In order to obtain the velocity of the particle from its range, assuming its mass to be about 14, the experimental range-velocity curves of Blackett and Lees[9] for nitrogen and oxygen together with the theoretical extrapolations of Knipp and Teller[10] have been used.

The relationship (1) must now be modified by the reduced mass. It becomes

$$V_N = 2V_F\left\{\frac{M_F}{M_F+M_N}\right\}\cos\theta, \qquad (2)$$

where V_N and M_N are velocity and mass of the nitrogen atom, and where V_F and M_F are velocity and mass of the fission fragment. The angle between the initial trajectory of the fission fragment and the trajectory of the nitrogen is θ. Knowing V_N and $\cos\theta$, one calculates V_F. Several of the shorter light particles when treated in this way as fragments with mass ~14, yielded satisfactory points on the range-velocity plot of Fig. 2A, and are plotted thereon.

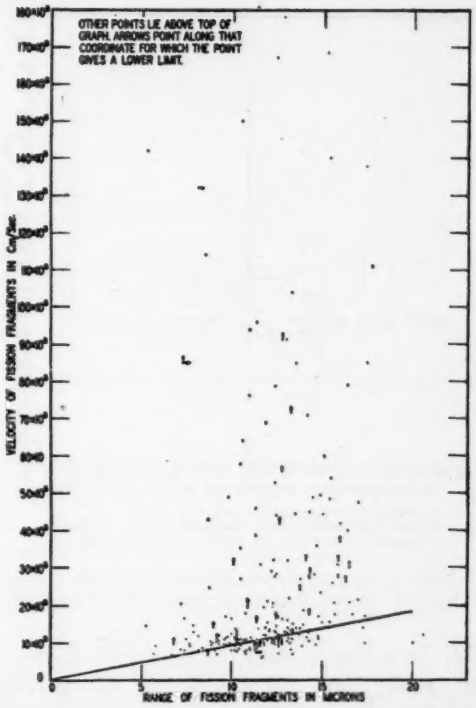
OTHER POINTS LIE ABOVE TOP OF GRAPH. ARROWS POINT ALONG THAT COORDINATE FOR WHICH THE POINT GIVES A LOWER LIMIT.
VELOCITY OF FISSION FRAGMENTS IN CM/SEC.
RANGE OF FISSION FRAGMENTS IN MICRONS
0
5
10
15
20

FIG. 2B. Simplification of Fig. 2A showing some of the points lying far from the range-energy region for fission fragments. The light particles branching from fission fragments which give such outlying points when treated as knock-on nuclei are consequently believed to be α-particles emitted in fission.

The dozen farthest outlying points to the southeast and the northwest are probably accounted for by a few excessively large experimental errors. The maximum velocity on the average for a fission fragment, namely that for a fragment of mass 93 and energy 94 Mev, is 13.9×10^8 cm/sec. This sets an average upper limit by which one can decide which points refer to proton recoils and which points refer to proper alpha-particles. However, in applying this limit it must be remembered that the lack of resolution due to straggling in the nonhomogeneous emulsion and due to errors in measurement may allow points corresponding to true proton recoils to lie above this limit.

The light fragments corresponding to all points lying above 18×10^8 cm/sec. are considered to be true alpha-particles. The fact that 90 percent of the points below 18×10^8 cm/sec. cluster in a region

[6] Bröstrom, Böggild, and Lauritsen, Phys. Rev. **58**, 651 (1940); Phys. Rev. **58**, 839 (1940); Phys. Rev. **59**, 275 (1941).
[7] Böggild, Arrøe, and Sigurgiersson, Phys. Rev. **71**, 281 (1947).
[8] R. Sherr and R. Peterson, Rev. Sci. Inst. **18**, 574 (1947).
[9] P. M. S. Blackett and D. S. Lees, Proc. Roy. Soc. **134**, 658 (1932).
[10] J. Knipp and E. Teller, Phys. Rev. **59**, 666 (1941).

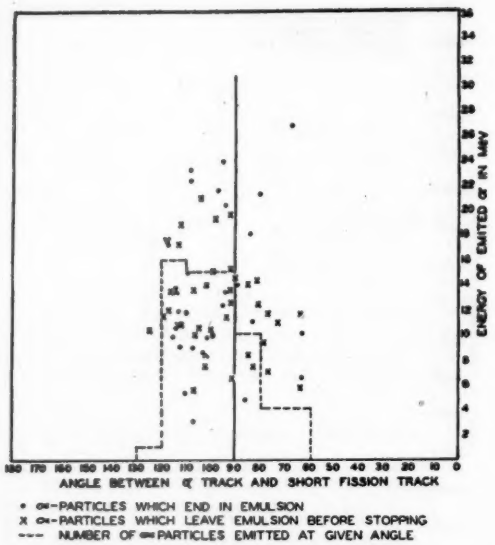
ENERGY OF EMITTED α IN MeV
ANGLE BETWEEN α TRACK AND SHORT FISSION TRACK
• α-PARTICLES WHICH END IN EMULSION
X α-PARTICLES WHICH LEAVE EMULSION BEFORE STOPPING
--- NUMBER OF α-PARTICLES EMITTED AT GIVEN ANGLE

FIG. 3. Energy of α-particles emitted in fission *vs.* angle between heavier fission fragment track and α-particle track.

suitable to a range velocity curve for fission fragments, and that the remaining 10 percent lie around the edges of this region means that almost all of the corresponding light fragments are proton recoils, and some few are recoils of carbon, nitrogen and oxygen. Quite probably none of these points, even those which lie outside the cluster, correspond to alpha-particles, since, if this were the case, one could expect an equivalent sprinkling of points in the regions away from the range-velocity region. Although it is possible that some few alpha-particles are not counted by using this criterion, it is not believed that they can represent more than 10–15 percent at the most.

Using the criteria discussed above for distinguishing the true alpha-particles from the knock-on protons and knock-on C, N, and O of the emulsion, there remain 80 long range alpha-particles from 18,500 fissions. This gives a frequency of 1 in 230, a figure which agrees with the frequency noted by Farwell *et al.*[8] These are then the light particles corresponding to points above 18×10^8 cm/sec. in Figs. 2A and 2B. Most of these points lie off the top of Fig. 2A by a large distance.

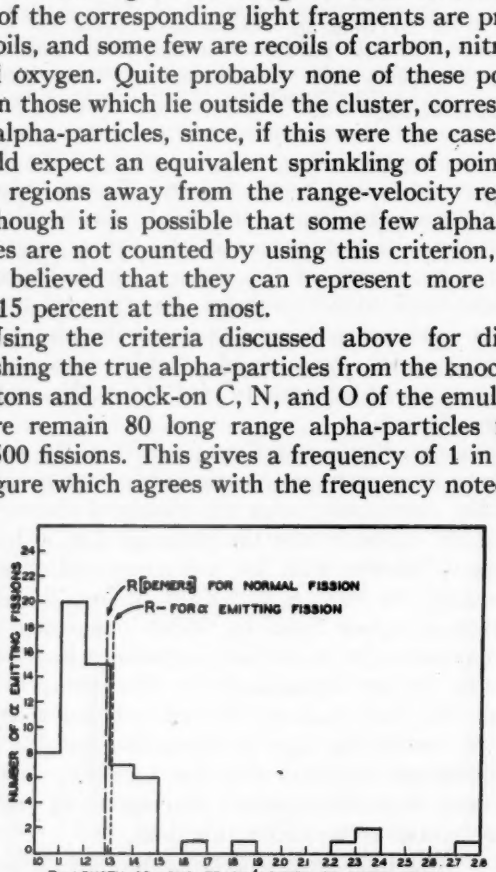
R[DEMERS] FOR NORMAL FISSION
R- FOR α EMITTING FISSION
NUMBER OF α EMITTING FISSIONS
R= LENGTH OF LONG TRACK/LENGTH OF SHORT TRACK

FIG. 4. Ratio: length of long fission fragment track ÷ length of short fission fragment track *versus* number of α-emitting fissions showing this ratio.

Out of 80, 31 alpha-tracks end in the emulsion. For the purposes of this analysis the remainder are not useless because they provide data on length of the total fission track, ratio of the lengths of the 2 fission fragments, and angle of emergence of the alpha-particle.

In Fig. 3 the energy of alpha-particles is plotted *vs.* angle of emission showing both those alphas which leave the emulsion and those which stop in the emulsion. The angle of emission is the angle between the heavy fragment track and the alpha-particle track. The energy of the alpha has been obtained from the range energy curves of Lattes, Fowler, and Cuer for alpha-particles in high density silver bromide emulsion. There is a slight tendency for the more energetic alphas to be emitted at an angle obtuse to the heavier fragment, although the statistics are poor and the effect is probably within the statistical accuracy. Also the greater number of alphas are emitted at angles slightly obtuse to the heavy (short) fragment. Both effects, if real, are in agreement with the greater Coulomb repulsion of the heavy fragment.

In Fig. 4 is plotted the ratio of lengths of long to short fragment against the number of alpha-emitting fissions showing that ratio. Within the experimental error the average ratio for alpha-emitting fissions is equal to the average ratio observed by Demers for normal fissions. Even if those ratios greater than 1.7 are considered as anomalous errors and are omitted, the ratio is 1.24, still equal to the ratio for normal fission well within the limits of error.

Since the ratio of the ranges of the fragments of a given fission is proportional[11–13] to the ratio of their masses, in principle, if straggling were small enough, Fig. 4 could be interpreted as a chemical yield curve. The ordinate would then be proportional to percent of fission into the mass ratio given by the abscissae, for alpha-emitting fissions. Because the error due to straggling in the non-homogeneous medium is so large, it is not possible to tell positively whether the width of the curve derives from a single type of fission or from all the types and frequencies of splitting observed for normal fission. Therefore, this curve unfortunately cannot be used as a chemical yield curve.

One may conclude, however, that alpha-emitting fissions either have approximately the same

[11] Freedman, Metcalf, and Sugarman, Manhattan Project Report CC-1559 (4/8/44).
[12] Finkle, Hoagland, Katcoff, and Sugarman, MPR CK-1806 (6/30/44); MPR CC-2076 (8/25/44).
[13] Katcoff, Miskel, and Stanley, Phys. Rev. **74**, 1225 (1948).

FIG. 5. Comparison of total length of α-emitting fission tracks with total length of normal fission tracks.

chemical yield curve as normal fissions or else approximately correspond to those types of splitting most abundant among normal fissions.

There is no obvious correlation either of angle or of energy with length of either fission fragment or with total length.

According to Fig. 5, the average total length of the alpha-emitting fissions is about 94 percent of the average total length of normal fissions. This is equal to the decreased total range calculated, assuming a 16 Mev alpha-particle emitted in such a way that 8 Mev subtracts from the kinetic energy of each fragment. Therefore, the energy of the alpha-particles seems to be obtained at the expense of the kinetic energy of the fission fragments on the average.

From Fig. 5 there can also be obtained some idea of the error due to straggling caused by inhomogeneity of the emulsion. It has been shown[13] that the total range in air of the two fission fragments of normal fission has practically the same value for all mass ratios. However, one sees in Fig. 5 that the lengths of normal fissions as measured in photographic emulsions range from less than 20 microns to more than 32 microns. This must be attributed to the fact that as the fission fragment goes through the emulsion it travels now through regions of gelatine, and now through erratically distributed grains of silver bromide in which it is slowed much faster than in the gelatine.

Figure 6 shows the actual energies observed for those alpha-particles which stopped in the emulsion. In order to find frequency of emission as a function of energy these various energies must be weighted by the corresponding probability to leave the emulsion, shown as the dashed curve. There are few alpha-particles emitted with low energy, the frequency of emission going through a maximum which is ill-defined due to the poor statistics of the observation.

In any given fission, one of the fission fragments is nearly always shorter than the other. In Fig. 7, three curves are given: the lengths of the short fission fragments are plotted against number, the same is done for the long fission fragments, and finally a third curve gives the sum of the first

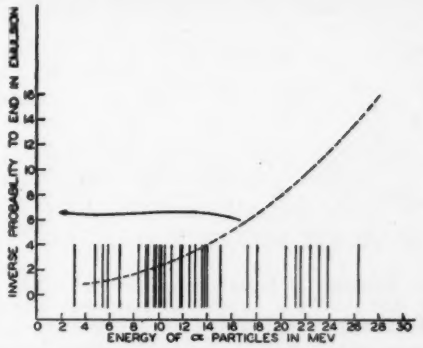

FIG. 6. Energies of α-particles emitted in fission and stopped in the emulsion.

two curves. These three curves all apply to alpha-emitting fission only. One sees from Fig. 7 that the curve for all the fission fragments from alpha-emitting fission shows a single peak; that is, that the peaks of the curves for long and for short fragments are not markedly separated. This is in contrast to similar curves given by Demers[2] for normal fission. The peaks of his curves for the long and for the short fragment are distinctly separated because they are much narrower (the average positions of the peaks have the same ratio as those for alpha-emitting fission), and consequently the curve which is the sum of the first two shows two well defined maxima.

However, Demers' curve for total length of the normal fission *vs.* number shows approximately the same spread as that observed here for normal fissions. Therefore, the widening of the range-number curves for long and for short fission fragments of alpha-emitting fissions would not seem to be due to a less homogeneous emulsion but rather to the alpha-emitting process itself. Probably it relates to the fact that the alpha-particles come out with a wide range of energies. It may perhaps be repeated that the ratio of the average lengths of long and short fragments is not changed by alpha-

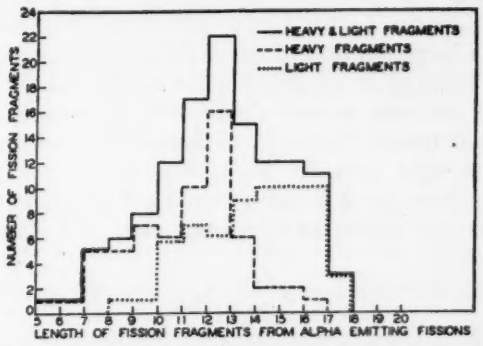
HEAVY & LIGHT FRAGMENTS
HEAVY FRAGMENTS
LIGHT FRAGMENTS
NUMBER OF FISSION FRAGMENTS
LENGTH OF FISSION FRAGMENTS FROM ALPHA EMITTING FISSONS

FIG. 7. Length of short fission fragment track *versus* number observed, and length of long fission fragment track *versus* number observed. The third curve gives the sum of the first two curves. All three curves refer to α-emitting fission only.

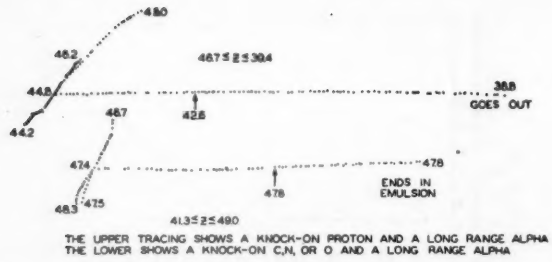

FIG. 8. Tracings of events coincident with fission shown enlarged 540×. They appear to represent emission of 2 α-particles at the instant of fission. However, the statistics of these events show that the correct interpretation is most probably that a nucleus of the emulsion has been knocked-on by a fission fragment immediately following emission of an α-particle in fission.

emission (although the average lengths themselves are decreased). This fact and the spread in alpha-particle energies together with the apparent broadening of the range number curves of the fission fragments gives separate evidence that the energy for the alpha-particle subtracts from the kinetic energy available to both fission fragments.

It should be pointed out that a curve, analogous to Fig. 7, is given for alpha emitting fission by Green and Livesey.[5] Their range number curve for all fission fragments together shows, however, two distinct peaks, apparently corresponding to the ranges of light and heavy fission fragments in emulsion. But the possibility exists that more than half of the light particles observed by them are proton recoils. Such an event does not divide the fission track into the lengths corresponding to the true ranges of the fission fragments. Consequently, their curve must be considered with this difficulty in mind.

In the same way in the collection of data for the present paper, the knock-on protons were at first confused with true alpha-particles. The differences in grain densities of the two kinds of tracks are not marked, at least not with the methods of development used here, although such critical development methods can probably be found with a little care. In the course of plotting the data, it became obvious that a large number of the shorter light fragments were emitted at an angle acute to the heavy fragment, and also in such a way that the ratio of long to short fission fragment, measured from the origin of the light particle track, was unusually large. These facts are difficult to explain if the light fragments are alpha-particles, but they are quite in keeping if the light fragments are knock-on protons. Consequently the criterion previously discussed was used to distinguish the knock-on light particles from the true long range alpha-particles.

In Fig. 8 are shown tracings of two events which on first sight appear to be the emission of two alpha-particles at the instant of fission. However, of the two events, the shorter light fragment of one fits very well in length and direction the requirements for a knock-on proton. In the second case the shorter light fragment has the range and angle for a knock on C, N, or O fragment. In both cases the long light fragment is a true long range alpha-particle, and in both cases it emerges at slightly more than 90° from the long (light) fission fragment. Two such events were found in 18,500 fissions. Also 80 long range alpha-events were found and about 150 knock-on protons, and knock on C, N, and O. The probability of the double events should be, therefore, of the order of $1/150 \times 1/80$ or 1 in 12,000 in agreement with what has been observed.

IV. CONCLUSIONS

The frequency of emission of long range alpha-particles in U^{235} fission was found here as 1 in 230, in agreement with the previous investigators.[2,3] The maximum energy of long range alpha-particle observed here is 26.4 Mev. There is a slight tendency for the alpha-particles of highest energy to be emitted at an angle slightly greater than 90° from the heavy fission fragment. Furthermore, the majority of alpha-particles emerge at an angle slightly obtuse to the heavy fragment. The energy of the alpha-particle is derived largely from the kinetic energy of the fission fragments. The magnitude of the ratio of average range of normal fission to average range of alpha-emitting fission checks well with that calculated, assuming a 16 Mev alpha-particle to be emitted in such a way that 8 Mev subtracts from the kinetic energy of each fission fragment. The straggling of the fission fragments due to the non-homogeneity of the emulsion is too great to allow the evaluation of a chemical yield curve for alpha-emitting fissions. It can be concluded, however, that the alpha-emitting fissions have approximately the same mass ratio as do normal fissions.

Acknowledgment is made to Professor Enrico Fermi for discussions during the progress of this work.

Angular Distribution of 1- to 3.5-Mev Protons Scattered by He^4

GEORGE FREIER, EUGENE LAMPI, W. SLEATOR, AND J. H. WILLIAMS
University of Minnesota, Minneapolis, Minnesota

(Received January 27, 1949)

The angular distribution of protons scattered by He^4 has been measured in the energy range from 1 to 3.5 Mev and over an angular range of 10° to 164° in the laboratory. The results are given as absolute cross sections per unit solid angle and show a broad resonance at approximately 2.2 Mev. The values for the cross sections are considered to be reliable to ±3 percent.

INTRODUCTION

THE scattering of protons by helium has been investigated by other groups interested in establishing the existence of resonance scattering similar to that originally found in neutron-helium scattering by Staub and Stephens.[1] The reaction investigated in $p-He$ scattering is

$$H^1+He^4\rightarrow Li^{*5}\rightarrow H^1+He^4,$$

where an excited state of the compound nucleus gives rise to resonance scattering.

The most extensive proton-helium scattering data up to the present time have been obtained by Heydenburg and Ramsey[2] where measurements were taken from 1 Mev to 3 Mev for the incident proton energies and over angles of 20° to 140° in the laboratory. Previous proton-helium scattering experiments were done by Roberts and Heydenburg[3] for incident protons up to 1 Mev. Experiments on the scattering of α-particles by hydrogen have been done by several workers.[4] By using α-particles up to 8.5 Mev they could obtain data corresponding to a maximum incident proton energy of 2.1 Mev. The present experiment extends the proton energy range to 3.5 Mev and extends the angular measurements down to 10° and up to 164° in the laboratory system of coordinates. These more complete data have made it possible to determine more exactly the shape of the differential cross-section curves.

EXPERIMENTAL PROCEDURE

The same apparatus was used in this work as in the experiments on proton-proton scattering[5] and deuteron-deuteron scattering.[6] The scattering chamber was filled with helium gas purified by storing it in a charcoal trap cooled with liquid nitrogen before letting it into the evacuated chamber. The number of scattering centers per cm^3 was determined by assuming the He^4 to be a perfect gas, measuring the pressure with an oil manometer, and measuring the temperature with a thermometer in equilibrium with the walls of the chamber. The total number of scattering centers was then determined by the volume common to the collimated incident beam and the imaginary column extending beyond and defined by the slit system of the counter. Pressures of approximately 1 cm of Hg were used in the chamber and were found to give no measurable multiple scattering in the gas.

The number of incident particles was measured by collecting them in a Faraday cage at the exit end of the chamber. The collector was in turn connected to a calibrated condenser and ballistic galvanometer system.

The number of scattered protons was measured with a proportional counter which rotated about a central axis through the small scattering volume described above. The factors for obtaining the differential cross section from the number of scattered particles were the same as in previous work.[5]

At low angles and high energies the recoil He^4 nuclei entered the proportional counter as well as the scattered protons. In general the He^4 pulses could be differentiated from the proton pulses by proper selection of bias voltages on the discriminator-scaler units. A typical bias curve is shown in Fig. 1. One discriminator set on the plateau *A* counted all the pulses, while the second set on plateau *B* counted only He^4 pulses. The number of protons scattered into the counter during any one

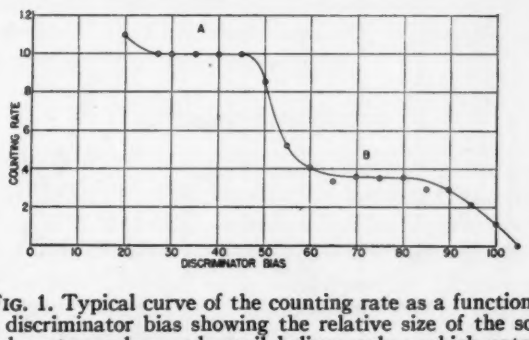

FIG. 1. Typical curve of the counting rate as a function of the discriminator bias showing the relative size of the scattered proton pulses and recoil helium pulses which entered the proportional counter.

[1] H. Staub and W. E. Stephens, Phys. Rev. **55**, 131 (1939).
[2] N. P. Heydenburg and N. F. Ramsey, Phys. Rev. **60**, 42 (1941).
[3] N. P. Heydenburg and R. B. Roberts, Phys. Rev. **56**, 1092 (1939).
[4] J. Chadwick and E. S. Bieler, Phil. Mag. **42**, 923 (1921); C. B. O. Mohr and G. E. Pringle, Proc. Roy. Soc. **160**, 190 (1937).
[5] J. M. Blair, G. Freier, E. E. Lamp, W. Sleator, and J. H. Williams, Phys. Rev. **74**, 553 (1948).
[6] J. M. Blair, G. Freier, E. E. Lampi, W. Sleator, and J. H. Williams, Phys. Rev. **74**, 1594 (1948).

TABLE I. Proton-helium scattering cross sections per unit solid angle in the center of mass coordinate system as a function of the proton energy in the laboratory and the scattering angle in the center of mass system of coordinates. Cross sections are in barns (10^{-24} cm^2). Proton energies are in Mev. The starred values are obtained from measurements with recoil helium atoms.

φ/E_p	0.95	1.49	1.70	2.02	2.22	2.53	3.04	3.58
12° 38′	62.8	22.9	15.92	9.97	8.12	6.46	5.32	4.33
18° 52′	12.35	4.05	2.50	1.564	1.405	1.500	1.520	1.348
25° 3′	4.04	1.090	0.654	0.496	0.600	0.823	0.921	0.834
31° 13′	1.713			0.291	0.441		0.728	
37° 20′	0.854	0.196	0.1461	0.271	0.398	0.554		0.554
43° 23′						0.502	0.523	0.481
49° 23′	0.322	0.1031	0.1057		0.331	0.474		
55° 21′							0.410	0.360
61° 10′	0.1735	0.0812	0.0940	0.1878		0.340		
66° 54′					0.238			
72° 37′	0.1217	0.0764		0.1540		0.253	0.246	0.224
90° 7′	0.0921	0.0828	0.0942	0.1262	0.1487			0.1390
94° 22′						0.1507	0.1408	
99° 28′	0.0833							
104° 36′				0.1402				
110° 14′								0.0997*
114° 22′		0.1202	0.1502	0.1795	0.1830	0.1740	0.1265	0.0985
120° 14′								0.0981*
132° 37′		0.1692	0.219	0.279	0.287	0.260	0.1710	0.1200
140° 14′							0.1950*	0.1428*
149° 22′		0.205	0.270	0.372	0.386	0.353	0.232	0.1663
150° 14′						0.345*	0.226*	0.1621*
160° 14′						0.407*	0.273*	0.1915*
164° 59′							0.280	
168° 2′			0.311	0.443	0.475	0.433	0.281	0.1935

run was the difference of the readings on these two scalers. At some angle and energy combinations the protons and recoil He^4 gave the same sized pulses. To obtain these data on the number of scattered protons an aluminum window which stopped the He^4 nuclei, but not the protons, was placed in front of the proportional counter. At the other angles the data from the recoil He^4 counts was used to calculate the differential cross sections of protons scattered in a backward direction and served as a check on direct measurements of protons scattered in a backward direction.

Measurements of the background counting rate were made by rotating a small brass shutter in front of the slit system of the counter. The number of background counts was in general only a fraction of a percent of the number of counts measured during a run. Enough runs were taken to get a total of at least 3000 counts at any one angle and energy.

The energy scale was calibrated on the basis of 1.882 Mev for the threshold of the $Li^7(p,n)Be^7$ reaction. The energies given are good to ± 20 kv.

CORRECTIONS

The observed number of counts was subject to some corrections. After the chamber was closed from the pumps, it would still outgas and con-

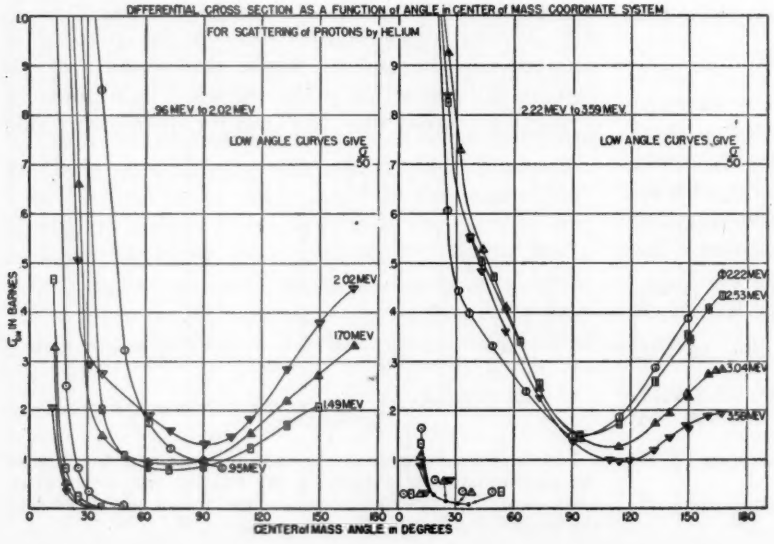
DIFFERENTIAL CROSS SECTION AS A FUNCTION of ANGLE in CENTER of MASS COORDINATE SYSTEM
FOR SCATTERING of PROTONS by HELIUM
96 MEV to 2.02 MEV
LOW ANGLE CURVES GIVE σ/50
2.22 MEV to 3.59 MEV
LOW ANGLE CURVES GIVE σ/50
σ IN BARNES
2.02 MEV
1.70 MEV
1.49 MEV
0.95 MEV
2.22 MEV
2.53 MEV
3.04 MEV
3.58 MEV
CENTER of MASS ANGLE in DEGREES

FIG. 2. Proton-helium scattering cross sections per unit solid angle in the center of mass coordinate system for various proton energies in the laboratory system of coordinates. The curves at small angles are reduced by a factor of 50.

taminate the scattering volume with some foreign gas. The time rate of accumulating contamination gases was measured by evacuating the chamber, closing the connection to the pumping system, and then counting the number of scattered protons at various small angles during a period of an hour or more. This value was found to be the linear function of the time for any given energy and angle and was used to correct the data at other angles and energies by assuming a Coulomb scattering law. A check on this correction was made by comparing data taken immediately after filling the chamber with data requiring up to a 4 percent contamination correction. Agreement was good to within statistical errors at the several angles and energies tested.

A second correction was made for residual air in the helium gas after purifaction. A sample of gas taken from the chamber immediately after filling and analyzed for us on one of Dr. A. O. C. Nier's mass spectrometers showed that the helium contained 0.1 percent air. The correction for this amounted to as much as 2 percent at some angles and energies, but was in general only a fraction of a percent.

The energy of the incident protons was corrected for losses in the Nylon entrance window to the chamber and for losses in the helium gas passed through before reaching the center of the scattering chamber.

Due to the finite size of the proton beam and the finite size of the solid angle subtended by the counter, "second-order geometry" corrections were made on the data similar to the corrections made on the proton-proton scattering data.[5]

RESULTS

The proton-helium differential cross sections in the center of mass system of coordinates are given in Table I and Fig. 2. The energies which are used as a parameter for the curves and which head the columns in the table are the incident proton energies in the laboratory system of coordinates. The errors given for the measured cross sections are the statistical errors which were calculated by using the reciprocal of the square root of the number of counts. The probable errors due to gas pressure measurements, charge measurement, measurement of geometrical factors, etc., amount to about 1.5 percent. When all errors are considered, the values of the cross section should be good to ± 3 percent. The 0.96-Mev data extend only to 99° as the scattered protons did not have enough energy to enter the counter at larger angles.

The differential cross-section curves have two interesting characteristics. First, as the energy increases, the curves depart markedly from the shape of Rutherford scattering curves down to angles as low as 25°. Second, at large angles the differential cross section increases with energy, passes through a maximum at approximately 2.2 Mev, and then decreases.

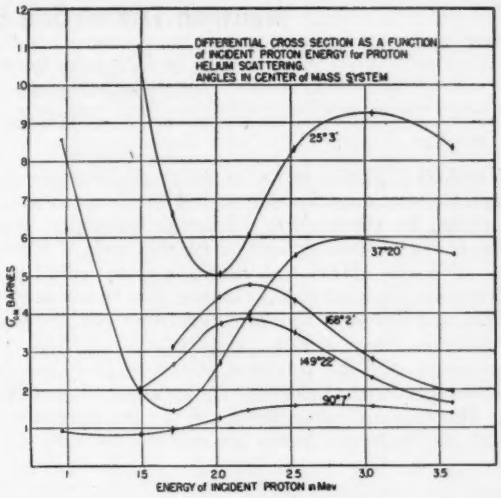
DIFFERENTIAL CROSS SECTION AS A FUNCTION of INCIDENT PROTON ENERGY for PROTON HELIUM SCATTERING. ANGLES IN CENTER of MASS SYSTEM
25°3'
37°20'
68°2'
149°22'
90°7'
σ_{cm} BARNES
ENERGY of INCIDENT PROTON in Mev

FIG. 3. Proton-helium scattering cross sections per unit solid angle in the center of mass coordinate system as a function of the energy of the incident protons in the laboratory system of coordinates. The angle parameter is the center of mass angle.

To see the nature of this resonance, the values of the cross section have been replotted in Fig. 3 as a function of energy with angles serving as parameters. These curves show a broad resonance in the neighborhood of 2.2 Mev for backward scattering. However, the maximum of the resonance appears to shift to higher energies as the angle increases. These curves also show that the preferential backward scattering is done at the expense of scattering in the forward direction as the cross sections for small angles have a minimum at approximately the same energy as cross sections in the backward direction have a maximum. With the rather limited number of points on the energy scale there does not appear to be a double resonance in these curves. However, the nature of the resonance can only be established after a phase shift analysis of the data is completed. This analysis is now being done by Professor C. L. Critchfield and Mr. D. Dodder and will appear in a later publication.

ACKNOWLEDGMENTS

This research was done with the partial support of the Office of Naval Research, Contract N5ori-147. It was also materially assisted by the University of Minnesota Technical Research Fund subscribed to by General Mills, Inc., Minneapolis Honeywell Regulator Company, Minneapolis Star Journal and Tribune Company, Minnesota Mining and Manufacturing Company, and Northern States Power Company.

Neutron Diffraction Study of the Structure of Ice*

E. O. WOLLAN, W. L. DAVIDSON** AND C. G. SHULL
Oak Ridge National Laboratory, Oak Ridge, Tennessee

(Received January 24, 1949)

The crystal structure of ice in which the location of the hydrogen atoms cannot be determined by x-ray means, has been studied by the neutron diffraction technique. The intensities in the neutron diffraction pattern from a powdered sample of heavy (D_2O) ice, maintained at −90°C, were measured and compared with the intensities which would result if ice possessed any one of four proposed structures. The oxygen atom positions have already been determined from x-ray measurements and the proposed structures are considered here with respect to the location of the hydrogen (or deuterium) atoms. The structures considered are (a) the Barnes model, in which the hydrogen atoms are midway between oxygen atoms, (b) the Bernal and Fowler model which maintains a molecular grouping of two hydrogen atoms close (0.96A) to each oxygen atom with a definite repeating orientation, (c) a model consisting of hydrogen molecules rotating about the oxygen atoms as centers, and (d) the Pauling model, suggested on the grounds of a residual entropy at low temperatures, in which hydrogen molecules possess some randomness of orientation under the restriction that one and only one hydrogen atom lies on each of the lines joining one oxygen atom to its neighbor. Structures (a), (b), and (c) are definitely ruled out by the neutron measurements while the Pauling structure agrees well with the measurement.

THE crystal structure of ice has been the subject of considerable study over a period of many years. X-ray diffraction studies[1–3] have led to a definite determination of the oxygen atom positions in the ice crystal lattice but the positions of the hydrogen atoms in the crystal cannot be determined by this means. Information on this point can be obtained from considerations of the physical and chemical properties of water and ice but this information is in some respects less definite than that obtained by x-ray studies where such studies are possible.

With the development of neutron diffraction techniques, we are now in a position to make a direct structure examination of hydrogen containing crystals. The coherent cross section for the scattering of neutrons by hydrogen and deuterium is quite comparable to that for oxygen and hence interference effects for neutrons scattered by these nuclei can be observed.

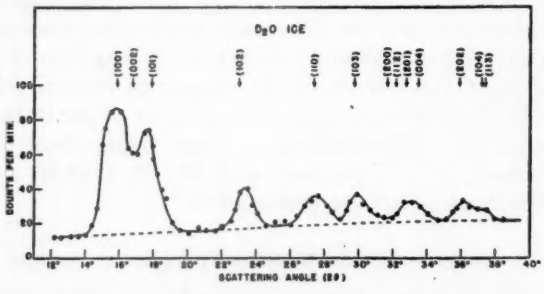

FIG. 1. Neutron diffraction powder pattern of heavy ice (D_2O) taken at −90°C with neutrons of wave-length 1.06A.

MEASUREMENTS

The neutron diffraction measurements have been made with heavy (D_2O) ice. D_2O was used because the coherent neutron scattering cross section for deuterium (~5 barns), is larger than for hydrogen (~2 barns), and also the diffuse scattering for deuterium is much smaller than for hydrogen.

The measurements were made with the powdered crystal technique with monochromatic neutrons from the ORNL pile as previously described[4] for other powdered crystal measurements. In this case the powdered ice was held in a special cold cell maintained at −90°C by a dry ice-acetone cooling mixture. The D_2O was frozen, powdered in a mortar and loaded into the cooling cell, the work being done in a dry box so as not to contaminate the D_2O with ordinary water.

The average results of a number of diffraction measurements with separately prepared powdered samples is shown in Fig. 1. The intensities in this pattern were obtained in terms of absolute cross sections by comparing the pattern for a known amount of ice with the pattern given by a known amount of diamond which is used as a standard since the carbon coherent cross section is accurately known. It will be noticed from the figure that some of the diffraction lines are not resolved. It is not possible with the presently available intensities to resolve the closely spaced lines in a crystal with hexagonal symmetry such as ice. This lack of resolution in the measurements can in some cases limit the significance of the data for structure determinations, but in the present case sufficient information is obtainable from the pattern so that a definite choice can be made between a number of proposed structures for ice. The absolute integrated intensities for the measured peaks are shown in the last

* This document is based on work performed under Contract No. W-7405, eng. 26 for the Atomic Energy Project at Oak Ridge National Laboratory.

** On leave (1946–1947) from B. F. Goodrich Company, Akron, Ohio.

[1] David M. Dennison, Phys. Rev. **17**, 20 (1921).
[2] W. H. Barnes, Proc. Roy. Soc. **A125**, 670 (1929).
[3] W. H. Bragg, Proc. Phys. Soc. (London) **34**, 98 (1922).
[4] E. O. Wollan and C. G. Shull, Phys. Rev. **73**, 822 (1948).

column of Table I, together with other information to be described below.

PROPOSED STRUCURES

Ice possesses hexagonal symmetry and the oxygen atoms are known from x-ray diffraction measurements to be located in a tetrahedral array, any one oxygen atom being located at the center with four other oxygen atoms occupying the corners of the tetrahedron. The distance between oxygen neighbors has been determined from the x-ray measurements to be 2.76A.

Several proposals have been made over a period of years with regard to the location of the hydrogen atoms in the ice structure. In 1929 Barnes[2] proposed a structure for ice in which the hydrogen atoms lie at the midpoints of lines joining neighboring oxygen atoms. The unit cell in this case contains 4 H_2O molecules with the atomic coordinates:

oxygen—$\frac{1}{3}, \frac{2}{3}, \frac{1}{16}$; $\frac{1}{3}, \frac{2}{3}, \frac{7}{16}$; $\frac{2}{3}, \frac{1}{3}, \frac{9}{16}$; $\frac{2}{3}, \frac{1}{3}, \frac{15}{16}$;
hydrogen—$0, \frac{1}{2}, \frac{1}{2}$; $0, \frac{1}{2}, 0$; $\frac{1}{2}, 0, \frac{1}{2}$; $\frac{1}{2}, 0, 0$; $\frac{1}{3}, \frac{2}{3}, \frac{1}{4}$; $\frac{1}{2}, \frac{1}{2}, \frac{1}{2}$; $\frac{1}{2}, \frac{1}{2}, 0$; $\frac{2}{3}, \frac{1}{3}, \frac{3}{4}$.

In 1933 Bernal and Fowler[5] proposed a structure for ice in which the H_2O molecules maintain in the crystal approximately the same structure that they have in the vapor state. The free H_2O molecule is known from dipole moment and spectroscopic data to have an angle between hydrogen bonds of about 105° and an O−H distance of about 0.96A. These molecular groups are placed in the crystal with one hydrogen atom along each of the tetrahedral lines joining neighboring oxygen atoms and there are then two hydrogen atoms close (∼0.96A) to each oxygen atom. The existance of molecular groups in the crystal is in line with data on the vibrational frequencies associated with the O−H bond which indicate that the O−H distance is increased by only about 3 percent in going from isolated H_2O molecules to ice. In this proposed structure the hydrogen molecules are assigned a definite arrangement which involves a unit cell of 12 molecules. (See original paper for atomic coordinates and see also, the note added in proof.)

It has been shown by Pauling[6] that the structure proposed by Bernal and Fowler in which the crystal is assumed to have a unique configuration with respect to the location of the hydrogen atoms is not in accord with the experimentally known fact that the entropy of the crystal does not tend to zero as the crystal is cooled to very low temperatures. Pauling assumes, as do Bernal and Fowler, that each water molecule is so oriented that its two hydrogen atoms are directed approximately toward two of the four surrounding oxygen atoms and that

[5] J. D. Bernal and R. H. Fowler, J. Chem. Phys. **1**, 515 (1933).
[6] L. Pauling, J. Chem. Soc. **57**, 2680 (1935).

TABLE I. Comparison of observed and calculated intensities in the neutron diffraction powder pattern of heavy ice. The calculated intensities are on an absolute scale and have been obtained using 5.2 and 4.2 barns for the coherent scattering cross sections of deuterium and oxygen, respectively.

	Bernal Fowler				Barnes		Rotating molecule		Pauling or half-hydrogen		Observed
$\sin\theta/\lambda$	hkl	P_{hkl}		hkl	P_{hkl}		P_{hkl}		P_{hkl}		P_{hkl}
0.1271	110	406		100	363		304		386		
0.1358	002	240	899	002	202	767	166	647	219	835	830
0.1442	111	253		101	212		177		230		
0.1860	112		128	102		79		97		104	118
0.2206	300		199	110		72		131		140	130
0.2401	113		212	103		14		101		70	95
0.2542	220	57		200	41		14		6		
0.2590	302	47		112	15	201	47	70	3	111	98
0.2639	221	66	304	201	67		9		63		
0.2717	004	32		004	78		0		41		
0.2745	311	102									
0.2856	213	29									
0.2885	222	35	104	202	199	253	6	6	77	106	97
0.3000	114	40		104	54		0		29		

only one hydrogen atom lies along each oxygen-oxygen line, but contrary to Bernal and Fowler he assumes that the crystal can exist in any of the many configurations which satisfy these conditions. He also assumes that the crystal can change from one configuration to another by rotation of some of the molecules or by motion of some of the hydrogen nuclei from a position near (∼0.96A) one oxygen atom to a corresponding position near an adjacent oxygen atom. Such motions would involve several hydrogen atoms simultaneously in order to satisfy the condition that there are always two hydrogen atoms near a given oxygen atom. The fact that at temperatures above about 200°K the dielectric constant of ice is of the same order of magnitude as that of water suggests that the molecules can orient themselves with considerable freedom. On the assumption that the crystal upon being cooled to very low temperatures is frozen into any one of the large number of configurations all of

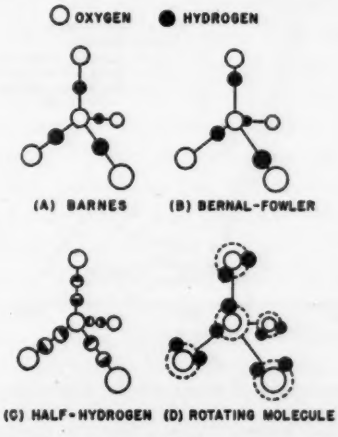

FIG. 2. Schematic diagram of four structural models which are used in calculating pattern intensities for various proposed structures of ice.

which satisfy the above mentioned conditions, the entropy of the crystal will tend towards a finite value as the temperature approaches zero. Pauling's calculation of this residual entropy leads to a value of 0.806 cal. per mole degree and this compares very favorably with the experimental values of 0.82 cal. per mole degree for ordinary ice and 0.77 cal. per mole degree for heavy ice.

The postulated models described above for the ice structure are shown schematically in Fig. 2. The oxygen atoms are at the center and corners of a tetrahedron. In the Barnes model (A) the hydrogen atoms are located midway between oxygen atoms whereas in the Bernal-Fowler model (B) there are two hydrogen atoms near each oxygen atom in a fixed repeating pattern which would require a larger cell to illustrate. For the Pauling model, which assumes a random molecular grouping, the expected intensities can be calculated on the basis of a half-hydrogen model (C) in which half the scattering amplitude of each hydrogen (or deuterium) nucleus is associated with the sites shown in (C). Calculations for a rotating molecule are based on the structure shown in (D) of the figure.

COMPARISON OF NEUTRON DIFFRACTION DATA WITH PROPOSED STRUCTURES

The results of the neutron diffraction measurement will now be considered by comparing the observed intensities for the heavy ice pattern with the calculated intensities for the various suggested structures. This comparison has been made for the structures proposed by Barnes, by Bernal and Fowler, for the case of D_2O molecules rotating about the oxygen atoms as centers and for the structure proposed by Pauling.

The smallest unit cell which accounts for the oxygen atom positions contains four D_2O molecules. This cell is satisfactory for the Barnes, rotating molecule and Pauling structures. The Miller indices for this cell are given in the fourth column of Table I. The Bernal-Fowler structure involves a larger cell of 12 D_2O molecules and the Miller indices corresponding to this structure are listed in the second column of the table. For this larger cell there are many more possible reflections over a given range of $\sin\theta/\lambda$ than for the Barnes cell. The structure factors*** and corresponding intensities have been calculated for all the possible reflections in the range of angles considered but in the case of those values of (hkl) not listed, the calculated intensities came out to zero or nearly zero.

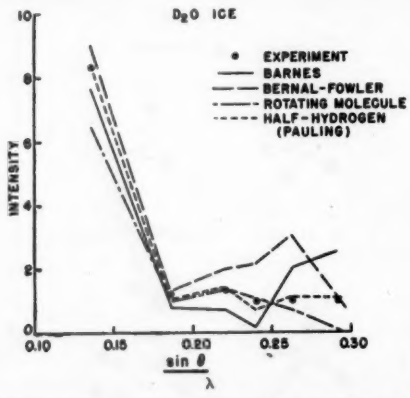

FIG. 3. Comparison of experimental intensities for D_2O ice with those calculated according to four proposed structures. The six observed intensity values listed in the last column of Table I are plotted as the experimental points in this figure. The lines joining the calculated intensity values are of no significance except for being a visual aid.

For the calculation of the absolute structure factors and the corresponding integrated intensities (listed as P_{hkl} in the table) the sign and magnitude of the coherent scattering amplitudes for the oxygen and deuterium nuclei must be known. In the case of oxygen it has been shown that the scattering is not spin dependent and that the phase of scattering is positive. Direct measurements of the coherent scattering by oxygen nuclei in crystals as well as measurements of the total scattering give 4.2 barns for the bound scattering cross section of oxygen. For the case of deuterium, recent unpublished powder crystal measurements with ThD_2 give a coherent scattering cross section of 5.2 barns for deuterium and this value has been used in the ice calculations. The phase of the deuterium scattering was shown to be positive in measurements with NaD.[7] This cross section is measurably smaller than the total scattering cross section of 7.5 barns for bound nuclei found by Rainwater and Havens and this difference indicates a spin dependent scattering for deuterium. On this basis a diffuse scattering caused by spin incoherence would be expected in the diffraction pattern along with the coherent and other diffuse scattering features.

Using these values for the coherent scattering cross sections, the integrated intensities (on an absolute scale) have been calculated using the structure factors for the various models. The comparison of the observed intensities with those calculated for the various models is given in Table I and also in Fig. 3 where the points represent the measured values and the lines show the trend of the calculated results. Column 3 in Table I lists the calculated intensities for the Bernal-Fowler structure, and these are to be compared with the observed intensities listed in the last column. It is seen that this model predicts intensities two and three times the observed intensity for the intermediate angle reflections and hence is not too suitable for describing the structure.

*** For a cell of this size the structure factor calculations are quite laborious and we have been assisted in these calculations by Miss E. A. Forbes.

[7] Shull, Wollan, Morton, and Davidson, Phys. Rev. **73**, 830 (1948).

The intensities calculated for the Barnes model, in which the deuterium atoms are assumed to be located half way between oxygen atoms, are listed in the fifth column of the table. The intensities of the reflections at the larger angles are seen to be very much higher than the measured values whereas at the smaller angles they are smaller than measured.

The intensities calculated for a rotating molecule in which the positional relationship present in the water molecule is maintained during rotation are shown in the sixth column of the table. A calculation for the case of deuterium nuclei rotating independently and at random on a shell of radius $r=0.96$A about the oxygen atoms gives essentially the same result. It is to be expected that this randomness in the orientation of the deuterium nuclei with respect to specific directions in the lattice will cause the coherent scattering to fall off with increasing angle of reflection, as is seen to be the case for the calculated values in the table. In any case the calculated intensities appear too small for both the small and large angle reflections.

The determination of the integrated intensities to be expected for the Pauling model of the ice crystal would require one to calculate the intensities for each of the many possible configurations which the crystal could assume under the previously mentioned assumptions that two and only two hydrogen atoms are at any given time located close to a given oxygen atom. When the problem is set up in this way it becomes evident that the solution with respect to the Bragg scattering by the crystal is just that which would be obtained by assuming the crystal to possess a substitution disorder with respect to hydrogen atoms in which half of the sites available for these atoms are unoccupied. This assumes that the occupied and unoccupied sites are randomly distributed and the requirement of molecular (D_2O) groups is disregarded. It is hence evident that the diffraction measurements are only capable of determining that on the average two hydrogen atoms will be found close to a given oxygen atom. The intensities calculated for what might now be called the half-hydrogen model in which an average scattering amplitude of $f_D/2$ has been taken for the $2N$ sites available to the N deuterium nuclei are listed in the seventh column of the table. The agreement of these calculated values of P_{hkl} with those observed experimentally is seen to be good, there being only one value which might be considered somewhat outside the experimental error. The fact that the measured peaks at the larger values of $(\sin\theta)/\lambda$ are lower than the calculated values can be due to a temperature effect or some of it may be due to the uncertainty in the deuterium scattering cross section.

This agreement constitutes strong evidence for the correctness of the Pauling structure. The neutron measurements cannot, however, in themselves prove the absence of any $(D_4O)^{++}$, $(D_3O)^{+}$, $(OD)^{-}$ or O^{-} groups in the crystal. That the number of such groups is small is borne out by the agreement of the calculated and experimentally determined residual entropy. A random distribution of the various possible groups would lead to a value of the residual entropy about three times greater than the measured value.

That there is a randomness in the location of the deuterium nuclei in the crystal is shown also by the magnitude of the diffuse scattering. With an average coherent scattering amplitude of $f_D/2$ for the $2N$ deuterium sites in the crystal, the average coherent cross section per deuterium nucleus will be $(4\pi/N)\sum_{2N}(f_D/2)^2=\frac{1}{2}(4\pi f_D^2)$. The coherent scattering cross section in a crystal with no randomness in the location of deuterium nuclei would be $4\pi f_D^2$ and the difference $4\pi f_D^2-\frac{1}{2}(4\pi f_D^2)$ will appear for the ice crystal as a diffuse scattering arising from the random character of the lattice. In addition to the diffuse scattering arising from this cause there will be diffuse scattering arising from spin dependence and a small amount from the usual Debye temperature effect. In addition to these true sources of diffuse scattering there is always present in our neutron experiments a small background which arises from multiple scattering of Bragg diffracted radiation.

Although, as yet, no real effort has been made to make an accurate determination of the diffuse scattering by ice, the measurements agree quite well with the calculated values. An approximate correction can be made for multiple scattering and the temperature diffuse scattering is negligible at small angles. The spin scattering per deuterium nucleus is given by $4\pi f_D^2(\text{total})-4\pi f_D^2(\text{coherent})=7.5-5.2=2.3$ barns and the corresponding random disorder scattering is, as we have shown above, equal to $\frac{1}{2}(4\pi f_D^2(\text{coherent}))=2.6$ barns. The sum of these cross sections, 4.9 barns per deuterium nucleus, agrees within experimental error with the observed value after correction for the multiple scattering. Thus the diffuse scattering constitutes an additional check on the random nature of the lattice.

We are not in a position at this time to discuss the relation of our results to the diffuse streaks which Owston and Lonsdale[8] has observed in their x-ray Laue photographs of ice. We hope, at a later date, to see whether or not this effect will also be observed with neutrons. The ice measurements represent the first real effort at applying neutron diffraction to the study of the location of hydrogen (or deuterium) nuclei in crystals and they show the potentialities of this technique in such structure analyses.

[8] P. G. Owston and K. Lonsdale, J. Glaciology I, 118 (1948).

Note added in proof: Since this paper went to press, Lonsdale and Owston have pointed out to us by correspondence that the parameters given by Bernal and Fowler, namely, $y=0.105$ and $Z=0.037$, are incorrect and should be changed to $y=0.115$ and $Z=0.0435$. This change in the value of the parameters would affect somewhat the intensity calculations given in column 3 of Table I but this change could almost certainly not produce good agreement between this model and our observed results since the coherent scattering by the hydrogen atoms in a model in which these atoms are fixed at definite sites will always be twice as great as that produced by the Pauling model. The calculated intensities given in Table I for the Bernal-Fowler model are all higher than the observed intensities given in column 7 of the table and it would not be expected that a revision of the parameters would alter this situation.

ACKNOWLEDGMENTS

We are indebted to Dr. H. M. James for valuable discussions in connection with the calculations of the intensities for the Pauling Model.

PHYSICAL REVIEW VOLUME 75, NUMBER 9 MAY 1, 1949

The Scattering of High Energy Neutrons by Nuclei

S. FERNBACH, R. SERBER, AND T. B. TAYLOR
Radiation Laboratory, Department of Physics, University of California, Berkeley, California

(Received January 19, 1949)

The experiments of Cook, McMillan, Peterson, and Sewell on the cross sections of nuclei for neutrons of about 90 Mev indicate that the nuclei are partially transparent to high energy neutrons. It is shown that the results can be explained quite satisfactorily using a nuclear radius $R=1.37A^{\frac{1}{3}}\times10^{-13}$ cm, a potential energy for the neutron in the nucleus of 31 Mev, and a mean free path for the neutron in nuclear matter of 4.5×10^{-13} cm. This mean free path agrees with that estimated from the high energy n-p cross section, but the results are not sensitive to the choice of mean free path.

IN a previous paper by one of the writers[1] it has been pointed out that to a high energy bombarding particle a nucleus appears partially transparent, since at energies of the order of 100 Mev the scattering mean free path for a neutron or proton traversing nuclear matter becomes comparable to the nuclear radius. This transparency effect is strikingly apparent in the experiments of Cook, McMillan, Peterson, and Sewell[2] on the scattering by nuclei of neutrons of about 90 Mev. In the present paper it will be shown that the observed scattering cross sections can be quite satisfactorily accounted for, using a mean free path of the expected magnitude.

The problem is that of the scattering of the neutron wave by a sphere of material characterized by an absorption coefficient and an index of refraction. The index of refraction is determined by the mean potential energy, V, of the neutron in the nucleus. If $k=(2ME)^{\frac{1}{2}}/\hbar$ is the propagation vector of the wave outside the nucleus, its propagation vector inside is $k+k_1$, with

$$k_1=k[(1+V/E)^{\frac{1}{2}}-1].$$

For $E=90$ Mev, $k=2.08\times10^{13}$ cm^{-1}. The potential V is generally taken to be about 8 Mev larger than the energy of the Fermi sphere. The latter depends on the assumed nuclear density. If we use for the nuclear radius the value $R=1.37A^{\frac{1}{3}}\times10^{-13}$ cm, deduced by Cook, McMillan, Peterson, and Sewell from the 14–25 Mev scattering results of Amaldi, Bocciarelli, Cacciapuoti, and Trabacchi,[3] and Sherr,[4] we find a Fermi energy of 22 Mev, and $V=30$ Mev. This gives $k_1=3.22\times10^{12}$ cm^{-1}. The absorption coefficient in nuclear matter is equal to the particle density times the cross section for scattering of the neutron by a particle in the nucleus,

$$K=3A\sigma/4\pi R^3.$$

In terms of the n-p and n-n cross sections,

$$\sigma=[Z\sigma_{np}+(A-Z)\sigma_{nn}]/A.$$

Cook *et al.*,[2] give for the scattering of a 90 Mev neutron by a free proton $\sigma_{np(\text{free})}=8.3\times10^{-26}$ cm^2. This cross section must be reduced to allow for the effect of the exclusion principle on the scattering by a proton bound in the nucleus; according to Goldberger,[5] the factor is $\sigma_{np}=\frac{2}{3}\sigma_{np(\text{free})}$. Assuming a $1/E$ dependence of the cross sections we find, for $E=90+30=120$ Mev, $\sigma_{np}=4.15\times10^{-26}$ cm^2. If, following Goldberger, we take $\sigma_{nn}=\frac{1}{4}\sigma_{np}$, and use the previously quoted radius formula, we obtain $K=2.4\times10^{12}$ cm^{-1} for $Z/A=\frac{1}{2}$, $K=2.1\times10^{12}$ cm^{-1} for $Z/A=0.39$ (U). It will be seen from these numbers that in the ensuing calculations it will be a reasonable approximation to suppose that $kR\gg1$, but k_1/k and $K/k\ll1$, so that k_1R and KR are of order one.

[1] R. Serber, Phys. Rev. **72**, 1114 (1947).
[2] L. J. Cook, E. M. McMillan, J. M. Peterson, and D. C. Sewell, Phys. Rev. **75**, 7 (1949).
[3] E. Amaldi, D. Bocciarelli, B. N. Cacciapuoti, and G. C. Trabacchi, Nuovo Cimento **3**, 203 (1946).
[4] R. Sherr, Phys. Rev. **68**, 240 (1945).
[5] M. L. Goldberger, Phys. Rev. **74**, 1268 (1948).

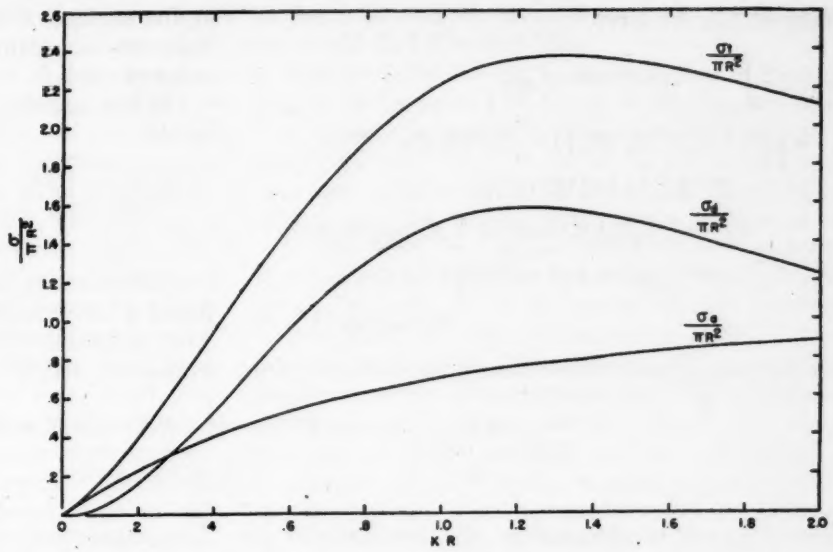

FIG. 1. Absorption, diffraction and total cross section as a function of the nuclear radius measured in mean free paths. These curves are for $k_1/K=1.5$.

The scattering cross section consists of two parts. The first, the "absorption cross section," is just πR^2 times the probability that the neutron collides with a particle in the nucleus. This is not true absorption: inelastic scattering and scattering with exchange are included. The second part, the "diffraction scattering," is elastic scattering arising from the disturbance of the incident plane wave by the nucleus. To illustrate the calculation, we first consider the scattering from a disk of radius R and thickness T. We suppose there is a boundary layer at the surface of the disk in which k_1 and K rise to their interior values in a distance larger than $1/k$.[6] There will then be no scattering at the surfaces, and, for unit amplitude of incident wave, the wave transmitted through the disk will have an amplitude and relative phase $a=\exp(-\frac{1}{2}K+ik_1)T$. The absorption cross section is

$$\sigma_a=\pi R^2(1-|a|^2)=\pi R^2(1-e^{-KT}). \quad (1)$$

The diffraction cross section can be found from the consideration that on a plane behind the disk the wave is no longer plane, but differs from a plane wave by an amplitude $1-a$ in the shadow of the disk. This amplitude represents a scattered wave, and the corresponding cross section is

$$\sigma_d=\pi R^2|1-a|^2 =\pi R^2(1-2e^{-\frac{1}{2}KT}\cos k_1T+e^{-KT}). \quad (2)$$

It can easily be shown that the angular dependence of the scattered amplitude is

$$f(\theta)=k\int_0^R(1-a)J_0(k\rho\sin\theta)\rho d\rho =(1-a)RJ_1(kR\sin\theta)/\sin\theta, \quad (3)$$

which gives the differential scattering cross section

$$d\sigma_d(\theta)=|f(\theta)|^2d\Omega =(\sigma_d/\pi)[J_1(kR\sin\theta)/\sin\theta]^2d\Omega. \quad (4)$$

The absorption cross section is, of course, always less than πR^2, but the diffraction cross section may be either larger or smaller, depending on the magnitude of the phase shift. For large KT, $\sigma_a=\sigma_d=\pi R^2$. In the opposite limit of small KT and k_1T, we have

$$\sigma_a=\pi R^2KT=A\sigma,$$
$$\sigma_d=\pi R^2(\tfrac{1}{4}K^2+k_1^2)T^2=\tfrac{1}{4}A\sigma[1+4(k_1^2/K^2)]KT.$$

Thus for low density or small thickness, σ_a approaches the sum of the scattering cross sections of the separate nucleons. The diffraction cross section, however, vanishes in the limit, being proportional to the probability of double scattering.

The corresponding calculations for a sphere are only slightly more complicated. The portion of the wave which strikes the sphere at a distance ρ from a line through the center of the sphere emerges after traveling a distance $2s$, with $s^2=R^2-\rho^2$. Its amplitude on emerging is $a=\exp(-K+2ik_1)s$, so that, in place of (1) we have

$$\sigma_a=2\pi\int_0^R(1-e^{-2Ks})\rho d\rho=2\pi\int_0^R(1-e^{-2Ks})sds =\pi R^2\{1-[1-(1+2KR)e^{-2KR}]/2K^2R^2\}. \quad (5)$$

This formula for the absorption cross section has previously been given by Bethe.[7] Similarly, in

[6] In terms of the model being employed, the finite intercept of the R *vs.* $A^{\frac{1}{3}}$ line obtained from the data on the lower energy scattering could be interpreted by the more careful examination of the boundary conditions which in this case would be necessary.

[7] H. A. Bethe, Phys. Rev. **57**, 1125 (1940).

place of (2), we have

$$\sigma_d=2\pi\int_0^R|1-e^{(-K+2ik_1)s}|^2\rho d\rho$$
$$=\pi R^2[1+(1/2K^2R^2)\{1-(1+2KR)e^{-2KR}\}$$
$$-(1/(\tfrac{1}{4}K^2+k_1^2)^2R^2)\{(\tfrac{1}{4}K^2-k_1^2)$$
$$+e^{-KR}[2k_1R(\tfrac{1}{4}K^2+k_1^2)+k_1K]\sin 2k_1R$$
$$-e^{-KR}[(\tfrac{1}{4}K^2-k_1^2)+KR(\tfrac{1}{4}K^2+k_1^2)]$$
$$\times\cos 2k_1R\}]. \quad (6)$$

In deriving (5) and (6) we have neglected refraction at the surface of the sphere. It can easily be seen that this is legitimate, since it gives an effect of order $(k_1/k)k_1R$.

For the angular distribution we find, in analogy to (3),

$$f(\theta)=k\int_0^R[1-e^{(-K+2ik_1)s}]J_0(k\rho\sin\theta)\rho d\rho. \quad (7)$$

For $KR\to\infty$, we again obtain (4), but we have not found a convenient expression in the general case. The amplitude for forward scattering is easily evaluated, and is found to be

$$f(0)=\frac{kR^2}{2}\left\{1+\frac{(k_1-\frac{1}{2}iK)^2[1-(1+KR-2ik_1R)e^{(-K+2ik_1)R}]}{2(\tfrac{1}{4}K^2+k_1^2)^2R^2}\right\}. \quad (8)$$

For purposes of calculation, the integral can be converted to a sum; letting $l+\frac{1}{2}=k\rho$ and using the relation $J_0((l+\frac{1}{2})\sin\theta)=P_l(\cos\theta)$, valid for large l and small θ, we find

$$f(\theta)=\tfrac{1}{2}k\sum_{l=0}^{l+\frac{1}{2}<kR}(2l+1)(1-e^{(-K+2ik_1)sl})P_l(\cos\theta), \quad (9)$$

where

$$s_l=[k^2R^2-(l+\tfrac{1}{2})^2]^{\frac{1}{2}}/k.$$

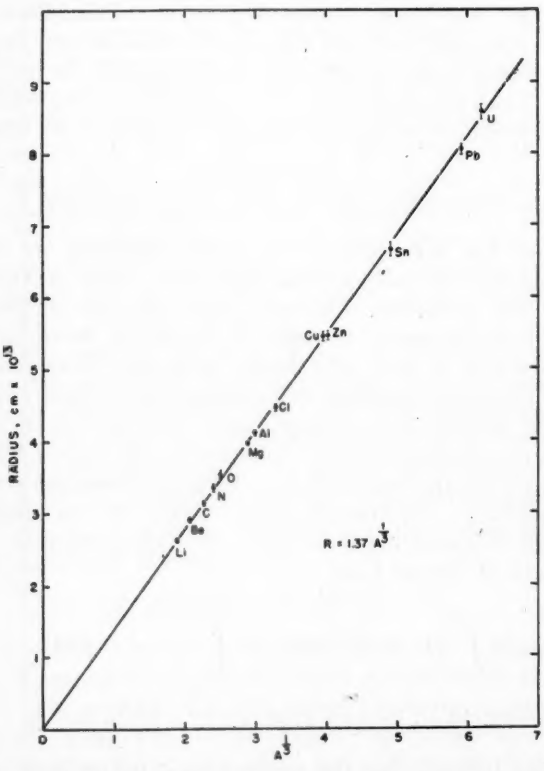

FIG. 2. Nuclear radii deduced from the total cross section measurements of Cook, McMillan, Peterson, and Sewell, plotted against the cube roots of the mass numbers. The straight line is $R=1.37A^{\frac{1}{3}}\times10^{-13}$ cm.

This expression can also be obtained by a partial wave analysis, using the WKB method to evaluate the phase shifts. This gives

$$\delta_l=(k_1+\tfrac{1}{2}iK)s_l,$$

whence we immediately obtain (9), and for σ_a and σ_d,

$$\sigma_a=(\pi/k^2)\textstyle\sum_l(2l+1)(1-e^{-2Ks_l}), \quad (10)$$

$$\sigma_d=(\pi/k^2)\textstyle\sum_l(2l+1)|1-e^{(-K+2ik_1)s_l}|^2. \quad (11)$$

Converting the sums in (10) and (11) to integrals we again obtain (5) and (6).

In Fig. 1 we have plotted $\sigma_a/\pi R^2$, $\sigma_d/\pi R^2$, and the total cross section $\sigma_t/\pi R^2=(\sigma_a+\sigma_d)/\pi R^2$ as functions of KR. The ratio $\sigma_a/\pi R^2$ is a function only of KR; the other two depend on k_1/K as well. The curves in Fig. 1 have been plotted for $k_1/K=1.5$, about the ratio indicated by our earlier consideration of the expected magnitude of the constants. Using this plot it is possible to determine, once a value of K is chosen, the radius required for each nucleus to give the measured total cross section. The radii calculated in this way from the observed cross sections, using the value[8] $K=2.2\times10^{12}$ cm^{-1}, are shown in Fig. 2. It will be seen that they lie quite closely on the line $R=1.37A^{\frac{1}{3}}\times10^{-13}$ cm; the self-consistency of our description of the scattering process is thus established. The value $K=2.2\times10^{12}$ cm^{-1} corresponds to a mean free path in nuclear matter of 4.5×10^{-13} cm. The associated value, $k_1=3.3\times10^{12}$ cm^{-1}, corresponds to $V=30.8$ Mev.

The question now arises as to the accuracy with which the constants K and k_1 are determined by the scattering data. If k_1 is decreased, keeping K constant, it is found that the radius curve, Fig. 2, is pulled up in the middle; the resultant curve can

[8] The small dependence of K on Z/A is unimportant, as we shall see later.

be approximated by two straight lines, the light elements lying on a steeper line through the origin, while the heavy elements lie on a less steep line with a positive intercept. Increasing k_1 has the opposite effect. A variation in k_1 of $\pm 0.2\times10^{12}$ cm^{-1}, or in V of ± 2 Mev, begins to produce appreciable bending. A reduction in K, with fixed k_1, introduces a curvature in the radius line, the center being pulled down and the two ends raised. The curvature becomes noticeable if K is reduced to less than $K=1.9\times10^{12}$ cm^{-1}, however K can be almost doubled before the opposite curvature becomes very pronounced. For example, $K=3.0\times10^{12}$ cm^{-1} gives an about equally good straight line, $R=1.39A^{\frac{1}{3}}\times10^{-13}$ cm. The total cross-section measurements thus determine the potential fairly well, but are quite insensitive to the absorption coefficient. Measurements of σ_a and of the differential diffraction scattering are required for a better evaluation of K. It should be noted that while k_1 and K are determined directly from the cross sections, the evaluation of V depends also on the energy of the incident neutrons. Cook *et al.* state that the energy of the neutrons detected in their experiment may be a little lower than 90 Mev, lying somewhere between 80 and 90 Mev. If we took $E=80$ Mev, we would find $V=28.8$ Mev.

For $K=2.2\times10^{12}$ cm^{-1}, the values of KR range from 0.58 for Li to 1.87 for U. It will be seen from Fig. 1 that the nuclear opacity, $\sigma_a/\pi R^2$, would vary from 0.52 for Li to 0.88 for U. It will also be seen that over this range of values of KR it would be expected that σ_d will be nearly twice as large as σ_a.

If one plots the angular distribution of the diffraction scattering given by (9) (i.e., $d\sigma_d(\theta)/d\sigma_d(0)$ *versus* $kR\sin\theta$) one finds curves for the heaviest nuclei which are indistinguishable from that for an opaque nucleus (Eq. (4)), at least as far as the first minimum of the diffraction pattern. For the lighter nuclei, the form of the curve is closely the same, but with an altered scale of abscissa, corresponding to using an effective radius somewhat smaller than the true radius. The increase in the half width of the diffraction peak is zero for $KR=1.78$ (Pb), 3.7 percent for $KR=1.20$ (Cu), 6.2 percent for $KR=0.90$ (Al) and 9.6 percent for $KR=0.63$ (Be). Measurements of the diffraction scattering and of the absorption are now in progress in this laboratory.

Work described in this paper was done under the auspices of the Atomic Energy Commission.

PHYSICAL REVIEW VOLUME 75, NUMBER 9 MAY 1, 1949

He³ Isotopic Abundance*

J. H. Coon
Los Alamos Scientific Laboratory, Los Alamos, New Mexico
(Received December 20, 1948)

The isotopic abundance of He³ in one sample each of "well" helium and "atmospheric" helium has been measured by detecting the He³(n,p)H³ disintegrations induced by thermal neutrons. The helium gas was put into a proportional counter, the disintegration rate compared to that with nitrogen in the counter, and the He³ content deduced from the known ratio of the He³ and N disintegration cross sections.

INTRODUCTION

PREVIOUS measurements[1,2] have indicated that He³ is present in natural helium in amounts of the order of one part in 10^6 to 10^7, and that the abundance varies by more than a factor of 10 depending on the source of the helium. He³ concentration determination is of special current interest in connection with nuclear investigations of interactions between elementary nuclei, and in connection with investigations of the thermodynamic behavior of He³ and He⁴ at temperatures of liquid helium.

In the present work measurements were made of the isotopic abundance of He³ in two samples of natural helium: one from wells near Amarillo, Texas, and one from air reduction processing. The presence of He³ was detected by counting ionization pulses arising from the disintegration products of the reaction He³(n,p)H³ induced by thermal neutrons. The cross section for this reaction is about 5000 barns,[3] which is sufficiently large to make it possible to detect the He³ in natural helium samples. Data were also taken with nitrogen in the counter, in which case one detects the N¹⁴(n,p)C¹⁴ disintegrations. Since the protons from the He³ and N reactions have very closely the same range, the "wall effect" corrections will be similar for the two cases. If counting is done on nitrogen and on

* This document is based on work performed at Los Alamos Scientific Laboratory of the University of California under Government Contract W-7405-eng-36.

[1] L. T. Aldrich and A. O. Nier, Phys. Rev. **70**, 983 (1946); **74**, 1225 (1948); **74**, 1590 (1948).

[2] L. W. Alvarez and R. Cornog, Phys. Rev. **56**, 613 (1939); **56**, 379 (1939).

[3] J. H. Coon and R. A. Nobles, Phys. Rev. **75**, 1358 (1949).

TABLE I. Determination of disintegration rates.

	Partial press. p of gas in atmos.	Press. of added argon in atmos.	Counter voltage	Approx. total number disintergrations counted	Additive correction Σw	Corrected counts per min. $=D$
N_2—run 1	0.258	1.71	3725	12,000	137.0	1314 \ Av. = 1278
run 2	0.258	1.71	3725	12,000	111.0	1243 /
"Well" helium	7.47	0.27	2010	7000	0.32	9.15
"Atmospheric" helium	1.143	0.65	1485	9000	0.54	10.55
Pure argon	1.95	—	2670	—	—	—

helium with the same neutron flux, then the disintegration rates D taking place within the sensitive volume of the counter will be related by:

$$D_N/D_{He}=(\sigma_N n_N/\sigma_{He^3} n_{He^3}), \quad (1)$$

where σ is the disintegration cross section and n the number of atoms per cm^3. If I is the relative concentration of He^3 in the helium and p is pressure, then the above ratio may be written

$$D_N/D_{He}=(\sigma_N/\sigma_{He^3})\cdot(2p_N/Ip_{He}). \quad (2)$$

Using the ratio σ_N/σ_{He^3} elsewhere reported,[3] we can therefore obtain I by determining the counting rates at measured pressures.

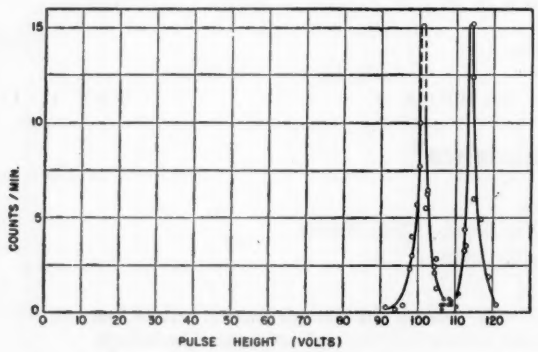

FIG. 1. Differential pulse height distribution curve obtained with a thin deposit of normal uranium mounted on the inner wall of the counter. The two peaks correspond to the alpha-particle groups from U^{234} and U^{238}. 3.0 atmos. argon pressure.

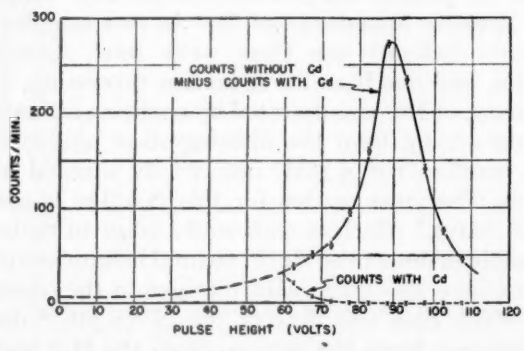

FIG. 2. Pulse height distribution curves obtained by counting $N^{14}(n,p)C^{14}$ disintegrations. The plotted points represent the number of pulses in a 5-volt pulse height interval and the point is plotted at the center of the interval. The vertical lines indicate standard deviations computed by taking the square root of the total number of counts obtained and adjusting this to the counting rate.

TABLE II. He^3/He^4 Ratio $\times 10^{-7}$.

	Present measurement	Aldrich and Nier
"Well" helium (Amarillo, Texas)	1.73	1.4
"Atmospheric" helium (Airco)	13.0	12.0
Beryl crystals (Amarillo, Texas)		0.6, 1.4, 1.4, 2.0
Radioactive ores		<0.3

APPARATUS AND PROCEDURES

The techniques and apparatus used were essentially the same as those reported in the article by Coon and Nobles in this issue of the Physical Review. There were a few exceptions as follows. A normal uranium alpha-particle emitter was used inside the counter instead of plutonium. A calcium purifier was attached directly to the counter in the manner reported by Klema and Barschall.[4] This purifier was desirable since the effect of a small N_2 impurity in the helium would not be distinguishable from the effect of He^3. The counter gas flowed continually over calcium turnings in the purifier at about 300°C. The effectiveness in removing nitrogen was tested by contaminating a pure argon filled counter with a small amount of air, and observing the drop in neutron induced counting rate as the calcium removed the nitrogen.

RESULTS

The pulse height distribution curves are shown in Figs. 1 to 4. The curves show counting data taken both with and without a cadmium cover over the counter. The count with cadmium is subtracted as a background except in the small pulse region where gamma-rays are detected, and where neutron capture gammas from the cadmium interfere. From Fig. 2 it is seen that in the case of nitrogen the count with cadmium is a very small fraction of the count without cadmium (about one part in 800)

[4] E. D. Klema and H. H. Barschall, Phys. Rev. **63**, 18 (1943).

except in the region of small pulses. In the case of helium (see Figs. 3 and 4) the count without cadmium is relatively high because of the presence of a few residual high energy neutrons getting to the region of the counter in spite of the large amount of graphite between the counter and the fast neutron source. The He^4 recoils from these fast neutrons are appreciable in number because of the tremendous abundance of He^4 as compared to He^3. Figure 3 also shows the cadmium difference curve obtained with 1.95-atmosphere pure argon in the counter. This count with argon serves as a background to be subtracted from the cadmium difference curves gotten with helium.

The number of disintegrations D taking place within the sensitive volume of the counter was obtained from

$$D=\sum C_1-\sum C_2-\sum A+\sum w,$$

where $\sum C_1$ is the counting rate without cadmium summed over all channels counted; $\sum C_2$ is the counting rate with cadmium summed over all channels counted; A is the background as determined with pure argon, this also being a cadmium difference count; and $\sum w$ is the "wall effect" correction determined by adding up the number of pulses under the extrapolated lower end of the corrected pulse height distribution curves. The correction $\sum w$ accounts at least in part for all small pulses whether they are due to "wall effect" or to other causes which reduce their size so much that they cannot be counted in the lowest pulse height counting channel.

Inserting values for p and D from Table I into relation (2), using[3] $\sigma_{He^3}/\sigma_N=2860$, and solving for I gives values listed in Table II, along with values obtained by Aldrich and Nier.[1] Differences between the two sets of values are probably not significant, especially in view of the variations which Aldrich and Nier find in the He^3 abundance for samples of different origin.

For correlating the He^3 abundance with the source of helium, the mass spectrograph is better than the present counter technique because of the large quantity of gas necessary in the counter method. For analysis of the He^3 content in enriched samples the counter technique may offer some advantages in ease and accuracy, depending of course on available facilities.

The accuracy of the present measurement is estimated at ± 15 percent, which does not include the error in the value of σ_{He^3}/σ_N which is about ± 5 percent. Of the 15 percent error, approximately 6

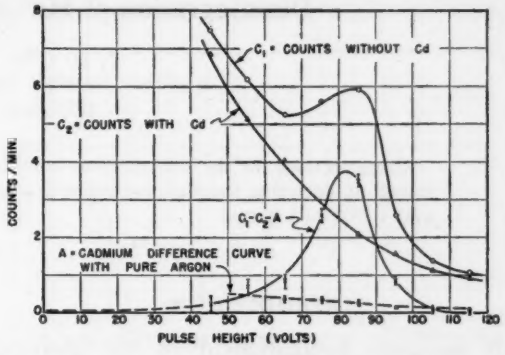

FIG. 3. Pulse height distribution curves obtained with "well" helium. The plotted points represent the number of pulses in a 10-volt pulse height interval and the point is plotted at the center of the interval. The difference curve, C_1-C_2-A, corresponds to the number of $He^3(n,p)H^3$ disintegrations.

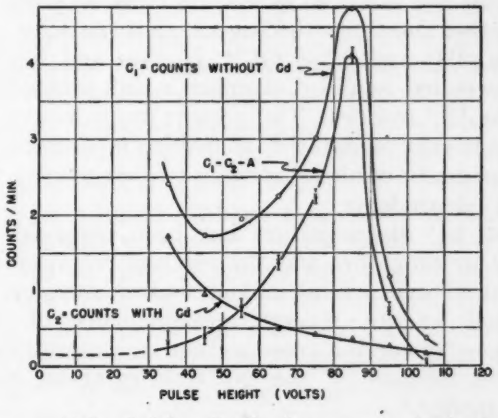

FIG. 4. Pulse height distribution curves obtained with "atmospheric" helium. The plotted points represent the number of pulses in a 10-volt pulse height interval and the point is plotted at the center of the interval. The difference curve, C_1-C_2-A, corresponds to the number of $He^3(n,p)H^3$ disintegrations.

percent is statistical error determined by considering the number of counts obtained. The correction $\sum w$ which involves extrapolation of the curve to zero pulse height may introduce 5 percent error. Background fluctuations from spurious electrical disturbances assume more importance because of the low counting rates. There is an undetermined effect of capture gammas from neutron capture in cadmium; these gammas cause a larger number of small pulses when cadmium surrounds the counter than when it does not.

Thanks are due Richard Taschek and E. R. Graves for helpful criticisms, and R. W. Davis, Warren Nyer, and Ralph Nobles for help in developing and assembling the apparatus.

Disintegration of He^3 and N^{14} by Thermal Neutrons*

J. H. Coon and R. A. Nobles**
Los Alamos Scientific Laboratory, Los Alamos, New Mexico
(Received December 20, 1948)

Cross sections for the n-p reactions induced in He^3 and N^{14} by thermal neutrons have been determined by detecting the disintegrations in a proportional counter. The values obtained are 5040 ± 200 and 1.76 ± 0.05 barns.

INTRODUCTION

An accurate measurement of the absorption cross section of boron for thermal neutrons has been made[1] and serves as a convenient standard for other determinations. In the present measurements it is assumed that the boron absorption is due entirely to the $B^{10}(n,\alpha)Li^7$ reaction and comparisons are made to determine cross sections for two other reactions yielding charged particles, *viz*[2] $He^3(n,p)H^3$ and $N^{14}(n,p)C^{14}$. Hughes and Eggler. first detected by cloud chamber a high probability for the He^3 reaction. The present measurement on He^3 is in part preparatory to making measurements with neutrons of higher energies for determining the energy dependence.

The N^{14} disintegration has been observed by many investigators and the reaction cross section measured[3] over a range of fast neutron energies. At thermal energy several measurements of the nitrogen absorption cross section, as distinguished from a measure of the n-p disintegration, have been made.[4,5]

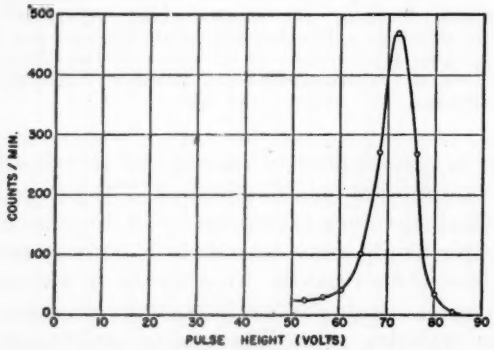

Fig. 1. Pulse height distribution curve obtained with the alpha-particles from a thin deposit of Pu^{239} located near the inner wall of the counter. Gas filling: 0.4205 cm^3 He^3 plus 87.8 cm pressure of argon.

In the present work measured quantities of He^3, N_2, and BF_3 were used in a proportional counter which was located in a fixed geometry in a region containing thermal neutrons. The disintegrations occurring in the gas were counted, and by suitable corrections the disintegration rate D occurring within the sensitive volume was determined. If σ represents disintegration cross section and n the number of atoms per cm^3, then:

$$\frac{D_B}{n_B\sigma_B}=\frac{D_{He^3}}{n_{He^3}\sigma_{He^3}}=\frac{D_N}{n_N\sigma_N}. \quad (1)$$

From this relation we can determine the unknown cross sections if we take σ_B as the known standard and use measured quantities of gas.

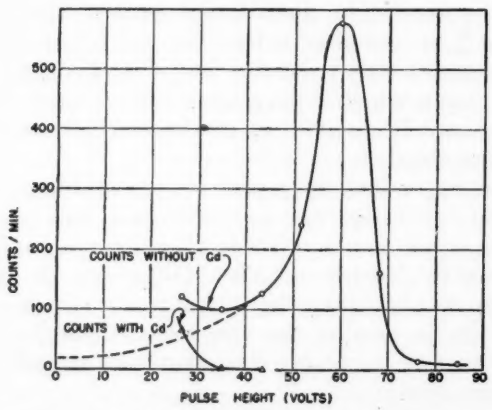

Fig. 2. Pulse height distribution curve obtained by counting $He^3(n,p)H^3$ disintegrations. The plotted points represent the number of pulses per minute in a pulse height interval which extends half way to the points immediately above and below. Gas filling: 0.4205 cm^3 He^3 plus 87.8 cm pressure argon.

APPARATUS AND PROCEDURES

The counter was a 3-inch diameter brass cylinder with a 0.005-inch diameter center wire and a sensitive length of about 6 inches. The sensitive length was limited by hypodermic tubing extending over the wire in the end regions of the counter, the design of which was similar to one previously described.[6] The voltage was adjusted to give a gas

* This document is based on work performed at Los Alamos Scientific Laboratory of the University of California under Government Contract W-7405-eng-36.
** Now at the University of New Mexico, Albuquerque, New Mexico.
[1] E. Fermi, J. Marshall, and L. Marshall, Phys. Rev. **72**, 193 (1947).
[2] D. J. Hughes, and C. Eggler, Phys. Rev. **73**, 809 (1948).
[3] H. H. Barschall and M. E. Battat, Phys. Rev. **70**, 245 (1946).
[4] H. Lichtenberger, H. Fowler, and A. Wattenberg, Argonne Laboratory Report No. CP 781, July 1943.
[5] Christian Lapointe and Franco Rasetti, Phys. Rev. **58**, 554 (1940).
[6] J. H. Coon and R. A. Nobles, Rev. Sci. Inst. **18**, 44 (1947).

multiplication of about 20. A Los Alamos Model 100 pulse amplifier[7] was used with a shortest between-stage coupling time constant of 20 microseconds to limit the low frequency response. The output of the amplifier was fed into a 10-channel differential pulse height selector[8] which analyzes the pulse height distribution by dividing a chosen range of pulse heights into 10 equal pulse height intervals and counting the number of pulses having heights within each interval.

A check on the operation of the detecting and counting apparatus was made by counting alpha-particles emitted from a thin deposit of Pu^{239} on a

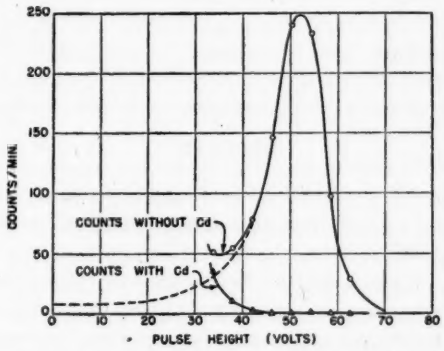

FIG. 3. Pulse height distribution curve obtained by counting $N^{14}(n,p)C^{14}$ disintegrations. Gas filling: 366 cm³ N_2 plus 88.7 cm pressure argon.

foil mounted near the inner wall of the counter. This source was mounted on a rotating disk and could be moved, so as not to see the counting volume, by a rotation of the counter. The value 5.15 Mev[9] was taken as the alpha-particle energy and served as an energy standard in looking for the disintegration particle groups. The observed pulse heights were correlated by use of a precision standard pulser and in this way one obtained a measure of disintegration energy (see Fig. 1).

The counting geometry was contained in a graphite prism built up of graphite blocks, the prism having dimensions 5 ft.×5 ft.×9 ft. high. The counter and a radioactive source yielding fast neutrons were placed in cavities within this prism near its vertical axis, the source being 48 inches above the counter. Under these conditions the neutrons arriving in the region of the counter have very nearly a Maxwell distribution in energy corresponding to room temperature.

Care was taken to obtain high purity and accurate quantity measurement of the gases used. The He^3 was the decay product of purified H^3 which had

[7] Matthew Sands, LADC-82, Los Alamos Laboratory, July 1946.

[8] E. W. Dexter, LADC-414, Los Alamos Laboratory, May 1947.

[9] O. Chamberlain, J. W. Gofman, E. Segrè, and A. C. Wahl, Phys. Rev. 71, 529 (1947).

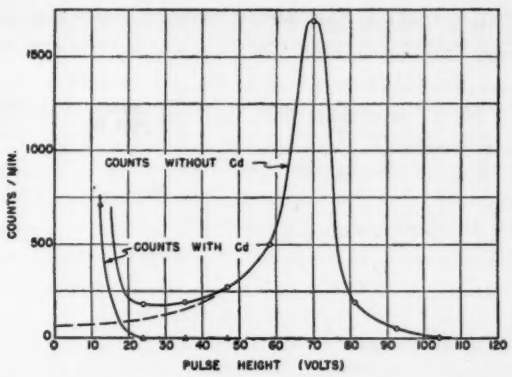

FIG. 4. Pulse height distribution curve obtained by counting $B^{10}(n,\alpha)Li^7$ disintegrations. Gas filling: 7.63 cm³ BF_3 plus 73.5 cm pressure argon.

been converted to heavy water. For use in a counter the residual H^3 content in the He^3 gas was reduced to a sufficiently low value by successive additions of hydrogen as a carrier in chemical purification. Likely impurities were removed by passing the gas through furnaces containing hot CuO and hot Ca, and then through a liquid air trap. Spectroscopic grades of N_2 and A were used. The BF_3 was frozen down in a liquid nitrogen trap, pumped, warmed and allowed to expand, frozen down again and recycled in this way several times. Then the BF_3 was flowed into the counter through a CO_2 trap.[10]

For each gas the quantity used was adjusted to give satisfactory counting rates, and argon then added to reduce the range of disintegration fragments to a suitably small fraction of the counter diameter. "Wall effect" corrections were small. Table I lists gas volumes and pressures and operating counter voltages.

The counting with any particular gas filling was done alternately with and without a cadmium cover over the counter for several cycles. The count with cadmium was then subtracted as a background, except in the small pulse region where gamma-rays were detected, and where neutron capture gammas from the cadmium interfered. Counting with and without cadmium was also done with pure argon in the counter and this count served as an additional background to be subtracted. These backgrounds were always less than one percent.

An approximate "wall effect" correction was calculated for each gas filling taking account of the range of the lighter disintegration particle and the stopping power of the gas. In this calculation it was assumed that the angular distribution of the particles was isotropic, and the following approximations were made: the counter walls were considered as plane instead of curved, the effect of

[10] The He^3 processing was done by E. S. Robinson and M. Goldblatt, and the BF_3 processing by R. M. Potter at this laboratory.

TABLE I. Experimental data and calculated cross sections for the n-p reaction induced in He^3 and N^{14}.

Gas	Vol. at 0°C in cm³	Press. at 15°C in cm Hg	Operating counter voltage	Corrected disint. per minute	Disintegration energy using Pu^{239} alphas as standard Mev	$\sigma=\sigma/\sigma_B\times 703$ in units of barns
He^3	0.4205	—	2250	1636	0.78	5040±200
A	—	87.8				
He^3	[0.503 initial]	—	1900	[1496]	—	[3850]
A	—	102.0				5000±1000
N_2	366.0	21.1	3120	1015	0.63	1.795
A	—	88.7				Av.=1.76 ±0.05
N_2	1007	57.1	3760	2680	0.65	1.724
A	none					
BF_3	7.63	—	1750	4152	2.25	705
A	—	73.5				Av.=703 (standard)
BF_3	24.1	—	2060	13,040	2.22	701
A	—	94.0				

corners was neglected, the range of the heavy recoil nucleus was neglected, and the specific ionization of the particle was assumed independent of energy. Let N_0 be the number of disintegrations per second per cm³ in the counter, and let R be the path length of a disintegration particle which expends all its energy in the gas. It can be shown that under the above approximations, the number of particles striking the counter wall per cm² per second is $N_0R/4$, and that the pulse height distribution arising from these particles is such that there are an equal number of pulses per unit pulse height interval for pulse heights ranging from zero to a maximum value, this maximum value being the pulse height arising from a particle which loses all its energy in the gas. By use of this calculation the measured pulse height distribution curves were extrapolated to zero pulse height as indicated in Figs. 2, 3, and 4.

The neutron absorption of the gas filling itself has the effect of depressing the neutron density in the region of the counter. The amount of this effect will differ for the different gas fillings. To prove this effect negligible a $\frac{1}{16}$-inch thick brass cylinder was slipped over the length of the counter. The observed drop in counting rate due to this added brass was 11 percent. The thermal neutron capture cross section of the Cu and Zn in this added brass was calculated to be 100 times or more greater than the capture by the gas in any case used. Therefore the gas absorption in no case depressed the neutron density by more than about 0.1 percent.

Neutron absorption in the counter walls will tend to shift the neutron spectrum from a Maxwell distribution at room temperature to a higher average energy. This effect cancels out if the cross sections in question vary inversely as the neutron velocity which is probably the case over the narrow range of neutron energy involved.

RESULTS

Figures 2, 3, and 4 show typical pulse height distribution curves for the counter filled with He^3, N_2, and BF_3. The width of the peaks is a characteristic of the counter behavior and the detecting equipment, one contributing factor being the width of the counting channels. No special attempt was made to minimize the effects contributing to the width of the peaks, since the significant datum is the area under the curve rather than its shape.

Because of the width of the pulse height peaks, the disintegration energy determinations listed in Table I are crude and serve principally only to identify the reaction under investigation. These energies are already known with greater precision than could be attained by this method. For example, Hughes and Eggler[2] gave Q values of 0.740 and 0.597 Mev for the He^3 and N^{14} reactions.

With reservations noted above regarding the small pulse region where gamma-rays are detected, the number of disintegrations D taking place within the sensitive volume of the counter was obtained from:

$$D=\sum C_1-\sum C_2-\sum A+\sum w,$$

where $\sum C_1$ is the counting rate without cadmium, summed over individual channels; $\sum C_2$ is the counting rate with cadmium, similarly summed over individual channels; $\sum A$ is the background determined with argon, this also being a cadmium difference count; and $\sum w$ is the small pulse and "wall effect" correction determined by adding up the number of pulses under the extrapolated lower end of the corrected pulse height distribution curves. The quantity $\sum w$ accounts for pulses which are small because of "wall effect" or other causes which reduce their size so much that they appear in the pulse height region where pulses due to gamma-rays appear.

Using values of D determined as above and using 703 barns[1] for boron, one obtains cross sections for He^3 and N from relation (1). The values so obtained, as listed in the last column of Table I, are:

$$\sigma_{He^3}(n,p) = 5040 \pm 200$$

and

$$\sigma_N(n,p) = 1.76 \pm 0.05 \text{ barns.}$$

Since the value of 703 barns applies to neutrons of 2200 meters per second or 293°K, the present determination applies to neutrons of this same energy even though there may have been a distorted spectrum in the region of the counter.

The second He^3 filling partially leaked out of the counter before any data were obtained. Counting with this unknown quantity of He^3 and assuming none was lost gave a value of $\sigma = 3850$ barns. Correcting this for the estimated loss gave a value of 5000 ± 1000.

The largest error was in the extrapolation of the pulse height distribution curves to zero and in evaluation of the number of small pulses. However, three sets of data on the good He^3 filling taken under somewhat different conditions and at intervals one week separated gave values with a total spread of only 2.3 percent. The data-taking was intermittent and extended over a period of three months, beginning and ending with the two nitrogen runs. Counting rates were such that statistical errors were negligible.

Values of the absorption cross section of nitrogen have been determined by Lapointe and Rasetti[5] and by Lichtenberger *et al.*[4] who obtained 1.4 ± 25 percent and 1.72 barns, respectively. These values have been adjusted so as to be dependent on a boron absorption cross section of 703. Comparison with the present measured value of 1.76 ± 0.05 for the n-p disintegration process gives a limit to the probability of other processes competing with the n-p process.

Note added in proof: Since submission of this manuscript two papers on the He^3 reaction have appeared in the literature. King and Goldstein,[11] from measurements with pure He^3 samples, obtain a value of 5000 barns for the total cross section of He^3 for 293° neutrons. This is in good agreement with the present value. In England, Batchelor *et al.*,[12] working with the very low concentration of He^3 in normal "atmospheric" helium, measure a cross section value of 3700 barns for the n-p reaction. They quote an error of ±250 barns plus whatever uncertainties there are in the values they used for the $N(n,p)$ reaction and for the He^3 isotopic abundance in their gas sample. The best information on these quantities does not reconcile the discrepancy between our value and the British value.

ACKNOWLEDGMENT

Thanks are due to E. R. Graves and to R. F. Taschek for helpful criticisms, and to R. W. Davis for help in carrying out the measurements.

[11] L. D. P. King and Louis Goldstein, Bull. Am. Phys. Soc. 24 (1), 31 (1949); also Phys. Rev. 75, 1366 (1949).
[12] R. Batchelor, J. S. Epstein, B. H. Flowers, and A. Whittaker, Nature 163, 211 (1949).

PHYSICAL REVIEW VOLUME 75, NUMBER 9 MAY 1, 1949

A Study of the Interaction of Protons with Tritium*

R. F. TASCHEK, G. A. JARVIS, A. HEMMENDINGER, G. G. EVERHART, AND H. T. GITTINGS
Los Alamos Scientific Laboratory, Los Alamos, New Mexico

(Received December 20, 1948)

Preliminary measurements of the scattering cross section of tritium for protons and the reaction cross section for $T^3(p,n)He^3$ have been made. A method of analysis for hydrogen in tritium samples is described. The neutron yield of the reaction is high and will make it a useful source; the threshold is sharp and can be used as a point on the energy scale of nuclear physics. Angular distributions for scattering and cross sections for the reaction are given.

INTRODUCTION

THIS is a preliminary report on experience with the interaction of protons and tritium for proton energies between 900 kev and 2.5 Mev as accelerated by the Los Alamos electrostatic generator. Tritium gas targets were used, the particular design reported elsewhere,[1] although this target has no immediate advantage for some of the work reported here.

* This document is based on work performed under U. S. Government Contract Number W-7405-Eng-36 at the Los Alamos Scientific Laboratory of the University of California.
[1] R. F. Taschek, Rev. Sci. Inst. 19, 591 (1948).

GAS HANDLING SYSTEM

Because of the small volume of precious gas available special methods of handling it were devised. Figure 1 is a schematic diagram of the tritium storage and handling system used; heated uranium shavings provided a completely satisfactory method of evolving the tritium-hydrogen mixture stored as hydride in the cold uranium when not in use. Titanium would probably have been as satisfactory. In case of small air or counter argon leaks into the target the uranium also acts

as a purifier for the hydrogen gases. Since the total amount of gas available was only about 10 cm³ at N.T.P., the mercury lift through the 500 cm³ bulb was used to make a complete transfer of gas at maximum efficiency from uranium pump to target and *vice versa* possible. Auxiliary connections could be made to suppplies of hydrogen and deuterium gas as shown in Fig. 1.

To guard against the possibility of breaking one of the thin aluminum foils sealing the target gas from accelerating tube vacuum and thus losing it, the "gas impedance" tube and trip valve shown schematically in Fig. 2 were used to connect target to accelerating tube. This device was to work by having the increase in gas pressure resulting from a broken foil fire either an ion gauge or spark plug, which in turn would trip the valve at the other end of the tube before an appreciable amount of the gas escaped through the high impedance flow tube. The gas was then to be recovered with the uranium pump. Up to the present time this device has not had the necessity for firing under the conditions for which it was designed.

ANALYSIS OF TRITIUM SAMPLES FOR HYDROGEN

In order to obtain absolute cross sections for particle interactions with tritium, it is necessary to know the amount of contaminating hydrogen (a product of the manufacturing process) with good accuracy. Early methods of analysis were quickly found to be unreliable and it was decided that 45° proton-proton scattering could be used to determine the amount of hydrogen. The following method was used for the analysis: tank hydrogen was first put into the target at about 10 cm mercury pressure, accurately measured. At a bombarding energy of about 2 Mev, the 45° scattered protons were counted. The shape of the pulse height distribution was recorded by a 10 channel pulse height analyser[2] with the Los Alamos Model 100 amplifier gain set so the peak of the distribution fell in the highest channels. Now leaving all variables unchanged but the gas, which was replaced to about the same pressure from the tritium sample a second pulse height distribution was recorded for the same number of microcoulombs of protons as in the hydrogen run. In Fig. 3 are shown typical pulse height distributions for tank hydrogen and for our tritium sample; smooth curves have been drawn through the total counts in each channel at the channel center for ease of representation. For the scattering from the tritium sample a double peak is observed, the smaller pulse height group corresponding to protons scattered from tritium, the

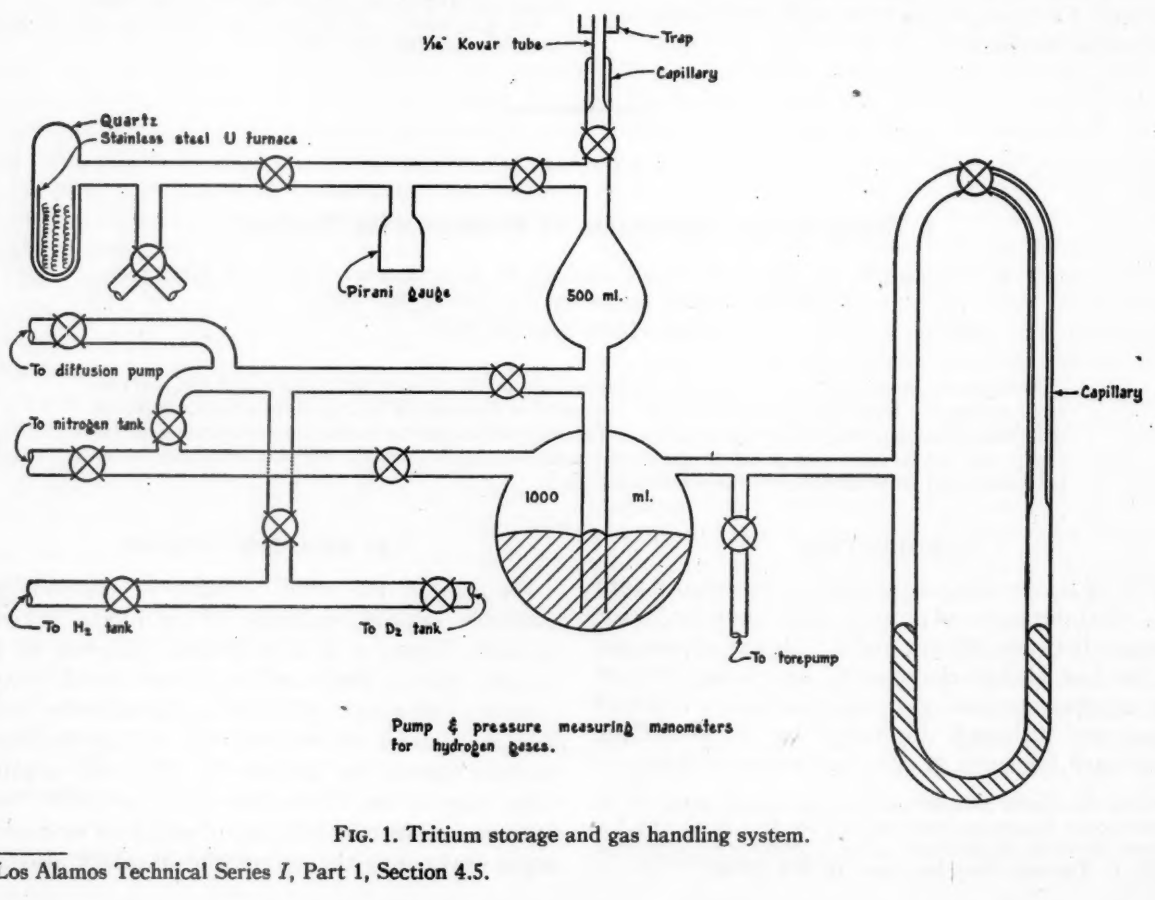

FIG. 1. Tritium storage and gas handling system.

[2] Los Alamos Technical Series *I*, Part 1, Section 4.5.

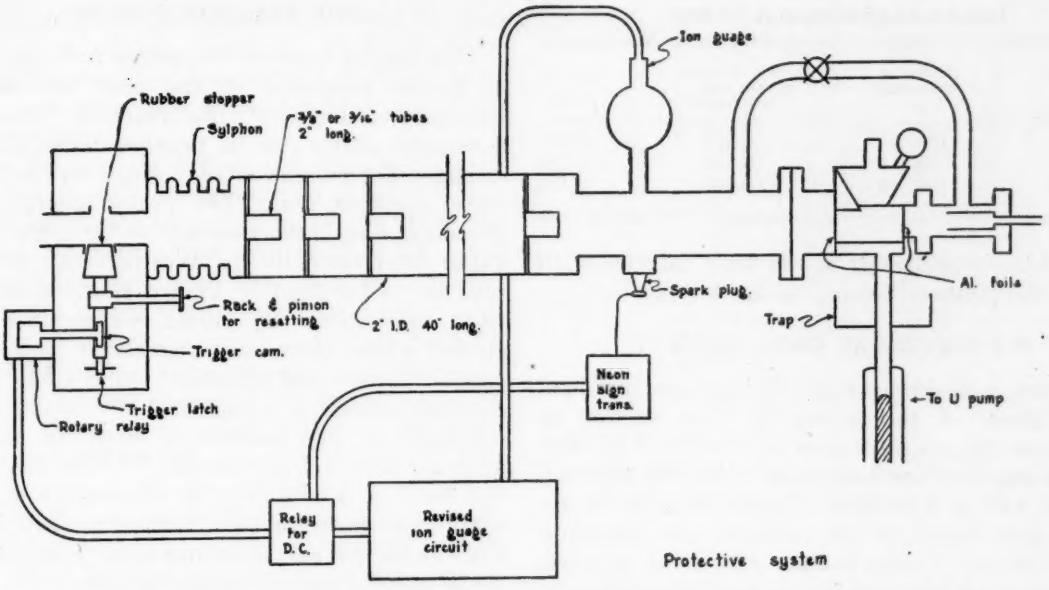

FIG. 2. Gas impedance tube and circuits for tritium recovery in case of foil breakage on target.

larger corresponding to hydrogen scattered protons; in this case counter pressure was set to make the energy loss from hydrogen scattered protons larger. With no further information than this, a direct comparison of the number of protons per centimeter of Hg target gas pressure under the tank hydrogen peak with the number under the hydrogen peak of the tritium sample gives the hydrogen concentration in the sample, from which the tritium concentration is immediately obtained. Concentration of tritium in the sample used here was 62 ± 2 percent obtained from three separate analyses. To check whether the sampling out of the tritium storage pump was adequate, the first and last analyses were made when only the minimum necessary gas was evolved, while the middle analysis was obtained from gas taken out of a complete evolution of the sample. Mean deviation of the three analyses was about one percent.

Obviously a very good analysis would require a palladium leaked hydrogen sample for a standard, but for the immediate needs this was not considered necessary. As a check on the method, one of the tank hydrogen runs was used to calculate a value of the proton-proton scattering cross section at 45°, since this is accurately known. Without attempting to correct for partial pressures of contaminating gases in tank hydrogen a cross section of 0.45_8 barn per unit solid angle was obtained comparing favorably with 0.472 barns given by Herb and his collaborators.[3] This measurement, in addition to checking the adequate purity of the hydrogen, is also a check on the accuracy of the proton detecting geometry factor of the proportional counter and indicates that measurement and calculation of this factor is correct to a few percent.

Considerable experience during the past year has shown that the gaseous tritium sample is not stable in our target against chemical exchange with hydrogen in stopcock grease. Using outgassed Apiezon *N* grease, this is most clearly shown by a progressive decrease in the tritium scattered protons and a corresponding increase in the hydrogen scattered protons. The use of a completely fluorinated grease did not greatly help since the tritium concentration still decreased, although the hydrogen concentration changed only slightly. It seems clear that this exchange phenomenon is greatly enhanced by passage of the beam through the target, since a sample left in the target overnight showed less than half the concentration change it

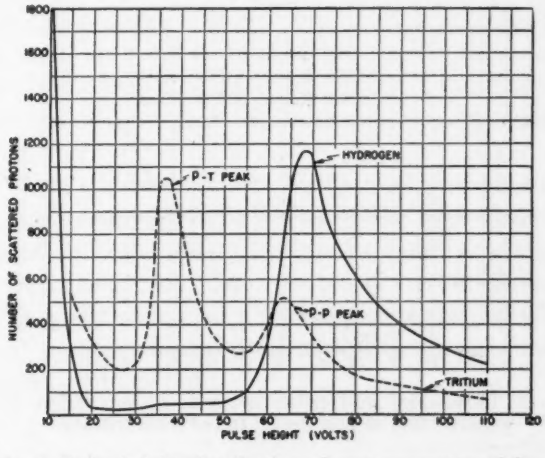

FIG. 3. Pulse height distribution of protons scattered from a tritium sample and from tank hydrogen.

[3] Herb, Kerst, Parkinson, and Plain, Phys. Rev. **55**, 998 (1939).

TABLE I. Cross sections at 2.0 Mev.

Laboratory angle θ	Center of mass angle ϕ	$\sigma(\theta)$ in barns per unit solid angle	$\sigma(\phi)$
45°	50°	0.325	0.217
67½°	86°	0.189	0.154
90°	109° 30′	0.145	0.154

would have experienced in the same interval with a one microampere beam passing through it.

P-T SCATTERING CROSS SECTION

In part a by-product of the analysis problem, three values of the scattering cross section of protons on tritium have been obtained at 2.01 Mev and an angular distribution of scattering between 45° and 135° at 1.59 Mev. These values are in absolute units based on the concentration measurements above. Table I lists the cross sections obtained at 2.0 Mev and Fig. 4 shows the laboratory and center of mass angular distributions at 1.59 Mev with the 2.0 Mev data also plotted.

It appears that for these two energies the differential cross sections are quite similar in value for the angular range in which measurements were made. The value of $\sigma_{P-T}(86°)$ of 0.154 may be compared with $\sigma_{P-P}(90°)=0.167$, both near 90° in the center of mass system.

It is obvious from the data that in the angular range shown the differential cross section is primarily caused by nuclear scattering. The general trend with angle and even absolute cross section is rather similar to that found in *p-d* scattering.[4] The absolute cross sections are probably good to only about 10 percent, the relative values to 5 percent or less. A more detailed and precise investigation of the scattering is to be undertaken in the near future. This work will be greatly facilitated by the higher tritium concentration available.

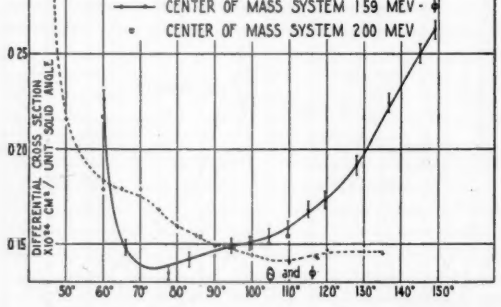
LABORATORY SYSTEM 1.59 MEV - θ
CENTER OF MASS SYSTEM 1.59 MEV - φ
CENTER OF MASS SYSTEM 2.00 MEV
DIFFERENTIAL CROSS SECTION X10²⁴ CM²/ UNIT SOLID ANGLE
0.30
0.25
0.20
0.15
θ and φ
50° 60° 70° 80° 90° 100° 110° 120° 130° 140° 150°

FIG. 4. Laboratory and center of mass system differential cross section of protons scattered from tritium.

[4] Sherr, Blair, Kratz, Bailey, and Taschek, Phys. Rev. **72**, 662 (1947).

THE REACTION $T^3(p,n)He^3$

The fiducial point of the energy scale of our Van de Graaff generator in the past has been the threshold of the $Li^7(p,n)Be^7$ reaction,[5] because the extremely sharp rise in neutron yield allows an accurate determination of voltage on the electrostatic analyzer scale. The proton energy of this threshold has been assumed to be 1.86_0 Mev, a value determined by the Westinghouse generator[6] relative to presumably known energies at certain (p,γ) resonances. By direct measurement on a curved plate electrostatic analyzer and voltage supply Hanson and Benedict[7] found 1.883 Mev for the same threshold; a value of 1.889 ± 0.004 was also obtained in this laboratory with an improved analyzer and voltage supply.** The existence of this large a discrepancy in the energy scale is a serious one both for the effect on neutron energies from endoergic reactions and even more so for the whole energy scale of nuclear physics.

If one now considers the system of reactions

$$T^3\rightarrow He^3+\tilde{\beta}+15 \text{ kev}, \quad T^3-He^3=15 \text{ kev}$$

and

$$p+T^3\rightarrow He^3+n-Q,$$

we find that in the laboratory system

$$Ep=4/3Q=4/3\{(n-p)-(T^3-He^3)\}.$$

Assuming that the neutron-proton mass difference is 755 kev,[8,9] then $Ep=986$ kev for the threshold of $T^3(p,n)He^3$. This shows that either of two things may be done; first, if the energy scale were very precisely known an extremely good value of the neutron-proton mass difference could be obtained by measuring proton energy at threshold even if the T^3-He^3 mass difference is known to only 20 percent or so; secondly, one may assume that, under the present circumstances, the *n-p* mass difference is known as well as the energy scale and in this way calibrate the latter. It was in this way that we redetermined our energy scale, the primary difficulty being, for our target, the thickness of the aluminum window at about one Mev. Using the calculated energy loss in the foil at one Mev, 185 kev, it appears that our energy scale based on 1.86 Mev for the $Li^7(p,n)Be^7$ threshold is about 25 kev too low, but if 1.89 Mev is used, the observed threshold for $T^3(p,n)He^3$ comes to 990 kev, which is about correct. This measurement is to be repeated

[5] R. F. Taschek and Arthur Hemmendinger, Phys. Rev. **74**, 373 (1948).
[6] Haxby, Shoupp, Stephens, and Wells, Phys. Rev. **58**, 1035 (1940).
[7] A. O. Hanson and D. L. Benedict, Phys. Rev. **65**, 33 (1944).
** Herb, Snowden, and Sala [Phys. Rev. **75**, 246 (1949)] report a recent and precise value of 1.882 Mev for this threshold.
[8] D. J. Hughes, Phys. Rev. **70**, 219 (1946).
[9] W. E. Stephens, Rev. Mod. Phys. **19**, 19 (1947).

with condensed tritium targets. At present the best determination of foil thickness is obtained by assuming the energy of the reaction threshold to be 986 kev and an energy scale based on 1.89 Mev for $Li^7(p,n)Be^7$.

Figure 5 shows the differential cross section for the reaction between threshold and about 2.2 Mev proton energy in the target gas for 0° and 90° in the laboratory system. The neutron yields were measured with eight inch long-counters[10] at distances of two meters from the source in order that near threshold no effects purely due to geometry be introduced. The long counters were calibrated with a standardized radium-beryllium source placed at the target position. It is believed that the cross sections are good to only about ±10 percent over most of the range because the target geometry is such that, for these relatively low energy neutrons, a rather large amount of scattering material is close to the source and not completely symmetrically disposed. Experience with measuring angular distributions would indicate that the zero degree data may be as much as 10 percent too high compared to 90°. The angular distributions are to be repeated in detail using a target assembly with a minimum of scattering material in the vicinity.

The advantages of $T^3(p,n)He^3$ as a monoenergetic neutron source are apparent, particularly with a low energy machine. With the present generator capable of about 2.7 Mev, neutrons up to 1.8 Mev can be obtained while only about one Mev neutrons are available from the $Li^7(p,n)Be^7$ reaction. In addition to this, the *cone*[5] of neutrons at threshold has 60 kev energy, making another strong neutron cone source available besides the 30 kev neutrons from $Li^7(p,n)Be^7$, which is very important for certain types of experiments. It should be pointed out that the cross sections obtained here are large and compare favorably indeed with those from $Li^7(p,n)Be^7$. The trend of the yield with energy indicates even larger yields above the maximum reached here.

It is not useful to compare center of mass cross sections since 90° in the laboratory changes continuously with energy in the center of mass system. As an example, however, at 2 Mev

$\theta=0°$	$\phi=0°$
$\sigma(\theta)=0.062$ barns,	$\sigma(\phi)=0.029$
$\theta=90°$	$\phi=117°$
$\sigma(\theta)=0.031$,	$\sigma(\phi)=0.035$

[10] A. O. Hanson and J. L. McKibben, Phys. Rev. **72**, 673 (1947).

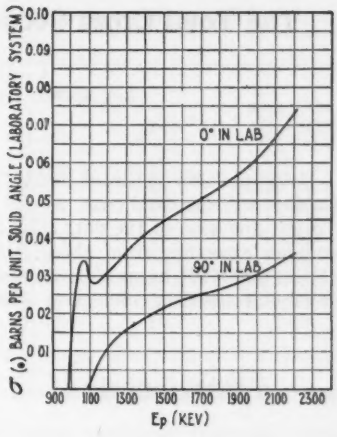

FIG. 5. 0° and 90° laboratory differential cross sections of $T^3(p,n)He^3$ as a function of proton energy.

indicating a rather symmetric distribution in the center of the mass system which is borne out by preliminary angular distributions at 1.2, 1.5, and 1.8 Mev. The peak in the 0° cross section data just above threshold is probably due primarily to the fact that up to $Ep=120$ kev above threshold all neutrons lie within some cone of half-angle less than 90°, due to center of mass motion, but above this energy they suddenly spread out over 4π solid angle resulting in a decrease in the 0° yield. A very similar phenomenon is observed in the corresponding lithium reaction, although possibly not so clean cut. It will be noted that there is no 90° yield until just at the turn over of the 0° curve.

One can feel reasonably certain that for proton energies even considerably larger than those used here the neutrons will remain monoergic. This arises from the knowledge that the neutrons from $D(d,n)He^3$ are monoergic at least up to 2.5 Mev deuteron energy and the residual nucleus He^3 is the same in both cases, meaning that no excited states of He^3 have been observed up to an excitation energy of over 20 Mev for the compound nucleus He^4.

With the measurement of the cross section of the inverse reaction $He^3(n,p)T^3$, a rather good check of the principle of detailed balance should be possible. Preparations are also underway to investigate $T^3(p,\gamma)He^4$ which has a Q of approximately 19 Mev and should complete the low energy proton interactions with tritium.

The Total Cross Section of the He_3 Nucleus for Slow Neutrons*

L. D. P. KING AND LOUIS GOLDSTEIN
Los Alamos Scientific Laboratory, Los Alamos, New Mexico
(Received January 24, 1949)

Using the slow neutrons available from the thermal column of the enriched uranium pile of this Laboratory, the total cross section of the He_3 nucleus was determined by the transmission method. To the precision of the data, this cross section obeys the $1/v$ law in the range of averaged neutron energies extending from about 0.001 to 0.03 electron volt. The product $(\sigma_{He_3} \times v)$ is found to be $(11.2 \pm 0.5) \times 10^6$ barns × meters × sec.$^{-1}$. The possible theoretical implications of these results are briefly discussed in connection with the properties of the compound He_4 nucleus.

I. INTRODUCTION

THE large thermal neutron cross section observed in the reaction $He_3(n,p)H_3$[1] suggested that it might be of interest to study the behavior of the neutron cross section of He_3 nuclei over a wide neutron energy range. These measurements appeared of interest also, in connection with a suggested method[2] of obtaining the distribution of He_3 atoms in the vapor and liquid phases of He_4-He_3 fluid mixtures. This same method might yield good absolute density values of pure He_3 in its vapor and liquid phases since a known small amount of this fluid may be experimented on while fully isolated thermally.

The large thermal neutron cross section of the $He_3(n,p)H_3$ reaction is readily explained in terms of the principle of detail balance[3] applied to the inverse reaction $H_3(p,n)He_3$ studied previously to some extent.[4]

The experiments reported here form the beginning for a more complete exploration of the neutron-proton exchange reaction in the He_3 nucleus. These studies could yield information[3] on some of the possible properties of the compound He_4 nucleus through which this reaction takes place presumably. Total neutron cross-section measurements have been made on He_3, using the low energy neutrons available in the thermal column of the enriched uranium pile of this laboratory. Previous studies at Chicago[5] as well as here[6] have shown that relatively intense neutron beams of low energies can be obtained from a cavity in a thermal column by filtration through graphite. Such neutrons have energies ranging from somewhat greater than thermal energy to about 0.001 electron volt, depending on the cavity and thickness of graphite filter used.

On quite general grounds it is to be expected that the variation of the absorption cross section of He_3 nuclei for slow neutrons should obey the $1/v$ law, v being the relative velocity of the neutrons and He_3 nuclei. This should, indeed be so, provided in this low neutron energy region the compound He_4 nucleus does not exhibit some narrow unstable excited energy level. The results described below indicate that such a level does not exist within the precision of our data.

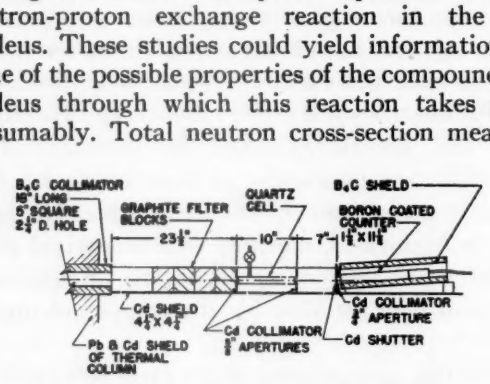

FIG. 1. Experimental arrangement.

II. EXPERIMENTAL PROCEDURE

The total transmission of a neutron beam through a known amount of He_3 gas has been compared to the transmission of the same beam through a known amount of normal boron trifluoride (BF_3) gas and also to the transmission through an evacuated reference cell. All three quartz absorption chambers were essentially identical. The experiment was performed by obtaining transmission data from a series of rapid exchanges, each of a few minutes duration, of the reference, helium, boron, and reference chambers, respectively. This method should tend to reduce errors caused by faulty alignment of the chambers, drifts in the neutron beam intensity, or neutron detector behavior. The close checks between exchanges indicated that these errors were small.

The detection equipment consisted of a boron coated proportional counter with a battery voltage supply; a scaler with a variable scaling rate of 64

* This work has been reported on at the New York meeting of the American Physical Society, January 28, 1949.

[1] Coon, Goldblatt, Nobles, and Robinson, Declassified Los Alamos Report, LADC No. 462, December, 1947; Phys. Rev. 75, 1358 (1949).

[2] L. Goldstein, Declassified Los Alamos Report, LADC No. 546, June 1948.

[3] L. Goldstein, Declassified Los Alamos Report, LADC No. 539, December 1947.

[4] Taschek, Jarvis, Hemmendinger, Everhart, and Gittings, Declassified Los Alamos Report, LADC No. 538, January 1947, and Phys. Rev. 75, 1361 (1949).

[5] H. L. Anderson, E. Fermi, and L. Marshall, Phys. Rev. 70, 815 (1946).

[6] L. D. P. King and J. Fox, unpublished.

TABLE I. Experimental results.

Graphite thickness (cm)	Transmission I/I_0* He	Transmission I/I_0* BF_3	σ barns He (total)	σ barns B (absorption)**	v(average) meters/sec.	$E=(\frac{1}{2}mv^2)$ volts	$T=E/k$*** degrees K	$(\sigma \times v)$ He 10^8 barns $\times$meters/sec.	Statistical fluctuations in $(\sigma \times v)$ (percent)
0	0.8832	0.8952	4660	625	2471	0.0319	370	11.52	0.25
0	0.8801	0.8917	4792	648	2385	0.0297	345	11.43	0.22
8.89	0.8666	0.8739	5373	764	2021	0.0213	248	10.86	0.26
17.78	0.7461	0.7644	10,990	1554	1004	0.00527	61.2	11.04	0.51
26.67	0.6078	0.6354	18,680	2623	593	0.00183	21.3	11.07	1.8
26.67	0.6158	0.6267	18,190	2702	575	0.00173	20.1	10.46	2.3
35.56	0.5554	0.5948	22,070	3004	517	0.00140	16.2	11.40	3.2

* I and I_0 are the respective counting rates through the helium or boron cells and the blank cell. All corrected for background.
** Obtained from $\sigma(BF_3)$ after correction for elastic cross section of boron and total cross section of F nuclei. This involves the omission of the possible coherent scattering effects caused by F nuclei in the BF_3 molecule.
*** k is Boltzmann's constant.

or 256 depending on the counting rates; together with a model 100 amplifier and preamplifier.[7] An independent neutron counter in the thermal column acted as a neutron intensity monitor.

The experimental arrangement is shown in Fig. 1. The neutron beam originates in a cavity, 4 ft. deep and 12×12 inches in cross section, in the thermal column of the pile. This cavity tapers toward the outer end of the column and terminates in an 18-inch long boron collimator shown in the figure. The average energy in the neutron beam is varied by inserting, in front of the absorption cells 3.5 inch (8.89 cm) long graphite blocks, 4.25″×4.25″ in cross section. The neutrons passing through the quartz absorption cells are collimated by $\frac{5}{8}$″ diameter circular apertures in cadmium shutters placed at both ends of the quartz tube. An additional collimator with a $\frac{3}{4}$″ diameter circular aperture is placed immediately in front of the boron counter. The entire set-up is enclosed in a $\frac{1}{32}$″ thick cadmium box. An additional boron carbide shield is placed around the boron counter. Counter background readings were obtained by placing a cadmium shutter over the $\frac{3}{4}$″ aperture in front of the counter. Background readings varied from 0.5 percent to 10 percent of the counting rate through the absorbers depending on the number of filter blocks used.

The quartz containers had a volume of about 200 cc and an effective length of 25 cm with 0.19-cm flat quartz windows on either end. Two of these chambers contained 50.44 cc NTP of BF_3 gas, with the natural isotopic abundance ratio, and 8.33 cc NTP of He_3, respectively.

The transmission measurement determines the total cross section of the He_3 nucleus and the BF_3 molecule. These are associated with a neutron velocity averaged over the distribution of the velocities in the incident neutron beam, i.e., if all the neutrons had this same average velocity. These average velocities can be determined from the known boron cross section and its $1/v$ behavior in the low energy region. This cross section was determined from the measured absorption of the BF_3 gas by correcting for the known boron scattering and total fluorine cross sections.

III. EXPERIMENTAL RESULTS

The data obtained have been collected in Table I. The first column gives the thickness of the graphite filter blocks in centimeters (1 block = 3.5 inches). The second and third columns give the transmission coefficients of the He_3 and BF_3 gases. The fourth and fifth columns contain the total He_3 and boron absorption cross sections. The latter of these has been obtained by taking the average elastic cross section of boron to be three barns[8] (1 barn = 10^{-24} cm^2), and the total fluorine cross section[9] to be 4 barns in the whole energy range investigated in this work. The average velocity, energy and associated temperature of the neutron beam are given in the sixth, seventh, and eighth columns, respectively. The individual determinations of the product $(\sigma_{He_3} \times v)$ are exhibited in the ninth column

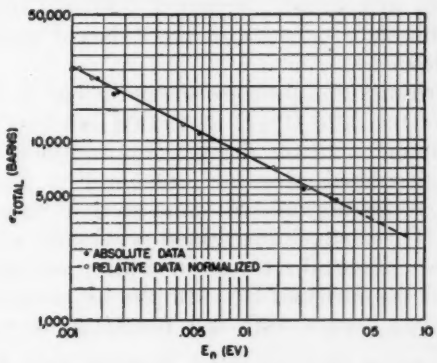

FIG. 2. The total cross section of He_3 as a function of the average neutron energy.

[7] M. Sands, Declassified Manhattan District Reports, MDDC No. 131 and 303, January and June 1946.

[8] H. Lichtenberger, unpublished.

[9] See H. H. Goldsmith, H. W. Ibser, and B. T. Feld, Rev. Mod. Phys. 19, 259 (1947).

while the corresponding relative statistical fluctuations are given in the last column.

The statistically weighted average of the product $(\sigma_{He_3}\times v)$ turns out to be 11.22×10^6 barns×meters/second. A weighting procedure resulting from the squares of the deviations Δ_i, where

$$\Delta_i=(\sigma\times v)_{\text{weighted}}-(\sigma\times v)_i$$

again leads to an average value almost identical to the statistically weighted average.

The constant for the He_3 cross section is given by

$$(\sigma_{He_3}\times v)=(\sigma_B\times v)\frac{n_{BF_3}l_{BF_3}}{n_{He_3}l_{He_3}}\frac{\ln I_0/I_{He_3}}{\ln I_0/I_{BF_3}}.$$

Here the constant $(\sigma_B\times v)$ has the value 1.545×10^6 barns×meters/second,[10] the n's are the number of the BF_3 molecules and He_3 atoms per cubic centimeter in the absorption cells, the l's are the effective lengths of these two gas columns. I_0's, I_{He_3}, and I_{BF_3} are counting rates, corrected for background, with the evacuated, He_3 and BF_3 filled cells, respectively.

Possible sources of absolute error are those resulting from the measurement of: (1) pressure, temperature, and degree of purity of the filling gases; (2) effective lengths of the gas columns; (3) the differences in the thicknesses of cell windows; (4) the variations in the alignment of the absorbing vessels. These together with the statistical fluctuations lead to a final value

$$\sigma_{He_3}\times v=(11.2\pm0.5)\times10^6 \text{ barns}\times\text{meters/sec.}$$

This excludes any errors inherent in the value of $(\sigma_B\times v)$, the elastic cross section of boron and the total cross section of fluorine used in the evaluation of $(\sigma_{He_3}\times v)$.[11]

The weighted root mean square deviation of $(\sigma_{He_3}\times v)$ expressed in percent fraction of the statistically weighted average $(\sigma_{He_3}\times v)$ is 2.7 percent. This lies well within the limits resulting from the more complete estimate of the different sources of error described above.

The results obtained are shown in Fig. 2. This is a plot of the total He_3 cross section as a function of the average neutron energy. In addition to the above described absolute cross-section measurements, some normalized cross-section values are shown. These were determined previously with the same experimental set-up. Since the composition of He_3 and B_{10} enriched BF_3 samples for these experiments was known with less precision, the results have been used to establish only the validity of the $1/v$ law. The energy range in these experiments extended to energy values as low as 0.001 electron volt (44.46-cm graphite filter).

The usual procedure of reducing the values to a definite temperature associated with a Maxwell distribution, according to a procedure suggested by Bethe,[12] has not been carried out for the following reasons. Although the neutron beam from the cavity of the pile proper is probably Maxwellian,[13] its distribution is distorted by the graphite filter blocks used. This is due to the very nature of the filtration process whereby neutrons with de Broglie wave-lengths larger than twice the lattice spacing of the poly-crystalline material are no longer scattered coherently. Furthermore, in order to obtain as close a comparison as possible between the boron and He absorption cells their gas concentrations were adjusted to give neutron transmissions within a few percent of each other. This was possible from the knowledge of the approximate value of $\sigma_{He_3}\times v$ at thermal energies.[1]

A Bethe type of correction which is determined by the magnitude of the natural logarithm of the transmission coefficients could be applied for the actual beams used if their distributions were relatively simple and known. Such a correction, however, would not alter the results obtained for $(\sigma_{He_3}\times v)$, to the precision of the data, as a result of the almost equal value of the natural logarithm of the transmission coefficients of the He_3 and BF_3 samples used.

IV. DISCUSSION AND POSSIBLE IMPLICATIONS OF THE RESULTS

In the interpretation of the results obtained with slow neutrons, whereby the absolute neutron velocities are of the same order of magnitude or smaller than the gas atom velocities, the question arises what actual velocities the observed phenomena correspond to.

It can be shown[14] that for any $1/v$ absorber in which the absorbing light nucleus is bound to a molecule the zero-point velocity of the absorbing nucleus does not alter the apparent relative motion between the nucleus and the neutron. This means that the absorption process is determined by the absolute neutron velocity only. A similar reasoning applies to the He_3 atoms as used in this experiment. This effect may be stated by saying that the cross section for a given neutron beam is independent of the temperature of the He_3 gas.

The precision of these experiments did not allow

[10] E. Fermi, J. Marshall, and L. Marshall, Phys. Rev. **72**, 193 (1947); see also, Sutton, McDaniel, Anderson, and Lavatelli, Phys. Rev. **71**, 272 (1941); and J. Rainwater and W. W. Havens, Jr., Phys. Rev. **70**, 136 (1946).

[11] An additional error may also result from neglecting the possible coherent scattering of the fluorine nuclei in the BF_3 molecules.

[12] H. A. Bethe, Rev. Mod. Phys. **9**, 135–136 (1937).

[13] Walter H. Zinn, Phys. Rev. **71**, 752 (1947); William J. Sturm, Phys. Rev. **71**, 757 (1947).

[14] See for instance, Willis E. Lamb, Jr., Phys. Rev. **51**, 187 (1937).

for a separation of the He_3 absorption and scattering cross sections for the slow neutrons used here. It is possible to show, on quite general grounds, that the nuclear scattering cross section in the thermal and subthermal energy range should be a constant. In view of this and the precision of the data it is justified to set an upper limit for the elastic cross section of He_3 for slow neutrons to be less than about 200 barns. An estimate of the lower limit can also be obtained as follows: It is to be remembered here that using the quantum mechanical collision cross-section formulas for the (n,p) exchange reaction and the (n,n) elastic scattering process, it is easy to show, that in the $1/v$ region of the former, we may write:

$$\frac{\sigma(n,n)}{\sigma(n,p)}=\frac{|H_{nn}|^2}{|H_{np}|^2}\left(\frac{E_n}{Q}\right)^{\frac{1}{2}},$$

where the $|H|s$ are the matrix element moduli for the processes indicated by the subscripts, E_n is the kinetic energy of relative motion of the $(n-He_3)$ system, while Q is the energy released in the (n,p) exchange reaction (kinetic energy of relative motion of the $p-H_3$ system $=0.75$ Mev). The ratio $|H_{nn}|^2/|H_{np}|^2\geqslant 1$, so that taking its lower limit, the scattering cross section, $\sigma_{He_3}(n,n)$ turns out to be, for thermal neutrons, ($E_n\sim 0.025$ volt),

$$\sigma_{He_3}(n,n)_{293^\circ K}=5100(0.025/0.75\times 10^6)^{\frac{1}{2}}\simeq 1 \text{ barn}.$$

As to the implications of the "$1/v$" law for the He_3 absorption cross section for slow neutrons, which is essentially measured in these experiments one may make a few qualitative statements.[15] One may say that in the slow neutron energy region the compound He_4 nucleus through which, presumably, the reaction takes place, has no unstable level. Furthermore, it is equally unlikely that there be in the α-particle a bound excited level near but below the reaction energy Q, for the process $He_4+Q\rightarrow He_3+n$, which is about 20.5 Mev. It is indeed probable, that if such a bound level existed not too far below 20.5 Mev, that it might have deformed the $1/v$ behavior of the He_3 slow neutron absorption cross section.

A final remark of some interest may be added here concerning the implications on the existence of an unstable energy level in He_4 above 20.5 Mev. Using the formalism of the dispersion theory of nuclear reactions it can be shown that such a level could be expected to exist on the basis of the $1/v$ region of the $He_3(n,p)H_3$ cross section. One finds, in particular, that the ratio (E_r/Γ), of the neutron resonance energy E_r to the total width Γ of the excited He_4 level in question, might be included between, about 0.5 and 2.0. By guessing a value of Γ, which could be done by analyzing similar situations in somewhat heavier nuclei, one is led to the conclusion that the existence of a broad unstable level in He_4, above 20.5-Mev excitation energy, is in the realm of possibilities.[3] This interesting point of the presence or absence of such a level in He_4 around the above mentioned energy could only be settled by experiments with higher energy neutrons or other types of experiments where this level might manifest itself in some way. Such experiments might help in disclosing limitations of the $1/v$ behavior of the $He_3(n,p)H_3$ cross section at higher neutron energies.

We should like to thank finally, Messrs. E. S. Robinson, M. Goldblatt, and R. M. Potter, from the Chemistry Department for their cooperation in preparing the helium and boron samples used in this experiment. Our thanks are also due to Mr. F. L. Bentzen who helped materially in setting up the counting equipment and the taking of the data.

This document is based on work performed at the Los Alamos Scientific Laboratory of the University of California under Government Contract W-7405-Eng-36.

[15] See, in this connection, reference 3.

Radioactive Isotopes of the Rare Earths. I. Experimental Techniques and Thulium Isotopes

GEOFFREY WILKINSON AND HARRY G. HICKS
Radiation Laboratory and Department of Chemistry, University of California, Berkeley, California
(Received January 19, 1949)

The experimental techniques used in the chemical separation and identification of radioactive isotopes of the rare earth elements are described. The isotopes are produced by bombardment of rare earth oxides with α-particles, deuterons, and protons from the 60-inch Crocker Laboratory cyclotron, and also by bombardment of tantalum with 200 Mev deuterons from the 184-inch cyclotron. The production and properties of three new thulium isotopes are described.

I. INTRODUCTION

THE extreme difficulty in achieving separation of the rare earth elements in a very pure state has been overcome in recent years by two main advances in experimental techniques. These have meant that not only macro, but tracer, amounts of rare earths can be reliably separated from each other in a few hours.

Methods of separation based on multiple oxidation states of the rare earth elements have been developed for europium, samarium, and other rare earths, particularly by McCoy[1] and Marsh,[2] using zinc and sodium amalgam reduction procedures, while the separation of rare earths by the use of columns of ion-exchange resins has been developed in the Manhattan Project, and has been described in a comprehensive series of papers.[3]

These procedures have given a great impetus to research on rare earth isotopes formed in fission of uranium and also by neutron capture.[4] Little work, however, has been done on neutron deficient isotopes formed by proton, deuteron, and α-particle bombardment of the rare earths. A systematic study has, therefore, been undertaken to remedy this deficiency in the knowledge of such isotopes, and further, to allow interpretation of the results of high energy particle bombardments of elements above the rare earths using the 184-inch cyclotron. In a previous note,[5] a list of new rare earth activities and their properties was given; the present paper describes the experimental procedures used, and the properties of the new thulium activities.

[1] H. N. McCoy, J. Am. Chem. Soc. **57**, 1756 (1935); **59**, 1131 (1937); **63**, 3422 (1941).
[2] J. K. Marsh, J. Chem. Soc. 398, 523 (1942).
[3] E. R. Tompkins, J. X. Khym and W. E. Cohn, J. Am. Chem. Soc. **69**, 2769 (1947); F. H. Spedding *et al.*, J. Am. Chem. Soc. **69**, 2777, 2786, 2812 (1947); E. R. Tompkins and S. W. Mayer, J. Am. Chem. Soc. **69**, 2859, 2866 (1947).
[4] E. R. Tompkins, J. X. Khym and W. E. Cohn, J. Am. Chem Soc. **69**, 2769 (1947); J. A. Marinsky, L. E. Glendenin, and C. D. Coryell, J. Am. Chem. Soc. **69**, 2781 (1947); D. H. Harris and E. R. Tompkins, J. Am. Chem. Soc. **69**, 2792 (1947); B. H. Ketelle and G. E. Boyd, J. Am. Chem. Soc. **69**, 2800 (1947); W. E. Cohn, G. W. Parker and E. R. Tompkins, Nucleonics **3**, 22 (1948).
[5] G. Wilkinson and H. G. Hicks, Phys. Rev. **74**, 1733 (1948).

II. EXPERIMENTAL

A. Bombardments

Where comparatively large quantities of material were available, hundred milligram amounts of rare earth oxide were spread on a ridged copper target plate, which was then covered with 0.2 mil tantalum foil. In all other cases, ten to twenty milligram samples of the oxides were bombarded on interceptor targets placed in the beam of the 60-inch Crocker Laboratory cyclotron. The finely powdered oxide was spread evenly on a small platinum tray with a grooved inner surface, which was silver soldered to a water-cooled copper holder. The oxide layer was wetted, and a few crops of dilute sodium silicate solution dropped on top of it. After evaporation and drying under an infra-red heat lamp, the oxide was very firmly bound in an even layer. Targets so prepared have withstood over a hundred microampere-hours of 20 Mev deuterons without loss. The targets were covered with 0.2 mil tantalum foil as additional protection.

Bombardments of rare earth oxides have been made with 38 Mev α-particles, 19 Mev deuterons, and 10 Mev protons from the 60-inch Crocker Laboratory cyclotron; runs with low energy α-particles were made by placing suitable thicknesses of tantalum foil over the interceptor target. Tantalum, as the metal foil, was bombarded with 200 Mev deuterons from the 184-inch cyclotron.

B. Chemical Separations

After bombardment, the rare earth oxide was dissolved in nitric acid, and insoluble matter removed by centrifugation. Carriers for contaminating activities likely to be formed from the target materials—copper, tantalum, platinum, sodium silicate, etc.—were added, and the rare earth fluoride precipitated from hot 2N nitric acid solution by addition of hydrofluoric acid. The washed fluoride was dissolved in a mixture of concentrated nitric acid and saturated boric acid; from this solution, the rare earth hydroxide was precipitated by addition of ammonium hydroxide. The washed

hydroxide was dissolved in nitric acid and a further fluoride precipitation made as before. Three or four such cycles were made, after which, the hydroxide was dissolved in a minimum of hydrochloric acid and the solution accurately adjusted to a known volume. Aliquots of this solution were taken for direct measurement of radioactivities, for chemical separation of the individual rare earth elements, and for estimation of the chemical yield of the bombarded oxide. Rare earths were determined for chemical yield measurement, by the precipitation of oxalate, followed by ignition to the oxide, and weighing.

The tantalum, after bombardment with 200 Mev deuterons, was dissolved in the minimum of nitric and hydrofluoric acids. To the boiling solution was added boric acid, to complex the fluoride, followed by cerium III solution as a carrier for the rare earth activities. After dilution, excess hydrofluoric acid was added to precipitate cerium III fluoride. The cerium was purified by hydroxide-fluoride cycles as above. To the final solution in strong nitric acid was added a small quantity of lanthanum (*ca.* 0.1 mg), and the cerium oxidized to the IV oxidation state by addition of sodium bismuthate. The cerium was then removed by precipitation of cerium IV phosphate from 3*N* nitric acid solution. The lanthanum, with the rare earth activities, was recovered as the fluroide, which was then converted to the chloride for subsequent separations on the ion-exchange columns.

C. Chemical Separation of the Rare Earth Elements

Chemical separation of the individual rare earth elements was made by ion-exchange resin columns, or for europium, by an amalgam reduction method. The principle of column separation involves first the adsorption of the rare earth ions in dilute acid solution on a small quantity of ion-exchange resin. This resin is then placed at the top of a resin column, through which is then passed a solution of a complexing agent for the rare earths, e.g., ammonium citrate. The rare earths are eluted under strictly controlled conditions and pass through the column at various rates; lutecium is the first to appear in the eluate, followed in succession by ytterbium, thulium, erbium, etc.

In preliminary experiments to determine the characteristics of column separations and optimum separation conditions for the rare earths, both inactive rare earths in milligram amounts, and Y^{91} radioactive tracer were used. The former were determined spectroscopically[6] and the Y^{91} determined by its radioactivity.

[6] Spectroscopic analyses of the rare earths were made in this laboratory by Mr. J. Conway and Mr. M. Moore, to whom we are greatly indebted for their assistance.

TABLE I. Production and properties of thulium isotopes.

Isotope	Decay	Half-life	Energy of radiation in Mev: Particles	Energy of radiation in Mev: γ-rays	Produced by
Tm^{166}	$K\beta^+\varepsilon^-\gamma$	7.7±0.1 hrs.	2.1 (β^+) 0.24, ~1 (ε^-)	*L*, *K* x-rays 1.7	Ho-α-3*n* Er-*p*-*n*
Tm^{167}	$K\varepsilon^-\gamma$	9.6±0.1 days	0.21 (ε^-)	*L*, *K* x-rays 0.22, 0.95	Ho-α-2*n* Er-*p*-*n* Ta-*d*-5*n*, 16α
Tm^{168}	$K\varepsilon^-\gamma$ (β^-?)	85±2 days	0.16, 0.5 (ε^-)	*L*, *K* x-rays 0.21, 0.85	Ho-α-*n* Er-*p*-*n* Tm-*n*-2*n*

1. *Preparation of the Column.*—All column separations were made using Dowex-50,[7] an aromatic hydrocarbon polymer containing many nuclear sulfonic acid groups. The resin used was the colloidal agglomerates, Batch 19891M supplied as the sodium form. The ammonium form of the resin was prepared by stirring with saturated ammonium chloride solution; excess ammonium chloride was removed by washing with water. The resin was graded to have a settling time of less than five minutes for five centimeters in water at room temperature. The length of the preliminary resin column was 50 cm, with a diameter of 0.4 cm, but in subsequent runs, it was found that 20 cm×0.4 cm and 20 cm×1.0 cm columns gave adequate separation.

2. *Adsorption of Rare Earths on Resin.*—The rare earth solution in hydrochloric acid was adjusted to give a *p*H between 0.5 and 1.5, the ionic strength being kept at a minimum; this solution was then agitated with about 0.2 ml of resin added in two or three successive portions. The solution and resin were agitated at about 70°C, but were not allowed to stand in contact for more than 15 minutes. This prevents diffusion of ions into the interior of the agglomerates, and subsequent slow elution with poor separations.

3. *Operation of the Column.*—The resin, with the rare earth adsorbed on it, was transferred to the top of the resin column, and the eluting agent passed through. The eluting agent used was a 0.25*M* solution of C.P. citric acid, accurately adjusted to *p*H 3.05 with ammonium hydroxide. Care was taken to approach this value from the acid side, so that readjustment with acid was not necessary, since it is important for good separations to keep the ionic strength at a minimum. The flow rate was approximately 0.03 milliliter per square centimeter column area per minute; with the columns used, of diameter 0.4 cm, and with a drop size of about 0.03 ml, this flow rate corresponded to one drop in 3.5–4 minutes.

The eluate was collected in 10×75 mm rimless test tubes placed in a perforated turntable, which was rotated automatically at various time settings,

[7] W. C. Bauman, Ind. Eng. Chem. 38, 46 (1946); W. C. Bauman and J. Eichhorn, J. Am. Chem. Soc. 69, 2830 (1947).

to place succeeding tubes under the column. Samples were normally collected for 15 minutes. In runs with active materials, aliquots were taken with micropipettes and evaporated on stainless steel disks for counting. Aliquots were also taken for spectroscopic analysis of macro amounts of rare earths present. The amount of rare earth, determined either spectroscopically or by activity measurements, was then plotted against the sample number. This allows estimation of the degree of separation achieved. In all column runs, samples collected before the elution of one "free column volume" were disregarded. After completion of a column run, any residual activity or rare earth was stripped from the column with 0.25*M* ammonium citrate of *p*H 7 as eluting agent. After thoroughly washing with water, the column was again ready for use.

After separation on the column, the rare earths were recovered by evaporation of the citrate solution with nitric and perchloric acids with subsequent ignition. The rare earth residue was then extracted with nitric acid and the hydroxide precipitated with ammonium hydroxide. If the solution contained only tracer amounts, a small amount of lanthanum was added as a carrier.

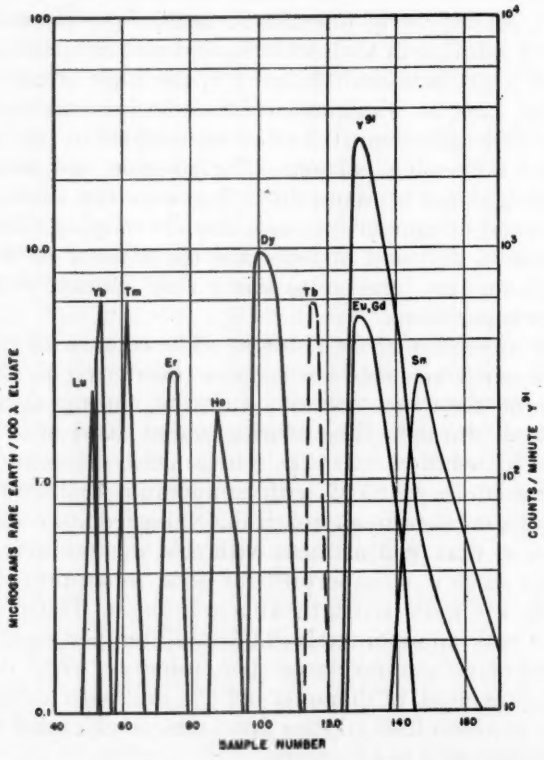

FIG. 1. Standard rare earth elution. 50×0.4 cm Dowex-50 column. Flow rate 0.08 ml/cm²/min. Sampling time 15 minutes; eluate volume in milliliters is 0.282×sample number. Y^{91} was measured by its radioactivity, other rare earths spectroscopically. Terbium is estimated since the cyanogen bands obscure the terbium lines. Eluting agent is citric acid adjusted to *p*H 3.05 with ammonium hydroxide.

In addition to strict control of the conditions mentioned above, it is also important for successful separations, that the capacity of the resin for adsorption of rare earth ions is not exceeded. For the columns described, the maximum capacity corresponds to approximately 10 mg and 100 mg of rare earth oxide, respectively. Where the starting materials contained significant amounts of other rare earth impurities, and purification was necessary before bombardment, a larger column, which had a capacity for about 1 g rare earth oxide was used. The area of the column and the drop rate were scaled up from the values used in the 0.4 cm and 1.0 cm diameter column runs, the amount of citrate flowing through unit cross-sectional area of resin being kept constant. The progress of any particular inactive rare earth through the column could be checked by using radioactive tracer for a neighboring heavier rare earth. After elution of the active tracer, the sample numbers of the desired inactive rare earth were estimated by comparison with the standard elution curve (Fig. 1). Aliquots of the samples were then examined spectroscopically to allow the pure rare earth fractions to be isolated.

4. *Results in Column Separations.*—In Fig. 1 is shown the "standard elution curve" obtained with inactive materials and Y^{91} tracer. It should be noted that while the lutecium and ytterbium are very close together, samples from the peaks of these curves have no detectable lines of each other or of other rare earths in their spectra. Thus samples of these neighboring elements can be obtained in which the separation factor is at least a thousand.

A typical column run on a bombarded sample is shown in Fig. 2, where the broken line shows the distribution of radioactivity produced by 38 Mev alpha-particle bombardment of holmium oxide. The solid lines show the distribution of inactive carriers of lutecium, ytterbium, erbium, and dysprosium, added as references, and determined spectrographically.

A further example of a column separation is shown in Fig. 3, where the rare earths are present in tracer quantities only. In such cases, separation is generally cleaner and there is less "tailing" of the peaks, than where macro amounts of rare earths are separated. The activities shown in Fig. 3 were spallation products, obtained by the bombardment of tantalum with 200 Mev deuterons from the 184-inch cyclotron. Lanthanum was used as a carrier for the radioisotopes. A study of the radiation characteristics and decays of the peak samples has shown no evidence of contamination.

D. Separation of Europium

Europium has been purified prior to, and recovered after bombardment by a modification of McCoy's method.[1] The europium in 6*N* hydro-

chloric acid solution was reduced to the divalent state by boiling with zinc amalgam. Rare earths other than europium were precipitated by carbonate-free ammonia using cerium as a carrier. After centrifuging, the supernatant solution was withdrawn, the europium oxidized by ozone, and then precipitated by ammonia. The procedure was repeated with both fractions to ensure complete separation.

E. Radioactive Measurements

Measurements were made with "end-on" type Geiger-Müller counters which had 3 mg/cm² mica windows, and were filled with 10 cm argon and 0.5

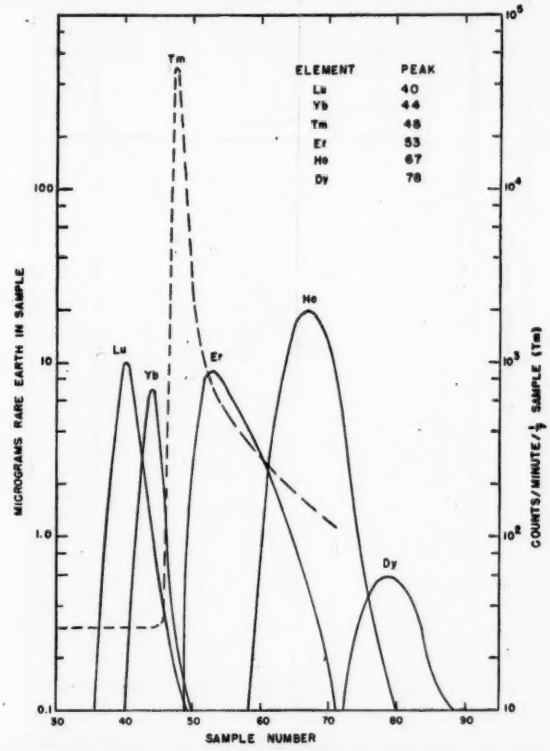

FIG. 2. Column separation of thulium activities from Ho+α bombardment.

cm alcohol; variations in counter efficiency were corrected for by use of a UX_2 reference. A "magnetic counter" was also used, which enabled recognition of positive and negative electrons and provided a check on data obtained from absorption measurements.

Radiation characteristics of active isotopes were determined by beryllium, aluminum, and lead absorption measurements. Electron and soft electromagnetic radiations were resolved by the technique of differential absorption in aluminum and beryllium.[8] The ranges of electrons reported have been taken as the total absorber thickness required for

[8] G. Wilkinson, Phys. Rev. **75**, 1019 (1949).

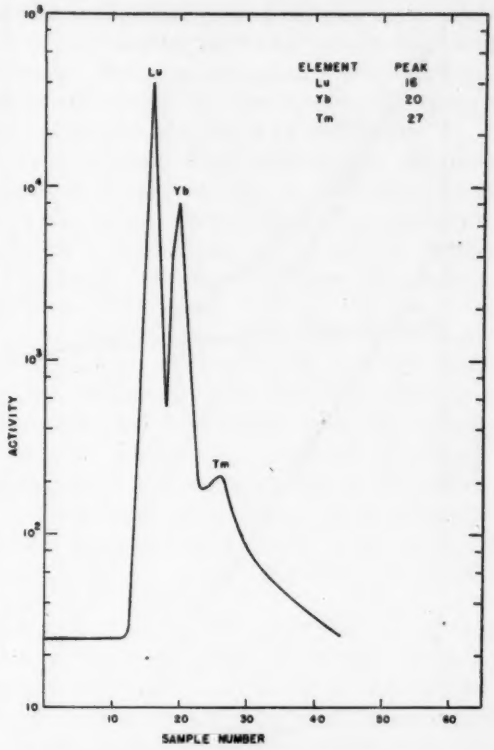

FIG. 3. Column separation of spallation products from 200 Mev deuteron bombardment of tantalum.

removal, i.e., added absorbers plus counter window, air gap, etc. Energies of electrons obtained by aluminum absorption measurements and by the magnetic counter, have been checked using the β^- radiation of P^{32} and the conversion electron of Tc^{99} as references.

In γ-ray absorptions, lead screens up to 45 g/cm² were used, with a beryllium absorber, sufficient to remove all secondary electrons, placed directly below the counter window. Measurements were taken on a counter tube without the usual lead housing, as scattering in the latter has been

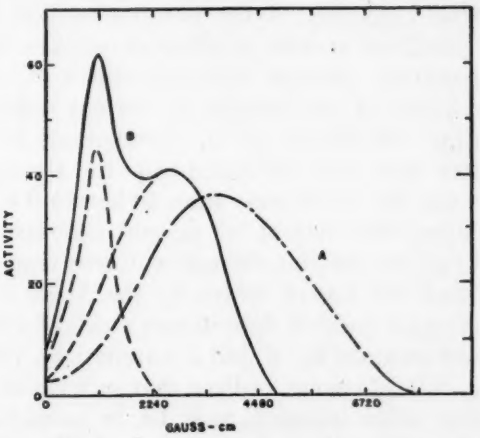

FIG. 4. Magnetic counter distribution of positrons (A) and electrons (B) of 7.7-hour Tm^{166} from Ho+α-bombardment.

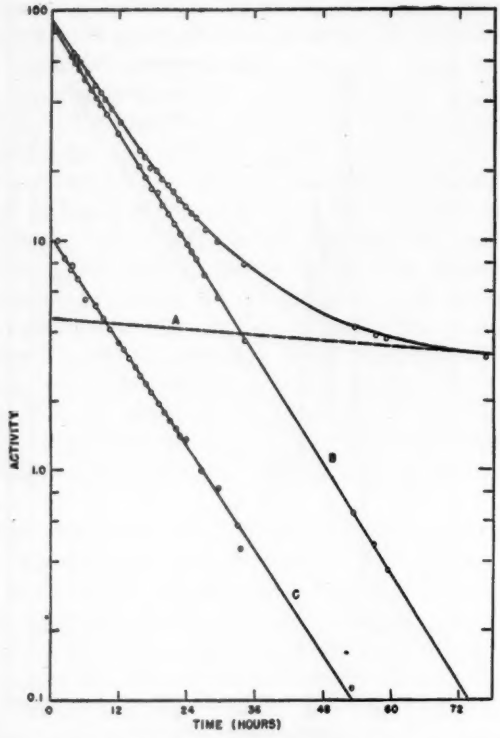

FIG. 5. Decay of 7.7-hour Tm^{166}, 9.6-day Tm^{167} background (A) and 7.7-hour Tm^{166} gross decay from Ho+α. (B) 7.7-hour Tm^{166} positron decay (C) from Er+p measured on magnetic counter.

found to give high values for the absorption half-thickness of hard γ-radiation.

Samples for counting were mounted on glass microscope cover slides. Where minimum back-scattering was required, as in measurements of ratios of electrons and electromagnetic radiation, samples were mounted on very thin mica.

For quantitative measurements, the counter geometries were calibrated by use of a weighed uranium (UX_2) standard.

The ratios of the various electron and electromagnetic radiations of the isotopes studied have been calculated in order to allow an estimate of the disintegration schemes, with the object of calculating yields of the isotopes in various reactions. Counting efficiencies of L x-radiation in the counters used were calculated from the absorption in the gas; for γ-radiation from 20 kev to 0.4 Mev a counting efficiency of 0.5 percent was assumed, and 1 percent per Mev thereafter. Corrections were also made for loss of x-rays by the Auger effect. In the region studied, fluorescence yields of 0.8 and 0.5 were assumed for K and L x-radiations, respectively. It is, of course, realized that such ratios, and absolute cross sections, may be in considerable error due to the uncertainties involved. The relative cross sections of the same isotope formed in various reactions are of more value. Beam intensities were taken from the cyclotron instruments.

III. THULIUM ISOTOPES

In the bombardment of holmium, which has a single isotope Ho^{165}, with 38 Mev, 30 Mev, and 20 Mev alpha-particles, three radioactive thulium isotopes were produced (see Table I). These were allocated to masses 166, 167, and 168 on the basis of the yields at various energies of the bombarding alpha-particles. The isotopes have been also produced and the mass assignments checked by proton bombardments of erbium. The chemical identity of the isotopes was established by column separations (see Fig. 2).

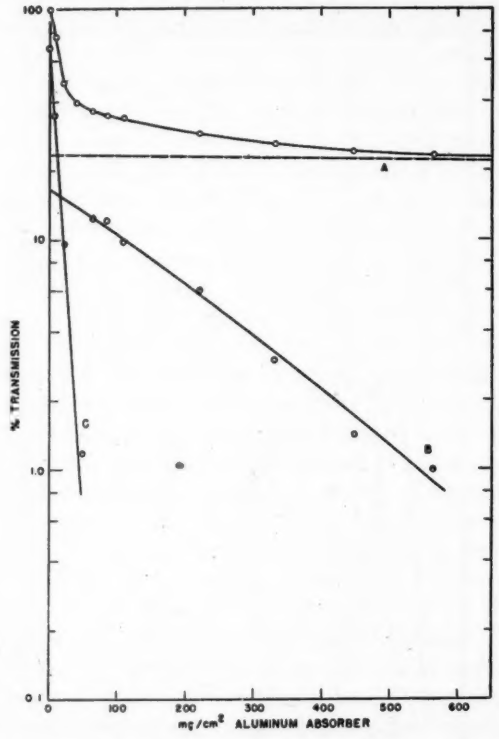

FIG. 6. Aluminium absorption of 7.7-hour Tm^{166} from Ho+α. K x-ray and γ-ray background (A), positrons and hard electrons (B), and soft electrons (C).

The holmium oxide used for bombardment was prepared by Dr. J. K. Marsh, Oxford University, England, and was supplied by Johnson, Matthey Company, London, as "Specpure" brand, laboratory number 1031. Analysis showed this oxide to contain about 15 percent dysprosium oxide and about 5 percent yttrium oxide.

The erbium used was Johnson, Matthey and Hilger, "H.S." brand, laboratory number 1755, prepared by Dr. J. K. Marsh. Spectrographic analysis gave ~0.2 percent yttrium and ytterbium impurities.

Initially the impure oxides were bombarded and the rare earths separated by the column method; in subsequent bombardments the recovered pure rare earths were used.

A. 7.7-hour Tm^{166}

The radiations of this isotope consist of positrons, several energies of negative electrons, K x-radiation, and very hard γ-radiation, all of which decay with the same half-life, the best value for which is 7.7 ± 0.1 hours. The gross decay of the isotope produced by 38 Mev alpha-particles on holmium was followed through eight half-lives.

Examination of the isotope on the magnetic counter showed unequivocally that positrons were

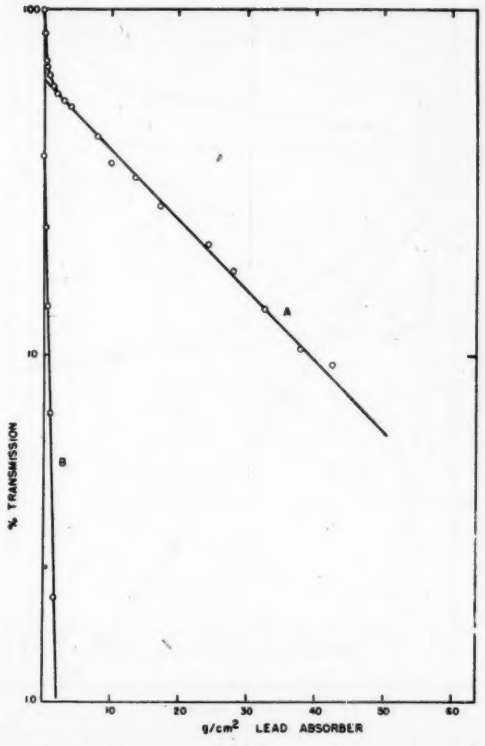

FIG. 7. Lead absorption of 7.7-hour Tm^{166} from Ho+α. Hard γ-radiation (A) and K x-rays (B).

present. Figure 4, curve A shows the measured distribution, with end point corresponding to 2.1 Mev maximum energy and with a mean energy of 0.6 Mev. The decay of the positrons (Fig. 5, curve C) was followed on the magnetic counter through six half-lives in both Ho+α and Er+p bombardments.

On the "negative sweep" of the magnetic counter, two groups of negative electrons were observed (Fig. 4, curve B) both of which decayed with the same half-life. While the lower energy peak probably represents a single conversion electron, the second group of harder electrons has a much broader distribution of energies, and may be a mixture of several conversion electrons which the simple instrument used is incapable of resolving. The maximum energy of this group corresponds to 1 Mev while the average is at $\sim$0.5 Mev.

The aluminum absorption of an infinitely thin sample is shown in Fig. 6. The electromagnetic background was determined after removal of all electrons by a 1400 mg/cm² beryllium absorber. No L x-radiation was observed here, although a direct beryllium absorption of the 7.7-hour activity suggests this to be present. The absorption curves show electrons of ranges 70 mg/cm² and $\sim$960 mg/cm² aluminum, corresponding respectively to 0.24 and 2 Mev; the harder radiation is a complex mixture of positive and negative electrons. Lead absorption of the electromagnetic radiations (Fig. 7), shows two components of half-thicknesses 80 mg/cm² and 14.3 ± 0.2 g/cm². The energy of the former, 50 kev, agrees well with the value for erbium K x-radiation.

An approximate ratio of positive to negative electrons was obtained by measuring the area under the curves (Fig. 4) from the magnetic counter. The ratio of both the soft and hard groups of electrons to the gross electromagnetic radiation was obtained from aluminum absorption measurements, the usual corrections being made for absorption of electrons is the counter window, etc. From the various measurements, the following ratios, neces-

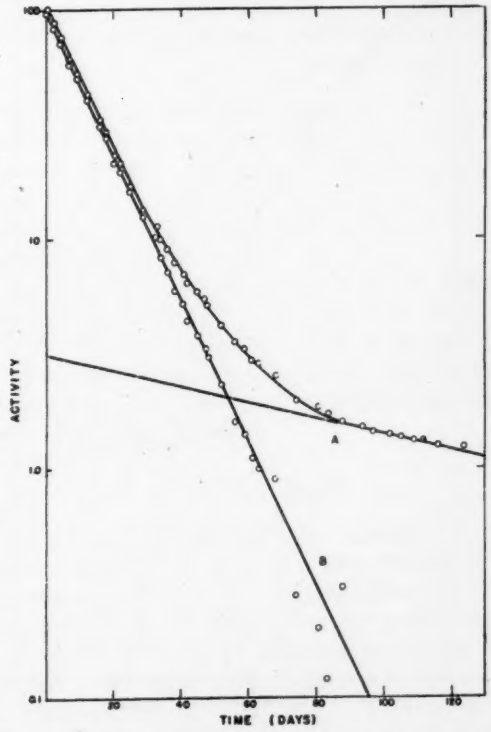

FIG. 8. Decay of 85-day Tm^{168} (A) and 9.6-day Tm^{167} (B) from Ho+α.

sarily approximate in view of the several corrections and uncertainties involved, were obtained.

$$e_1:e_2:\beta^+:K \text{ x-rays}:\gamma = 0.05:0.003:0.004:1:0.3,$$

where e_1 and e_2 are respectively the soft and hard electron intensities. The very complex radiations can be attributed to orbital electron capture in thulium, leading to excited or metatstable levels of the daughter nucleus. Electrons arise from converted γ-ray transitions between the various levels or between these and the ground state. Positron emission may go to an excited level of the daughter nucleus or to the ground state. Since the ratio of electrons to K x-radiation is only $\sim$0.05, approximately 95 percent of the K x-rays measured must arise from orbital electron capture, and it is assumed that 0.95 K quanta represent one disintegration. Thus, the branching ratio for disintegration by positron emission is around 0.5 percent.

It should be noted that the wide distribution of hard negative electrons observed (Fig. 4, curve B) could be due to a continuous β^--spectrum of maximum energy about 1 Mev arising from β^--branching in Tm^{166}, since it is very possible that Yb^{166} is an unreported stable isotope of low abundance. The postulation of stable ytterbium isotope at mass 166 involves no great heresy, since an isotope in such a position would, according to well-known empirical rules of the stability of isotopes, be either long lived or stable, and since stable isotopes of erbium, Er^{162},[9] and dysprosium, Dy^{156},[10] which are in analogous positions, are known. A similar situation has arisen with the 16 day Ta^{178},[5] which has been found to decay almost completely by β^--emission, thus implying the existence of an unreported stable isotope of tungsten at mass 178.

If the hard negative electrons of Tm^{166} are, then, a β^--particle spectrum, the disintegration by β^--emission is approximately 0.4 percent of that by orbital electron capture. The branching by β^-- and β^+-emission is thus almost the same.

The cross sections for formation of the 7.7-hour isotope were calculated from the intensity of K x-radiation, with the above assumptions for counting efficiencies and quanta per disintegration. The K x-radiation was measured for weighed samples of unseparated bombarded pure holmium, since no activities other than those of the thulium isotopes were observed. It is possible, however, to determine the specific activity by integrating the counts of the thulium peak in the column separation of a known quantity of bombarded holmium. This method is of general application for calculation of cross sections where activities of two or more elements are present, e.g., in the rare earth fraction of spallation products

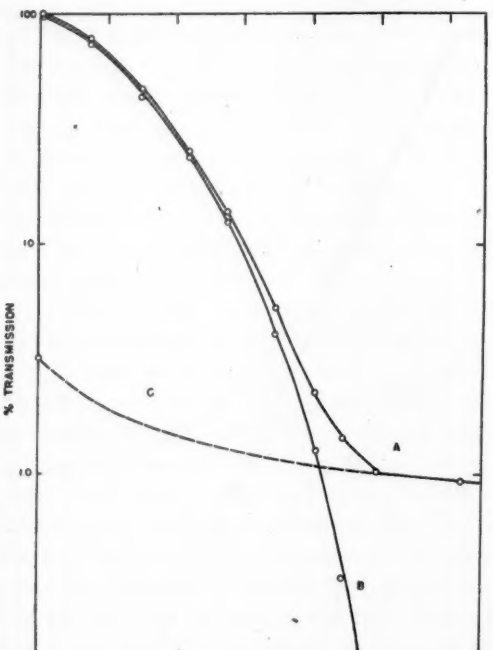

FIG. 9. Aluminum absorption of 9.6-day Tm^{167} from Ho+α. K x-ray and γ-ray background (A), electrons (B) and L x-rays (C).

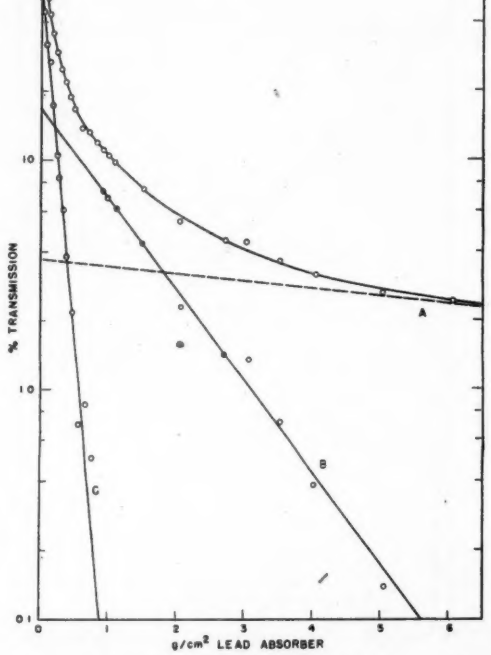

FIG. 10. Lead absorption of 9.6-day Tm^{167} from Ho+α. 0.95 Mev γ-ray (A), 0.22 Mev γ-ray (B) and K x-rays (C).

[9] W. Wahl, Finska Kemistsamfundets Medd. **50**, 10 (1941).
[10] D. C. Hess, Jr., M. G. Inghram, Phys. Rev. **74**, 1724 (1948).

from tantalum with high energy particles, or in deuteron bombardments of rare earths.

B. 9.6-day Tm^{167}

After decay of the 7.7-hour isotope from both Ho+α and Er+p bombardments, a residual activity consisting of 9.6-day and long-lived components was observed in the thulium fraction (see Fig. 8). The half-life of the shorter-lived isotope obtained from Ho+α bombardments is 9.6±0.1 days; the gross decay was followed through ten, and γ-radiation, through nine half-lives. The samples were studied on the magnetic counter, no positrons being

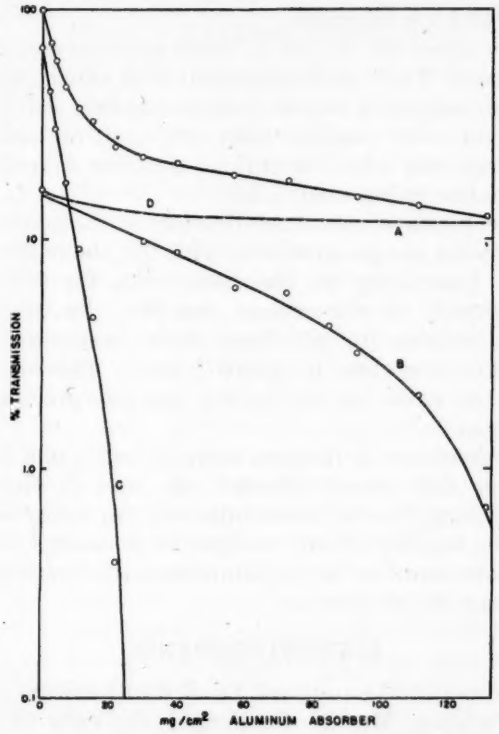

FIG. 11. Aluminum absorption of 85-day Tm^{168} from Ho+α. K x-ray and γ-ray background (A), hard electrons (B), soft electrons (C) and L x-rays (D).

observed. The aluminum absorption curve of an infinitely thin, column separated sample of the 9.6-day activity from Ho+α bombardment is shown in Fig. 9. The electrons have a range of 52±2 mg/cm² aluminum, corresponding to 0.21 Mev energy. The electromagnetic radiation consists of four components of half-thicknesses 7.5 mg/cm² aluminum, 80 mg/cm² lead, 770±20 mg/cm² lead and 9.6 g/cm² lead, corresponding, respectively, to energies of 6 kev, 50 kev, 220 kev and 0.95 Mev. The two soft radiations agree well with the energies of erbium L and K x-radiations. The lead absorption curve is shown in Fig. 10.

From absorption measurements, making corrections for absorption of electrons in counter

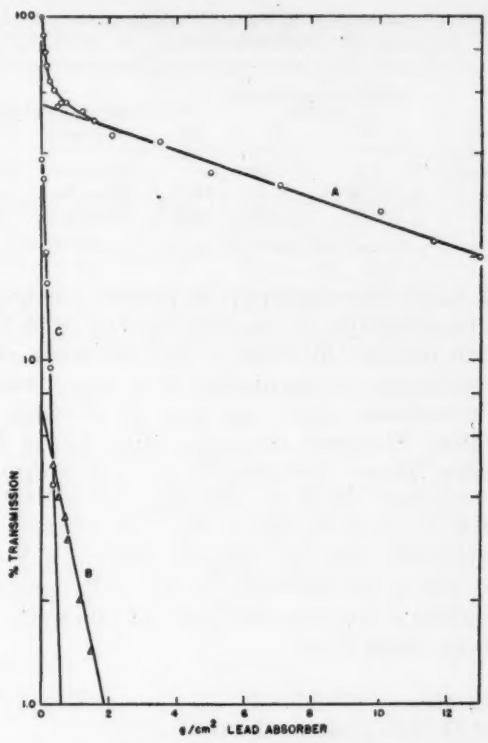

FIG. 12. Lead absorption of 85-day Tm^{168} from Ho+α. 0.85 Mev γ-ray (A), 0.21 Mev γ-ray (B) and K x-rays (C).

window, etc., for counting efficiencies of electromagnetic radiation and for loss of x-rays by Auger effect, the following ratios were obtained:

electrons: L x-rays: K x-rays: 220 kev γ: 0.95 Mev γ = 0.3:0.2:1:0.1:0.01.

Assuming that K x-radiation arises from production of the conversion electrons, then 0.7 K x-ray quanta probably represent one disintegration by orbital electron capture. This figure has been assumed in the calculation of cross sections for production of the isotope.

The isotope has also been produced by the bombardment of tantalum with 200 Mev deuterons from the 184-inch cyclotron. The measured radiation characteristics were identical with those described above. The reaction producing the isotope is designated Ta-d-5z16a.

C. 85-day Tm^{168}

After decay of the 9.6-day isotope, a small residual activity of long-life was found in the column separated thulium fractions from the Ho+α bombardments at 38 Mev. A more active sample was obtained from a 54 microampere-hour bombardment of 80 mg of pure holmium oxide with 19 Mev alpha-particles. The decay of electron and electromagnetic radiations of the isotope have been followed through three half-lives to give a value of

TABLE II. Cross sections in barns for alpha-particle reactions with holmium.

Activity	Energy of α-particles in Mev 38	30	19	Probable reaction	Probable isotope
7.7 hours	1.1	5×10^{-4}	—	Ho-α-3n	Tm^{166}
9.6 days	7×10^{-3}	0.1	10^{-3}	Ho-α-2n	Tm^{167}
85 days	10^{-4}	3×10^{-3}	0.2	Ho-α-n	Tm^{168}

85±2 days. The aluminum absorption curve (Fig. 11) shows electrons of ranges 29 mg/cm² (0.16 Mev) and 150 mg/cm² (0.5 Mev). The soft electromagnetic radiation corresponding to L x-ray energies was determined after removal of electrons by beryllium. The lead absorption (Fig. 12) of hard radiation shows components of half-thicknesses 77±3 mg/cm² (49 kev), ~740 mg/cm² (0.21 Mev) and 8.8 g/cm² (0.85 Mev). The first of these corresponds well with the value for erbium K x-radiation. The ratios obtained for the radiations after the various corrections for counting efficiency, etc. had been made were:

0.16 Mev e^-:0.5 Mev e^-:L x-rays:K x-rays:
0.21 Mev γ-ray:0.85 Mev γ-ray
=0.15:0.02:0.2:1:0.2:0.8.

The energy of the soft electrons agrees well with that to be expected for K shell conversion of the 0.21 Mev γ-ray. The conversion coefficient is ~0.8. Assuming that K x-rays arise from conversion, then ~0.75 of the observed K-radiation may be considered to represent one disintegration by orbital electron capture. The cross sections for production of the isotope have been calculated accordingly. Since the 85-day activity is allocated to Tm^{168}, the possibility of β^- branching exists, and the 0.5 Mev electrons observed may be β^- radiation. With the previous assumptions regarding K x-rays, about 2 percent of the disintegrations would, then, proceed by β^- emission.

The 85-day isotope has been also observed in bombardments of erbium with 10 Mev protons and thulium with fast neutrons. In both cases, the 127-day Tm^{170} is also formed. The latter is reported to have no γ-radiation, and the x- and γ-radiation observed in the thulium fraction decays with a half-life of 85 days. The allocation to mass 168 on the basis of reaction yields is thus confirmed.

D. Discussion

In Table II are given the cross sections for production of the three thulium isotopes by alpha-particle bombardment of holmium at various energies. The absolute values of the cross sections may be in considerable error in view of the several assumptions which had to be made. The relative yields of the isotopes at various energies are significant, however, and allow allocation of the 7.7-hour, 9.6-day, and 85-day activities to masses 166, 167, and 168, respectively, on the basis of α,3n, α,2n, and α,n reactions.

The allocation of the 7.7-hour positron-emitting isotope to Tm^{166} is in agreement with observations that for elements of odd atomic number, only isotopes of even mass number are positron active, and then only when the ratio of neutrons to protons is equal to or less than 1.43.

The yields of the three isotopes in Er+p bombardments are in agreement with the above allocations. Correcting the observed yields for isotopic abundances of the erbium isotopes, the isotopic cross sections for all three cases, assuming p,n reaction, are close to 2×10^{-2} barn. This agrees with the value for the Lu-p-n reaction previously reported.[11]

No evidence of thulium activities with half-lives shorter than those reported was seen in Ho+α, Er+p, and Tm+n bombardments; an upper limit for the half-life of any shorter-lived isotope, from measurements on non-column-separated materials, is about 15 minutes.

ACKNOWLEDGMENTS

We would like to thank Dr. J. G. Hamilton, Mr. T. Putnam, Mr. B. Rossi, and the crew of the 60-inch Crocker Laboratory cyclotron for their most helpful cooperation and assistance in bombardments. We are further indebted to Professors G. T. Seaborg, I. Perlman, and B. B. Cunningham for their continued interest and advice.

This paper is based on work done under the auspices of the Atomic Energy Commission.

[11] G. Wilkinson and H. G. Hicks, Phys. Rev. **75**, 696 (1949).

The Effects of Nuclear Stability on the Formation of the Chemical Elements*

J. S. SMART
*University of Minnesota, Minneapolis, Minnesota***
(Received January 21, 1949)

Nuclear stability considerations are applied to the neutron capture theory of the formation of the chemical elements. It is shown that the matter density during the time of formation must have remained within the limits 10^{-1} g/cm³ and 10^{-11} g/cm³. The nuclei were probably formed with some neutron excess so that both neutron capture and β-decay were effective in determining relative abundances. The chain of formation followed a path such that the β-decay and capture probabilities were approximately equal. The abundance of nuclei of even atomic weight over those of odd atomic weight can be explained from the general features of the nuclear energy surface, regardless of the neutron excess at the instant of formation.

I. INTRODUCTION

A NEUTRON capture theory of the formation of the chemical elements has recently been proposed by Gamow and Alpher.[1-3] It is assumed that the elements are formed and their relative abundances determined in a pre-stellar stage of the universe. During the first stages of universal expansion, the primordial matter was a gas of neutrons at high density and temperature. As the expansion continued, protons were formed by β-decay of neutrons and the temperature became low enough to make capture of free neutrons by the protons a relatively probable event. Heavier nuclei were then built up by successive neutron captures. The formation process ceased when the neutron density became very small because of expansion and β-decay. According to this theory, the maximum period of time allowed for the formation process was only a few hours, due to the radioactive decay of the neutrons. The significant feature of the relative abundance data is the isobaric abundances and not the isotopic abundances, as in the thermal equilibrium theories.

The differential equations describing the formation process may be written

$$dN_A/dt=\lambda_{A-1}N_{A-1}-\lambda_A N_A, \quad A=1, 2, 3\cdots \quad (1)$$

if one neglects the effects of universal expansion in reducing the density of matter. Here N_A is the number of nuclei per unit volume of atomic weight A, and λ_A is the probability per second of a nucleus of mass A capturing a neutron. It is implicitly assumed that neutron captures occur at a much higher rate than other transmutation reactions. Alpher and Herman[4] have computed relative abundances by this theory, neglecting the effects of universal expansion but considering the variation of the λ_A's with time because of neutron decay. They find that in order to obtain the best fit to the relative abundance curve, an initial density of $\rho=5\times10^{-9}$ g/cm³ must be assumed. In their treatment it is not necessary to specify the temperature during the formation process, but it seems clear that the temperature could not be much higher than that corresponding to a kinetic energy of 1 Mev since the capture probabilities would be quite low, and there would be enough high energy neutrons to dissociate a large fraction of the nuclei that were formed. Alpher[3] has pointed out that, if the average energy were lower than 10^3 ev, resonance capture would predominate and the results would be reflected in the abundance data, e.g., the nuclei with high resonance capture cross sections would be very scarce. Since no such variations are noticed, it is assumed that the formation process occurred at a temperature of about 0.1 Mev. It should also be pointed out, however, that this argument considers only the known cross sections for stable elements. Actually, the elements were probably formed with some neutron excess, and later β-decayed down to their present stable state. Then some of these unstable nuclei may have had resonance capture cross sections which would be responsible for the present distribution.

The above theory has had considerable success in explaining the general shape of the abundance curve[3,4] and some of the fine structure features such as the scarcity of Li, Be, and B,[5] and the existence of isobars.[6] The purpose of this paper is to discuss several points which have not been covered in previous work, in particular, the effect of β-decay of the newly formed nuclear species in controlling the formation process.

* This paper is based in part on a thesis submitted in partial fulfillment of the requirements for the degree of Doctor of Philosophy, at the University of Minnesota, August, 1948.

** Now at Naval Ordnance Laboratory, White Oak, Silver Spring 19, Maryland.

[1] G. Gamow, Phys. Rev. **70**, 572 (1946).

[2] R. Alpher, H. Bethe, and G. Gamow, Phys. Rev. **73**, 803 (1948).

[3] R. Alpher, Phys. Rev. **74**, 1577 (1948).

[4] R. Alpher and R. Herman, Phys. Rev. **74**, 1737 (1948).

[5] R. Alpher, R. Herman, and G. Gamow, Phys. Rev. **74**, 1198 (1948).

[6] J. S. Smart, Phys. Rev. **74**, 1882 (1948).

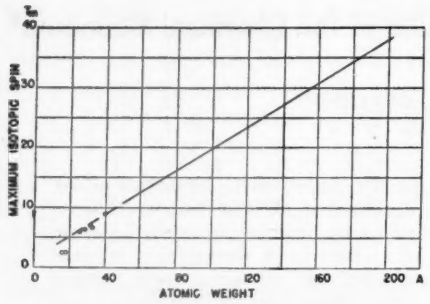

FIG. 1. Maximum isotopic spin as a function of A. The circled points were computed using Barkas' atomic mass formula. (Walter H. Barkas, Phys. Rev. **55**, 691 (1939).)

II. THE EFFECTS OF THE NEUTRON DENSITY ON THE FORMATION PROCESS

The previous papers have assumed, either explicitly or implicitly, that the mean time between neutron captures is large enough for the nuclei to have time to adjust their charges by β-decay. Actually, this assumption corresponds to one of three possible sets of physical conditions under which formation may have occurred, and there is no *a priori* reason for choosing one over the others. We list them here.

A. *Low Density.*—If the density is very low, the captures will come very slowly, there will be sufficient time for β-decays between captures, and the only nuclei formed will be stable ones and those with an excess of one neutron. It seems unlikely that this extreme condition was realized since some of the β-emitters just above the floor of the Heisenberg valley, such as P^{32} and Sc^{46}, have lifetimes of many days.

B. *High Density.*—If the density is sufficiently high, there will be a rapid succession of captures and the nucleus will not have time to adjust its charge by β-decay. The process will be brought to a temporary halt when so many neutrons have been added that the next one would not be bound. Then it would be necessary to wait until a β-decay occurred. After this another neutron or two could be captured until the limit of neutron stability was again reached. In this case the β-decay probability and not the capture probability would control the rate of formation. The set of differential equations describing the formation would still be those of Eq. (1) but λ_A is now related to the mean β-lifetime of the nucleus of mass A which has the highest neutron-proton ratio it can sustain without emitting a neutron.

C. *Intermediate Density.*—If the density is somewhere between the two extreme cases, then the nuclei when formed will lie along the slope of the Heisenberg valley, between the floor of the valley and the region of neutron instability. Then both capture times and β-decay times will be important in controlling the rate of formation. We shall show later that the process must follow a path such that $\lambda(\beta\text{-decay}) \cong \lambda(\text{capture})$ and that the particular path will be determined by the existing physical conditions.

III. THE FORMATION PROCESS AT HIGH DENSITIES

It is of interest to investigate the possibility that the formation process took place at high densities. The first step is to determine the highest neutron-proton ratio that a nucleus of mass A can sustain without emitting a neutron since it is the β-transition probabilities of these nuclei which control the formation process at high densities. The model of the nucleus which we have used is based on Wigner's theory of the symmetric Hamiltonian.[7] Wigner assumes that the binding energy of a nucleus can be written as a sum of three terms,

$$B = K + C + P, \tag{2}$$

where K is the total kinetic energy of the particles in the nucleus, C the potential energy due to the repulsions of the protons, and P the potential energy due to specifically nuclear forces. If the energies are given in $m\mu$,

$$\begin{aligned} K &= 14.6A + (32.5/A)(P_1^2 + P_2^2 + P_3^2), \\ C &= 0.635(Z(Z-1)/A^{\frac{1}{3}}), \\ P &= -\tfrac{1}{2}A(A-1)L' - \Xi L. \end{aligned} \tag{3}$$

A is the number of particles in the nucleus; P_1, P_2, and P_3 are the partition quantum numbers for the nucleus; L and L' are combinations of exchange and direct interactions due to Majorana and ordinary forces. Ξ is the difference between the number of symmetric and number of antisymmetric couplings in the nucleus. L' and L are expected to be inversely proportional to A, but their numerical values must be determined empirically. For $A > 50$, we have[8]

$$\begin{aligned} L' &= (96/A)[1 - (1.28/A^{\frac{1}{3}})], \\ L &= (152/A)[1 - (2.4/A^{\frac{1}{3}})]. \end{aligned} \tag{4}$$

Since the nuclei in which we are interested have a large neutron excess, $T_\zeta = \frac{1}{2}(A - 2Z)$ will in general be much larger than the other quantum numbers. Accordingly we shall make the simplifying assumption that each nucleus belongs to the $(T_\zeta, 0, 0)$ multiplet, i.e., $P_1 = T_\zeta$, $P_2 = P_3 = 0$.*** Then any nuclear species can be completely described by any two of the three quantities, A, Z, and T. (The subscript ζ has been dropped for convenience.)

The condition that the next neutron added to the

[7] E. P. Wigner, *Nuclear Physics* (University of Pennsylvania Press, Philadelphia, 1940).

[8] G. Gamow and C. L. Critchfield, *Theory of the Atomic Nucleus and Nuclear Energy Sources* (Clarendon Press, Oxford (in print)).

*** Actually, this multiplet is possible only for nuclei with $A = 4n$.

nucleus not be bound is

$$B(A, Z)-B(A+1, Z)=0, \quad (5a)$$

or if we consider A and Z as continuous variables, this condition may be written as

$$(\partial B/\partial A)_Z=0. \quad (5b)$$

By combining Eqs. (2)–(5) we get a relation between the maximum T and A. The equation has been solved numerically for various values of A. Surprisingly enough, the acceptable solution gives a near linear relation between T_M and A, as is shown in Fig. 1. The relation can be expressed quite accurately by the empirical formula

$$T_M=0.183A+1.6. \quad (6)$$

A convenient approximation to the above formula is that nuclei which are about 70 percent neutrons are just at the limit of neutron stability.

The next step is to determine the total energy available for β-decay. This is

$$W_0=\Delta B+\Delta M, \quad (7)$$

where ΔB is the difference in binding energy of the initial and final nuclei, ΔM is the neutron-proton mass difference, and m_0 is the electron rest mass. In this instance,

$$\Delta B=B(A, Z)-B(A, Z+1)$$
$$=B(A, T_M)-B(A, T_M-1), \quad (8)$$

so that W_0 can be computed for any A by combining Eqs. (2), (3), (4), and (6).

For $W_0/m_0c^2\gg 1$, the decay constant for a nucleus of mass A and charge Z is given by

$$\lambda_A=[\gamma(Z, W_0)/\tau_0]|M|^2(W_0^5/30), \quad (9)$$

where W_0 is given in units of m_0c^2, M is the matrix element for the transition, $\gamma(Z, W_0)$ is a function showing the effect of the Coulomb field on the electron emission, and τ_0 is a constant, approximately equal to 8800 seconds. This expression must be summed over all excited levels of the daughter nucleus to obtain the total decay constant. As the parent and daughter nucleus belong to different multiplets, these transitions are all unfavored on the basis of Wigner's theory. However, for $A>40$, any given state of a nucleus is a mixture of several multiplet states because of the Coulomb perturbations; this means there is no longer any clear-cut distinction between favored and unfavored transitions. We shall assume that there is always one final state with an M much larger than the others, so that we need consider only this possibility if the corresponding energy release is large enough. We shall also assume that the shape of the nuclear wave function is mainly determined by the kinetic energy of the particles so that the most probable transition is the one in which there is no change in kinetic energy.[9] Then, instead of Eq. (7), an alternative formula may be used to compute the actual β-disintegration energy.

$$W_\beta=\Delta C+\Delta P+\Delta M. \quad (10)$$

For transitions between the ground states of parent and daughter nuclei, the spin—isotopic spin part of the matrix element is $2T_M$ for Fermi selection rules and $6T_M$ for Gamow-Teller selection rules. For transitions to excited states, the matrix element is somewhat less but still proportional to T_M. We shall assume $2T_M$ as a reasonable value. The orbital part of the matrix element for unfavored but allowed transitions has been estimated to be about 1/25.[8] Using these results, we obtain as a final expression for the disintegration probability of the T_M nuclei

$$\lambda_A(T_M)=(\gamma T_M W_\beta^5/375\tau_0), \quad W_\beta/m_0c^2\gg 1. \quad (11)$$

The results are tabulated in Table I. The values for γ were obtained from the charts in Konopinski's article on β-decay.[10]

We see that the mean β-lifetime for the neutron saturated nuclei is about 0.1 second and is practically independent of A.

In order to find the nuclear abundance trend that such a λ-behavior predicts, it is necessary to examine the solutions of the differential Eqs. (1). These equations are well known as those governing a family of radioactive substances. Bateman[11] has investigated their solutions for λ independent of t and for various boundary conditions. The feature of the solutions of most importance to us is that for large t, $N_A\sim 1/\lambda_A$ (corresponding to radioactive equilibrium).

One would like to assume that the formation process was carried out to equilibrium because then the critical dependence on time could be eliminated. But we have seen that at high densities the λ_A's are practically constant for $A>50$. An equilibrium solution would not show the hundred-fold decrease in abundance between mass 50 and mass 100. On the other hand, if the process were cut off before equilibrium was attained, the heavy elements would show a rapid decrease in abundance with A. It seems therefore that a neutron capture process at high density with β-decay controlling the rate of formation is incapable of explaining even the primary features of the abundance curve. The poor results for $A>50$ make it unnecessary to compute decay constants for $A<50$.

The transition from high to intermediate density occurs when the density is such that the capture

[9] This hypothesis has been checked for some β-emitters, such as N^{16} and O^{19}, where the total and transition energies are known. The agreement is reasonably good.

[10] E. J. Konopinski, Rev. Mod. Phys. 15, 209 (1943).

[11] H. Bateman, Proc. Camb. Phil. Soc. 15, 423 (1910).

TABLE I. λ_A for (A, T_M) nuclei.

A	T_M	$W_\beta(m_0c^2)$	W_β	γ	$\lambda_A(\text{sec.}^{-1})$
50	10.8	17.3	15.5×10^5	1.37	6.9
64	13	16.5	12.2×10^5	1.55	7.4
100	20	16.3	11.5×10^5	1.93	13.5
125	24.5	14.7	6.9×10^5	2.32	11.8
180	34.5	11.6	2.1×10^5	3.48	7.6

probabilities near neutron saturation are equal to the β-decay probabilities. For lower densities, the β-decays will occur before the limit of neutron stability is reached. To fix the lower limit of the high density case, we note that the capture probability for 0.1 Mev neutrons may be written

$$\lambda_c(A)=n\sigma_A v\cong 3\times10^8\rho\sigma_A, \tag{12}$$

if σ_A, the neutron capture cross section for the nucleus of mass A, is given in barns and ρ is the density in grams per cubic centimeter. Hughes' experimental data[12] for 1-Mev neutrons indicate that the capture cross sections of a stable nucleus is about 10^{-4} barns for $A\sim15$, rises exponentially to 0.1 barn at $A\sim100$, and remains roughly constant thereafter. The cross sections for the nuclei near neutron saturation are considerably less; we shall assume that they are reduced by a factor of about 1000 from an argument to be given in the next section. Assuming that the σv product is a slowly varying function of energy near 1 Mev, we find $\rho=10^{-1}$ g/cm^3 the lower limit to the high density conditions. For densities equal to or greater than this, all of the nuclei would have been formed with β-decay as the rate controlling agent. Since we have seen that the high density case does not explain the shape of the abundance curve, we assume that most of the formation process must have been carried out at a density less than 0.1 g/cm^3.

IV. THE FORMATION PROCESS AT INTERMEDIATE DENSITIES

A study of the problem of element formation at intermediate densities must necessarily be more detailed than a discussion of the high density conditions. In particular, one must consider both β-decay probabilities and capture probabilities for each individual nuclear species. Since both of these quantities depend upon energy differences between neighboring nuclei, a detailed knowledge of the features of the nuclear energy surface is required. We have already seen that the β-decay probability varies with the fifth power of the transition energy. The capture probability depends in turn upon the excitation energy of the compound nucleus formed when the neutron is captured; the nature of the dependence is not known exactly. However, we have

$$E=E_n+B_n, \tag{13}$$

where E is the excitation energy, E_n the neutron kinetic energy, and B_n the binding energy of the neutron in the compound nucleus. (Here we consider B_n positive if the neutron is bound.)

We shall now try to show that the formation process follows a path along the nuclear energy surface such that the β-decay probabilities and capture probabilities are approximately equal. As a specific example, consider an O^{16} nucleus in the neutron gas. The first three events that occur will be captures as O^{17} and O^{18} are stable. The next nucleus to be formed, O^{19}, may either β-decay to F^{19} or capture a neutron and become O^{20}. If O^{20} is formed, then it has the possibility of becoming either F^{20} or O^{21} and so on. The important feature of the process is that successive neutron captures carry us into a region of increased β-decay energy and decreased neutron binding energy. On the other hand, successive β-decays carry us into a region of low β-transition energy and high neutron binding energy.

We may picture the building of heavier and heavier nuclei as represented by a path traced along the floor and slopes of the Heisenberg valley. The allowed moves are $\Delta A=1$, $\Delta N=1$ (neutron capture) and $\Delta Z=1$ (β-decay). From the discussion in the preceding paragraph, it is apparent that, regardless of the initial starting-point, the path first moves toward a region where the capture and β-decay probabilities are equal. When this region is reached, the formation then follows a path such that $\lambda(\text{capture})\cong\lambda(\beta\text{-decay})$. At first thought, it might seem that there would be enough branching, i.e., enough times when the less probable event happens first to make the actual process very complicated to follow in detail. However, by the same argument, it can be shown that the branches always tend to return and unite with the main path.

The probability of β-decay is independent of the physical conditions, while the capture probability increases linearly with the density. Thus the particular path which the formation process follows depends upon the physical conditions existing at the time. The higher the density, the nearer the path will be to the neutron saturation limit. Also, variations in capture cross section, excluding the dependence on excitation energy, will be effective in determining the path of formation. Alpher[3] has already pointed out the inverse relationship that exists between the relative abundance of a nuclear species and its neutron capture cross section.

The cross section for radiative capture of a neutron may be written

$$\sigma(n,\gamma)=\sigma_n(\bar{\Gamma}_\gamma/\bar{\Gamma}_\gamma+\bar{\Gamma}_n), \tag{14}$$

if one assumes that the only two competing processes are capture and scattering. σ_n is the cross section for formation of the compound nucleus, $\bar{\Gamma}_\gamma$

[12] D. J. Hughes, Phys. Rev. 70, 106A (1946).

is the average radiation width, and $\bar{\Gamma}_n$ the average neutron width of the excited state. The quantities with subscript n are averaged over different angular momentum states. For neutrons of 0.1 Mev, the inelastic scattering can be neglected; then the formation of the compound nucleus and the emission of a neutron are inverse processes. Weisskopf[13] has shown that under such conditions $\sigma_n \propto \bar{\Gamma}_n$. Then if $\bar{\Gamma}_n \gg \bar{\Gamma}_\gamma$, $\sigma(n,\gamma) \propto \bar{\Gamma}_\gamma$. Reference 13 also indicates that $\bar{\Gamma}_\gamma$ varies as E^5 for transitions to the ground state and as E^6 if there are appreciable transitions to excited states. Apparently the capture probability has about the same dependence on E as the β-decay probability has on W_β.

If the topography of the nuclear energy surface were known accurately enough, so that values of W_β and B_n were available for all nuclei below the neutron saturation line, one could map out the path of formation that was followed in building the heavy elements from the light ones. All that would be necessary would be to begin with some logical initial nucleus and proceed by β-decay and neutron capture moves, the particular move depending on the relative size of $T_\frac{1}{2}[W_\beta(A,Z)]^5$ and $n[E(A+1,Z)]^5$. The average neutron density, n, could be estimated by seeing which value of n gave the best fit to the abundance curve. However, there is at present no method of estimating W_0 and E accurately enough to make such a computation profitable.

One easily noticeable feature of the relative abundance data is that nuclei of even A are in general more abundant than those of odd A. Alpher has pointed out that it is not correct to use the even-odd variation in capture cross sections to explain the even-odd variation in abundances, because the nuclei were formed with a different neutron-proton ratio than they now have. We shall show here that an abundance of nuclei of even A over those of odd A is a consequence of the neutron capture theory, regardless of the neutron excess at formation.

The behavior of W_0 and B_n as functions of A and Z is tabulated below:

A	W_0
Odd	decreases monotonically with increasing Z.
Even	decreases with increasing Z but values for odd Z are larger than for even Z.
Z	B_n
Odd	decreases with increasing A, values for odd A are larger.
Even	decreases with increasing A, values for even A are larger.

Remembering that the formation takes place in a region where β-decay and capture are about equally probable, and that the respective probabilities for the nuclear species (A,Z) depend on $W_0(A,Z)$ and $B_n(A+1,Z)$, we can estimate which process is favored for different types of nuclei.

A	Z	Most probable event
Odd	Odd	β-decay
Odd	Even	Capture
Even	Odd	No choice
Even	Even	No choice

Thus there is a tendency for each nuclear species to be formed with even Z. This is a sufficient condition for the formation of more even nuclei than odd, as can be seen by observing the variation of B_n with A for even Z nuclei.

We have previously rejected the possibility of the formation process having taken place under low density conditions because of the high β-lifetimes involved. However, we can obtain a practical lower limit to the intermediate density case by assuming the formation path to run along the Heisenberg valley, detouring the very long-lived β-emitters such as P^{32}. The mean β-lifetime in this region is about 1000 seconds. This leads to 10^{-11} g/cm^3 as the minimum density at which the entire process could occur under intermediate density conditions.

The limits of 10^{-1} and 10^{-11} g/cm^3 on the density during formation are in agreement with the results obtained by Alpher and Herman[4] by fitting the abundance curve. Alpher and Herman computed the N_A as a function of A, using the capture probabilities alone. As we have shown that the formation occurs under conditions such that $\lambda(\text{capture}) \cong \lambda(\beta\text{-decay})$, this procedure is justified for obtaining the general behavior of the relative abundance curve. In order to compute individual relative abundances, however, it would be necessary to consider both probabilities.

V. THE FORMATION OF LIGHT ELEMENTS

It seems worthwhile to add a note concerning the formation of light elements. There are two special features of the formation process at small A. First, since no stable nuclei of atomic weights 5 and 8 exist, some reaction other than neutron capture will be necessary to bridge the gap at these points. Second, for $A<16$ and at energies of 10^6 electron volts, there are many reactions which can compete favorably with neutron capture and all of these must be considered in computing nuclear abundances.

The long (12 year) half-life of H^3 makes it impossible to build even as far as He^4 by the neutron capture theory unless H^4 is not a neutron emitter, and this seems very unlikely. Apparently a description of the formation process up to He^4 must take into account all possible combinations of reactions involving neutrons, protons, deuterium,

[13] V. Weisskopf, *Lecture Series in Nuclear Physics* (Government Printing Office, Washington, D. C., 1947), p. 112.

tritium, He^3, and α-particles. To build across the mass 5 and 8 gaps, it is necessary to assume triple collisions such as α—n—n and α—α—n and processes such as $Li^7(\alpha, n)B^{10}$. Difficulties of another type arise at masses 10 and 14. Be^{10} and C^{14} both have half-lives of more than 1000 years while Be^{11} and C^{15} are probably neutron unstable. From $A=15$ on, there seem to be no breaks in the formation chain due to nuclear instability or long-lived β-emitters which cannot be bypassed.

The formation of the elements then appears to be divided into two distinct parts. For $A>16$, the process is essentially one of building heavy nuclei by successive neutron captures interspersed by β-decays. In this region, there are two other reactions which are of some importance to the formation process. They are the nuclear photo-effect, which may be responsible for the creation of isobars,[6] and fission in the heaviest elements, which sets an upper limit on the size of nuclei formed. For $A<16$, there are many types of reactions having probabilities of the order of magnitude of the neutron capture probability, and any attempt to compute the relative abundances of light elements must consider all of them.

VI. ACKNOWLEDGMENTS

The writer is greatly indebted to Professor C. L. Critchfield for suggesting and guiding this research. He is also indebted to Drs. R. A. Alpher and R. C. Herman for the privilege of seeing some of their results before publication. The experimental relative abundance data used in making calculations were kindly furnished by Dr. Harrison Brown.

PHYSICAL REVIEW VOLUME 75, NUMBER 9 MAY 1, 1949

Tensor Forces and the Triton Binding Energy*

HERMAN FESHBACH
Department of Physics, Massachusetts Institute of Technology, Cambridge, Massachusetts

AND

WILLIAM RARITA**
Physics Department, Brooklyn College, Brooklyn, New York

(Received January 6, 1949)

The binding energy of the triton has been calculated variationally employing the Hylleraas expansion for the trial wave functions, thus permitting a systematic improvement in the binding energy. The procedure used was tested by applying it to the binding energy problem of the deuteron with tensor forces. The present theory, assuming a rectangular-well shape with a range of 2.8×10^{-13} cm for all the internucleon potentials, yields a H^3 binding energy 40 percent to 50 percent of the experimental value. Various suggestions for resolving this dilemma are discussed.

I. INTRODUCTION

THE explanation of the properties of the triton is a severe test of the phenomenological theory of nuclear forces. Prior to the introduction of tensor forces, its calculated[1] binding energy was in good agreement with experiment. It was realized at an early date by Inglis[2] that this situation might be substantially altered when tensor forces are included in spite of the rather complete explanation of two-body problems[3] afforded by the Rarita-Schwinger theory. In the H^3 problem, their interaction potential, a rectangular well, is tested for larger relative momenta of the constituent nucleons. Inglis' argument was based on perturbation theory. A more complete discussion has been given by Gerjuoy and Schwinger,[4] using the variational method with results in substantial agreement with Inglis. It is the aim of the present paper to enlarge the scope of the former's work by the use of the method of Hylleraas which has been applied successfully to problems of this type in the past.[1] We shall use the two-body law of force as given by Rarita and Schwinger.[5] Their results do not determine the exchange character of the nuclear force but this property does not enter crucially into our discussions. The main conclusion of the present paper is that the simple theory which works so well

* Assisted by the joint program of the ONR and the AEC.
** This work was done while the second author (W.R.) was in residence at Massachusetts Institute of Technology. He takes this opportunity to express his appreciation for the hospitality shown him during his stay there.

[1] W. Rarita and R. D. Present, Phys. Rev. **51**, 788 (1937).
[2] David R. Inglis, Phys. Rev. **55**, 988 (1939).
[3] See for example: Bailey, Bennet, Bergstralh, Nuckolls, Richards, and Williams, Phys. Rev. **70**, 583 (1946). Russell, Sachs, Wattenberg, and Field, Phys. Rev. **73**, 545 (1948). R. Wilson, C. H. Collie, and H. Halban, Nature **162**, 185 (1948).
[4] E. Gerjuoy and J. Schwinger, Phys. Rev. **61**, 138 (1941).
[5] W. Rarita and J. Schwinger, Phys. Rev. **59**, 436 and 556 (1941).

for two-body problems fails for H^3. We shall discuss some possible modifications in the concluding section.

II. TRITON BINDING ENERGY

We shall employ the relative coordinates $\mathbf{r}_1$, $\mathbf{r}_2$, $\boldsymbol{\rho}$ illustrated in Fig. 1. After the coordinates of the center of mass are eliminated the Hamiltonian for this problem may be expressed in terms of these coordinates:

$$H=-(\hbar^2/M)(\nabla_1^2+\nabla_1\cdot\nabla_2+\nabla_2^2) + V(r_1)+V(r_2)+V(\rho). \quad (1)$$

The potential energy V is

$$V(\rho)=-\{1-\tfrac{1}{2}g+\tfrac{1}{2}g\sigma_1\cdot\sigma_2+\gamma S_{12}\}J(\rho). \quad (2)$$

Here σ_i is the Pauli spin vector associated with the ith particle, and

$$S_{12}=[3(\sigma_1\cdot\boldsymbol{\rho})(\sigma_2\cdot\boldsymbol{\rho})/\rho^2]-\sigma_1\cdot\sigma_2. \quad (3)$$

$V(r_1)$, the potential between particles 1 and 3 is obtained by replacing σ_2 by σ_3 in (2) and (3) and $\boldsymbol{\rho}$ by $\mathbf{r}_1$. The constants g and γ, are given by Rarita and Schwinger[5] for a rectangular potential well of depth V_0 and range r_0:

$$g=0.0715,\quad \gamma=0.775,$$
$$V_0=6.40\times\text{binding energy of the deuteron}, \quad (4)$$
$$r_0=2.80\cdot10^{-13}\text{ cm}.$$

The ground state of H^3 has a total angular momentum of $\frac{1}{2}\hbar$. For a three-particle system the possible orbital angular momentum states are S, P, D. The S states must be doublets, the D states quartets, while the P states may be either doublet or quartets. The angular and spin dependence may be removed either in terms of the Eulerian angles associated with the plane containing the three particles[6] or much more conveniently by the use of spin operators as performed by Gerjuoy and Schwinger. From the measured magnetic moment[7] of H^3, it may be seen that the principal state is an S state. Of the two S states which can be formed, the most important will be that one symmetric in r_1 and r_2; its angular and spin dependence will be represented by $^2S_{\frac{1}{2}}^0$; the other S state $^2S_{\frac{1}{2}}^1$ will be antisymmetric in r_1 and r_2. In virtue of Hamiltonian the $^2S_{\frac{1}{2}}^0$ state will interact directly with the $^2S_{\frac{1}{2}}^1$ state and with the $^4D_{\frac{1}{2}}$ states. These latter may be formed as shown by Gerjuoy and Schwinger from the four operators which may be realized by combining the dyadic $\sigma_1\sigma_3$ with the space dyadics $\mathbf{r}_1\mathbf{r}_1$, $\mathbf{r}_1\mathbf{r}_2$, etc. However, it has been shown by L. H. Thomas[8] that an identity exists between these four so that there are

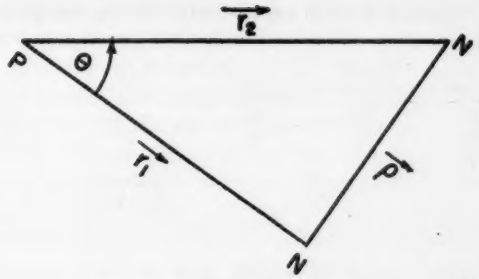

FIG. 1. Coordinates for H^3.

only three independent D states, which we shall call $^4D_{\frac{1}{2}}^0$, $^4D_{\frac{1}{2}}^1$, $^4D_{\frac{1}{2}}^2$. This may be verified directly using the more explicit Eulerian angular dependence.[9] Only one of these D states has a dependence on r_1 and r_2 which is even in their exchange:

$$^4D_{\frac{1}{2}}^0=(r_1^2S_{13}+r_2^2S_{23})\,{}^2S_{\frac{1}{2}}^0. \quad (5)$$

It will be assumed here as in Gerjuoy and Schwinger that this state is the principal one combining with the ground state $^2S_{\frac{1}{2}}^0$. The qualitative argument upon which this is based relies on the fact that the $^4D_{\frac{1}{2}}^{1,2}$ states are odd in the exchange of r_1 and r_2 and thus must have a node whenever $r_1=r_2$, i.e., whenever the two neutrons are close together. From the short range character of the forces it follows that $V(\rho)$ will have relatively little average value for these states. A similar argument may be applied to the $^2S_{\frac{1}{2}}^1$ state which is known to be present in a relatively small amount in the ground state of H^3.

We therefore write for the wave-function Ψ:

$$\Psi=f\,{}^2S_{\frac{1}{2}}^0+g\,{}^4D_{\frac{1}{2}}^0, \quad (6)$$

where f and g will depend only upon r_1, r_2, and ρ. Finally

$$^2S_{\frac{1}{2}}^0=(1/8\pi)^{\frac{1}{2}}\alpha(3)[\alpha(1)\beta(2)-\beta(1)\alpha(2)], \quad (7)$$

where α and β are the usual spin functions. Expression (6) may now be introduced into the variational principal to obtain the energy E:

$$E=(\Psi, H\Psi)/(\Psi, \Psi). \quad (8)$$

The explicit expressions are given in the Appendix.

The functions f and g were determined by the method of Hylleraas. The functional forms assumed first were

$$f=A\exp[-\lambda(r_1+r_2)-\nu\rho],$$
$$g=B\exp[-\mu(r_1+r_2)-\sigma\rho]. \quad (9)$$

When a variational function of the type f is used in the Rarita-Present theory, one obtains immediately 90 percent of the binding energy of H^3, which indicates that it is an excellent description of the S state. Once the proper values of λ, μ, ν, σ are determined both f and g are to be multiplied

[6] E. C. Kemble, *The Fundamental Principles of Quantum Mechanics* (McGraw-Hill Cook Company, Inc., New York, 1937), p. 230.
[7] H. Anderson and A. Novick, Phys. Rev. 71, 372 (1947).
[8] Private communication.
[9] Herman Feshbach, Phys. Rev. 61, 544A (1942).

TABLE I. Percent experimental binding energy.

Nucleus	S state (no tensor forces)	S and D	S	D
H^2	74	66	−46	112
H^3	70	32	18	14
H^3			28 Equivalent Two Body	

by power series in r_1, r_2, and ρ. For variational functions (9) it was found that $\lambda \simeq \nu$ and $\sigma \sim 0$ although equalities did not occur precisely at the minimum. However, because the difference in binding energy involved was slight (about 3 percent) the simpler expressions obtained by assuming equality were used with

$$\lambda = \nu = 1.5/r_0; \quad \sigma = 0; \quad \mu = 5.0/r_0. \tag{10}$$

The binding energy found using function (10) was 32 percent of the experimental binding energy, and the percent D state = 1.7 percent.

The next step involved the use of the Hylleraas expansion for both f and g. In the present calculation terms up to the squares of r_1+r_2, and ρ and their crossproducts were included. Thus ten more terms, five for the S state and five for the D state were considered. *No marked improvement in the binding energy was obtained when the coefficients of these terms were varied, indicating that form (9) was already a good approximation to the correct wave functions.* The final value for the calculated H^3 binding energy was 40 percent of the experimental value.

To buttress this conclusion, we have checked upon our results by comparing with similar calculations for the deuteron and by employing the equivalent two body[10] method to estimate the contribution of the S state to the total energy. These results, are summarized in Table I.

We have given our results for the case of the simple function (10). For the more complicated Hylleraas expansion, we estimate that the entries in columns (3) and (4) for H^3 would change to 21 and 19, respectively.

The first column S gives the energy computed using the potential energy required to obtain the binding energy of H^2 before the discovery of the deuteron quadrupole moment, and thus in the absence of tensor forces. The second column yields the total energy when potential energy (2) is used. The decomposition in the third and fourth columns gives the energy obtained from the S state alone and the energy obtained from the D state together with the coupling energy between the S and D states.

We first note that the equivalent two body method gives for the binding energy from the S state alone, the value 28 percent of the experimental binding energy of H^3. This value is to be compared with 18 percent for the trial function (10) and 21 percent for the Hylleraas expansion, remembering that the two body method may give a value 10 to 15 percent too large in absolute value. The rough agreement obtained indicates that our representation of the S state is excellent. No such check is available for the D state energy so that we must rely on the indirect evidence offered by the above S state comparison, and the data in the table. Here we see that for the simplest variational form used for H^2 the energies computed with and without tensor forces are very close. Moreover when a power series expansion was added on to the deuteron wave functions the rate of improvement was similar to that obtained for H^3 with the Hylleraas expansion. We would like to emphasize the drastic change in the comparison between the computed energies for the binding energy of H^3 with and without tensor forces. Moreover the decomposition in S and D energy given in columns (3) and (4) lends additional weight that no gross inaccuracy can be ascribed to our final values.***

As a final check, the contribution of the $^2S_{\frac{1}{2}}{}^1$ state was computed using form (10) for the $^2S_{\frac{1}{2}}{}^0$ and $^2D_{\frac{1}{2}}{}^0$ terms. The $^2S_{\frac{1}{2}}{}^1$ state couples directly to the $^2S_{\frac{1}{2}}{}^0$ state. It is fairly representative of the many omitted states noted above. We then let

$$\Psi = f\,{}^2S_{\frac{1}{2}}{}^0 + g\,{}^4D_{\frac{1}{2}}{}^0 + h\,{}^2S_{\frac{1}{2}}{}^1. \tag{11}$$

The function h must be odd in exchange of r_1 and r_2 so that as in Rarita and Present h must be taken proportional to r_1-r_2. Then

$$h = D(r_1-r_2)\exp[-\alpha(r_1+r_2+\rho)],$$

where D and α are to be determined variationally. The resulting increase in binding energy is only 0.4 percent indicating that these additional terms will not affect the binding energy of H^3 to any great extent. We thus conclude that the computed binding energy of H^3 employing nuclear potentials (2) and (4) is not appreciably greater than 40 percent of the experimental value.

III. DISCUSSION

It is appropriate now to discuss some of the possible changes in the internucleon potentials which might bring the theoretical value for the binding energy of H^3 into agreement with experiment. One might hope to resolve the difficulty by (1) keeping the Rarita-Schwinger potential intact

[10] Eugene Feenberg, Phys. Rev. **47**, 850 (1935); **48**, 906 (1935).

*** One of us (W.R.) has used a joining method (described Phys. Rev. **74**, 1799 (1948)), to compute the binding energy. Here f and g are assumed to have different radial dependence inside and outside of an arbitrary radius. The best binding thus obtained was 36 percent.

and adding forces which are of some importance in H^3 and of relatively little importance in H^2, and (2) changing the shape and range of the interaction potential.

Considering method (1) first, a measure of the additional potential required is given by the ratio τ of the V_0 needed to the V_0 used in (4). We estimate $\tau \sim 1.1$. Such additional potentials can in principle arise from relativistic effects since v^2/c^2 of a nucleon in H^3 is appreciable. Relativistic effects include three body forces[11] beside relativistic corrections[12] to two body forces. The latter will probably be made available as a result of experiments on high energy neutron-proton scattering. It should be noted however that such additional potentials as contemplated above would not correct other difficulties of the Rarita-Schwinger interaction potential.[13]

In category (2) we have investigated briefly the effects of a change in range, or shape, or both, of the interaction potential. *Decreasing* the range of *both* the central and tensor forces *decreases* the calculated binding energy of H^3. For example using the range[14] $2.66 \cdot 10^{-13}$ cm with a rectangular well potential for $J(r)$, the calculated binding energy of H^3 decreases to 24 percent of the experimental value for the same trial functions which yield 32 percent. The qualitative reason for this behavior may be given. Reducing the range requires a greater relative amount of tensor force, i.e., a greater γ, for only in this way is it possible to obtain the experimental quadrupole moment for the deuteron. However a large γ requires a smaller V_0 (in order to obtain the experimental binding energy of the deuteron), leading to a reduction in the calculated binding energy of H^3. Since present two body data requires, if anything, a reduction in range, changing the range of both central and tensor forces does not seem to be a fruitful idea.

Another possibility then would involve maintaining the range of the central force to that given by p–p scattering data, but using a longer range tensor force. Primakoff and Feenberg[15] have pointed out that by taking the tensor range sufficiently long the tensor force would have no effect on binding energy problems, so that the binding energy problem would return to the pre-tensor situation. Here however a difficulty encountered by Rarita and Present would recur, for although H^3 binding would be precisely correct, the calculated binding energy for He^4 would be too large. This has been verified for other potential wells by Svartholm.[16] It is essential, therefore that the tensor force be of sufficient strength as to effect the binding of H^2 considerably, of H^3 somewhat, and of He^4 not at all. This adjustment is very sensitive to the *shape* of the interaction potential.†

Finally one might give up the luxury of charge independent nuclear forces as suggested by Blatt.[13] It would be necessary to keep the (n–n) and (p–p) forces the same because of evidence obtained from the energy differences of mirror nuclei, particularly the H^3–He^3 binding energy difference. It is, however, possible to reduce the range of either the singlet n–p force or the central (non-tensor) part of the triplet (n–p) force. It should be noted that such an interaction potential would in addition yield results closer to the present scattering data than the Rarita-Schwinger ansatz.

ACKNOWLEDGMENT

We are indebted to Miss Hannah Paul for computational aid.

APPENDIX

Variational Calculation for the Deuteron

The deuteron serves as a useful introduction and control to the more difficult triton problem. The energy E of the deuteron ground state is

$$E\int_0^\infty [(Au)^2+(Bw)^2]dr$$
$$=\int_0^\infty \{[d(Au)/dr]^2 - JA^2u^2 - 4\sqrt{2}\gamma JABuw$$
$$-(1-2\gamma)JB^2w^2+(6B^2w^2/r^2)+[d(Bw)/dr]^2\}dr. \quad \text{(A1)}$$

Here Au/r is the S radial wave function and Bw/r is the D radial function. Varying the coefficients leads to a secular equation

$$\|E_{ij}\|=0, \quad E_{ij}=P_{ij}-L_{ij}-EN_{ij}. \quad \text{(A2)}$$

Using the binding energy of the deuteron $|E_0|$ as the unit of energy:

$$P_{11}=1/\alpha^2\int_0^\infty (du/dr)^2dr, \quad \alpha^2=M|E_0|/\hbar^2,$$
$$P_{12}=0,$$
$$P_{22}=1/\alpha^2\int_0^\infty [(dw/dr)^2+6(w^2/r^2)]dr, \quad N_{11}=\int_0^\infty u^2dr,$$
$$L_{11}=\int_0^\infty Ju^2dr, \qquad N_{12}=0, \quad \text{(A3)}$$
$$L_{12}=2^{\frac{1}{2}}\int_0^\infty \gamma Juwdr, \qquad N_{22}=\int_0^\infty w^2dr,$$
$$L_{22}=\int_0^\infty (1-2\gamma)Jw^2dr.$$

Let J be the rectangular well. Use r_0, its range, as the unit of distance. Let $u=re^{-\lambda r}$, $w=r^3e^{-\mu r}$. All the integrals are easily

---

[11] H. Primakoff and T. Holstein, Phys. Rev. **55**, 1218 (1939).
[12] Gregory Breit, Phys. Rev. **56**, 153 (1938).
[13] D. Bohm and C. Richman, Phys. Rev. **21**, 567 (1947); J. Blatt, Phys. Rev. **74**, 92 (1948).
[14] William G. Guindon, S.J., Phys. Rev. **74**, 145 (1948).
[15] Henry Primakoff, Phys. Rev. **72**, 118 (1947).
[16] N. Svartholm, Thesis.

† Since the calculations reported here were completed, one of us (H.F.) has shown that a potential

$$V(\rho)=-[(1-\tfrac{1}{2}g)+\tfrac{1}{2}g\sigma_1\cdot\sigma_2]V_c(\rho)+S_{12}V_\tau(\rho)$$
$$V_c=V_{0c}(e^{-\mu\rho}/\mu\rho) \quad V_\tau=V_{0\tau}(e^{-\tau\rho}/\tau\rho)$$
$$\mu=326\ \text{mc}/\hbar \quad \tau=\mu/1.8$$

yields on a variational calculation 85.5 percent of the experimental H^3 binding.

evaluated. The integrals involved are of the form

$$\int_0^1 r^n e^{-\nu r} dr = I_n^{\nu}, \quad \int_0^\infty r^n e^{-\nu r} dr = S_n^{\nu}. \tag{A4}$$

Variational Calculation for H^3

We list the elements of the matrices P_{ij}, L_{ij}, N_{ij}. The determinant is, of course, of the form (A2). The elements P_{11}, L_{11}, and N_{11} listed first are well known being given in Rarita and Present.

$$P_{11}=\int\left\{\left(\frac{\partial f}{\partial r_1}\right)^2+\left(\frac{\partial f}{\partial r_2}\right)^2+\left(\frac{\partial f}{\partial \rho}\right)^2+\frac{\mathbf{r}_1\cdot\mathbf{r}_2}{r_1 r_2}\frac{\partial f}{\partial r_1}\frac{\partial f}{\partial r_2}+\frac{\mathbf{r}_1\cdot\mathbf{r}_{21}}{r_1\rho}\frac{\partial f}{\partial r_1}\frac{\partial f}{\partial \rho}+\frac{\mathbf{r}_2\cdot\mathbf{r}_{12}}{r_2\rho}\frac{\partial f}{\partial r_2}\frac{\partial f}{\partial \rho}\right\}d\tau;$$
$$d\tau=4r_1r_2\rho dr_1dr_2d\rho. \tag{A5}$$

$$L_{11}=(1-2g)L^S(12)+(1-g/2)[L^S(13)+L^S(23)],$$
$$L^S(12)=\int f^2J(\rho)d\tau, \quad L^S(13)+L^S(23)=\int f^2[J(r_1)+J(r_2)]d\tau.$$

The coupling term E_{12} is:

$$E_{12}=-2\gamma\int f\,{}^3S_1^0 J(r_1) g\,{}^3D_1^0 d\tau$$
$$=-2\gamma\int fJ(r_1)g[6r_1^2+(3-9\cos^2\theta)r_2^2]d\tau. \tag{A6}$$

The kinetic energy for the D state P_{22} is:

$$-P_{22}=(g\,{}^4D_1^0|\nabla_1^2+\nabla_1\cdot\nabla_2+\nabla_2^2|g\,{}^4D_1^0)$$
$$=\int\left\{\left[\frac{g}{r_1^2}\frac{\partial}{\partial r_1}\left(r_1^2\frac{\partial g}{\partial r_1}\right)+\frac{g}{r_2^2}\frac{\partial}{\partial r_2}\left(r_2^2\frac{\partial g}{\partial r_2}\right)+\frac{g}{\rho^2}\frac{\partial}{\partial\rho}\left(\rho^2\frac{\partial g}{\partial\rho}\right)\right.\right.$$
$$+\frac{\mathbf{r}_1\cdot\mathbf{r}_{21}}{r_1\rho}g\frac{\partial^2 g}{\partial r_1\partial\rho}+\frac{\mathbf{r}_2\cdot\mathbf{r}_{12}}{r_2\rho}g\frac{\partial^2 g}{\partial r_2\partial\rho}$$
$$\left.+\frac{\mathbf{r}_1\cdot\mathbf{r}_2}{r_1r_2}g\frac{\partial^2 g}{\partial r_1\partial r_2}+\frac{2}{\rho}g\frac{\partial g}{\partial\rho}\right](^4D_1^0/{}^4D_1^0)$$
$$+[6r_1^4+3r_1^2r_2^2(1-3\cos^2\theta)]\frac{4g_1}{r_1}\frac{\partial g}{\partial r_1}$$
$$\left.+[6r_2^4+3r_1^2r_2^2(1-3\cos^2\theta)]\frac{4g}{r_2}\frac{\partial g}{\partial r_2}\right\}d\tau, \tag{A7}$$

where $(^4D_1^0|{}^4D_1^0)=6[r_1^4+r_2^4+r_1^2r_2^2(1-3\cos^2\theta)]$.

$$L_{22}=[L^D(12)+L^D(13)+L^D(23)]$$
$$+\gamma[L_T^D(12)+L_T^D(13)+L_T^D(23)], \tag{A8}$$

where the subscript T denotes tensor, the terms involved being diagonal values for the D state for the tensor terms.

$$L^D(12)=\int g^2J(\rho)d\tau; \quad L^D(13)=\int g^2J(r_1)d\tau;$$
$$L^D(23)=\int g^2J(r_2)d\tau, \tag{A9}$$
$$L_T^D(13)=\int[6(r_2^4-r_1^2r_2^2-2r_1^4)$$
$$-3(1-\cos^2\theta)(r_2^4+r_1^2r_2^2)]g^2J(r_1)d\tau.$$

For $L_T^D(23)$ make substitutions $r_1\rightleftarrows r_2$ in multiplication factor in square brackets and in $J(r_1)$.

$$L_T^D(12)=\int\left\{12\left[r_1^4+r_2^4+r_1^2r_2^2\left(\frac{3\cos^2\theta-1}{2}\right)\right]\right.$$
$$-\frac{12}{\rho^2}[2r_1^6+2r_2^6+(r_1^2+r_2^2)r_1^2r_2^2$$
$$\left.-3(r_1^4+r_2^4)r_1r_2\cos\theta]\right\}g^2J(\rho)d\tau. \tag{A10}$$

Finally

$$N_{22}=\int g^2d\tau(^4D_1^0/{}^4D_1^0). \tag{A11}$$

Assuming (10) for the D state and the rectangular well shape $N_{22}=(192)(6!)/\mu^{10}$; $P_{22}=(96)(6!)/\mu^8$;

$$L^D(12)=+V_0\left[\frac{8}{21}I_6^{\mu}+(S_4^{\mu}-I_4^{\mu})\right.$$
$$\left.-\frac{24}{35}(S_2^{\mu}-I_2^{\mu})+\frac{1}{15}(S_0^{\mu}-I_0^{\mu})\right];$$
$$L^D(13)+L^D(23)=+96V_0[S_6^{\mu}I_2^{\mu}+S_2^{\mu}I_6^{\mu}];$$
$$L_T^D(12)=V_0\left\{-\frac{32}{49}I_6^{\mu}-\frac{1}{3}(S_6^{\mu}-I_6^{\mu})\right. \tag{A12}$$
$$\left.-(S_4^{\mu}-I_4^{\mu})+\frac{183}{245}(S_2^{\mu}-I_2^{\mu})-\frac{1}{15}(S_0^{\mu}-I_0^{\mu})\right\};$$
$$L_T^D(13)+L_T^D(23)=\mp 96V_0[+S_6^{\mu}I_2^{\mu}-S_4^{\mu}I_4^{\mu}-2S_2^{\mu}I_6^{\mu}].$$

When the more complicated variational function (9) or the Hylleraas expansion are used more difficult integrals appear. Two auxiliary integrals had to be introduced.

$$H_{m,n}^{\alpha,\beta}=\int_0^1 s^m e^{-\alpha s}ds\int_0^s \rho^n e^{-\beta\rho}d\rho,$$
$$G_{l,m,n}^{\alpha,\beta\gamma}=\int_0^1 r_1^l e^{-\alpha r_1}dr_1\int_0^\infty r_2^m e^{-\beta r_2}dr_2\int_{|r_1-r_2|}^{r_1+r_2}\rho^n e^{-\gamma\rho}d\rho, \tag{A13}$$

where $s=r_1+r_2$. By means of recurrence relations these may be reduced to the I and S integrals defined above.

S-Wave Proton-Proton Scattering from 0.2 to 40 Mev for the Yukawa and Gauss Error Potentials

R. D. HATCHER, G. B. ARFKEN, AND G. BREIT
Sloane Physics Laboratory, Yale University, New Haven, Connecticut*
(Received January 28, 1949)

Tables of the phase shift expected for the *S*-wave in proton-proton scattering are presented. The energy range covered is from 0.2 to 40 Mev. The accuracy obtainable by means of them is stated in the text and is believed to be sufficient for most applications. For energies below 5 Mev use is made of the function f which varies nearly linearly with energy. Representations of f in terms of depth and range of the potential wells are studied and some questions arising in comparing potentials with each other and with experiment are briefly discussed.

I. INTRODUCTION AND NOTATION

THE calculation of phase shifts arising in the collision of two protons has been treated by many authors.[1,2] Differences in methods, in intended accuracy of numerical work, in the choice of values of fundamental physical constants, and in the manner of presenting results make it difficult to make use of the material effectively. It was felt, therefore, that there is a need for a set of calculations giving the expected values of the *S*-wave phase shift through the range of energies of probable interest for comparison with experiment. The lower end of this energy range is at[2] about 0.2 Mev for incident protons. Plans of the Berkeley group to experiment at about 30 Mev made it desirable to go somewhat beyond this energy and the calculations have been made, therefore, in the range from 0.2 to 40 Mev.

One of the objects of the present paper is to provide experimental groups with sufficiently complete and simple information to facilitate the interpretation of their results during the progress of the measurements. Presentation of phase shifts in numerical form proved to be the simplest and is probably the most adequate means for this purpose. The more essential data are given in Tables I, II, III. Additional values for other widths and depths of potential energy wells are available. These are useful for improving the interpolation properties of the tables and can be furnished to those needing them. The interpolation properties of the tables are sufficiently good for most purposes. Together with Tables I–V of BTE the numerical formulas listed for each scattering angle therein and supplemented by Eqs. (3.1), (3.2), (3.3) of BTE for other scattering angles the results reported on here make it possible to interpret experimental material without complicated mathematics. The isolation or elimination of effects of phase shifts for angular momenta greater than zero is not taken care of by the material listed. It is partly covered by the work of BTE,[1] BCP,[1] and BKT[2] and has given rise so far only to minor and uncertain corrections.

In order to facilitate interpolation at the lower energies use is made of the function f of BCP. This quantity varies nearly linearly with energy. The intercept, slope, and quadratic coefficient of E for the (f, E) line vary smoothly with convenient combinations of potential well parameters. Representations of these are given below under Eqs. (3) to (4.52) in terms of range and depth times square of range. The square well parameters which reproduce the intercept and slope of the (f, E) curve have been calculated and are given by Eqs. (4.6), (4.7) and the explanations adjoining them. The employment of the f function provided an additional check on the calculation. The distinction between the equivalence of two potential wells for zero energy and for a fit to each other at two energies is discussed and the relation of some fits of potential well parameters to experiment is considered from this viewpoint.

Notation

The notation of this paper is that of BTE[1] and HSB[2] except for the following changes and additions.

Well parameters:

$A/mc^2=A'$, $\alpha\hbar^2/(Mmc^2)=\alpha'$, $C/mc^2=C'$, $amc^2/e^2=a'$.

Bohr collision radius $a_B=\hbar^2/\mu e^2$.

Coulomb functions F_0, G_0 are denoted by F, G, respectively.

Phase amplitude quantities $\tilde{a}$, φ introduced by $F=\tilde{a}\sin\varphi$, $G=\tilde{a}\cos\varphi$.

R = cut-off distance for potential tail.

$r_e=rmc^2/e^2$, $R_e=Rmc^2/e^2$, $b_e=bmc^2/e^2$.

* Assisted by the ONR.

[1] Experimental and theoretical work up to 1939 is summarized by G. Breit, H. M. Thaxton, and L. Eisenbud, Phys. Rev. **55**, 1018 (1939). This paper is referred to in the text as BTE, the experimental work of Herb *et al.* as HKPP, of Tuve *et al.* as HHT.

[2] A more recent collection of references is found in G. Breit and W. G. Bouricius, Phys. Rev. **75**, 1029 (1949). The work of Hoisington, Share, and Breit is referred to as HSB, that of Breit, Broyles, and Hull as BBH, that of Blair, Freier, Lampi, Sleator, and Williams as BFLSW, that of Hoisington and Thaxton as TH, that of Breit, Kittel, and Thaxton as BKT.

TABLE I. Values of phase shift K_0 in degrees for meson potential $-Ce^{-r/a}/(r/a)$. Potential is cut off at $r=3e^2/mc^2$. Notation in headings: $C'=C/(mc^2)$, $a'=a/(e^2/mc^2)$.

E (Mev)	$a'=$ / $C'a'^2=$ / $C'=$	0.4 / 16.32 / 102	0.4 / 15.84 / 99	0.42 / 15.36 / 96	0.4 / 15.81 / 89.6*	0.45 / 17.01 / 84	0.45 / 16.40 / 81*	0.45 / 15.79 / 78*	0.45 / 15.19 / 75*	0.45 / 14.58 / 72	0.5 / 16.50 / 66	0.5 / 15.75 / 63	0.5 / 15.00 / 60	0.55 / 15.73 / 52
0.2		7.79	6.54	5.60	6.71	11.14	8.66	7.00	5.82	4.92	9.56	7.41	5.97	7.85
0.4		17.60	14.70	12.52	15.07	25.22	19.53	15.70	12.98	10.94	21.50	16.60	13.29	17.53
0.6		25.69	21.55	18.40	22.06	35.95	28.28	22.89	19.00	16.09	30.85	24.09	19.39	25.30
**0.8		32.08	27.43	23.27	27.69	43.55	34.97	28.66	23.93	20.32	37.76	30.13	24.33	31.28
1.0		37.09	31.66	27.32	32.25	48.92	40.06	33.25	27.98	23.85	42.85	34.57	28.35	35.88
1.4		44.19	38.38	33.55	38.94	55.63	46.98	39.89	34.11	29.40	49.50	41.07	34.34	42.22
1.8		48.82	43.00	38.02	43.48	59.38	51.28	44.31	38.42	33.46	53.43	45.28	38.47	46.21
**2.0		50.52	44.81	39.79	45.18	60.66	52.81	45.97	40.09	35.09	54.79	46.82	40.06	47.64
2.2		51.93	46.27	41.30	46.67	61.67	54.06	47.36	41.52	36.50	55.87	48.08	41.40	48.81
2.4		53.13	47.56	42.63	47.92	62.45	55.10	48.53	42.77	37.74	56.74	49.16	42.55	49.77
2.6		54.13	48.67	43.79	48.98	63.08	55.96	49.53	43.84	38.83	57.46	50.06	43.55	50.58
3		55.67	50.40	45.63	50.64	63.92	57.20	51.06	45.51	40.57	58.45	51.40	45.09	51.72
4		58.03	53.24	48.78	53.28	64.92	59.00	53.45	48.31	43.61	59.72	53.40	47.57	53.34
5		59.17	54.76	50.59	54.67	65.07	59.71	54.63	49.84	45.38	60.06	54.28	48.86	53.94
6		59.69	55.59	51.69	55.39	64.85	59.91	55.18	50.69	46.46	59.96	54.60	49.52	54.05
7		59.90	56.04	52.33	55.75	64.46	59.86	55.41	51.16	47.13	59.68	54.65	49.82	53.93
8		59.87	56.21	52.70	55.85	63.95	59.62	55.41	51.36	47.50	59.26	54.48	49.90	53.62
9		59.75	56.28	52.90	55.86	63.45	59.32	55.31	51.44	47.72	58.82	54.26	49.87	53.26
10		59.52	56.19	52.95	55.73	62.90	58.96	55.12	51.39	47.81	58.32	53.96	49.73	52.90
12		59.01	55.91	52.88	55.35	61.86	58.20	54.63	51.14	47.77	57.38	53.31	49.35	52.10
14		58.41	55.50	52.64	54.88	60.86	57.43	54.06	50.77	47.57	56.46	52.63	48.87	51.32
16		57.78	55.02	52.30	54.34	59.92	56.67	53.47	50.33	47.27	55.60	51.94	48.36	50.57
18		57.16	54.52	51.93	53.83	59.05	55.92	52.88	49.88	46.94	54.80	51.29	47.85	49.86
20		56.56	54.02	51.52	53.29	58.24	55.25	52.31	49.41	46.57	54.04	50.66	47.35	49.18
22		55.96	53.51	51.10	52.76	57.47	54.58	51.74	48.94	46.19	53.32	50.05	46.84	48.55
24		55.40	53.03	50.70	52.26	56.75	53.96	51.21	48.49	45.82	52.66	49.49	46.37	47.96
26		54.85	52.55	50.28	51.76	56.06	53.35	50.68	48.04	45.44	52.02	48.94	45.90	47.37
28		54.33	52.09	49.88	51.28	55.45	52.85	50.20	47.61	45.07	51.42	48.42	45.45	46.86
30		53.82	51.64	49.48	50.82	54.84	52.26	49.71	47.19	44.71	50.85	47.92	45.02	46.34
32		53.34	51.20	49.08	50.37	54.26	51.74	49.23	46.78	44.35	50.30	47.43	44.60	45.84
36		52.42	50.38	48.35	49.53	53.20	50.78	48.38	46.01	43.67	49.30	46.54	43.80	44.92
40		51.60	49.62	47.67	48.75	52.24	49.90	47.59	45.30	43.04	48.39	45.72	43.08	44.10

* The values used in the numerical integrations in these column headings are more accurately given by 89.648 instead of 89.6, and 15.1875, 15.7950, 16.4025 instead of 15.19, 15.79, 16.40, respectively.

** The K_0 at $E=0.8$, 2.0 Mev have been obtained by means of the function f starting with directly computed K_0 at $E=0.6$, 1.0 Mev and $E=1.8$, 2.2 Mev, respectively.

b = radius of square well
$Q'=dQ/d\rho=dQ/kdr$; Q is any quantity.
$\chi=(M/\hbar^2)[E/2-V-e^2/r]$.
$Y=rd\mathfrak{F}/\mathfrak{F}dr$.
$x_G=r\alpha^{\frac{1}{2}}$, $x_Y=r/a$, $x=(8r/a_B)^{\frac{1}{2}}$.
$f=f^{(0)}+f^{(1)}E+f^{(2)}E^2+\cdots$.

II. CALCULATIONS AND TABLES

The numerical integrations by means of which the logarithmic derivative of $\mathfrak{F}$ has been obtained have been performed at intervals of 0.1 in x_G, x_Y. The solution was started at $r=0$ by a power series expansion for the Gauss potential and an equivalent though formally different procedure was used for the meson potential. The results of the modified procedure have been compared with the power series procedure in several cases to make sure of its reliability. The phase shift was then determined by means of the formula

$$\cot(\varphi+K_0)=\tilde{a}^2\cdot\mathfrak{F}'/\mathfrak{F}-\tilde{a}'\tilde{a}, \qquad (1)$$

or in some cases by means of the equivalent formula

$$\cot(\varphi+K_0)-\cot\varphi=(\mathfrak{F}'/\mathfrak{F}-F'/F)\tilde{a}^2, \qquad (1.1)$$

where the symbols are as in the list of notation. At energies overlapping the work of BTE the formulas referred to in that reference have been used. For both potentials the above formulas were applied at $r_e=3$. In this way there resulted a value of K_0 corresponding to a purely Coulombian potential for $r_e>3$. For the Gauss error potential the effect of the tail of the potential energy curve beyond $r_e=3$ was found to be negligible. For the meson potential a correction for the tail effect has been worked out by perturbation methods and is reproduced in one of the tables. The phase φ and the amplitude $\tilde{a}$ of the Coulomb functions have been calculated by means of Eqs. (9) and (10) of J. A. Wheeler[3] so that

$$\tilde{a}=1+a_1/\rho+a_2/\rho^2+\cdots. \qquad (1.2)$$

In the formula for a_3 Wheeler's $-\eta/8$ was replaced by $-\eta/4$. The additional term for

$$a_6=4641\eta^6/1024-2431\eta^4/128+281\eta^2/32 \qquad (1.3)$$

was found useful. These equations suffice for the calculation of the amplitude $\tilde{a}$. The phase φ has been obtained by means of Eq. (4b) of Wheeler.[3]

[3] John A. Wheeler, Phys. Rev. 52, 1123 (1937).

TABLE II. Values of correction to K_0 in degrees for meson potential. These should be added to K_0 of Table I in order to allow for effect of potential in region $r>3e^2/mc^2$.

E (Mev) \ a′ C′	0.4 102	0.4 99 and 96	0.42 89.65	0.45 84	0.45 78	0.45 75	0.45 72	0.5 69	0.5 66	0.5 63	0.5 60	0.5 57
0.2	0.02°	0.02	0.03	0.07	0.05	0.04	0.03	0.16	0.12	0.09	0.08	0.09
0.4	0.05	0.04	0.06	0.14	0.09	0.08	0.07	0.31	0.23	0.19	0.15	0.13
0.6	0.06	0.05	0.07	0.16	0.12	0.10	0.09	0.33	0.27	0.23	0.20	0.17
1.0	0.06	0.05	0.08	0.13	0.12	0.11	0.10	0.25	0.24	0.23	0.21	0.19
1.4	0.04	0.04	0.06	0.09	0.10	0.10	0.09	0.16	0.17	0.18	0.18	0.17
1.8	0.03	0.03	0.05	0.06	0.07	0.08	0.08	0.10	0.12	0.13	0.14	0.14
2.2	0.02	0.02	0.03	0.04	0.05	0.06	0.06					
2.4	0.02	0.02	0.03	0.03	0.04	0.05	0.05					
2.6	0.01	0.02	0.02	0.02	0.04	0.04	0.04					
3.0	0.01	0.01	0.02	0.01	0.02	0.03	0.03					
4.0	0.00	0.00	0.00	0.00	0.01	0.01	0.01					

This equation gives in the notation of the present paper

$$\varphi' = \tilde{a}^{-2}. \tag{1.4}$$

Substitution of the power series in $1/\rho$ for $\tilde{a}$, expansion in powers of $1/\rho$ and integration term by term gives an addition to the asymptotic form $\rho - ln2\rho + \sigma_0$ in the form of a power series in $1/\rho$. This series starts with the term $(2a_2 - 3a_1^2)/\rho$ in Wheeler's notation. The calculations have been checked against semiconvergent expansions for F and G and other known methods. Some divergences from the values listed by TH[2] have been found and accounted for by their use of 0.0489 for $\rho\eta$ at $r_e=1$ rather than the value used here and in BTE. Making allowance for this difference in constants it proved possible to make use of most of their work.

The fundamental physical constants enter the work through

$$q = (M/m)(e^2/\hbar c)^2 = 0.0977(17) \tag{1.5}$$

and the value of mc^2 in Mev. The Coulomb functions involve dimensionless quantities

$$\rho\eta = r/a_B = (rmc^2/e^2)q/2 = r_e q/2, \tag{1.51}$$

$$\eta = (q/2)^{\frac{1}{2}}(mc^2/E)^{\frac{1}{2}}(M_H/M)^{\frac{1}{2}}. \tag{1.52}$$

The differential equations for the two potentials can be written as

$$\{d^2/d\xi_G^2 + E/(2mc^2) + A' \exp(-\alpha'\xi_G^2) - q^{\frac{1}{2}}/\xi_G\}\mathfrak{F} = 0, \tag{1.53}$$

$$\{d^2/d\xi_Y^2 + q[E/2mc^2) + C'(a'/\xi_Y) \times \exp(-\xi_Y/a') - 1/\xi_Y]\}\mathfrak{F} = 0, \tag{1.54}$$

where

$$\xi_G = r/l_G, \quad \xi_Y = r/l_Y \tag{1.55}$$

with the units of length

$$l_G = \hbar/(Mmc^2)^{\frac{1}{2}}, \quad l_Y = e^2/mc^2. \tag{1.56}$$

The application of the joining Eq. (I) requires the identification of corresponding values of ρ or $\rho\eta$ with ξ_G or ξ_Y. For ξ_Y the unit of length l_Y is the same as for the Coulomb functions. For ξ_G the ratio of the units of length is

$$l_Y/l_G = q^{\frac{1}{2}}. \tag{1.57}$$

Effects of changes in the values of fundamental constants can thus be traced through the effects of q and E/mc^2. The numerical integrations matter only through $\mathfrak{F}'/\mathfrak{F}$. In most cases the quantities $\mathfrak{F}$, $\mathfrak{F}'$ were interpolated for at $r_e=3$. For the meson case the interpolation was usually parabolic; for the Gauss potential it was usually linear.

Numerical integration of differential equations is subject to cumulative errors. The adequacy of the choice of interval length, the number of significant figures carried and the choice of interpolation formula for the second difference has been tested, therefore, by several methods in a number of representative cases. Some of the tests were based on the equation

$$Y_1 - Y_2 + (r/\mathfrak{F}_1\mathfrak{F}_2)\int_0^r (\chi_1 - \chi_2)\mathfrak{F}_1\mathfrak{F}_2 dr = 0, \tag{1.6}$$

which applies to solutions of

$$d^2\mathfrak{F}_i/dr^2 + \chi_i(r)\mathfrak{F}_i = 0, \quad (i=1, 2) \tag{1.61}$$

with vanishing $\mathfrak{F}$ at $r=0$. This relation is closely related to similar formulas occurring in derivations of Green's function for one dimensional problems, to Eqs. (10.3) of BCP (9.1) of BTE, and to Eq. (10) of Ramsey.[4] Values of the homogeneous logarithmic derivative Y obtained from the numerical solution of the wave equation have been used in Eq. (1.6) and their differences have been thus compared with the integral occurring in that equation. The function χ was changed either by changing the energy, keeping the potential fixed or by changing the potential. The work for the two potentials which was carried out by different methods was thus intercompared. The differences in $Y_1 - Y_2$ were always interpretable in terms of

[4] W. H. Ramsey, Proc. Camb. Phil. Soc. 44, 87 (1948).

TABLE III. Values of phase shift K_0 in degrees for Gauss error potential $-A\exp(-\alpha r^2)$. Potential is cut off at $r=3e^2/mc^2$. Notation in headings corresponds to $A'=A/mc^2$, $\alpha'=\alpha\hbar^2/Mmc^2$.

E (Mev)	A'* 42.89	45.38	47.65	50.03	51.44	47.54	49.92	52.42	55.04	57.79	54.46	57.18	60.04	61.95
	α' 18	20	20	20	21.59	22	22	22	22	22	24	24	24	26
	A'/α' λ	λ/w	λ	λw	λ	λ/w^2	λ/w	λ	λw	λw^2	λ/w	λ	λw	λ
0.2	7.40	5.86	7.09	8.89	6.89	4.75	5.63	6.84	8.59	11.40	5.42	6.61	8.34	6.40
0.4	16.56	13.07	15.92	20.04	15.46	10.55	12.57	15.34	19.39	25.79	12.12	14.84	18.83	14.38
0.6	24.06	19.12	23.18	28.93	22.56	15.49	18.41	22.41	28.10	36.66	17.80	21.72	27.35	21.09
**0.8	29.94	24.08	28.97	35.67	28.26	19.65	23.25	28.09	34.77	44.30	22.51	27.30	33.96	26.56
1.0	34.56	28.13	33.55	40.73	32.81	23.15	27.24	32.63	39.84	49.65	26.44	31.80	39.04	31.03
1.4	41.07	34.24	40.11	47.52	39.42	28.64	33.33	39.25	46.78	56.26	32.49	38.43	46.07	37.67
1.8	45.27	38.50	44.45	51.63	43.83	32.70	37.63	43.68	51.04	59.89	36.84	42.94	50.47	42.24
**2.0	46.79	40.14	46.05	53.09	45.48	34.34	39.32	45.34	52.56	61.08	38.54	44.65	52.05	43.99
2.2	48.05	41.53	47.38	54.26	46.86	35.76	40.76	46.72	53.79	62.00	40.02	46.09	53.34	45.47
2.4	49.10	42.74	48.50	55.19	48.02	37.01	42.01	47.91	54.80	62.73	41.30	47.31	54.41	46.75
2.6	49.97	43.76	49.43	55.96	49.01	38.11	43.08	48.90	55.63	63.28	42.42	48.36	55.30	47.84
3	51.28	45.38	50.86	57.05	50.51	39.90	44.78	50.42	56.84	63.99	44.21	50.00	56.61	49.54
4	53.08	47.91	52.91	58.42	52.76	42.91	47.54	52.72	58.45	64.68	47.15	52.49	58.42	52.23
5	53.70	49.16	53.77	58.74	53.75	44.64	48.99	53.76	58.94	64.51	48.76	53.70	59.09	53.59
6	53.76	49.74	54.00	58.55	54.12	45.63	49.71	54.16	58.90	63.96	49.63	54.22	59.18	54.24
7	53.50	49.92	53.89	58.10	54.13	46.17	50.02	54.17	58.57	63.25	50.05	54.36	58.96	54.49
8	53.06	49.84	53.58	57.51	53.92	46.40	50.06	53.96	58.10	62.45	50.20	54.25	58.57	54.48
9	52.51	49.60	53.12	56.86	53.55	46.44	49.92	53.62	57.52	61.60	50.16	54.00	58.07	54.31
10	51.88	49.23	52.60	56.14	53.08	46.34	49.66	53.17	56.87	60.74	49.97	53.63	57.49	54.01
12	50.60	48.40	51.46	54.66	52.09	45.88	48.95	52.17	55.55	59.05	49.41	52.76	56.29	53.26
14	49.26	47.41	50.26	53.24	50.98	45.25	48.09	51.08	54.21	57.45	48.67	51.78	55.04	52.39
16	47.97	46.38	49.06	51.85	49.81	44.50	47.17	49.97	52.90	55.92	47.84	50.76	53.81	51.44
18	46.73	45.37	47.89	50.52	48.70	43.70	46.24	48.88	51.63	54.48	46.99	49.74	52.61	50.49
20	45.53	44.36	46.75	49.25	47.60	42.89	45.30	47.81	50.41	53.11	46.12	48.73	51.45	49.54
22	44.38	43.38	45.66	48.04	46.50	42.08	44.38	46.77	49.26	51.82	45.25	47.74	50.33	48.60
24	43.30	42.43	44.62	46.90	45.46	41.28	43.49	45.78	48.16	50.61	44.40	46.79	49.27	47.69
26	42.27	41.52	43.62	45.81	44.51	40.50	42.62	44.82	47.10	49.46	43.57	45.87	48.25	46.82
28	41.29	40.65	42.68	44.78	43.63	39.74	41.78	43.90	46.10	48.37	42.77	44.99	47.28	45.96
30	40.36	39.81	41.77	43.80	42.75	39.00	40.97	43.02	45.15	47.34	41.99	44.13	46.35	45.13
32	39.47	39.00	40.90	42.87	41.89	38.27	40.19	42.17	44.23	46.36	41.24	43.30	45.45	44.32
36	37.84	37.49	39.29	41.16	40.32	36.90	38.71	40.59	42.54	44.55	39.80	41.76	43.79	42.82
40	36.37	36.13	37.83	39.60	38.89	35.65	37.37	39.16	41.00	42.91	38.49	40.34	42.27	41.42

* The values of A' indicated to within ± 0.01 in the column headings have been used as 42.887, 45.383, 47.652, 50.035, 51.440, 47.544, 49.921, 52.417 55.038, 57.790, 54.460, 57.183, 60.042, 61.948. The values of A'/α' are given in terms of $\lambda=2.3826$, $w=1.05$.

** The K_0 at $E=0.8$, 2.0 Mev have been obtained by means of the function f starting with directly computed K_0 at $E=0.6$, 1.0 Mev, and $E=1.8$, 2.2 Mev, respectively.

smaller errors in Y_1, Y_2 than the error tolerance for K_0.

The cumulative effects of omitted terms in the interpolation formulas for the step by step numerical integrations have been estimated and found to be sufficiently small. In addition to the above tests calculations of much higher accuracy have been made in a few cases for comparison with the routine type of numerical integration. For the Gauss potential these tests were made for $\alpha'=21.59$, $A'=51.44$ at $E=20$ and 40 Mev. For the meson potential similar tests were made at the same energies for $C'=63$, $a'=0.5$. The Coulomb function F for 36 Mev was checked on by a similar method, outlined below, with an interval of 0.1 for ρ. A comparison with the value as calculated by the semiconvergent series was satisfactory within the accuracy claimed for that method. The specially accurate calculations have been made following the plan developed by D. R. Hartree. For a differential equation of type

$$Ou=0, \tag{1.7}$$

one expresses

$$u=u_0+u_1 \tag{1.71}$$

in terms of a known function u_0 which is picked so as to be an approximation to u and to satisfy a differential equation

$$O_0u_0=0 \tag{1.72}$$

in which O_0 is such that

$$O-O_0=O_1 \tag{1.73}$$

is not too large. Then one can obtain a high accuracy for u by integrating numerically the differential equation

$$Ou_1+O_1u_0=0 \tag{1.74}$$

for the smaller quantity u_1. In the present application the region $O<r<3e^2/mc^2$ was subdivided into two or more intervals. In the first interval, corresponding to the smallest r, the solution was obtained by means of a power series for u. The second interval of r was treated by arranging for u_0 to be a sine curve of suitable wave-length to make O_1 reasonably small. The function u_0 and its first derivatives were joined smoothly to the solution in the first interval. The function u_1 was then determined by numerical integration by means of Eq. (1.74). Both u_1 and its first derivative were made

to vanish at the boundary adjoining the first interval.

The boundary between the two intervals was at $x_Y=1.8$ and $x_G=1.4$ for the meson and Gauss potentials, respectively. For the check on the Coulomb function the boundary was at $\rho=0.7625$. These tests indicated a higher accuracy than that claimed for the results. An additional check was made through the function f. This check will be described in a later section.

In Table I values of the phase shift K_0 in degrees are tabulated against the energy E in Mev for various values of the meson potential parameters. The unit of length for the range a is e^2/mc^2, the unit of energy for the well depth is mc^2. The quantity $C'a'^2$ gives the product of depth times square of range in these units. This parameter is often more convenient for interpolation than the depth C'. The phase shifts in this table as well as those in the analogous Table III for the Gauss error potential have an intended accuracy of about 0.03° in the sense of maximum deviation from correct value. The accuracy is occasionally better than that and especially so regarding the consistency of neighboring values. The above statements concerning accuracy do not take into account possible revisions in the numerical values of fundamental physical constants. The potential was supposed to extend only to $r_e=3$ in calculations for Table I. Corrections for the tail effect which is the effect of the tail of the potential energy curve in the region $r_e>3$ are listed separately in Table II. The reason for this arrangement of the material is that some of the values in the literature have been calculated neglecting the tail beyond $r_e=3$. There is besides an advantage in making a comparison with the f function if one cuts off the potential at a reasonable distance. Most of the numbers in Table I have been obtained by direct calculation. The values indicated by ** have been calculated indirectly by interpolation employing the function f. The $C'a'^2$ in some of the column headings are approximate only as indicated in the first footnote to Table I. There are on hand additional values of K_0 for triplets of values $(a', C', C'a'^2)=(0.5, 57, 14.25)$, $(0.5, 69, 17.25)$, $(0.55, 49, 14.8225)$, $(0.55, 55, 16.6375)$, $(0.6, 41, 14.76)$, $(0.6, 44, 15.84)$, $(0.6, 47, 16.92)$ which will be supplied on demand to those wishing to improve the quality of interpolation obtainable from Table I.

Table I is suitable for two- or three-way interpolation. Interpolation against E when carried out by standard second difference formulas is good to better than 0.02° from 0.2 to 1 Mev, 0.05° from 1 to 4 Mev, 0.03° from 4 to 10 Mev, 0.01° from 10 to 40 Mev. Above 14 Mev linear interpolation is good to better than 0.02°, an inaccuracy smaller than the intended error tolerance of the tables.

Parabolic interpolation against C' gives errors $<0.03°$ from 0.2 to 3 Mev and $<0.01°$ from 3 to 40 Mev.

Interpolation against a' may be made by first obtaining values of K_0 employing interpolation against $C'a'^2$ keeping a' constant for the particular value of $C'a'^2$ required. This is done for a triplet of values of a' nearest to the required value. Parabolic or linear interpolation is then used on these derived values. Parabolic interpolation for $C'a'^2=15.80$ gives an accuracy of 0.01° and for $C'a'^2$ in the region 14.80 to 16.80 it gives an accuracy of 0.02°. Linear interpolation is good to 0.03° over the same region.

In Table II the values of the tail effect correction are listed for the more important cases. In this Table the region for $E>14$ Mev has been omitted. The tail effect has been studied in this energy region for the first 7 pairs of well parameters in the table which are entered in the block starting with the second and ending with the eighth columns. In all of these cases the tail effect does not exceed 0.02°. It reaches this value between 12–18 Mev for $a'=0.45$, $C'=72, 75, 78$; $a'=0.42$, $C'=81.648$ and also for the region 8–10 Mev for $a'=0.45$, $C'=81, 84$. In many cases the effect is $<0.01°$ and in some $<0.005°$. These values can be furnished through correspondence if desired. The accuracy of the tail effect calculations for the last 5 columns of Table II is not claimed to be better than $\pm0.02°$. For the preceding columns which correspond to $a'=0.4$ to 0.45 the accuracy is believed to be $\pm0.01°$.

In Table III the values of K_0 in degrees for the Gauss error potential are listed in a manner similar to that of Table I. The quantities A', α' are the usual A, α expressed in units $mc^2, \hbar/(Mmc^2)^{\frac{1}{2}}$ for energy and length, respectively. Attention should be called to the first footnote to Table III which explains the notation used in listing the A'/α'. These have been arranged in a geometric progression and the values of A' have been chosen so as to correspond to the preassigned values of A'/α'. The latter quantity is the depth times the square of range parameter and corresponds to $C'a'^2$ of the meson case. As in Table I the K_0 at $E=0.8$ and 2 Mev have been obtained by interpolation making use of the function f. In addition to the numbers listed in the table there are available values of K_0 at the energies listed in Table III for $A'/\alpha'=\lambda/w^2$ and λw^2 with $\alpha'=30, 24, 20$; for $A'\alpha'=\lambda/w$ and λw with $\alpha'=30, 26, 18, 16$; for $A'/\alpha'=\lambda$ with $\alpha'=30, 16$. The results can be furnished to those needing them for improving the quality of interpolation obtainable by means of Table III. The methods employed for checking were essentially the same as for Table I. In addition a good check was furnished by joining the external and internal wave functions at $r_e=2.5$ and estimating the

practically negligible effect of the potential in the region $2.5<r_s<3$. The potential tail for $r_s>3$ had a negligible effect and a table analogous to Table II did not prove necessary. The interpolations which led to values of the logarithmic derivative of the internal function were made linearly rather than parabolically for $\mathfrak{F}$ and $\mathfrak{F}'$. In this respect the Gauss error calculations are less accurate than those for the meson potential. No definite inaccuracy exceeding the intended tolerance of 0.03° has been detected, however.

For energy the interpolation properties of Table III are the same as those of Table I. Parabolic interpolation (i.e., interpolation by 2nd difference formulas) against A/α for fixed α introduces errors $<0.01°$ for fixed α in the region 2.5 Mev$<E<$40 Mev. A uniform scale in $\log(A'/\alpha')$ makes it possible to use convenient interpolation formulas. Parabolic interpolation against A'/α' for $\alpha'=22$ gives errors of $\sim$0.06° from 0.2 to 1 Mev, 0.02° at 1.4 Mev, 0.01° at 1.8 Mev, and negligible errors otherwise. Linear interpolation against A'/α' introduces errors of 0.1° at 3 Mev, 0.05° at 5 Mev, 0.02° at 10 Mev and 0.01° at $E>20$ Mev.

Interpolation against α is even more satisfactory. From 0.2 Mev to 7 Mev the error introduced by linear interpolation does not exceed 0.01° and it reaches 0.02° at 10 Mev. At 20 and 40 Mev linear interpolation against α is accurate to $\sim$0.02°. Parabolic interpolation is good to 0.01° or better throughout the whole range of values.

The employment of second difference formulas (parabolic interpolation) can be avoided by drawing a good set of graphs for either of the two Tables I, III.

III. PROPERTIES OF f

The function f of Eq. (7.6) of BCP[1] should vary approximately linearly with E as follows from that equation. For a vanishing range of force the values of the phase shift satisfy the equation

$$f=f^{(0)}, \tag{2}$$

where the right side is energy independent. This relation has been used in a transformed form as Eq. (7.9) by BCP in connection with some of the graphs in that paper. The approximate linearity of f with energy at the lower energies is a consequence of Eq. (7.6) of BCP. The constancy of f for zero range has been used by Landau and Smorodinsky[2] with the result that experiment could not be satisfied as has been previously known and a linear relation was postulated instead. This matter was further investigated by Blatt and Jackson[5] who following the variational method for phase shifts in Schwinger's[6] form have given another justification for the approximate linearity of f. The same question has been independently studied by Breit and Bouricius.[2] The present work has received some stimulus through informal reports of the successes of Schwinger and of Blatt and Jackson in the employment of the variational method. It follows from any of these considerations that the function f, being very linear at low energies, should be useful in comparing the values of K_0 and especially so at the lower energies. It is also useful to employ an expansion of f in E as a check on the calculations. It is understood that the equivalent of the formulas for the coefficients in the expansion has been discussed by Schwinger in his Harvard lectures. The formulas are related to those for vanishing Coulomb potential in a manuscript by Blatt and Jackson[5] on neutron-proton scattering. These have been derived by Bethe[7] without the use of the variational method and independently in connection with the present paper.[8] The value of f for zero energy is found in G. Breit and W. G. Bouricius.[2] From the latter one has

$$f_{E=0}=4\frac{\mathrm{K}_0-(2/x)\mathrm{K}_1Y_0}{I_0-(2/x)I_1Y_0}+4\gamma-2, \tag{2.1}$$

which is obtained by an easy transformation from the unnumbered formula between their Eqs. (8.58), (8.6) and is equivalent to their Eq. (8.6). The functions I_ν, K_ν are used here in the same notation as in Whittaker and Watson's book on modern analysis. One also has[8]

$$[\partial f/\partial(E/mc^2)]_{E=0}=\int_0^\infty (u_0^2-u^2)dr_s, \tag{2.2}$$

where u_0 is the solution of the radial equation for F or G at $E=0$ for a purely Coulombian potential. Here

$$u_0=-x[\mathrm{K}_1(x)+(\gamma-\tfrac{1}{2})I_1(x)]+xI_1(x)f_{E=0}/4 \tag{2.3}$$

in the same notation as in the paper by Breit and Bouricius.

The function u_0 plays the part of a comparison function for vanishing range of force arranged to

[5] J. M. Blatt and J. D. Jackson, private communication. This was received when the present work was nearly completed.

[6] Julian Schwinger, Phys. Rev. **72**, 742 (1947); J. M. Blatt, Phys. Rev. **74**, 92 (1948).

[7] H. A. Bethe, preliminary report at ONR conference on classical nuclear physics at the University of Chicago, December 1948. The exact form for proton-proton scattering was not stated by Bethe.

[8] While the exact form of Eq. (2.2) in the text has been derived only in connection with the present paper it should be stated that it is not essentially different from other relations following from Eqs. (9), (9.1) of BTE. The methods employed for interchecking calculations for different potentials in BTE employ relations differing only superficially from the relations of Blatt and Jackson and of Bethe. By the method outlined in BTE it is only a matter of patience to work out the coefficient of any power of E in f.

give the desired value of f at $E=0$. The function u is the solution of the radial equation for $\mathfrak{F}$ at $E=0$. The function u is normalized so as to be asymptotic to u_0 at $r=\infty$. The checks by means of Eqs. (2.1), (2.2) were made for potentials terminating at $r_e=3$. The normalization was, therefore, such as to make $u=u_0$ at that value of r_e. The difference between the values obtained from Eq. (2.2) and the value derived by fitting the computed phase shifts was in all cases smaller than amounts which would be accounted for by computational uncertainties in the K_0.

In the meson case checks were made at $C'=99$, $a'=0.4$ and at $C'=63$, $a'=0.5$. For the Gauss error potential a check was made at $\alpha'=22$, $A'/\alpha'=2.3826$. Checks on the value of f at $E=0$ were made by means of Eq. (2.1) and were also satisfactory.

In the meson case three checks were made at $C'=99, a'=0.4$; $C'=63, a'=0.5$ and $C'=44, a'=0.6$, the percentage difference in all cases being less then 0.1 percent. Similar results were obtained from a series of checks for the Gauss error potential at $A'/\alpha'=2.2692$, $\alpha'=18$, 22, 26; $A'/\alpha'=2.3826$, $\alpha'=18$, 22, 24, 26; and $A'/\alpha'=2.5017$, $\alpha'=18$, 22, 26.

The computed values of K_0 have been used to ascertain the coefficients in the expansion of f in powers of E in the form

$$f=f^{(0)}+f^{(1)}E+f^{(2)}E^2+\cdots. \tag{2.4}$$

Only the first three coefficients have been calculated. In some of the calculations the procedure was equivalent to making a parabolic fit to judiciously chosen sets of three points. If comparison of results indicated that the values were not sufficiently consistent with those for neighboring pairs of potential well parameters improved calculations were made by making a least square fit to the available values of f from 0.2 to 10 Mev by a quadratic in E. The point of view in this work was that it might be more important to have a practically adequate representation of K_0 than to have a mathematically correct set of coefficients. Since the checks by means of Eqs. (2.1), (2.2) were satisfactory, it is believed that the coefficients are nearly correct in a mathematical sense as well and that the higher powers of E have not distorted the values too strongly. On obtaining the values of $f^{(0)}$, $f^{(1)}$, $f^{(2)}$ their behaviour with well parameters was studied. The following striking facts were noticed:

(1) Plots of $f^{(0)}$, $f^{(1)}$ against $(C'a'^2)^{-\frac{1}{2}}$ for fixed a' are nearly straight lines. For $f^{(0)}$ these lines intersect in a point which is nearly the same for any pair of lines. The intersection is at $(C'a'^2)^{-\frac{1}{2}}=0.2342$. At this point the extrapolated value of f at $E=0$ is independent of the range parameter a'. Such a condition can be expected on the following basis. Neglecting the effect of the Coulomb potential, i.e., considering the colliding particles as though they were a proton and a neutron, there is a resonance condition at zero energy for a value of $C'a'^2$. This condition corresponds to a vanishing slope of $\mathfrak{F}$ at $r=\infty$. Calculations of Hoisington and Share in connection with HSB[2] have indicated that this condition obtained for

$$d^2\mathfrak{F}/dx^2+\lambda'(e^{-x}/x)\mathfrak{F}=0, \tag{2.5}$$

where

$$\lambda'=1.68\cdots.$$

The value of $C'a'^2$ corresponding to this λ' is $\lambda'/q=17.2$ while the value of $C'a'^2$ as determined from the intersection is 18.2. The difference of 0.9 is of the order which would be expected for the Coulomb effect since for a square well the effective depths with and without Coulomb potential are in the approximate ratio $(10.5+0.83)/10.5=1.079$ which would put the estimated value of $C'a'^2$ at 18.4. Since the Coulomb effect cannot be expected to change effective depths in a manner independent of well shape, the above agreement is doubtless the correct one although not the complete explanation of this very good approximation. For the Gauss error potential the situation is similar. The resonant condition for uncharged particles corresponds to $A'/\alpha'=2.684$ in accordance with unpublished calculations made in connection with the paper by BTE. The lines representing $f^{(0)}$ as a function of $(\alpha'/A')^{\frac{1}{2}}$ are nearly straight and intersect at approximately $(\alpha'/A')^{\frac{1}{2}}=0.590$ corresponding to $A'/\alpha'=2.88$ while the Coulomb correction made by analogy with the square well gives $1.079\times2.684=2.90$.

(2) Tables and graphs of K_0 for the Gauss error potential indicate that for fixed A/α the values of K_0 are nearly independent of α at an energy of $\sim$5 Mev. This is to be expected because the scattering properties of the square and Gauss error potential wells are very similar. The resonant depth of a square well for $b_e=1$ is $5.233\times2.4674=12.91$ Mev which may be compared with the approximate depth of 10.5 Mev which fits experiment for this b_e. The difference in these depths is 2.4 Mev for a kinetic energy of 2×2.4 Mev$=5$ Mev. The kinetic energy inside the potential well has such a value that the wave function could be joined to a cosine curve if the wave-length outside the well were infinite. If this were the case then K_0 would depend only on the product of depth times square of range for the square well. These conditions are not satisfied closely because the parameter ρ is $\sim$0.69 and the square well width measured in wave-lengths is $\sim$0.11 and the argument is only a qualitative one. The curves do not exactly intersect at a point but are tangent to an envelope which extends

through ~2 Mev centered at an energy between 4 and 8 Mev depending on the value of A/α. As a consequence the interpolation of K_0 against α is very good in the vicinity of this energy. The value of A/α is supposed to be kept fixed in this interpolation.

For the meson potential the condition is similar, the center of the envelope falling in the region from ~1 Mev to ~6 Mev.

The results of fitting the values of $f^{(0)}$ can be summarized by the following formulas for the meson case:

$$f^{(0)}=\alpha_{Y0}+\alpha_{Y1}[(C')^{-\frac{1}{2}}/a'-0.25147], \quad (3)$$

where

$$\alpha_{Y0}=7.8240-11.0754(a'-0.42)+16.747(a'-0.42)^2, \quad (3.1)$$

$$\alpha_{Y1}=274.329-665.992(a'-0.42)+1108.69(a'-0.42)^2. \quad (3.2)$$

The method of obtaining this representation was to fit each curve of $f^{(0)}$ against $(C')^{-\frac{1}{2}}/a'$ by least squares making use of Eq. (3) and then to fit the five values of α_{Y0} and α_{Y1} thus obtained to a parabola given by Eqs. (3.1) and (3.2). Checks made on all the points used in the fits indicated an accuracy of 0.1 percent. A similar procedure was followed in obtaining representations for $f^{(1)}/a'$ and $f^{(2)}/a'^2$. Both of these quantities were found to vary nearly linearly with $(C')^{-\frac{1}{2}}/a'$. The accuracy is believed to be 0.1 percent for $f^{(1)}/a'$ and 0.3 percent for $f^{(2)}/a'^2$

$$f^{(1)}/a'=\beta_{Y0}+\beta_{Y1}\{(C')^{-\frac{1}{2}}/a'-0.25147\}, \quad (3.3)$$

where

$$\beta_{Y0}=2.2577-0.4655(a'-0.42)-0.718(a'-0.42)^2, \quad (3.4)$$

$$\beta_{Y1}=21.91-11.68(a'-0.42)-18.2(a'-0.42)^2. \quad (3.5)$$

$$f^{(2)}/a'^2=\gamma_{Y0}+\gamma_{Y1}\{(C')^{-\frac{1}{2}}/a'-0.25147\}, \quad (3.6)$$

where

$$\gamma_{Y0}=-0.03058+0.00864(a'-0.42)+0.0678(a'-0.42)^2, \quad (3.7)$$

$$\gamma_{Y1}=-0.3001+0.624(a'-0.42)+0.243(a'-0.42)^2. \quad (3.8)$$

Identification of notation will be aided by a few samples of triplets of values of $(f^{(0)}, f^{(1)}, f^{(2)})$. For the meson potential they are (6.920, 0.8719, −0.00472) if $a'=0.40$, $C'=102$; (6.342, 0.9652, −0.00587) if $a'=0.45$, $C'=81$. For the Gauss error potential these quantities have the values (8.743, 1.0597, 0.00485) if $\alpha'=20$, $A'/\alpha'=2.2692$; (7.918, 0.9419, 0.00354) if $\alpha'=24$, $A'/\alpha'=2.3826$. In calculating K_0 from f one needs C_0^2/η and q_0/η. Formulas for these quantities are found in BCP and occur in more convenient form in Breit and Bouricius[2] as Eqs. (2.1), (2.3). The real part of the expression involving the gamma-function in these formulas and values of C_0 have been tabulated in good detail by the New York Computation Laboratory of the National Bureau of Standards.

In the case of the Gauss error potential the values of $f^{(0)}$, $f^{(1)}$, and $f^{(2)}$ obtained by least squares fits may be represented as follows:

$$f^{(0)}=\alpha_{G0}+\alpha_{G1}\{(\alpha'/A')^{\frac{1}{2}}-0.64788\}+\alpha_{G2}\{(\alpha'/A')^{\frac{1}{2}}-0.64788\}^2, \quad (4)$$

where

$$\alpha_{G0}=7.686+0.1194(\alpha'-22)-0.00178(\alpha'-22)^2, \quad (4.1)$$

$$\alpha_{G1}=85.06+2.105(\alpha'-22)-0.0256(\alpha'-22)^2, \quad (4.2)$$

$$\alpha_{G2}=59. \quad (4.3)$$

For the values of the parameters $\alpha'=18$ to 26 and $A'/\alpha'=2.2692$ to 2.5017 these equations give values of $f^{(0)}$ accurate to 0.05 percent.

$$f^{(1)}\alpha'^{\frac{1}{2}}=\beta_{G0}+\beta_{G1}\{(\alpha'/A')^{\frac{1}{2}}-0.64788\}, \quad (4.4)$$

where

$$\beta_{G0}=4.6076+0.00377(\alpha'-22)-0.000217(\alpha'-22)^2, \quad (4.41)$$

$$\beta_{G1}=8.7833. \quad (4.42)$$

The accuracy of this representation over the range of parameters mentioned in connection with Eq. (4) is 0.1 percent.

$$f^{(2)}\alpha'=\gamma_{G0}+\gamma_{G1}\{(\alpha'/A')^{\frac{1}{2}}-0.64788\}, \quad (4.5)$$

where

$$\gamma_{G0}=0.0869-0.00103(\alpha'-22)+0.0000475(\alpha'-22)^2, \quad (4.51)$$

$$\gamma_{G1}=0.4817. \quad (4.52)$$

These formulas give values of $f^{(2)}$ to within ± 0.00012 of the "least squares" values.

By means of the above expressions and Eq. (2.4) f may be determined over the tabulated range of α' and A'/α' up to about $E=10$ Mev to within 0.05 percent.

By means of the procedure described by Breit and Bouricius[2] in connection with their Eq. (8.61) the equivalent square well radius b_e for zero energy has been determined for typical combinations of parameters for the two potentials. The following two equations give an approximate representation of the results:

$$b_e/a'=2.318-0.23(a'-0.42)-0.088[C'a'^2-15.814], \quad (4.6)$$

$$b_e(\alpha')^{\frac{1}{2}}=4.75-0.0058(\alpha'-22)-0.211[(A'/\alpha')-2.3826]. \quad (4.7)$$

The equivalent square well range is here expressed in units e^2/mc^2. The accuracy of the representations is about 0.2 percent. The equivalent square well depth for zero energy is obtainable by solving for Y_0 either Eq. (2.1) of the present paper or Eq. (8.6) of Breit and Bouricius. Replacing χ_1 by Y_0 in Eq. (8.6′) of BTE one finds Db_e^2 in the form of a rapidly converging series. The series starts as $5.233(2.4674-2Y_0\cdots)$. For the Gauss error well with $\alpha'=21.59$, $A'=51.44$ the value of Db_e^2 is 10.47(2) with Mev as the unit of D. A 10 percent change in range produces approximately a 2 percent change in Db_e^2. For fixed range the quantity Db_e^2 changes nearly in the same ratio as A'/α'. The behavior with corresponding quantities for the Yukawa potential is similar.

IV. ON THE EQUIVALENCE OF POTENTIALS

Two kinds of potential energy curves may be said to be equivalent if they give the same value of K_0 at two energies $E_{\rm I}$, $E_{\rm II}$. This definition of equivalence contains an explicit reference to two energies. If the f curves were exactly straight the reference to the two energies would be irrelevant since all pairs of values would lead to the same answer. One could then speak of an absolute equivalence. It is well known that in an energy region of several Mev there is no striking difference between the shapes of the (K_0, E) curves which are obtained for different plausible potentials. This followed from Eqs. (10.3) of BCP was verified by direct computation and further developed by HSB[2] and BBH[2]. It was also found in the work referred to that, for the potentials tried, there exist differences in values of K_0 at energies other than $E_{\rm I}$ and $E_{\rm II}$ which are not beyond possible detection by improved experiments. It becomes necessary to explain the connection of this situation with the nearly linear nature of the (f, E) curves. The two views are not contradictory if one takes into account the quadratic terms in E. For two potentials such as the Yukawa and the square well, designated in the formulas by subscripts Y and S respectively and fitted to each other at energies $E_{\rm I}$, $E_{\rm II}$ one has

$$f_Y^{(0)}=f_S^{(0)}+(f_Y^{(2)}-f_S^{(2)})E_{\rm I}E_{\rm II}, \quad (5)$$

$$f_Y^{(1)}=f_S^{(1)}+(f_S^{(2)}-f_Y^{(2)})(E_{\rm I}+E_{\rm II}), \quad (5.1)$$

and

$$(f_Y-f_S)_{E=\langle E\rangle}=(f_S^{(2)}-f_Y^{(2)})(E_{\rm II}-E_{\rm I})^2/4, \quad (5.2)$$

where

$$\langle E\rangle\equiv(E_{\rm I}+E_{\rm II})/2. \quad (5.3)$$

A proper change of subscripts makes the formulas applicable to any pair of potential energy types. For the Yukawa and square well potentials approximate values are $f_Y^{(2)}=-0.0054$, $f_S^{(2)}=0.0061$. It will be noted that these values have opposite signs so that the effect becomes magnified. As an example it will be supposed that the two types of potential have been fitted to experimental data at 1 and 2.2 Mev. The value of $f_Y^{(1)}-f_S^{(1)}$ is then approximately 0.037. Since within a few percent each of the $f^{(1)}$ is equal to 1 these fits will disagree with each other at low energies by ~3.7 percent in the effective ranges. More explicitly this disagreement appears as follows. For $a'=0.42$, $C'=89.65$, values which correspond to an approximate fit to experiment by HSB, the equivalent square well range at zero energy is 0.975 in units e^2/mc^2. This means that a square well of proper depth with the above range reproduces the slope of the (f, E) curve for the Yukawa potential at zero energy. The above estimate shows that the square well which reproduces the meson phase shifts at 1 and 2.2 Mev has a smaller slope than the Yukawa well and that its range is approximately 0.938 or 2.64×10^{-13} cm. This is in agreement with the fact that in fitting experimental material HSB paid more attention to the data of HKPP than to that of HHT while BTE have worked with the two sets of data on an approximately equal footing. According to Breit and Bouricius the fit to the combined Wisconsin and Minnesota material indicates a square well range of approximately the above amount.

It should be mentioned that the change caused in $f^{(0)}$ by a readjustment of the fit in the above example is of the order 0.0025 and produces a negligible effect on the equivalent square well range b_e. The quantities $f^{(2)}$ are proportional to the square of the range. In the above example a 7 percent change in $f^{(2)}$ is immaterial but for a more accurate fit it would have to be taken into account.

In BTE a fit of the then available experimental data was made by the Gauss error potential with $\alpha'=21.59$, $A'=51.44$. The value of the phase shift at 0.67 Mev was fitted together with values at about 2 Mev. The range of this potential should be, therefore, somewhat too long even in comparison with the square well range $b_e=1$. The equivalent square well range for zero energy is in this case 1.022. The value of $f^{(2)}$ for the Gauss error potential is ~0.0037. By means of Eq. (5.1) a square well agreeing with the Gauss error potential at two energies is found to have an $f^{(1)}$ smaller than that of the Gauss potential by $\sim0.0024(E_{\rm I}+E_{\rm II})$. For $E_{\rm I}\sim0.7$, $E_{\rm II}\sim2$ Mev the correction to $f^{(1)}$ of the square well becomes -0.007 bringing the equivalent square well range down to 1.015 according to expectation. Small changes in a value of the range parameter correspond to nearly the same fractional

changes in the value of the equivalent square well range.

ACKNOWLEDGMENTS

The writers are indebted to Dr. L. H. Thomas for arrangements to have the numerical integrations for the meson potential performed at the Watson Computing Laboratories of the International Business Machines and to Drs. L. S. Dederick and F. Alt for similar arrangements at the Ballistic Research Laboratories concerning the Gauss error potential. Thanks are also due to Messrs. W. G. Bouricius and G. E. Brown for their help in some of the work.

PHYSICAL REVIEW VOLUME 75, NUMBER 9 MAY 1, 1949

An Accurate Determination of the Threshold for the Nuclear Reaction $C^{12}(d,n)N^{13}$

T. W. BONNER, J. E. EVANS,* AND J. E. HILL**
The Rice Institute, Houston, Texas

(Received January 17, 1949)

The threshold for the production of neutrons from the bombardment of C^{12} by deuterons was found to occur at a bombarding energy of 328 kev. The Q value of the reaction calculated from this threshold is -0.281 ± 0.003 Mev. From this Q value and other disintegration energies, the calculated mass difference between the neutron and proton ($n-H$) is 0.77 Mev.

INTRODUCTION

WHEN carbon is bombarded by deuterons, neutrons and radioactive N^{13} are formed according to the following reactions:

$$C^{12}+H^2\rightarrow N^{13}+n+Q_1, \quad (1)$$

$$N^{13}\rightarrow C^{13}+e^{+}+Q_2. \quad (2)$$

The value of Q_1 has been reported by Bonner and Brubaker,[1] Cockcroft and Lewis,[2] and by Bennett and Richards.[3] The experimental values of Q_1 vary from -0.25 to -0.28 Mev. Several determinations of the maximum energy of the positrons from N^{13} have been made.[4] Probably the most accurate determinations[5] of this energy are those of Lyman who obtained an end-point energy of 1.198 ± 0.006 Mev, and Siegbahn and Slatis who found an end-point energy of 1.24 ± 0.02 Mev.

A precise determination of the value of Q_1 from the threshold energy of the reaction is important so that the mass difference between the neutron and proton ($n-H$) may be calculated by combining the values of Q_1, Q_2, and the energy release Q_3, in the following reaction:

$$C^{12}+H^2\rightarrow C^{13}+H^1+Q_3. \quad (3)$$

If the mass difference ($n-H$) is accurately obtained by other methods, then the rest mass of the neutrino may be obtained from precise values of Q_1, Q_2, and Q_3. The absolute yield of neutrons near the threshold is of interest since this reaction can be used as a source of monoenergetic neutrons to supplement the reactions $Li(p,n)Be^7$ and $H^2(d,n)He^3$. To get the number of neutrons per incident deuteron, positrons from N^{13} were counted, since there are an equal number of neutrons and N^{13} atoms formed. This method of counting the neutrons indirectly has the advantage that Geiger counters have nearly 100 percent efficiencies for the positrons and also the positrons are emitted with spherical symmetry in contrast to the neutrons which are asymmetrical about the direction of the deuteron beam.

APPARATUS

The Rice Institute Van de Graaff generator was used as a source of deuterons. The slit width of the magnetic analyzer was adjusted so that deuterons with an energy spread of 1 kev could pass through the slits and strike the carbon target. This opening of the slits was three times as large as previously described;[6] this arrangement was used in order to get nearly all the deuteron beam through the slit. However, from visual observation of the fluorescence of the deuteron beam striking a Pyrex plate, it was estimated that more than 90 percent of the deuterons which hit the target were within an energy interval of 300 volts at the threshold energy.

---

* Now at Los Alamos Scientific Laboratory, Los Alamos, New Mexico.

** Clinton National Laboratory, Oak Ridge, Tennessee.

[1] T. W. Bonner, and W. M. Brubaker, Phys. Rev. **50**, 309 (1936); T. W. Bonner, Phys. Rev. **53**, 496 (1938).

[2] J. D. Cockcroft and W. B. Lewis, Proc. Roy. Soc. **A154**, 261 (1936).

[3] W. E. Bennett and H. T. Richards, Phys. Rev. **71**, 565 (1947).

[4] W. A. Fowler, L. A. Delsasso, and C. C. Lauritsen, Phys. Rev. **49**, 561 (1936); C. S. Cook, L. M. Langer, H. C. Price, and M. B. Sampson, Phys. Rev. **74**, 502 (1948).

[5] E. M. Lyman, Phys. Rev. **55**, 1123 (1939); K. Siegbahn and H. Slatis, Arkiv. f. Mat. Astr. O. Fys. **32A**, No. 9 (1945).

[6] W. E. Bennett, T. W. Bonner, C. E. Mandeville, and B. E. Watt, Phys. Rev. **70**, 882 (1946); T. W. Bonner and J. E. Evans, Phys. Rev. **73**, 666 (1948).

The carbon target was made by evaporation of ceresin wax onto a silver disk, 0.0045 inch in thickness. Since the target had been used in a previous experiment, the thickness of the target was determined at the end of this experiment by comparing the relative number of gamma-rays obtained under deuteron bombardment with a newly evaporated target, which was weighed on a microbalance. The calculated weight of the ceresin target was 45 micrograms per cm². Its original weight at the time of evaporation about six months earlier was 56 micrograms per cm².

A thin-walled Geiger counter, 60 mm long and 18 mm in diameter with a wall thickness of 0.15 mm of glass, was placed as close to the carbon target as possible. The counter was mounted inside a thin copper tube which had a window covered with an aluminum foil of thickness 0.0005 inch. The positrons had to pass through a total thickness of 0.163 g/cm² of material to go from the carbon target into the counter. About half of the positrons were transmitted through this amount of material. Lead absorbers 4 cm thick were placed around the counter in order to reduce the background.

PROCEDURE

Bombardment of the target was carried out in the following manner. At the moment the beam was brought on the target, the electrical clock and current integrator were started. The target was bombarded for 1200 sec., that is, for two half-lives. The reading of the current integrator was taken every 100 seconds to see that the bombarding current remained reasonably constant throughout the run. After 1200 seconds, the voltage of the statitron was turned off, and the reading on the Geiger tube was recorded. A scale of 64 was used but readings were taken to the individual count by means of the interpolation lights. The number of counts over the half-life following bombardment were used to determine the relative numbers of N^{13} atoms which are formed. On some of the runs the

TABLE I. Relative yield of N^{13}.

Magnet current in amperes	Energy of deuterons in kev	Number of counts in 10 minutes	Background, including residual activity in 10 minutes	Saturation activity per 5000 integrator counts	Relative yield of N^{13} (above 370-kev cross section in barns)*
2.200	323	246 (May 31)	243	0.2	3.0×10^{-7}
2.220	329	223 (May 28) 265 (May 31)	239 243	−0.9 1.3	3.0×10^{-7}
2.230	332	292 (May 28) 339 (May 31)	239 243	2.6 5.0	6.0×10^{-6}
2.240	335	410 (May 28) 435 (May 31)	239 243	8.5 9.7	1.43×10^{-5}
2.250	338	554 (May 28) 632 (May 31)	242 243	14.3 17.9	2.53×10^{-5}
2.260	341	699 (May 28) 742 (May 31)	244 245	21.1 23.1	3.47×10^{-5}
2.300	353	1020 (May 29) 918 (May 29) 1008 (May 31)	289 247 260	63.2 67.9 60.7	9.80×10^{-5}
2.350	369	1912 (May 29) 1903 (May 31)	271 263	113 112	1.78×10^{-4}
2.380	378	2521 (May 28) 2507 (May 31) 2519 (June 1)	255 263 274	145 142 143	2.26×10^{-4}
2.410	387	3163 (June 1)	286	179	2.83×10^{-4}
2.450	399	4073 (June 1)	293	231	3.64×10^{-4}
2.500	415	6283 (June 1)	320	346	5.45×01^{-4}
2.550	432	8416 (June 1)	311	477	7.54×10^{-4}
2.800	520	36,800 (June 1)	356	2066	3.27×10^{-3}
3.100	636	46,700 (June 1)	453	6720	1.06×10^{-2}
4.280	1184	42,500 (June 1) 43,700 (June 1)	530 650	88,800 87,800	0.139

* Since the target is 42 kev thick, the cross sections are the average value over this range of bombarding energy. Below 370 kev, disintegrations are only produced in the top part of the target, and hence the values given in the table are considerably smaller than the true cross sections.

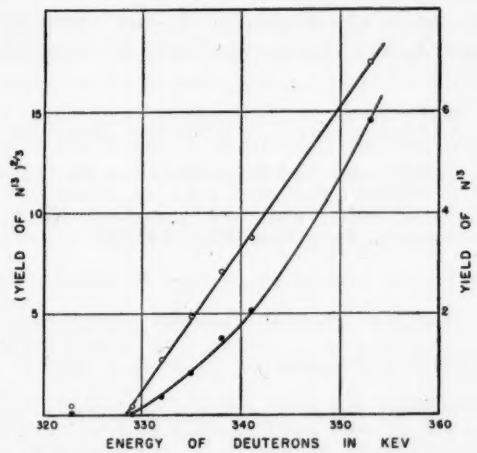

FIG. 1. Solid circles refer to yield of N^{13} *versus* the energy of the deuterons. Open circles give (yield of neutrons)$^{\frac{1}{2}}$ as a function of deuteron energy.

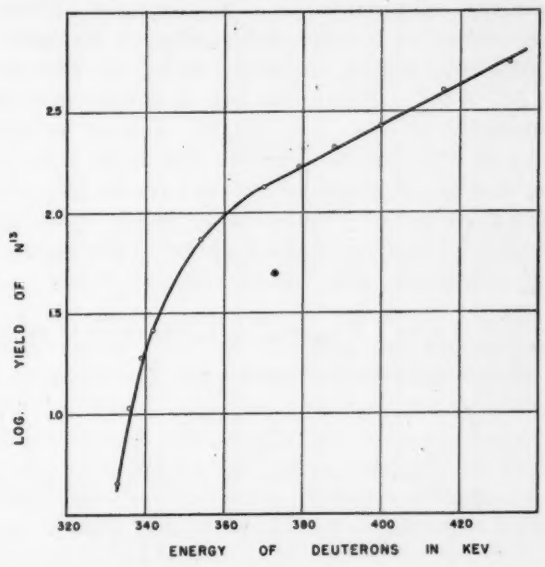

FIG. 2. Logarithm of the yield of N^{13} *versus* energy of deuterons. The linear portion of the curve above 370 kev shows exponential increase with energy for a thin target. Below 370 kev, the target is thick and the yield is not exponential.

number of counts in 100-sec. intervals were plotted to make certain that the effect being counted had a half-life of 10 minutes. Before going through the above procedure for a different current in the magnetic analyzer, the activity was allowed to decay through at least five half-lives. Allowance was made for any activity remaining.

Experiments were carried out in the region of the threshold and also at a bombarding voltage of 1188 kev. Absolute cross sections were assigned to our excitation curve by making use of the accurate determination of the cross section for this reaction at higher energies as determined by Bonner, Evans, Harris, and Phillips.[7]

Upon completion of the experiment, the magnetic analyzer was calibrated by means of the two narrow resonances at 485 kev and 873.5 kev in the reaction $F^{19}(p,\alpha)^*O^{16}$. The precise energy of the higher resonance is that recently obtained by Herb.[8] In the case of the lower resonance 1.3 percent has been added to the older result of 479 kev, in view of the more recent results of Herb. A very thin target of ZnF_2 which weighed 2 micrograms per cm^2 was used in these experiments. The peak of the lower resonance was observed at a current of 1.902 amperes in the magnetic analyzer. The maximum of the higher resonance was obtained at 2.562 amperes. The threshold for the production of N^{13} was obtained at an intermediate value of 2.223 amperes, and so the voltage scale was probably known at the threshold to an accuracy of better than one percent.

RESULTS

Table I gives the relative yield of N^{13} obtained from the individual runs. The averaged values of the number of N^{13} atoms formed as a function of bombarding energy are shown in Fig. 1. The yield of N^{13} is not a linear function of energy near the threshold. In the case of the similar reaction $C^{14}(p,n)N^{14}$, Stephens, Spruch, and Schiff find that the number of neutrons should vary as $(E_p-E_t)^{\frac{1}{2}}$ for a thick target. Consequently, in Fig. 1 we have plotted (yield of N^{13})$^{\frac{1}{2}}$ as a function of the energy of the deuterons. The result appears linear with energy near the threshold, and an accurate value of the threshold (328 kev) is obtained. The Q value of the reaction is $-6/7\cdot 0.328=-0.281$ Mev. The limit of error is estimated to be ± 3 kev, which corresponds to an uncertainty in the absolute value of the bombarding voltage of one percent. Figure 2 shows the variation of yield with deuteron energy on a logarithmic scale. Above 370 kev, the cross section increases exponentially with energy; below 370 kev, the curve is no longer exponential. At bombarding energies less than 370 kev, the target is "thick," and above this value it becomes "thin." A target thickness of $370-328=42$ kev is indicated. From the mass of the carbon target its thickness was calculated to be about 45 kev at 350-kev bombarding energy.

The difference between the mass of the neutron and proton $(n-H)$ neglecting the mass of the neutrino is equal to $Q_3-Q_1-Q_2$ minus the mass of two electrons. The range of the protons from Eq. (3) has been determined by Cockcroft and Lewis,[2] and a calculated value[9] of Q_3 is 2.71 ± 0.05 Mev. The computed energy difference $(n-H)$ is 0.773 Mev from a value of $Q_1=-0.281$ Mev, $Q_2=1.198$ Mev, and $Q_3=2.71$ Mev. If the higher value of $Q_2=1.24$ Mev is used, the $(n-H)$ difference is 0.73 Mev which appears to be too low a value, particularly in view of the recent accurate value of $(n-H)=0.804\pm 0.009$ Mev obtained by Bell and Elliott.[10] Stephens[11] has pointed out that values of Q_3 of comparable accuracy can be obtained from mass spectrographic data. The combined data of Ewald[12] and Mattauch[13] yield a value of $Q_3=2.673$ Mev. The resulting $(n-H)$ difference is either 0.74 or 0.69 Mev, depending on the values taken for Q_2. These mass differences seem too low. The older mass spectrographic data of Bainbridge and Jordan[9] give a value of $Q_3=2.76$ Mev; this leads to values of $(n-H)$ of either 0.82 or 0.78 Mev, depending on the value of Q_2 which is used.

This work was supported by the Research Corporation and by the joint program of the ONR and the AEC.

[7] T. W. Bonner, J. E. Evans, J. C. Harris, and G. C. Phillips, Phys. Rev. **75**, 1401 (1949).
[8] R. G. Herb, private communication.
[9] M. S. Livingston and H. A. Bethe, Rev. Mod. Phys. **9**, 245 (1937).
[10] R. E. Bell and L. G. Elliott, Phys. Rev. **74**, 1552 (1948).
[11] W. E. Stephens, Rev. Mod. Phys. **19**, 19 (1947).
[12] H. Ewald, Zeits. f. Naturforschgung **1**, 131 (1946).
[13] J. Mattauch, Phys. Rev. **57**, 1155 (1940).

The Neutrons and Gamma-Rays from the Disintegration of C^{12} by Deuterons

T. W. Bonner, J. E. Evans, J. C. Harris, and G. C. Phillips
The Rice Institute, Houston, Texas

(Received January 17, 1949)

The excitation curves for the production of gamma-rays and neutrons resulting from the bombardment of carbon by deuterons have been determined over the deuteron energies 0.7 to 1.9 Mev. A careful study of the very narrow gamma-ray resonance occurring at 1.435 Mev has shown that the half-width of the resonance is 5.5 kev and the cross section is 0.62 barn at resonance. Other gamma-ray resonances were observed at 0.91, 1.16, 1.30, and 1.73 Mev with cross sections, respectively, of 0.29, 0.34, 0.39, and 0.97 barn. No resonance for the production of neutrons has been observed at, or near, 1.435 Mev. Resonances for the production of neutrons were observed at energies of 0.91, 1.16, 1.30, 1.62, and 1.76 Mev with the total cross section at resonance, respectively, of 0.12, 0.14, 0.19, 0.19 and 0.22 barn. The angular distributions of the neutrons have been studied; the distributions are quite complex and vary radically with changes in the bombarding energy. At 1.26 Mev there are about five times as many neutrons at 160° as at 0° to the direction of the deuteron beam.

INTRODUCTION

RESONANCE yields occurring in the deuteron bombardment of carbon were first observed in 1940 by Bennett and Bonner. In a series of experiments done at the Rice Institute[1–4] and at the University of Minnesota[5,6] the excitation yields for the various disintegration products were determined. The nuclear reactions occurring in C^{12} and the energy released in each reaction are

(1) ${}_6C^{12}+{}_1H^2\rightarrow{}^*N^{14}\rightarrow{}_6C^{13}+H^1+2.7$ Mev,[7]
(2) ${}_6C^{12}+{}_1H^2\rightarrow{}^*N^{14}\rightarrow{}_6{}^*C^{13}+H^1-0.5$ Mev,[3]
(3) ${}_6C^{12}+{}_1H^2\rightarrow{}^*N^{14}\rightarrow{}_7N^{13}+n^1-0.281$ Mev.[8]

The gamma-rays emitted from the excited $^*C^{13}$ of reaction (2) have been determined to have an energy of 3.11 Mev,[9] which is to be compared to a value of 3.2 expected from the measured values of the energy released in reactions (1) and (2). The energy of the gamma-ray involved in the very narrow resonance at 1.435 Mev was checked and found to be about 3 Mev,[3] the same as for the other broader resonances.

One of the objects of the present experiment was to obtain the natural width of the sharp resonance at 1.435 Mev. In the previous experiments the observed width of this resonance was 10 kev, but since this was the width expected from the spread in energy of the beam of deuterons, the data showed only that this level was narrower than 10 kev. With the improved resolution of our apparatus, the natural width could be obtained.

Another object of these experiments was to find if neutrons from reaction (3) showed a resonance at 1.435 Mev. The earlier experiments indicated no resonance, but a careful search for resonant effects is important since it is very difficult to understand theoretically why any level in the excited ${}_7{}^*N^{14}$ nucleus, no matter what its parity and angular momentum, cannot break up into N^{13} and a neutron.

A study of the angular distribution of the neutrons of reaction (3) has been prompted by the somewhat different form of excitation curves obtained by measurements of the positron activities of N^{13} (a measure of total neutron production over all angles) and curves obtained by direct detection of the neutrons emitted in a small solid angle from a carbon target. Similarly Bailey, Freier, and Williams[6] have discovered a very marked difference between the excitation curves for the production of neutrons taken at 0° and 90° to the bombarding deuteron direction.

APPARATUS

The Rice Institute Van de Graaff generator was used to accelerate the deuterons. Regulation of the beam-analyzing electromagnet (supplied now by a bank of high capacity storage batteries instead of a generator as in previous descriptions[10]), in combination with a potential stabilizer used to modulate an electron beam to the central electrode, gave a deuteron beam with an estimated resolution of 0.01 percent, or less, of the operating voltage.[10] A beam current integrating device, designed by B. E. Watt,[11] gave a count on a mechanical register for each 0.0416 microcoulomb of deuteron charge collected at the target.

[1] W. E. Bennett and T. W. Bonner, Phys. Rev. **58**, 183 (1940); Bonner, Hudspeth, and Bennett, Phys. Rev. **58**, 185 (1940).
[2] Rogers, Hudspeth, Bonner, and Bennett, Phys. Rev. **58**, 186 (1940).
[3] Bennett, Bonner, Hudspeth, Richards, and Watt, Phys. Rev. **59**, 781 (1941).
[4] W. E. Bennett and H. T. Richards, Phys. Rev. **71**, 565 (1947).
[5] Bailey, Phillips, and Williams, Phys. Rev. **62**, 80 (1940).
[6] Bailey, Freier, and Williams, Phys. Rev. **73**, 274 (1948).
[7] W. E. Stephens, Rev. Mod. Phys. **19**, 19 (1947).
[8] Bonner, Evans, and Hill, Phys. Rev. **75**, 1398 (1949).
[9] Dougherty, Hornyak, Lauritsen, and Rasmussen, Phys. Rev. **74**, 712 (1948).
[10] Bennett, Bonner, Mandeville, and Watt, Phys. Rev. **70**, 882 (1946).
[11] B. E. Watt, Rev. Sci. Inst. **17**, 334 (1946).

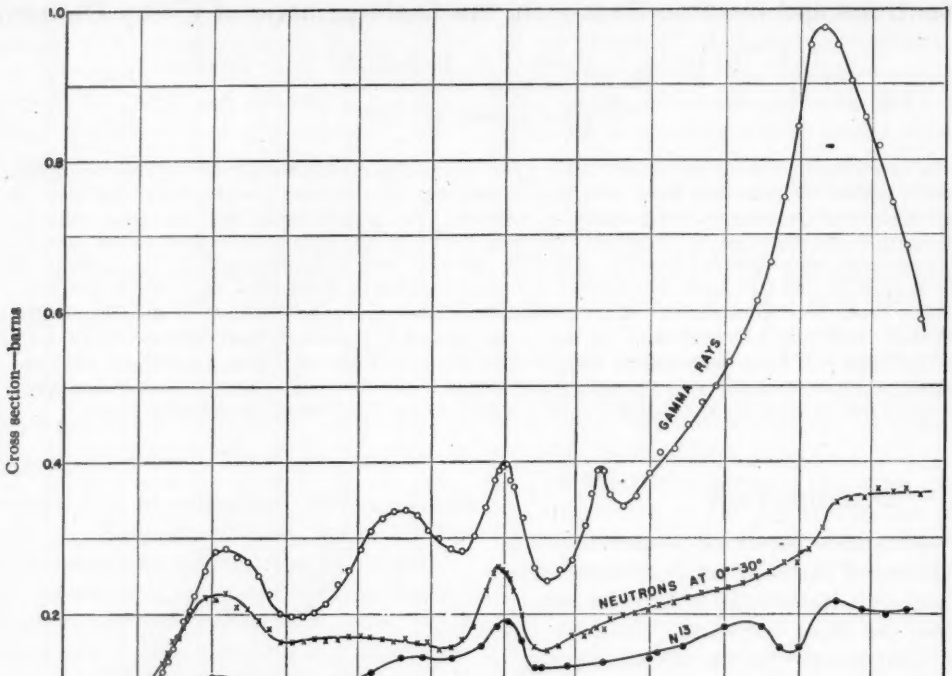

FIG. 1. Experimentally determined cross sections for the production of gamma-rays and N^{13} as a function of the energy of the bombarding deuterons. The yield of neutrons at $0°\pm30°$ is not in terms of absolute cross section, but shows only relative shape of this yield function.

Some of the carbon targets were prepared by heating small volumes of ceresin wax in a vacuum and collecting a thin film of the wax on a polished silver disk. The target thickness in μ g/cm^2 was determined by weighing the wax deposit on a microbalance. These targets did not collect carbon or deuterium in quantities sufficient to be detected as an increase in gamma-rays or neutrons. However, ceresin wax targets when deposited on very thin silver foils and exposed to the deuteron beam in a vacuum were found to become thinner. More satisfactory targets of pure carbon were made by cracking benzene in an atmosphere of helium onto the surface of silver foils.[12]

The counter used to determine the angular distribution of the neutrons was a cylindrical proportional counter of 4.5-cm inner diameter and a sensitive length of 4.5-cm, with a one mil tungsten wire. The counter was filled with one atmosphere of hydrogen and two percent methane, and operated at 1920 volts with an Atomic Instrument Company type 204-B Linear Amplifier.

[12] G. C. Phillips and J. Richardson (to be published).

DETERMINATION OF THE EXCITATION CURVES

The Gamma-Rays

In order to study the gamma-rays that accompany the short range proton group of reaction (2), a thin-walled, argon-filled Geiger counter was placed at about 8 cm from the center of the target and at about 90° to the direction of the deuteron beam. Large lead blocks were used to shield the counter from stray gamma-rays originating from carbon contamination along the beam path. In addition, about an inch of lead was placed around the counter to absorb scattered x-rays coming from the high voltage electrode of the Van de Graaff generator and annihilation radiation coming from the N^{13}. The counting rate for this arrangement of the Geiger counter became too great above 1.5 Mev. To keep the counting rate of the background radiation a small percentage of the total counting rate, a much smaller Geiger counter was used in preference to moving the original counter farther from the target. Background determinations were usually made by allowing the entire beam to fall just on the low energy side of the analyzing slit system, thus blocking the beam from the target, but giving essentially the same amount of radiation from carbon

contamination elsewhere along the beam path. Under these conditions this background counting rate was about 10 percent of the total rate for a very thin target that was only 3.0 μ g/cm^2 of ceresin. For the thicker targets, which were ordinarily used, the background was correspondingly less.

To determine accurately the cross section for the production of gamma-rays, a thick, pure graphite target was bombarded with deuterons of 1.30-Mev energy. Since the "thin" target relative yield of gamma-rays as a function of energy was known, the cross section for gamma-rays could be calculated from the observed thick target yield by integrating the thin target curve from 0 to 1.30 Mev. A small counter with a copper cathode was placed 17 cm from the target and surrounded by 1.4 cm of lead. A counter efficiency of 1.65 percent was assumed for the 3.1-Mev gamma-rays.[13] The transmission of the lead under identical geometrical conditions was determined experimentally by means of 2.62-Mev gamma-rays from mesothorium and found to be 48 percent. These data gave a cross section at 1.30 Mev of 0.39 barn. The gamma-ray data of Fig. 1 are all adjusted to this cross section. It is to be noted that in Fig. 1 the narrow resonance at 1.435 Mev does not have its true cross section indicated since the target was much thicker than the true resonance width.

The 1.435-Mev gamma-ray resonance has been observed in the present experiment with ceresin targets varying in thickness from 3 to 80 μ g/cm^2, which correspond to the range of 1 to 27 kev for deuterons of 1.4 Mev. Just previous to one of these observations with a 6-kev target, the beam analyzing magnet was calibrated using the narrow gamma-ray resonances found in the bombardment of fluorine by protons for reference energies.[14] The resonances at 0.669 and 0.8735 Mev were studied using the molecular beam, and so calibrations were obtained at 1.338 and 1.742 Mev. With this calibration the peak of the narrow resonance, which had previously been designated as the 1.43-Mev resonance,[15] was found to occur at 1.435 Mev.

The shape of the 1.435-Mev resonance was determined with good resolution by using a 1-kev thick ceresin target and by changing the bombarding energy in 1-kev steps (see Fig. 2). The energy width measured midway between the dotted line of Fig. 2 and the resonance peak was found to be 5.5 kev. This is thought to be nearly the natural width since the energy spread in the beam was less than 1.4 kev and the target was very thin. The asymmetry observed on the sides of this resonance has been observed in all of the twelve separate examinations of the resonance made during this experiment. By using a 1-kev target, the ratio of yields at the peaks of the 1.30-Mev and the 1.435-Mev were carefully determined to be 1.58 so that the cross section at resonance peak for the 1.435-resonance is 0.62 barn.

The angular distribution of the gamma-rays was investigated at 1.73 Mev with the small Geiger counter. To do this it was necessary to rotate the counter about the target at a distance greater than had been used for the excitation curves. The background count was ~10 percent of the true counts. No asymmetry was found greater than 10 percent, the background counting rate.

The N^{13} Positrons

The total yield of neutrons integrated over all angles can be obtained by observing the positron activity of the residual N^{13} nucleus of reaction (3). To determine the relative number of positrons as a function of energy a quantity of N^{13} was prepared by deuteron bombardment for a half-life (600 seconds) of a thin ceresin target on a thick silver disk placed at 30° to the beam. Immediately after this bombardment the positron activity was observed through an aperture of 0.5-cm diameter at a distance of 6.7 cm from the target and at right angles to the beam. A thin-walled Geiger counter

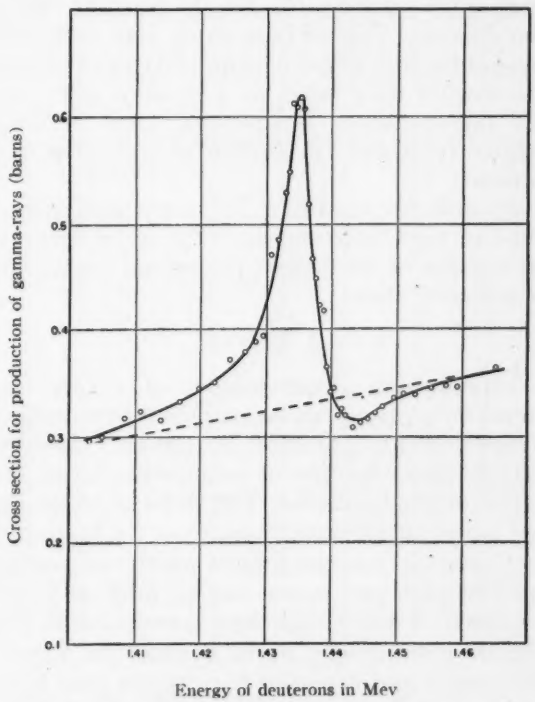

FIG. 2. Experimentally determined cross section in barns for the production of gamma-rays from a thin (1-kev) ceresin target at the narrow 1.435-Mev resonance.

[13] Bradt, Gugelot, Huber, Medicus, Preiswerk, and Scherrer, Helv. Phys. Acta **19**, 77 (1946).
[14] Bernet, Herb, and Parkinson, Phys. Rev. **54**, 398 (1938); R. G. Herb (1948) private communication.
[15] Harris, Bonner, Evans, and Phillips, Phys. Rev. **73**, 649 (1948).

TABLE I. Data pertaining to the neutron and gamma-ray resonances.

Position of resonance Mev	Width at half-height kev (gamma-ray and neutron resonances)	Cross section at resonance peak in barns		Estimated relative intensity	
		Gamma-ray	Neutron	Gamma-ray	Neutrons
0.91	200	0.29	0.12	2.5	1.0
1.16	200	0.34	0.14	2.5	1.0
1.30	80	0.39	0.19	2.5	1.4
1.435	5.5	0.62		2.5	<0.1
1.62	200		0.19		1.0
1.73	200	0.97		9.0	
1.76	200		0.22		1.0

and a scale of 64 units were used to detect and record the number of positrons passing through the aperture. These measurements could not be used to determine the cross section because of backscattering of the positrons by the thick target backing, but the measurements gave relative yields. The cross section was determined by using a pure carbon target of 23.5 μ g/cm^2 on a thin silver foil (7.75 mg/cm^2). The target was placed normal to the deuteron beam and was bombarded for two half-lives (20 minutes). It was then quickly removed from the vacuum system and placed over the axis of a bubble-window Geiger counter, of window thickness 3 mg/cm^2. The only absorbing material in the path of the positrons (end-point energy 1.24 Mev)[16] was from the few centimeters of air and the counter window, and so nearly 100 percent of the positrons reached the sensitive region of the counter. The backscattering was negligible because of the thin target backing. Five independent measurements were taken at 1.30 Mev, with different target-counter separations; cross sections calculated from these measurements agreed within 10 percent.

If dN/dt is the number of N^{13} atoms decaying at the end of the bombardment of 20 minutes and n is the number of N^{13} formed per second during the bombardment, then

$$n = -4/3(dN/dt).$$

The experimental determination of dN/dt was obtained by plotting the logarithms of the number of Geiger counts obtained in 100-sec. intervals *versus* the time, for ten or so intervals after the cessation of bombardment. The times at which the points were plotted were 53 sec. from the beginning of each interval; i.e., the time at which the average number of positron counts over an interval would be expected. A line with a slope corresponding to a 10-minute half-life was drawn through the experimental points and extended back to the time bombardment ceased, thus obtaining dN/dt at $t=1200$ sec.

The thickness of the pure carbon target on the silver foil was obtained by comparing the ratios of the gamma-rays from this target and the thick target previously mentioned. These data were taken at 1.30 Mev with several geometrical arrangements of the counter about the targets, and gave the same ratio of yield to within 10 percent.

These measurements gave a cross section of 0.192 barn at 1.30 Mev for the production of N^{13}. The cross section for N^{13} production as a function of deuteron energy is shown in Fig. 1.

Table I gives the collected data pertaining to the neutron and gamma-ray resonances which were observed.

The Neutrons

The yields of neutrons at 0° ($\pm 30°$) as shown in Fig. 1 were obtained using a proportional counter 6 cm long and 1.6 cm in diameter filled with ethane at a pressure of 43 cm of Hg. The counter had a 4-mil wire and was operated in the proportional region at 2200 volts. These data are relative yields and not absolute cross sections.

The protons recoiling from the neutrons entering the counter were counted if their energy exceeded 300 kev, a value set by means of a discriminator attached to the output of a 204-B linear amplifier and before the input of an Atomic Instrument Company scale of 64. Gamma-rays from reaction (2) were not observable at this bias. A discussion of this type of counter has been given by Bethe and Barschall,[17] who show that the counter sensitivity (assuming a proton track length small in relation to the counter diameter) is relatively insensitive to neutron energy.

Stray fast neutrons were partially shielded from the ethane counter by means of paraffin blocks interspersed among the lead blocks used to shield the gamma-ray counter. The counter was placed to subtend the largest solid angle possible at the target and was surrounded by about 5 cm of paraffin except on the side adjacent to the target. The paraffin shielding was effective in reducing the background counting rate.

The region in the vicinity of the 1.435-Mev gamma-ray resonance has been investigated for neutron resonances by means of the hydrogen-filled counter at laboratory angles of 45°, 90°, and 160°, and by means of the ethane counter at 0°. These data are shown in Fig. 3. There is no evidence for a sharp neutron resonance in this energy region.

[16] K. Siegbahn and H. Slatis, Arkiv. f. Mat. Astr. O. Fys. **32A**, No. 9 (1945).

[17] H. H. Barschall and H. A. Bethe, Rev. Sci. Inst. **18**, 147 (1947).

The Neutron Angular Distributions

Neutron angular distributions were taken at nine deuteron energies. The hydrogen-filled proportional counter with a linear amplifier, discriminator, and scaler was used to count the fast neutrons. This counter was non-directional and the bias setting corresponded to 0.15-Mev recoil protons as was determined by 3 bias *versus* counting rate curves for neutrons of different known energies. The counter was insensitive to the gamma-rays when set at its standard bias. By lowering the bias the over-all gain of the system was checked frequently with a radium source in a standard position. The counter was rotated about the target at a distance of 10 centimeters and it subtended a laboratory angle of $\pm 12°$ at the target. The data was taken in 15° steps in the laboratory system. The carbon target was 135 μ g/cm^2 of ceresin wax on a thick silver disk. Data was taken by going several times through the angles and averaging. These averages are believed to be correct to within 10 percent. The background count was obtained by letting the beam fall on the defining slits only. The background was less than 10 percent.

The laboratory angles θ were converted into center of gravity angles φ by the relation

$$\sin(\varphi-\theta)=\left(\frac{E_{\text{deuteron}}}{78E_{\text{deuteron}}-25.5}\right)^{\frac{1}{2}}\sin\theta$$

and the counting rates at each c.g. angle φ were corrected because of the variation of the solid angle subtended by the counter in the center of gravity coordinates.

The counting rates at each deuteron energy and at each angle were also corrected for the efficiency of the counter. The efficiency of the counter is given by

$$F=\sigma_0\mathfrak{N}DPE_n^{-\frac{1}{2}}$$

where $\sigma_0=4.16\times10^{-24}$ cm^2 is the neutron-proton cross section at 1 Mev, E_n is the neutron energy in Mev, $\mathfrak{N}$ is the number of hydrogen atoms/cm^3, D is the effective depth of hydrogen gas that the neutrons see, and P is the probability that if a recoil occurs inside the counter it will be counted as a pulse above the bias. P is not only a function of bias energy (the size of the "cone" of recoiling protons that will release the bias energy) but also of the ratio of proton track length L to counter radius R. P and F have been calculated for the counter.[18]

The efficiency of the hydrogen counter may also be experimentally determined. By integration of the observed angular distribution curves and comparison of this total yield into 4π-radians with the yield of N^{13} as determined from the positron measurements an efficiency of the counter for the average neutron energy in that distribution is obtained. These experimental determinations agreed with the theoretical within about 15 percent. The corrections in yield were made using the theoretical efficiency. The angular distributions are shown in Fig. 4 and are believed to be correct to within 10 percent. A subsequent paper will analyze the neutron angular distributions.

[18] J. C. Harris and G. C. Phillips (to be published).

CONCLUSIONS

In general, reactions (2) and (3) are competing reactions, and at the three lower resonances there are about equal probabilities of breaking up with the emission of neutrons or short range protons. However, certain marked differences in the resonance phenomenon of reaction (2) and (3) can be noted. There are resonances for neutron emission at 1.62 and 1.76 Mev that do not correspond to the large gamma-ray resonance at 1.73 Mev. It is interesting that the 1.73-Mev gamma-ray resonance occurs at the point of maximum slope of the neutron cross section suggesting that the neutrons show something akin to dispersion about this point. Although the resonance at 1.62 Mev was not observed at 0°, similar curves when counting neutrons at 90° have been obtained by Williams *et al.*[6] for this region.

At the 1.435-Mev resonance there is no indication of a neutron resonance within the limits of the experiment. If a neutron resonance exists it must be relatively weak and $\sigma_\gamma/\sigma_{\text{neut.}}>25$. The shape of the 1.435 resonance for gamma-rays is markedly asymmetrical; this resonance has been observed many times with different targets and different experimental arrangements and so it is certain that the asymmetry is real. It is interesting that a

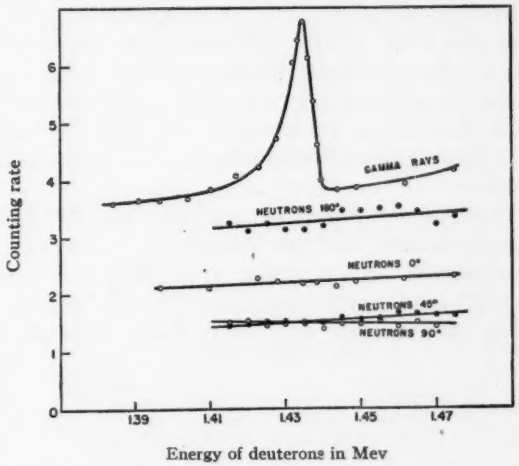

FIG. 3. The yields of gamma-rays and neutrons at 0°, 45°, 90°, and 160° at the narrow 1.435-Mev resonance. The 45°, 90°, and 160° neutron counting rates are correct ratios while the 0° counting rate is arbitrary.

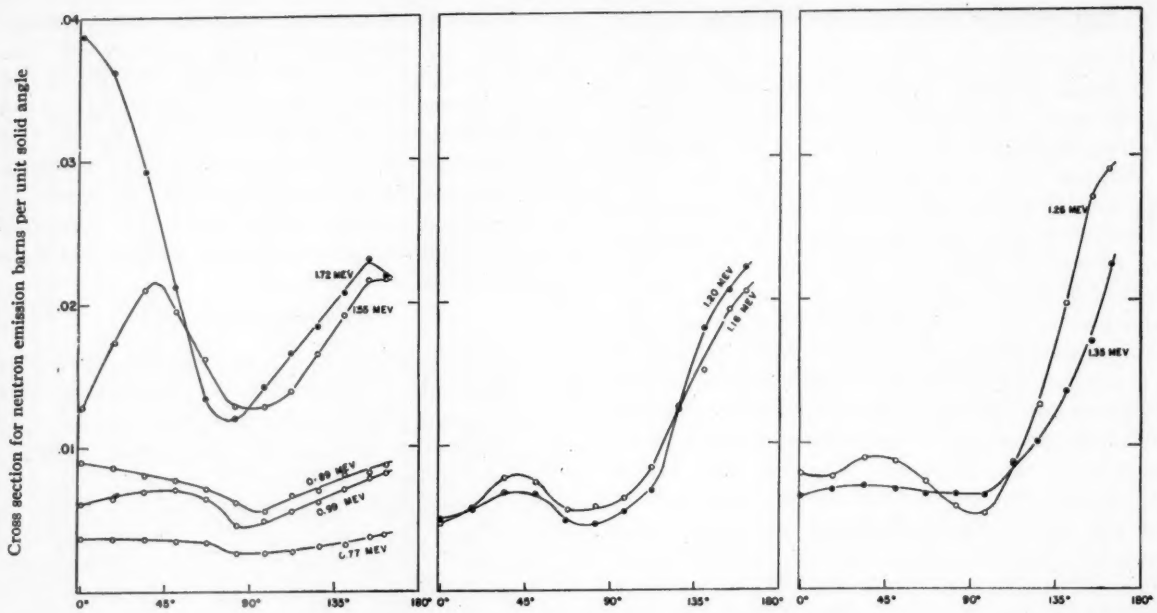

FIG. 4. The angular distributions of the neutrons in center of gravity coordinates for the deuteron bombarding energies indicated.

superposition of resonance and dispersion formulas will produce this shape. Similar shapes have been observed in the resonances associated with the bombardment of fluorine by protons.

The ratio of the cross sections for reactions (2) and (3) are several orders of magnitude different from what would be expected if the deuteron is captured by the C^{12} nucleus and the excited $*N^{14}$ nucleus subsequently breaks up with the emission of either a short-range proton or a neutron. At the 0.91-Mev resonance the ratio of the number of short-range protons to neutrons is $\sigma_\gamma/\sigma_n \sim 2.5$. At this bombarding energy the short-range protons have only an energy of 230 kev in the center of mass coordinates; the penetrability through the Coulomb barrier for $l=0$ is only approximately 10^{-4}. The effect of the Coulomb barrier should make the emission of neutrons far more likely than the emission of short-range protons; and indeed the cross section for reaction (2) should be much smaller than is observed.

In the case of the narrow resonance at 1.435 Mev the penetrability of the short-range protons is approximately 1/30, while the observed ratio $\sigma_\gamma/\sigma_n > 25$, and so the discrepancy in the expected number of neutrons and short range protons is >750.

Since the discrepancies are so large in the cross sections, it seems possible that the assumed mechanism of disintegration is wrong. There is the possibility that the entire deuteron does not enter the C^{12} nucleus in the case of low energy proton emission. The difficulty in proposing an Oppenheimer-Phillips reaction to interpret the results is that sharp resonances like the 1.435 Mev should not be observed. The lifetime of the nucleus would be expected to be of the order of the transit time of the proton across the nucleus, or about $5\times10^{-13}/10^{9} = 5\times10^{-22}$ sec. From the relation $\Delta E \cdot \Delta t \sim \hbar$, a width of 1.3 Mev is obtained, and this is completely incompatible with the sharp resonance that is observed. In view of this difficulty in the width of the level it seems that some other mechanism must be sought.

Critchfield has suggested an explanation in terms of a special model of the excited $*N^{14}$ nucleus with a large rotational angular momentum. If the $*C^{13}$ has high rotational angular momentum the probability of transition from $*N^{14}$ to $*C^{13}$ may be much greater than to a N^{13} nucleus without this high angular momentum.

This work was supported by the Research Corporation and by the joint program of the ONR and AEC.

Measurements of the Absolute Intensity of Cosmic Radiation at Sea Level

R. A. MONTGOMERY*
California Institute of Technology, Pasadena, California
(Received January 24, 1949)

A cosmic-ray telescope is described which measures the absolute intensity of the cosmic radiation through the use of trays of overlapping Geiger counters to eliminate insensitive areas. The results obtained, carefully corrected for accidentals, counter efficiency, side showers, absorption, and barometric pressure, are compared with those of previous authors.

I. INTRODUCTION

PREVIOUS sea level determinations of the total cosmic ray intensity show surprising discrepancies in the values obtained by different authors, over a range of thirty to forty percent.[1–5] These discrepancies are much greater than the normal daily and seasonal variations. The greatest single sources of error are in the corrections for side showers and absorption in the counter walls and material overhead.

The Geiger-counter telescope described below utilizes larger and symmetrical sensitive areas and yet retains good angular resolution. The larger areas give greater real counting rates so that good statistical accuracy can be achieved in short periods of time. This advantage, together with that of using thin-walled counters of relatively low absorbing power, and a novel method of minimizing errors due to variations in the effective length of the counter, indicated that more reliable results could be obtained than those previously reported.

This work was done as a supplement to that previously described[6,7] using equipment largely adapted from the previous work.

II. COUNTER TELESCOPE FOR ABSOLUTE DETERMINATION OF COSMIC-RAY INTENSITY

The telescope is composed of three trays of Geiger counters rigidly supported, one below the other, by a boxlike aluminum framework. Each tray is made up of eleven counters, nine of which have their axes parallel and which overlap so that there is no insensitive area between the counters. The other two counters are placed transversely, one across each end of the main group. Each tray of the telescope has 25.69-cm effective length and 24.52-cm effective width. The spacing between the two outer trays of the telescope is 98.5 cm between corresponding planes through the trays.

The Geiger counters used,[6] were made from copper-plated steel cylinders of 0.025-cm wall thickness. The diameter is 3.3 cm and the length approximately 25 cm. The counters were carefully chosen to have nearly equal thresholds and were operated at constant battery voltage approximately 100 volts above threshold. The individual counting rates of the counters agreed very closely when they were tested under identical conditions, using a thorium source to stimulate rapid counting rates.

From purely geometrical considerations it is possible to calculate the ratio of the counting rate of the telescope, n, in counts per minute, to the absolute intensity, j_0, of the cosmic rays, in ionizing particles per unit solid angle per cm² per minute, considering only cases where one particle strikes all three trays. If the telescope is pointing vertically, if the trays are of dimensions "$2a$" and "$2b$," if the separation between the outer trays is "d," and if the intensity of the radiation is assumed to vary as the square of the cosine of the zenith angle, then we have

$$n/j_0 = 16a^2b^2(1-2a^2/d^2)(1-2b^2/d^2)/d^2, \qquad (1)$$

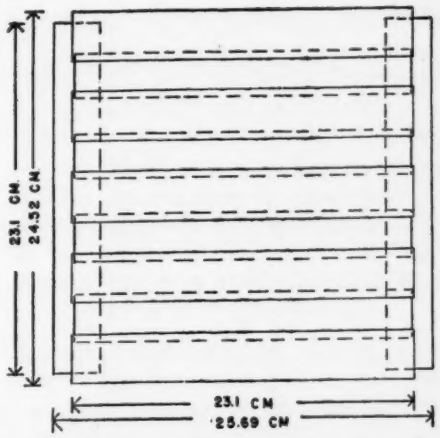

FIG. 1. Plan view of a single tray of Geiger counters. The effective dimensions of the individual counters are shown. Note that the counters overlap so that only about ⅓ of the effective area of each is utilized.

*Now at General Electric Company, Schenectady, New York.

[1] T. H. Johnson, Phys. Rev. **43**, 307 (1933).
[2] J. C. Street and R. H. Woodward, Phys. Rev. **46**, 1029 (1934).
[3] D. K. Froman and J. C. Stearns, Can. J. Research **A**, 29 (1938).
[4] K. Greisen, Phys. Rev. **61**, 212 (1942).
[5] K. Greisen and N. Nereson, Phys. Rev. **62**, 316 (1942).
[6] A. T. Biehl, R. A. Montgomery, H. V. Neher, W. H. Pickering, and W. C. Roesch, Rev. Mod. Phys. **20**, 360 (1948).
[7] See reference 6, p. 353.

TABLE I. Counting rate of apparatus.

	Counting rate (coincidences per minute)	Date	Barometer (inches Hg)	Total counts	j_0 (uncorrected)
Transverse counters connected	28.05	Nov. 5–7, 1947	29.42	72,000	0.726
Transverse counters unconnected	23.40	Nov. 13–14, 1947	29.21	22,500	0.724

where if a/d is less than $\frac{1}{8}$, then any higher order terms may be neglected with an error of less than $\frac{1}{4}$ percent.

For the particular telescope used, we must make a correction for the insensitive areas at the corners of the tray and also a correction for the finite thickness of the trays. Figure 1 shows a plan view of one of the trays showing the sensitive areas of the counters making up the tray. The effective width of each counter is assumed to equal the inside diameter of the cylinder.[4] The effective counter length was determined by the method of Street and Woodward[2] to be 23.1 cm as an average for five counters. Figure 2 shows the experimental curve for this determination.

The insensitive area constitutes 0.66 percent of the total area so that the correction due to this factor is -1.3 percent because of the dependence of the counting rate on the square of the tray area. The cylindrical shape of the counters may be shown to add to the effective tray area in amount of 0.5 percent when the transverse counters are effective in the circuit.

Applying these two geometrical corrections and substituting for "a," "b," and "d," we have $n/j_0=38.60$.

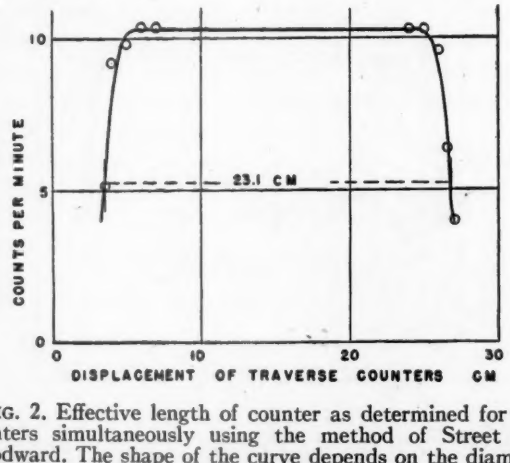

FIG. 2. Effective length of counter as determined for five counters simultaneously using the method of Street and Woodward. The shape of the curve depends on the diameter of the counters, the effective length being given by the distance between half-maximum points.

If the transverse counters are disconnected, then we have an entirely different telescope admittance. The circular ends of the counters now contribute to the effective area and solid angle of the telescope. An integration is performed to determine the number of rays that can pass through one set of circular ends on one tray, and which are so directed as to pass through the other extreme tray. This result, multiplied by four for the other similar sets of counter ends, amounts to a total of 3.2 percent for the geometry used. The cylindrical shape of the counters affects only the effective width in this case and hence the correction is but half of that when the traverse counters are connected, i.e., 0.25 percent. If we apply these two corrections and now use the effective length of a single counter as that of the tray, we now have, using Eq. (1), $n/j_0=32.30$.

The ratio of the geometrical factors for the telescope with and without the transverse counters connected is $38.60/32.30=1.195$. It is possible to get an internal check on the consistency of these results by comparing the counting rates of the telescope with and without the transverse counters connected. This was done using both double and triple coincidences. The results were: for triples, 1.19 ± 0.01; for doubles, 1.215 ± 0.01.

III. DETERMINATION OF ABSOLUTE INTENSITY OF COSMIC RAYS

The counting rate of the above apparatus was determined at Pasadena on the roof of Bridge Laboratory. The residual absorbing material, in addition to the counter walls, was $\frac{1}{4}$-inch plywood. (See Table I.)

IV. CORRECTIONS FOR ABSOLUTE DETERMINATION

These results must be corrected for the following factors:

(1) Accidental coincidences and loss of efficiency;
(2) changes in barometric pressure;
(3) absorption in the counter walls and wood overhead;
(4) additional coincidences due to side showers.

Measurements were taken over 24-hour periods to minimize the daily variations.

V. CORRECTIONS FOR ACCIDENTALS AND EFFICIENCY

The resolving time of the electronic circuits is such that the number of sea-level accidental coincidences is completely negligible for a three-tray arrangement.

As discussed by Johnson,[8] the efficiency of a train of "n" coincidence counters is E^n where $E=E_\sigma E_p$. E_σ is the efficiency as limited by the "dead time" of the counters, and E_p is the efficiency

[8] T. H. Johnson, Rev. Mod. Phys. 10, 206 (1938).

as limited by the pressure in the counters and the kind of gas used to fill them.

The measurements of the efficiency due to "dead time" have been described.[6] The efficiency in this respect is 99.9 percent since the sea-level counting rate per tray is only about 20 counts per second.

The probability of detection of a single particle of path length "L" through a counter, filled to pressure "p" with a gas of specific ionization "N," is $(1-\exp(-NLp))$. The over-all efficiency is obtained by integrating the efficiency for a given path length over the distribution of possible path lengths. For a cylindrical counter of diameter "D," the over-all efficiency for particles whose paths are normal to the axis of the cylinder is

$$E_p = 1 - \int_0^1 \exp(-NpD(1-y^2)^{\frac{1}{2}})dy,$$

where "y" is the distance of closest approach of the ray to the counter axis, measured in units of the cylinder radius. Taking the value of $N=30$ ions per cm per atmos. for argon,[8,9] $p=0.075$ atmos., and $D=3.25$ cm, then NpD equals 7.4.

The integration performed graphically in Fig. 3 shows that the over-all counter efficiency is 97.9 percent if the counter is used singly. In the trays used for the absolute determination, the counters overlapped in such a manner that only $\frac{4}{5}$ of the effective diameter of each counter is utilized. The efficiency under these conditions is given by the same expression as above, with the upper limit now 0.8 in the integral. This works out to be 99.8 percent. The tray efficiency is now 99.6 percent if we consider the tray as made up of eight counters, each 99.8 percent efficient and one counter 97.9 percent efficient. The over-all efficiency for three trays in coincidence is 98.8 percent for rays traveling parallel to the axis of the telescope.

The correction for inefficiency of the mechanical recorder is negligible since the resolving time is approximately 0.01 second, and the counting rate is only about 0.5 count per second.

VI. PRESSURE COEFFICIENT OF COSMIC-RAY INTENSITY

Widely different values have been reported in the literature for the pressure-intensity coefficient of the vertically incident cosmic rays at sea level. Clay and Bruins[10] give a value of -6.4 percent per cm Hg change in pressure, from ionization measurements with the chamber shielded with from 12- to 120-cm iron, for rays incident at any angle. Barnothy and Forro[11] report values of -3.74 ± 0.59 percent per cm Hg at the vertical with an angular opening in their Geiger-counter telescope of $10°\times40°$. Their results indicated that the coefficient was slightly smaller away from the vertical. These results differ by nearly a factor of two from those of Clay and Bruins. Unpublished measurements by Pickering show -3.65 percent per cm Hg change in pressure from sea-level observations.

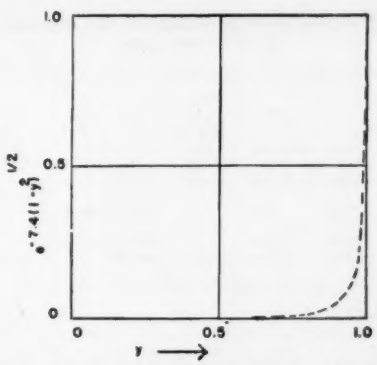

FIG. 3. Graphical integration of $\exp-7.4(1-y^2)^{\frac{1}{2}}dy$. The area under the dotted curve gives the fractional loss in efficiency due to the probability that no ions will be formed by some of the ionizing rays in passing through the counter.

In order to redetermine this coefficient, two of the cosmic-ray balloon telescopes[6] were mounted in a truck and operated at three different altitudes ranging from zero to 1300 feet above sea level. The pressures were recorded with an accurate Paulin barometer which was calibrated against a meteorological standard. The counting rate at each altitude was determined to within a statistical probable error of less than 0.5 percent. Figure 4 shows a curve of the natural logarithm of the counting rate *vs.* the pressure in inches of Hg for several instruments. The average slope corresponds to a coefficient of -9.1 ± 0.6 percent per inch of Hg or -3.6 ± 0.3 percent per cm Hg. These results agree very well with those of Barnothy and Forro, and those of Pickering.

The assumption is made in these measurements that the pressure change due to a change in altitude is equivalent, in its effect on the cosmic-ray intensity, to an equal pressure change at the same altitude. This assumption is justified if an atmosphere in equilibrium is postulated.[12]

VII. ABSORPTION IN THE COUNTER WALLS AND WOOD OVERHEAD

The change in the counting rate of a two-tray telescope was measured as absorbers, corresponding to equivalent numbers of counter wall thicknesses, were placed between the two trays. In Fig. 5 the logarithm of the counting rate is plotted against the number of equivalent wall thicknesses of ab-

[9] J. Cosyns, Bull. Tech. Assn. Eng. Brussels, 173 (1936).
[10] J. Clay and E. M. Bruins, Rev. Mod. Phys. 11, 158 (1939).
[11] J. Barnothy and M. Forro, Zeits. f. Physik. 100, 742 (1936); and 104, 535 (1936).
[12] B. Rossi, Rev. Mod. Phys. 11, 297 (1939).

TABLE II. Principal determinations of the absolute intensity, j_0 of cosmic rays.

Author	Date	Altitude	Pressure inches/Hg	j_0	Corrected	Magnetic lat.
Johnson	1933	189 m	—	0.70		57°
Street and Woodward	1934	0 m	—	0.80±0.028		55°
Froman and Stearns	1938	37 m	—	0.973±0.032		58°
Greisen	1941	259 m	29.2	0.735	0.709*	55°

* Behind ¼-inch of wood.

sorber. Sheets of copper-plated steel, identical to those from which the cylinders were rolled, are used as absorber. Six thicknesses total 1.4-g/cm² of absorber.

If we consider that as many rays are produced as absorbed in the upper wall of the top tray,[13] then the correction for the absorption in the other five counter walls of a triple coincidence telescope would be 4.0±0.5 percent by extrapolation of the curve. The absorption in the ¼-inch of wood overhead is approximately 1.5 percent, as determined by noting the change in counting rate when an additional equivalent layer of wood is placed above the telescope.

VIII. CORRECTION FOR ADDITIONAL COUNTS DUE TO SIDE SHOWERS

A first estimate of the effect of side showers can be obtained by displacing the center tray of the triple-coincidence telescope so that no one particle can traverse all three trays if it travels in a straight line. If the telescope is vertical, and the center tray is displaced in a horizontal plane, a curve may be obtained showing the variation of counting rate with the distance of displacement.

We consider the totality of coincidences due to side showers in two groups, *viz.*, (1) those coincidences due to the passage of only two associated rays, and (2) those coincidences due to the passage of more than two associated rays. The number of the latter will be nearly independent of small displacements, relative to the shower extent, of the center tray.

The number of counts due to only two particles, $n_2(x)$, will be proportional to the number of shower particles which pass at discrete intervals of time through a sub-telescope, made up of the middle tray of the main telescope and one of the outer trays, multiplied by the probability that each particle will be accompanied by another shower particle which excites the third tray. If this probability be considered constant, and if the angular distribution of the discrete shower particles is assumed to vary as the square of the cosine of the zenith angle, then $n_2(x)=KA(\theta)w(\theta)\cos^2\theta$, where $A(\theta)$ is the tray area normal to the sub-telescope axis at angle θ, and $w(\theta)$ is the sub-telescope solid angle. If "d" and "x" are respectively the separation between the outer trays of the telescope and the distance of horizontal displacement of the intermediate tray from the telescope axis, then $\cos\theta=d/(d^2+x^2)^{\frac{1}{2}}$.

Now $A(\theta)=A(0)\cos\theta$ and $w(\theta)=A(0)\cos^3\theta/(d/2)^2$, hence, $n_2(x)=C_1\cos^6\theta$ where C_1 is a constant of the geometry. The total number of counts due to side showers, $n_s(x)$ is therefore of the form $n_s(x)=C_1\cos^6\theta+C_2$, where C_2 represents the coincidences due to the passage of more than two rays. The number of counts due to side showers when the three trays are in the normal telescope arrangement, may be estimated from the extrapolation of

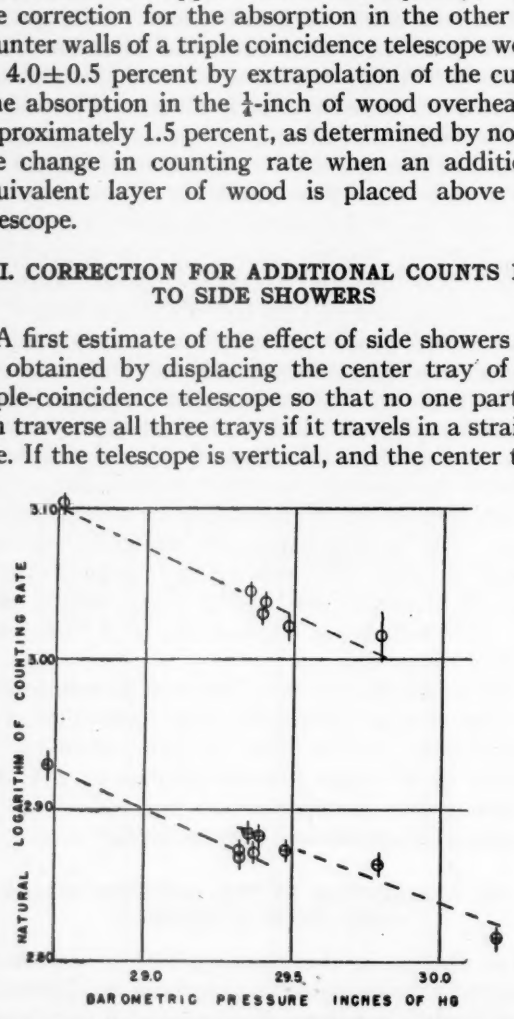

FIG. 4. Variation of intensity of vertically incident cosmic radiation with pressure at sea level. The average slope corresponds to a coefficient $k=0.091$ for the variation of the natural logarithm of counting rate with barometric pressure, measured in inches of Hg.

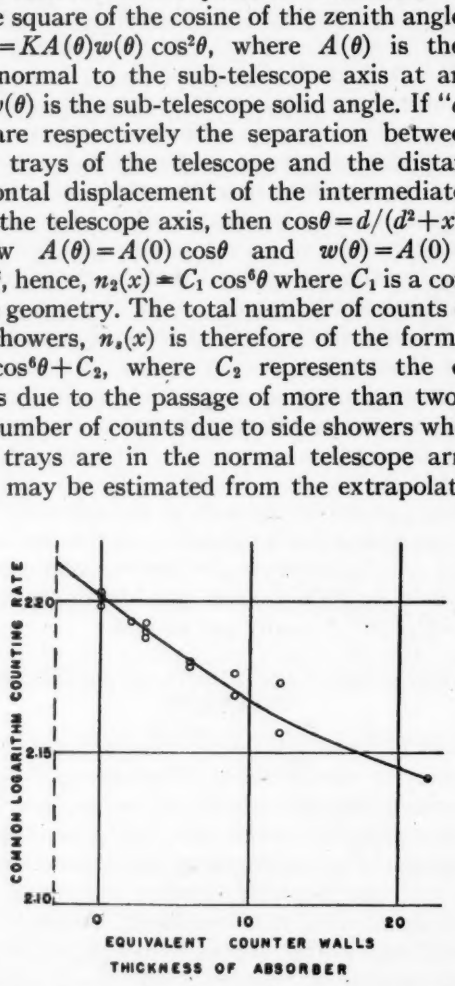

FIG. 5. Variation of coincidence counting rate with equivalent counter walls thickness of absorber using double coincidences. The curve is extrapolated to give the absorption in three additional counter walls.

[13] H. Schwindler, Zeits. f. Physik, **72**, 625 (1931).

the curve of $n_s(x)$ *versus* x or it may be independently determined in the following manner.

The standard telescope is arranged with four evenly spaced trays and counting rates are determined with double, triple, and quadruple coincidences. When the results are corrected for pressure changes and for accidentals, the differences represent the contributions of the side showers since the absorbing material is held constant. The results corrected to a common pressure of 29.07 inches Hg are, if s_2, s_3, and s_4 are the number of counts due to side showers for double, triple, and quadruple coincidences, respectively,

Counting rate (counts/min.)			s_2-s_3	s_3-s_4
Doubles	Triples	Quadruples		
31:70	29.15	28.20	2.55	0.95

If we assume that $s_4/s_3=s_3/s_2$, then solving we have $s_3=1.5$ counts per minute.

Figure 6 shows the experimental points obtained for the coincidence counting rate as a function of the horizontal displacement distance superimposed on the theoretical curve which fits s_3 equal to 1.5 counts per minute for $x=0$ and a background of 0.30 count per minute. The theoretical curve fits the experimental points quite well, indicating that the results of the two methods of estimating the shower effect are consistent.

In considering the number of counts observed with the one tray displaced, we must allow for the fact that we can observe coincidences between particles, one of which arrives in the permitted cone of the telescope, and the second, traveling in a parallel path, strikes the displaced tray. That these occurrences are relatively rare is shown by the following experiment.

Two counter telescopes are arranged side by side, both pointing in the vertical direction. It is arranged to count only simultaneous coincidences in both telescopes. The observed counting rate in this experiment is only 0.11 count/min., a number small compared with the contribution due to side showers.

The correction to be made to the triple-coincidence measurements is therefore $1.5/29.15=0.05$ or a 5 percent correction with a probable error of about $\frac{1}{2}$ percent.

IX. SUMMARY OF CORRECTIONS

The corrections other than geometrical are then:

(1) efficiency, 1.3±0.5 percent;
(2) absorption, 4.0±0.5 percent in counter walls plus 1.5±0.5 percent in the wood overhead;
(3) side showers, −5.0±0.5 percent;
(4) barometric pressure −3.6±0.3 percent per cm Hg.

No corrections are made for temperature variations. The results, corrected to standard atmosphere pressure of 76-cm Hg are

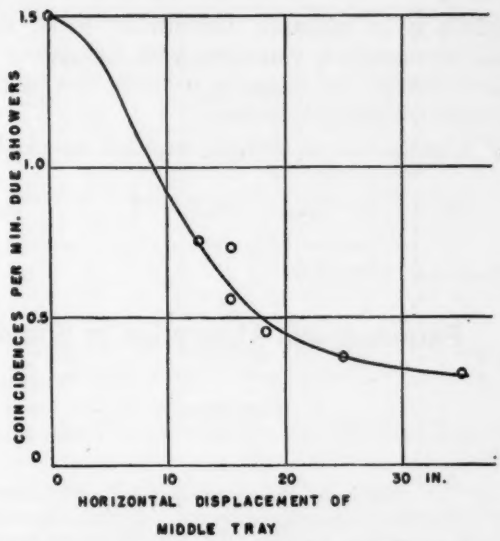

FIG. 6. Variation of number of triple coincidences observed due to side showers with the horizontal displacement of the middle tray of the telescope. The curve shown is the theoretical one adjusted to give correct values on the axis and at a distance large compared to the tray size.

	¼″ wood overhead	no absorber
Transverse counters connected	0.695	0.705
Transverse counters unconnected	0.680	0.690

The results are expressed in ionizing particles per unit solid angle per cm² per minute.

X. COMPARISON WITH PREVIOUS RESULTS

The results given above serve generally to confirm those of Greisen,[4] as corrected in the later paper by Greisen and Nereson,[5] when their results have also been corrected for the residual absorbing material which consists of 2.3 g/cm² of brass plus ¼-inch wood.

The results calculated from Greisen's data for absorption are consistent with the results given in Section VII, each being about 3 percent per g/cm² of absorber. Greisen's results must also be corrected for the shower factor which he estimates at 3 percent from his data on sixfold coincidences.

Table II summarizes the principal determinations to date, which may be compared with those in Section IX.

The present results are therefore approximately three percent lower than those of Greisen. It is interesting to attempt to correlate the experimental difference in terms of the world-wide changes in cosmic-ray intensity as measured by Forbush.[14] These records show that the mean daily sea-level cosmic-ray intensity as measured at Cheltenham, Maryland, was higher in the midsummer of 1941 by 5 percent than the daily average in the period of these measurements in the fall of 1947. Since

[14] Records made available to Dr. H. V. Neher through the kindness of Dr. S. E. Forbush.

Pasadena is at magnetic latitude of 40°N, there should be negligible variation with latitude of the sea-level cosmic-ray intensity between this location and more northerly locations.[15]

[15] R. A. Millikan and H. V. Neher, Phys. Rev. **50**, 15 (1936).

In conclusion the author wishes to record his deep appreciation for the invaluable advice and counsel of Dr. H. V. Neher and Dr. W. H. Pickering. He sincerely thanks the Carnegie Institution of Washington for their financial assistance.

PHYSICAL REVIEW VOLUME 75, NUMBER 9 MAY 1, 1949

Paramagnetic Absorption in Single Crystals of Copper Sulfate Pentahydrate*

JOHN WHEATLEY AND DAVID HALLIDAY
Department of Physics, University of Pittsburgh, Pittsburgh, Pennsylvania
(Received December 30, 1948)

We have studied paramagnetic resonance in $CuSO_4 \cdot 5H_2O$, at 9375 mc/sec. Although two absorption peaks were expected, only one was found; Van Vleck has explained this in terms of exchange coupling between Cu^{++} ions. We have found electronic gyromagnetic ratios for a large number of orientations of the crystal (with respect to the external field). Theory agrees with experiment if the gyromagnetic ratios that correspond to the three principal susceptibilities are 2.39, 2.39, and 2.07. We also find a variation in absorption line width with orientation. The shapes of the absorption lines agree with a theory of exchange coupling advanced by Gorter and Van Vleck.

I. INTRODUCTION

THE paramagnetic anisotropy of $CuSO_4 \cdot 5H_2O$ has been studied, both experimentally by Krishnan and Mookherji[1] and theoretically by Polder.[2] Since the discovery of paramagnetic resonance absorption, further studies of this salt in the form of single crystals have been made by Kip,[3] by us,[4] and by Bagguley and Griffiths.[5] In microwave resonance experiments, the measured quantity is usually the electronic gyromagnetic ratio (g factor).

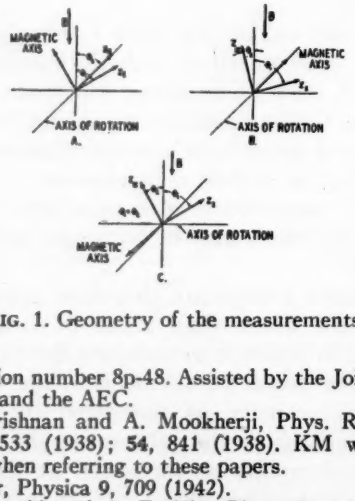

FIG. 1. Geometry of the measurements.

II. CRYSTAL STRUCTURE

Beevers and Lipsom[6] have worked out the structure of copper sulfate. The unit cell contains two Cu^{++} ions. Each ion is surrounded by four negatively charged oxygens (parts of water molecules) in an approximate square, 2.8A on a side; there are also two other oxygens (parts of sulfate groups), each of which is 3.1A from any one of the oxygens in the square. These six oxygens form an octahedron about the cupric ion; the body diagonal perpendicular to the square is the longest. Polder[2] has calculated that this arrangement produces an electric field of nearly tetragonal symmetry at each Cu^{++} ion. The x-ray measurements show that the configuration about each ion is nearly the same and that the angle between the two tetragonal axes is 98°. Magnetic measurements show that this angle is close to a right angle.

III. PREVIOUS MAGNETIC MEASUREMENTS

Krishnan and Mookherji[1] found that two of the principal susceptibilities of the crystal—those along the bisectors of the angles between the tetragonal axes—are nearly equal. They are greater than the third—which is taken normal to the plane formed by the two tetragonal axes. We shall call these tetragonal axes Z_I and Z_{II} following KM.[1] The direction of lowest susceptibility is an axis of magnetic symmetry; we will call it the magnetic axis. From their measurements of the principal susceptibilities of the crystal, KM were able to calculate susceptibilities for directions both parallel

* Publication number 8p-48. Assisted by the Joint Program of the ONR and the AEC.

[1] K. S. Krishnan and A. Mookherji, Phys. Rev. **50**, 860 (1936); **54**, 533 (1938); **54**, 841 (1938). KM will be used hereinafter when referring to these papers.

[2] D. Polder, Physica 9, 709 (1942).

[3] R. D. Arnold and A. F. Kip, Phys. Rev. **73**, 1247(A) (1948).

[4] J. Wheatley, D. Halliday, and J. H. Van Vleck, Phys. Rev. **74**, 1211(A) (1948).

[5] D. M. S. Bagguley and H. E. Griffiths, Nature **162**, 538 (1948).

[6] C. A. Beevers and H. Lipsom, Proc. Roy. Soc. London **A146**, 570 (1934).

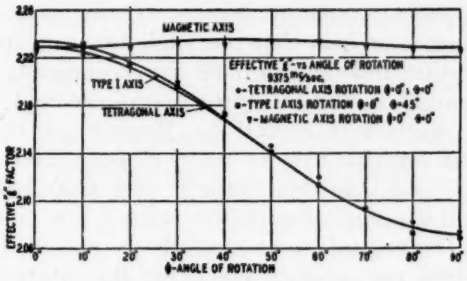

FIG. 2. Variation of g factor with angle of rotation for $CuSO_4 \cdot 5H_2O$ at 9375 mc/sec.

and perpendicular to each of the tetragonal axes. From these values they found effective Bohr magneton numbers for these same directions. The effective Bohr magneton number, n, for any direction is given by

$$n=(3kT\chi_0)^{\frac{1}{2}}/N\beta^2, \tag{1}$$

where k is Boltzmann's Constant, T is the absolute temperature, χ_0 is the static susceptibility of the crystal in the direction in question, N is Avogadro's number, and β is the Bohr magneton. KM found $n_{\parallel}=2.13$ and $n_{\perp}=1.80$. Also

$$g=n[J(J+1)]^{\frac{1}{2}}, \tag{2}$$

where J is the total angular momentum quantum number, and "g" is the g factor for the direction in question. If the electric fields acting on the ion are asymmetrical enough to quench the orbital part of the angular momentum, we have instead[7]

$$g=n[S(S+1)]^{\frac{1}{2}}, \tag{3}$$

where S is the spin quantum number. Polder's work suggests that in $CuSO_4 \cdot 5H_2O$ the orbital angular momentum is quenched and the spin is free. Assuming the spin ($S=\frac{1}{2}$) to be free, KM's results predict $g_{\parallel}=2.46$ and $g_{\perp}=2.08$.

IV. PARAMAGNETIC ANISOTROPY—DISCUSSION

Paramagnetic resonance absorption is a useful tool[8] for studying magnetic properties of copper sulfate single crystals. In microwave absorption experiments, the crystal is subjected to an oscillating magnetic field of microwave frequency, and a static magnetic field, normal to the oscillating field. The microwave frequency, ν, is constant and the magnetic field is varied. An absorption maximum occurs at the value of magnetic induction, $\mathbf{B}$, that satisfies the resonance relation

$$h\nu=g\beta B. \tag{4}$$

For a given crystal orientation it would seem that

[7] J. H. Van Vleck, *Electric and Magnetic Susceptibilities*, Chapter XI (Clarendon Press, Oxford, 1932).

[8] R. L. Cummerow, D. Halliday, and G. E. Moore, Phys. Rev. 72, 1233 (1947).

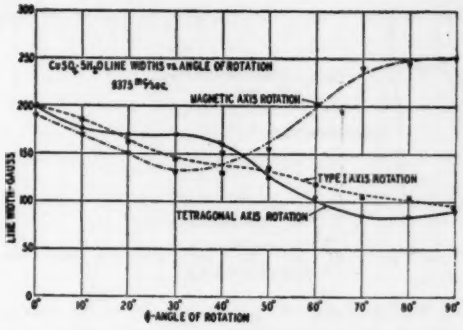

FIG. 3. Variation of absorption line width with angle of rotation for $CuSO_4 \cdot 5H_2O$ at 9375 mc/sec.

Eq. (4) would be satisfied for two different $\mathbf{B}$ values; this is because there are two different orientations of Cu^{++} ions, each with its own g value.

The g factor for any direction with respect to a tetragonal axis may be calculated simply by finding the static susceptibility in that direction and substituting in Eq. (1) and Eq. (3). The static susceptibility in any direction in terms of $\chi_{\parallel}$ and $\chi_{\perp}$ (the static susceptibilities parallel and perpendicular to a tetragonal axis) can be calculated from simple geometrical considerations. The result is

$$\chi_\theta=\chi_{\parallel}\cos^2\theta+\chi_{\perp}\sin^2\theta, \tag{5}$$

where θ is the angle between the direction specified and a tetragonal axis.

The g factor for any direction with respect to a tetragonal axis is then evidently given by

$$g=(g_{\parallel}^2\cos^2\theta+g_{\perp}^2\sin^2\theta)^{\frac{1}{2}}, \tag{6}$$

where θ is the angle between the direction specified and a tetragonal axis.

It follows that for the two ions in the unit cell the values of g will be given by

$$g_1=(g_{\parallel}^2\cos^2\theta_1+g_{\perp}^2\sin^2\theta_1)^{\frac{1}{2}}$$

and

$$g_2=(g_{\parallel}^2\cos^2\theta_2+g_{\perp}^2\sin^2\theta_2)^{\frac{1}{2}}, \tag{7}$$

where θ_1 and θ_2 are the angles which the direction of the external field makes with Z_I and Z_{II}, respectively. In an absorption experiment, then, we expect to find two absorption maxima, those corresponding to g_1 and g_2 in Eq. (7). At 3.2 cm, however, we find only one peak. Van Vleck[9] attributes this to a strong exchange coupling between the cupric ions; the single effective "g" is the arithmetic mean of g_1 and g_2,

$$g_{eff.}=(g_1+g_2)/2. \tag{8}$$

V. EXPERIMENTAL ARRANGEMENT

The experimental arrangement is like that used in previous work.[8] The output of a square-wave

[9] J. H. Van Vleck, private communication.

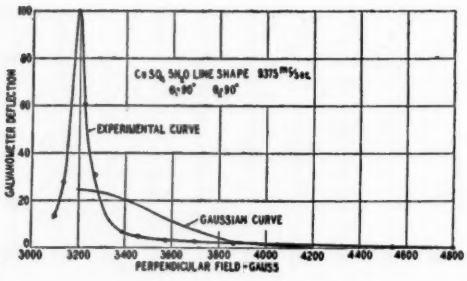

FIG. 4. Comparison of the line shape of an experimental $CuSO_4 \cdot 5H_2O$ absorption line at 9375 mc/sec. with a Gaussian curve having the same area and second moment.

modulated low power oscillator passed through a resonant cavity that contained the copper sulfate crystal. The power was detected by a crystal rectifier. The voltage output of the crystal rectifier was amplified, rectified, and then compared with a stable d.c. battery voltage; the difference between the two was displayed as a galvanometer deflection. If the crystal in the cavity absorbs power, there will be a galvanometer deflection; it can be shown that the galvanometer deflection is proportional to χ'', the imaginary part of the high frequency susceptibility of the salt. The magnetic field was calibrated using the proton moment; we think it is correct to ± 6 gauss. The absorption peaks are reproducible to within ± 10 gauss.

In order to study the anisotropy, the crystal specimen was mounted on the end of a shaft that protruded slightly into the resonant cavity. The shaft was normal to the steady field. We could measure relative shaft rotation angles. Three orientations of the crystal with respect to the axis of rotation were studied. They are shown in Fig. 1. The drawings (and all later discussion) are based on the assumption that the angle between Z_I and Z_{II} is a right angle. Figure 1A shows rotation of the crystal about an axis parallel to one of the *tetragonal axes* of the unit cell, the angle of rotation, φ, being equal to θ_1 plus a constant. In Fig. 1B the crystal is rotated about an axis parallel to the *magnetic axis* of the crystal; the angle of rotation again is equal to θ_1 plus a constant. Figure 1C shows rotation about such an axis that the angle between the axis of rotation and the magnetic axis is constant and a right angle; further, the direction of the field makes equal angles with Z_I and Z_{II}. We will call this last type of rotation axis a "*Type I*" *axis*. The angles that Z_I, Z_{II}, and the magnetic axis make with the crystallographic axes of the crystal are given by KM. The crystals were carefully ground into small cylinders, the cylinder axis being the rotation axes of Fig. 1.

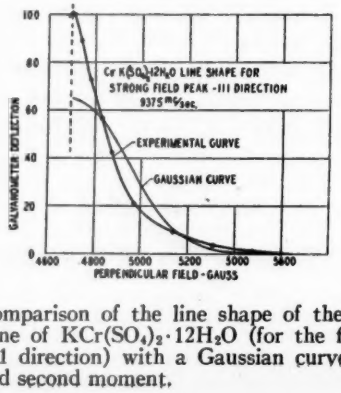

FIG. 5. Comparison of the line shape of the strong field absorption line of $KCr(SO_4)_2 \cdot 12H_2O$ (for the field oriented along the 111 direction) with a Gaussian curve having the same area and second moment.

VI. RESULTS

The experimental data for all three axes are shown in Fig. 2. The values of g for the tetragonal and Type I axis rotations should repeat every 90°; the values of g for the magnetic axis rotation should repeat every 45°. This comes about because the angle between Z_I and Z_{II} is nearly a right angle.

The theoretical curves that best fit the experimental data are shown as full lines in Fig. 2. They are found in the following way from Eq. (7) and Fig. 1: for the tetragonal axis rotation $\theta_1=\phi$ and $\theta_2=90°$. Thus, Eq. (7) reduces to

$$g_1=(g_{11}^2\cos^2\varphi+g_\perp^2\sin^2\phi)^{\frac{1}{2}}, \quad g_2=g_\perp. \tag{9}$$

Finally, according to Van Vleck, the measured g is given by

$$g=(g_1+g_2)/2. \tag{10}$$

From the indicated geometry (and with a similar procedure) we may compute curves for the magnetic axis rotation and Type I axis rotation. For the magnetic axis rotation, $\varphi=0°$, $\theta_1=0°$; for the type I axis rotation, when $\varphi=0°$, $\theta_1=45°$. The theoretical curves depend on g_{11} and $g_\perp$; g_{11} and $g_\perp$ are chosen so as to best fit the data at the ends of the experimental curves. These values are $g_{11}=2.39$ and $g_\perp=2.07$.

VII. ABSORPTION LINE WIDTHS

Besides the anisotropy in the g factors, we found that the widths (at half-amplitude) of the absorption lines varied with the orientation of the crystal in the steady field. The experimental results for the three axes of rotation are shown in Fig. 3. The relationship between φ and θ for each of the curves is the same as that in Fig. 2. Van Vleck[10] has developed a formula for the variation of the mean square line width with angle of rotation for tetragonal axis rotation; it assumes that the exchange energy is a function only of the total crystalline spin; our results are consistant with this theory.

VIII. ABSORPTION LINE SHAPES

We have studied, in detail, the shapes of the absorption lines. The copper sulfate absorption lines

[10] J. H. Van Vleck, private communication.

are much narrower than one expects on the basis of known internal magnetic fields. Also, we find that the absorption in $CuSO_4 \cdot 5H_2O$ reaches negligible values only after the applied field is about 1500 gauss greater than that at the absorption maximum. This is shown in Fig. 4. A line shape theory has been worked out by Gorter and Van Vleck,[11] and in detail by Van Vleck,[12] on the assumption of exchange interaction between the cupric ions. Their results show that when exchange is important, the usual assumption of a Gaussian curve for the absorption line is a poor one. Instead, they find that the absorption line should be peaked in the center and should have a long tail. To test this, we have drawn a Gaussian curve with the same area and second moment as the absorption line (Fig. 4). The Gaussian curve is a very poor approximation to the experimental curve. In Fig. 5 is shown the strong field side of the upper absorption line of $CrK(SO_4)_2 \cdot 12H_2O$ (steady field oriented along the 111 crystallographic direction). Exchange effects here are probably small. We draw here, too, a Gaussian curve with the same area and second moment as the absorption line. In this case the Gaussian curve is a reasonable approximation to the experimental curve. The difference between the absorption line shapes of the two salts can thus be explained on the basis that there is exchange interaction between the cupric ions.

We wish to acknowledge the continued aid and encouragement of Dr. A. J. Allen.

[11] C. J. Gorter and J. H. Van Vleck, Phys. Rev. **72**, 1128 (1947).
[12] J. H. Van Vleck, Phys. Rev. **74**, 1168 (1948).

PHYSICAL REVIEW VOLUME 75, NUMBER 9 MAY 1, 1949

The Second Viscosity of Liquids*

L. N. LIEBERMANN
University of California, Marine Physical Laboratory, San Diego, California
(Received January 3, 1949)

The second coefficient of viscosity is concerned with the viscous forces generated by compression (or dilatation). In the absence of knowledge of its magnitude in liquids it has been customary in hydrodynamics to assume that the coefficient of dilatational viscosity, n', could be approximated by the ideal gas value $n' = -2n/3$, where n is the coefficient of shear viscosity. A method has been developed for obtaining values for the dilatational viscosity which is based on Eckart's theory of acoustical streaming; the non-periodic motion of the fluid in the vicinity of a sound source is dependent on the two coefficients of viscosity. Values for the coefficient of dilatational viscosity for a variety of organic liquids and for water are given in the table. The coefficient of dilatational viscosity was found to be positive in sign and greater in magnitude than the shear viscosity. For example, the dilatational viscosity of water was found to be 2.4 centipoise and that for carbon disulfide greater than 200 centipoise. There is no correlation between the magnitude of the shear and dilatational viscosities for the liquids studied. Temperature variation measurements on water show that the temperature dependence of dilatational and shear viscosity in this substance is identical. Introduction of values for the dilatational viscosity into acoustical calculations eliminates the well-known discrepancy between theory and observation of sound absorption in liquids at very high frequencies.

I. INTRODUCTION

THE classical theory of viscosity is closely analogous to the theory of elasticity. In the classical elasticity theory two coefficients of elasticity appear, the Lamé coefficients, λ and μ. In an analogous manner there are two coefficients of viscosity, n and n'. The coefficient, n is familiar; it is simply the coefficient of shear viscosity. Values for this coefficient are determined with the use of a rotating cylinder or a transpirational viscosimeter and are to be found for a variety of substances in handbooks.

The second coefficient of viscosity, n', is less familiar; it might be called the coefficient of dilatational viscosity. It is a measure of the viscous forces which arise when a volume of fluid is compressed or dilated without change in shape. The magnitude of the viscous forces depends on the *rate* of compression or dilatation. A conventional viscosimeter does not measure the dilatational viscosity inasmuch as the dilatation or compression in these instruments is obviously negligible. No dilatational viscosimeter exists nor may values for the dilatational viscosity be found in the literature.

In hydrodynamics it has been customary in dealing with actual liquids to assign for the value of the dilatational viscosity, that calculated for an ideal gas; the dilatational viscosity of an ideal gas may be shown to be equal to $-2n/3$.[1] Most textbooks[2] do not attempt to justify this assumption

* This work represents one of the results of research carried out under contract with the Bureau of Ships, Navy Department.

[1] Horace Lamb, *Hydrodynamics*, 6th edition (Cambridge University Press, London, 1932), p. 574.
[2] For example: Lord Rayleigh, *Theory of Sound* (Dover Publications, New York, 1945), p. 314.

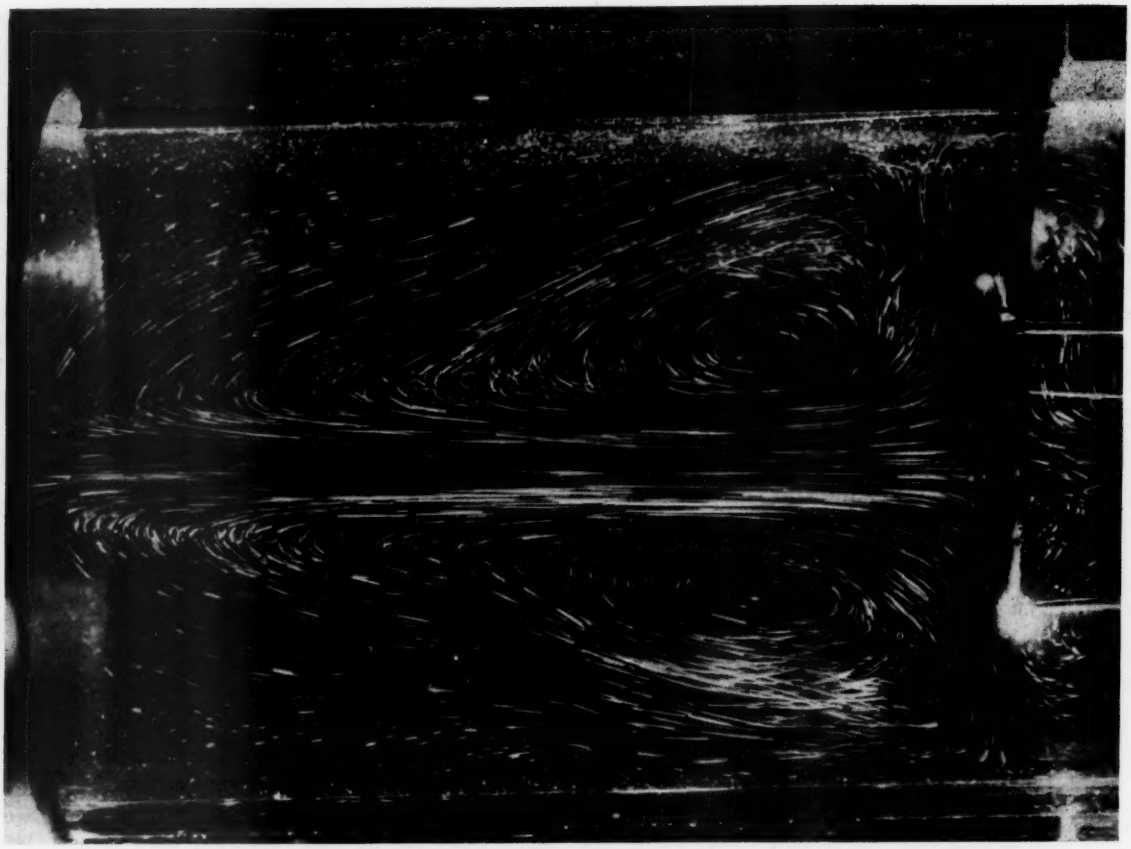

FIG. 1a. Photograph of acoustic streaming from a sound source; the motion of the liquid is made visible by a suspension of tiny particles of aluminum.

but attribute the proof of the argument to Stokes. However, Stokes was well aware of the deficiencies of his argument: ". . . I have always felt that the correctness of the value $n/3$ for the last term of this equation (the term which includes the dilatational viscosity) does not rest on as firm a basis as the correctness of the equation of motion of an incompressible fluid, for which the last term does not come in at all."[3]

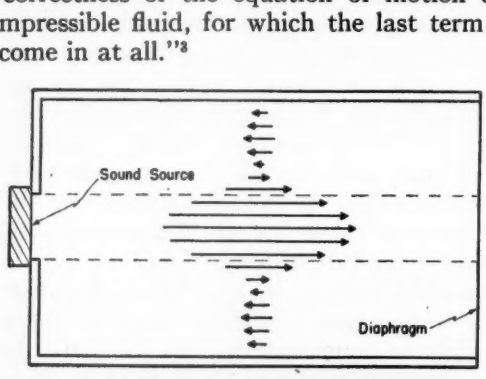

FIG. 1b. A schematic of the experimental arrangement used in a. The liquid is contained in a glass cylinder; the sound beam is circular in cross section and is transmitted through the diaphragm without reflection. The arrows indicate the theoretical distribution of velocity in the mid portion of the cylinder.

[3] G. G. Stokes, Math. Phys. Papers, 3, 136 (1851).

It is not surprising that this assumption should have persisted so long in hydrodynamical theory. In most problems liquids may be treated as incompressible and the value of the dilatational viscosity does not arise. Even when the compressibility may not be neglected the motion is often divergenceless; the stress in this type of motion may be shown to be independent of n'. However the generation of acoustical waves in liquids and in gases does produce divergent motion; in acoustics the effect of the dilatational viscosity can be expected to be an extremely important factor. It is in this subject particularly that one may expect to find defects in the theory which result from the neglect of dilatational viscosity.

The succeeding sections will discuss in turn, the effect of dilatational viscosity on the absorption of sound; an unusual second-order acoustical effect which has its origin in part in the dilatational viscosity; and finally, actual values of the dilatational viscosity obtained experimentally for a variety of liquids.

II. VISCOSITY AND SOUND ABSORPTION

As previously mentioned, divergent motion is associated with acoustic waves; hence the dilata-

tional viscosity as well as the shear viscosity can be expected to exert an important influence on the propagation of these waves. The effect of the two viscosities is conveniently studied by beginning with the usual second-order equation of hydrodynamics,[4]

$$\rho(Du/Dt)+\nabla p=n\nabla^2 u+(n+n')\nabla\nabla\cdot u, \quad (1)$$

where u is the particle velocity, ρ is the density, and p the pressure. This equation may be considerably simplified for the study of acoustic waves: for plane waves in the x direction Eq. (1) becomes

$$\rho(\partial u/\partial t)+(\partial p/\partial x)=(2n+n')(\partial^2 u/\partial x^2). \quad (2)$$

Equation (2) together with the equation of continuity gives the usual plane wave solution:

$$u=u_0\exp[-i(\omega t+kx)] \quad (3)$$

in which k is complex if ω is real. The imaginary part of k is the negative of the absorption coefficient. To a sufficiently good approximation the absorption coefficient is given by:

$$\alpha=\omega^2(2n+n')/2\rho c^3, \quad (4)$$

where ω is 2π times the frequency, and c is the velocity of sound. In the ideal gas approximation $n'=-2n/3$ and the quantity $(2n+n')$ in Eq. (4) becomes $4n/3$. The latter will be recognized as the form given in most textbooks on sound for the calculation of absorption.

It is well known that the observed sound absorption, with few exceptions, is always in excess of the calculated values. Equation (4) suggests a reason for this disagreement: errors in the calculated absorption may be attributable to the use of the ideal gas approximation rather than the actual dilatational viscosity. This proposal has been advanced by several writers in recent years,[5] but unfortunately, sound absorption data, alone, cannot be used to establish unambiguous values for the dilatational viscosity. Absorption data do not necessarily represent the sound energy dissipated by viscous forces alone; for example, heat conduction and scattering processes may also dissipate sound energy. However it will be shown in a later section that sound absorption can, in fact, be correctly attributed to the combined effects of the dilatational and shear viscosities in the case of all liquids studied here.

III. ACOUSTICAL STREAMING AND VISCOSITY

The streaming of liquids or gases away from a vibrating sound source is a phenomenon which is

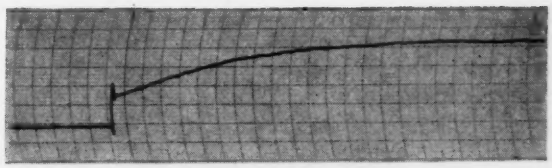

FIG. 2. A sample recording of forces on the suspended disk. The source was turned on: the abrupt rise is proportional to the radiation pressure on the disk; the slow increase represents the force of the streaming liquid as it approaches equilibrium velocity. The suspension is underdamped.

familiar to some experimenters. Figure 1a is a photograph illustrating this phenomenon. The streaming of a liquid is made visible by a suspension of fine particles of aluminum; an oscillating quartz crystal which is the sound source is on the left of the photograph.

Eckart[6] has recently developed a set of second-order equations of acoustics which include the streaming phenomenon as one of their solutions. The force which drives the motion is dependent on both the dilatational and shear viscosities; the retarding force is dependent only on the viscous shear forces. Eckart suggested therefore that the ratio n'/n might be determined from a study of the streaming phenomenon.

The solutions to Eckart's equations show that acoustical streaming consists of vortex motion, generated at the boundaries of the sound beam. As is generally true of vortex motion, these vortices diffuse from their origin, following closely the laws of heat diffusion. Quantitative considerations of these vortices are considerably simplified if the fluid is confined to a cylinder whose length is long compared to the radius; the sound beam is directed

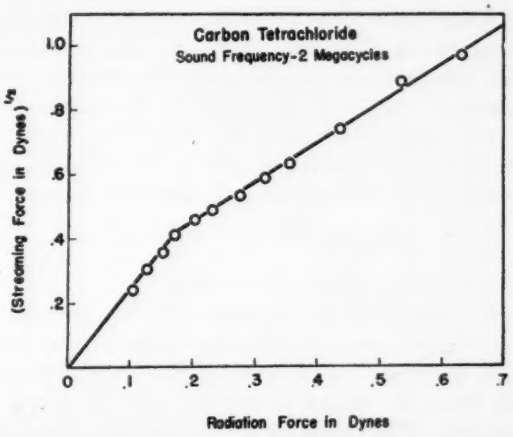

FIG. 3. Sample data for one liquid. The ordinate is proportional to the velocity of streaming; the abscissa is proportional to the sound intensity. Measurements were made over a range of sound intensities in order to define the two slopes. The slope which passes through the origin is used for the determination of the viscosity; the decrease in slope at higher streaming velocities represents turbulent motion.

[4] Compare with reference 2, pp. 574, 577.

[5] For example see: Laszto Tisza, Phys. Rev. 71, 531 (1942); William Pitt Mason, *Electromechanical Transducers and Wave Filters* (D. Van Nostrand Company, Inc., New York, 1942), p. 306.

[6] Carl Eckart, Phys. Rev. 73, 68 (1948).

TABLE I. Summary of viscosity ratio for a number of liquids.

Liquid	Frequency (megacycles)	Viscosity ratio (n'/n)	Coefficient of shear viscosity[a] (n in centipoise)	Coefficient of dilatational viscosity (n' in centipoise)	Viscosity ratio from sound absorption[b] (n'/n)
Water	5	2.4	1	2.4	2.1
Methyl alcohol	5	1.3	0.60	2.2	1.1
Ethyl alcohol	5	3.8	1.2	3.2	3.6, 2.6, 2.3
Acetone	5	3.1	0.30	10	3.8, 3.1, 2.9
Propyl alcohol (*iso*)	5	5.1	2.2	2.3	
Amyl acetate	5	9.9	0.89	11	10.2, 12.3
	2	9.6		11	
Xylol (*m*)	5	11	0.62	18	7.7, 6.5
	2	11		18	
Ethyl formate	5	15*	0.40	37*	21, 10
	4	22*		55*	
	3	31*		77*	
	2	85*		210*	
Chloroform	2	24	0.57	48	27, 34, 35
Carbon tetrachloride	2	28	2.0	14	27, 21, 22
Benzene	2	107	0.65	160	140, 130, 150
Carbon disulphide	2	>200	0.37	>500	

* These values are for the unmodified Eq. (5). Using the modified form (See Section IV, Part C) $n'/n=700$ for all frequencies.

[a] Taken from *International Critical Tables* (McGraw Hill Book Company, Inc., New York).

[b] Absorption data for water were taken from J. Pinkerton, Nature **160**, 128 (1948); the others are from Ludwig Bergmann, *Der Ultraschall* (Edwards Brothers Inc., Ann Arbor, 1944).

along the axis and passes without reflection through the region in which the liquid is confined. A schematic diagram of such an arrangement is shown in Fig. 1b. For the above conditions Eckart's equations lead to a velocity of streaming on the axis of the tube given by**

$$v=(\omega^2r^2GI/\rho c^4)(2+n'/n). \tag{5}$$

The sound beam has a radius r and an intensity I. The constant G in this equation is a geometrical factor which takes into account the relative size of the sound beam and the tube. If the sound beam fills the tube, $G=0$ and the streaming stalls; an increased axial velocity results as the tube diameter increases. For the special case outlined above

$$G=(r^2/r_0^2-1)/2-\log r/r_0, \tag{6}$$

where r_0 is the radius of the tube.

The predicted distribution of the velocity in other regions of the tube as well as on the axis is also of interest. The streaming flows along the axis away from the sound source and returns along the periphery. The result of a distribution calculation carried out for one set of dimensions used in these experiments is illustrated in Fig. 1b; the relative magnitude and direction of the velocity is illustrated by the vectors in the diagram; end effects of the tube have, or course, been neglected. This velocity distribution may be directly compared with the distribution of velocity in the photograph inasmuch as the geometry was identical.

** A typographical error occurs in Eq. (33) of Eckart's paper which if uncorrected leads to the first power of the frequency rather than the square of the frequency in the above equation.

IV. THE MEASUREMENT OF THE RATIO OF THE VISCOSITIES

A. Basis of the Method

It is seen from the preceding section that the ratio of the viscosities n'/n may be obtained from Eq. (5) provided all the other quantities in this equation are measurable or obtainable. Of these quantities, it is the measurement of the axial velocity of streaming and the absolute intensity of the sound beam which presents the major experimental problem.

The measurement of the axial streaming velocity can be made in either of two ways: particles can be suspended in a liquid in order to make the streaming visible and the velocity measured with the aid of intermittent photography; or the velocity can be obtained by calculation from the measurement of the forces on a disk set in the stream. The latter method makes use of the well-known relation between fluid velocity and the force on a disk,

$$F_S=K\rho v^2 \tag{7}$$

which obtains solely from momentum considerations. Viscous drag effects are eliminated inasmuch as the disk blocks the flow around itself.

Actually both methods were used in the determination of the streaming velocity. The constant of proportionality K, in the above expression, was determined experimentally by direct comparison with the velocity obtained by the photographic method for two liquids, water and carbon tetrachloride. As was expected, the value of the constant reproduced over a wide range of velocities. The more convenient disk method could then be used henceforth for all other liquids for which the geometry of the experiment was identical.

The use of the force on a disk for measuring streaming velocity conveniently lends itself to the simultaneous determination of the intensity of the sound beam. A disk suspended in a sound beam will, in general, be acted upon by the force of radiation pressure as well as by the force of streaming. The force of radiation pressure is given by,

$$F_R=2\pi IRr^2/c, \tag{8}$$

where I is the incident intensity of the sound beam and R is the reflection coefficient of the disk.***

*** The discussion of streaming in the previous section neglects the possibility of reflection. In the presence of sound reflection of relatively small intensity, the effective intensity is given by the difference between the incident and reflected intensities.

The use of radiation pressure to determine the intensity in a sound beam is a well-known method, but the fact that both radiation and streaming forces act simultaneously on the disc has long plagued investigators who were interested only in measuring the sound intensity.

The separation of the two forces can be effected by making use of the inertia of streaming. While radiation forces respond instantly to abrupt changes in sound intensity, the streaming velocity has a relatively long time constant. Hence a force-measuring device, capable of rapid response, will differentiate between the effects of radiation and of streaming.

A sample recording of the forces on the disk is shown in Fig. 2. Initially, the source was turned on; the abrupt rise is proportional to the force produced by radiation pressure; the slow increase represents the force on the disc as the streaming velocity increases and eventually approaches a maximum exponentially. On interruption of the source, the decay is analogous to the growth. Hence, the two effects of radiation and of streaming are separated but still may be measured practically simultaneously.

The actual determination of the ratio of the two viscosities is best illustrated by examining some typical data. Figure 3 gives a number of observations obtained for carbon tetrachloride at different sound intensities during one series. The abscissa of each point is the force on the disk (in dynes) due to radiation pressure. The ordinate of each point is the square root of the force of streaming on the disk. The ordinate is proportional to the streaming velocity; the abscissa is proportional to the sound intensity.

The slope of the curve shown in Fig. 3 like all others studied, surprisingly possesses two values, one at low sound intensities and one at high. The reason lies in the difference between laminar and turbulent streaming which is discussed at greater length in a succeeding section. The theory of streaming clearly applies only to laminar flow; hence the need for obtaining data in the form shown in the sample which clearly defines the two flow regions.

B. Apparatus for Studying the Viscosity Ratio

The apparatus used for these measurements is shown schematically in Fig. 4. The disk is mounted on a vertical magnesium deflection arm which is suspended by a stiff horizontal suspension ribbon. The deflection of the disk which is proportional to the force is electrically recorded by a variable reluctance device, consisting of an iron slug which changes the inductance of one of two iron core inductances forming part of an alternating current inductance bridge. The unbalance voltage is amplified and applied to a recording galvanometer.

The system was calibrated before and after each measurement by deflecting the suspension with a known force. A fine glass fiber is arranged in such a manner that its known bending force (of the order of 0.2 dyne) can be applied to the suspension.

The suspension is damped by an unconventional procedure. A tiny permanent magnet is mounted on the suspension; an electro-magnet mounted on the suspension support attracts or repells the magnet depending on the polarity of the polarizing voltage. The polarizing voltage is obtained after suitable amplification, from the derivative of the current supplied to the recording galvanometer. By varying the amount of the polarizing voltage the exact amount of the damping can be controlled. Usually the equipment was operated slightly underdamped rather than at critical damping.

Interchangeable disks, semitransparent to sound were used. These consisted of thin aluminum foils mounted on supporting rings. The accuracy of the final measurement is dependent on the accuracy with which the reflection coefficient of the various foils is known. These reflection coefficients were calculated using the usual expression for the reflection at normal incidence from a thin plate:

$$R=\frac{[\rho_1c_1/\rho_2c_2-\rho_2c_2/\rho_1c_1]^2}{4\cot^2\omega\tau/c+[\rho_1c_1/\rho_2c_2+\rho_2c_2/\rho_1c_1]^2}, \quad (9)$$

in which τ is the foil thickness; the subscripts 1 and 2 refer to the liquid and to the aluminum. The practical application of this equation to thin foils was tested by measuring the reflectivity as a function of thickness for a wide variety of aluminum foils ranging in thickness from 2.5×10^{-4} to 10^{-2} cm.

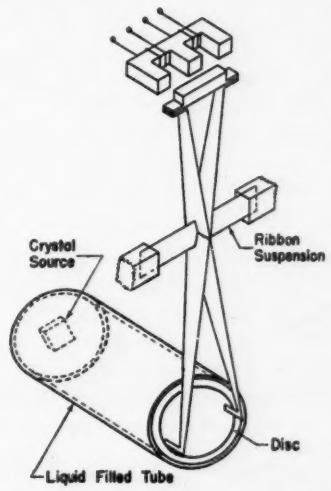

FIG. 4. A schematic diagram of the construction of the apparatus. The deflection of the disc produces an unbalance in the variable reluctance bridge located at the top.

Deviations from the above equation were found only for the foils which were thinner than 10^{-3} cm. The thinner foils were found to reflect more than is predicted, presumably owing to the slight contribution of the supporting ring. The foils used for the actual measurement were thicker than 10^{-3} cm.

V. THE RATIO OF THE VISCOSITIES

A. The Measured Viscosity Ratios

Table I summarizes the results of the determination of the viscosity ratio for a number of liquids. Several important conclusions are immediately evident from an inspection of the values in Table I: first, the viscosity ratios for all of the liquids studied have *positive values* rather than the value $-\frac{2}{3}$ which is predicted for an ideal gas. Secondly, the value of the ratio varies widely; there is *no direct correlation* between shear viscosity and dilatational viscosity. Thirdly, the value of the coefficient of dilatational viscosity for most liquids is *considerably greater* than the coefficient of shear viscosity; in benzene and carbon disulfide the dilatational viscosity is more than 100 times the shear viscosity. Clearly the ideal gas theory applied to the dilatational viscosity in liquids is a poor approximation.

B. Viscosity Ratios from Sound Absorption Data

Section II discussed the possibility of obtaining values for the dilatational viscosity with the use of absorption data. Absorption data for a number of liquids are given in Bergmann's book;[7] data on absorption in water has also been obtained from Pinkerton's work.[8] The consistency of the absorption measurements of liquids with the exception of water are rather poor. Water has been investigated with considerable care by several workers and Pinkerton's measurements are undoubtedly an excellent example as well as being the latest published work; his value is also in approximate agreement with previous work.

In accordance with the discussion in Section II, calculations were made assuming the observed sound absorption resulted exclusively from viscous dissipation. The values obtained in this manner with the aid of Eq. (4) are listed in the last column of Table I. It is seen that these values, in general, agree with those obtained from the present experiment within the consistency of the absorption data. In the case of water for which there exists reliable absorption data the agreement is excellent. This general agreement presents strong evidence that *the major part, if not all, of the sound absorption in most liquids is a result of viscous dissipation;*[****] the Stokes theory is found to agree with observation of liquids provided the dilatational as well as the shear viscosity is included in the calculation.

C. Temperature Dependence of the Viscosity Ratio

The data given in Table I were all taken with the temperature at approximately 17.4°C. The room temperature of the underground room in which these measurements were performed conveniently remained constant to within a few tenths of a degree and no attempt was made to control the temperature more precisely.

A set of observations were made on water to ascertain the temperature dependence of the viscosity ratio of this substance. The temperature was varied from 4°C to 25°C and the viscosity ratio measured at 2° intervals. Although the shear viscosity of water varies by the factor 2 in this temperature range, *the viscosity ratio showed no significant variation.* Absorption data for water as a function of temperature[8] also lead to the same result.

D. Frequency Dependence of the Viscosity Ratio

It will be noted that most of the liquids were studied at the five megacycle frequency; some were studied at two megacycles and a few were studied at both frequencies. The choice of frequencies was dictated by the magnitude of the viscosity ratio. Increasing the frequency increases the streaming forces. Hence, liquids having small viscosity ratios were studied at five megacycles; liquids having very large ratios were more conveniently studied at two megacycles; intermediate ratios could be studied at both frequencies.

Of the three liquids studied at the two frequencies, one liquid, ethyl formate, showed a remarkable dependence on frequency; the ratio increases with decreasing frequency. In order to explore this phenomenon further, additional measurements were made. The viscosity ratio of ethyl formate was found to be 15, 22, 31, and 85, at the respective frequencies 5, 4, 3, and 2 megacycles.

This behavior of the viscosity ratio may be explained if the assumption is made that the dilatational viscosity mechanism possesses a relaxation time which is considerably greater than that of the shear viscosity. (The relaxation time of the shear viscosity is usually assumed to be the mean free travel time of the molecules, of the order of 10^{-12} second.) This assumption of the relaxation time influences the frequency dependence of the streaming velocity. From Eq. (5) the streaming

[7] Ludwig Bergmann, *Der Ultraschall* (Edwards Brothers, Inc., Ann Arbor, 1944).

[8] J. Pinkerton, Nature 160, 128 (1948).

[****] One exceptional liquid is sea water. Recent work has shown that in addition to sound absorption resulting from the two viscosities, absorption at frequencies below one megacycle results from a chemical reaction involving one of the dissolved salts. Another well known exception is mercury, whose sound absorption results largely from its high heat conductivity.

velocity is proportional to

$$(2+n'/n)\omega^2 \equiv (4/3+\kappa/n)\omega^2, \qquad (10)$$

where κ is defined as $n'+2n/3$. If the dilatational viscosity mechanism exhibits relaxation, the term $\kappa\omega^2/n$ in the above expression should be replaced by

$$\kappa\omega^2/n(1+\omega^2\theta^2) \qquad (11)$$

in which θ is the relaxation time of the dilatational viscosity. In case Eq. (5) is applied without modification to streaming data where relaxation exists the viscosity ratio will be found to apparently decrease in the region of relaxation and to approach the limiting value $-\frac{2}{3}$ at extremely high frequencies. The application of the modified Eq. (5) to the ethyl formate data is found to give the approximately constant value $n'/n=700$ at the four frequencies. The relaxation time, θ, which was chosen to give the best fit, is 2×10^{-7} second.

VI. DISCUSSION

A. Dilatational Viscosity and Molecular Theory

It might be satisfying, if at this point a molecular model of dilatational viscosity could be presented. Considering the complexity of the structure of liquids it is not surprising that none can be given which has a real foundation in fact. There have, however, been numerous attempts in the past to formulate a molecular theory of shear viscosity in liquids. A brief review of a current theory is of interest in that it is indicative of the form which future theories of dilatational viscosity will undoubtedly assume.

The usual theory of shear viscosity assumes a liquid to be constructed of molecules which are bonded to one another but which may change equilibrium positions under the action of a shearing motion. The introduction of a relaxation time or transition probability for the transition process, following the Poisson-Maxwell procedure, gives the dependence of viscosity on the rate of shear. The number of molecules possessing sufficient energy to effect bond rupture, and hence transition, depends on the Boltzmann expression, $\exp(-B/RT)$, which leads to a reasonably correct temperature dependence of shear viscosity for some liquids,

$$n_T = n\exp(B/RT).$$

In a similar manner it might be proposed that dilatational viscosity is a result of molecular rearrangement induced by compression or dilatation. Presumably there would exist in a liquid two or more stable molecular configurations possessing different energies. Transitions between these states would be actuated by compression (or dilatation). A dependence of viscous dissipation on the rate of compression results as above from a finite relaxation time for the transition process. The temperature dependence of this process would be expected to be given by the Boltzmann expression just as in the shear viscosity model. Inasmuch as the activitation energy, B, of the process would be expected to be nearly the same as that for the shear process, the temperature dependence of the two viscosities might be expected to be nearly identical; this would agree with the observed equivalence of the temperature dependence of the shear and dilatational viscosities in water (see Section V, Part C). The similarity of the activiation energies of the two processes would not preclude large variations in the viscosity ratio; the magnitude of the viscosity depends on the relaxation time as well as on the activation energy of the process.

B. Flow Phenomena Associated with Acoustical Streaming

The hydrodynamics of the observed acoustical streaming is of interest quite apart from the study of dilatational viscosity. Several unusual phenomena are apparent from a study of the motion of the fluid: As can be seen from Fig. 3, the relationship between sound intensity and fluid velocity is not the same for all values of the sound intensity; instead there appear to be two clearly defined flow regions. In both regions the flow velocity is a linear

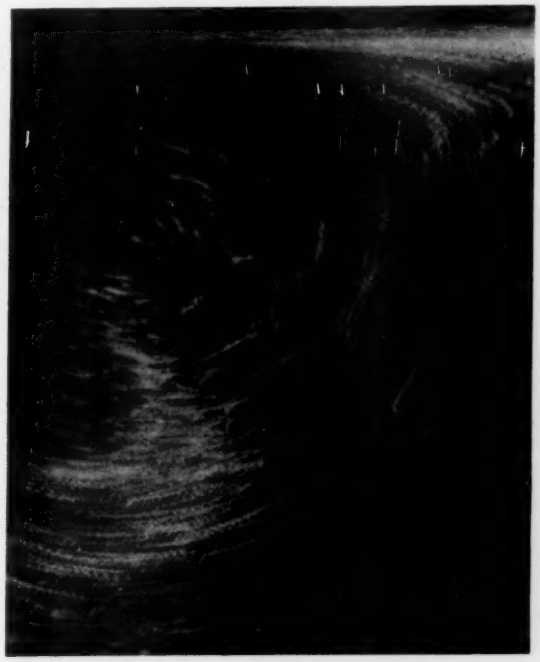

FIG. 5. A photograph of acoustical streaming similar to that shown in Fig. 1. A portion of the streaming has been enlarged in order to show that, surprisingly, the particle tracks are sinuous. It is believed that the particles rotate, which results in an epicycloidal motion.

function of the sound intensity but with different constants.

This behavior is strongly reminiscent of laminar and turbulent flow. For example, fluid flow in pipes is proportional to the pressure head up to a critical velocity; beyond this velocity the flow becomes turbulent and the constant of proportionality changes, or the relation may even be no longer linear. Such an explanation of the two flow regions in acoustical streaming has one disturbing feature: The Reynolds' Number at the critical streaming velocity is of the order of 100 which is a factor 20 less than the generally accepted value. Possibly the Reynolds' criterion for turbulence must be modified when applied to vortex motion of this kind. Visual inspection with the aid of dye or suspended particles exhibits no striking change during the transition between the two flow regions.

Photographs of the suspended particles in the stream show two phenomena which have not been mentioned earlier. It is apparent in Fig. 1a that the streaming lacks symmetry about a vertical line through the center of the photograph. On the other hand, Eckart's theory of streaming would predict perfect symmetry about the median line. Eckart has suggested[9] that this phenomenon may be related to 4th-order terms which were neglected in the theory. The significant 4th-order terms would take into account inertial effects in the fluid flow. In addition to disturbing the symmetry the magnitude of these terms at high fluid velocities might also be sufficient to disturb the linear relationship between fluid velocity and sound intensity. If this were the case, the linear relationship would be approached asymptotically with decreasing sound intensity. These 4th-order terms should become significant at a Reynolds' Number of about unity.

Another phenomenon associated with acoustical streaming may be seen in Fig. 5. This photograph is similar to Fig. 1 except that a portion of the acoustical streaming has been enlarged in order to make visible the individual tracks of the suspended particles. Close inspection shows that, surprisingly, each track is sinuous. It is believed that each particle rotates about an axis which is displaced from its center; when combined with translation this motion would be epicycloidal. The explanation for the rotation of the suspended particles is not obvious and this phenomenon must be given further study.

The author is indebted to Messrs. Stanley Lai and Victor Anderson for assistance in experimental work. He also wishes to express his appreciation to Professor Carl Eckart for valuable discussions.

[9] Carl Eckart, private communication.

PHYSICAL REVIEW VOLUME 75, NUMBER 9 MAY 1, 1949

On the Theory of Diffraction by an Aperture in an Infinite Plane Screen. II.

HAROLD LEVINE AND JULIAN SCHWINGER
Lyman Laboratory of Physics, Harvard University, Cambridge, Massachusetts
(Received January 13, 1949)

The diffraction of a scalar plane wave by an aperture in an infinite plane screen is examined theoretically. The wave function at an arbitrary point of space is expressed in terms of the discontinuity in its normal derivative at the screen, where the boundary condition is that of vanishing wave function. An integral equation for the discontinuity in normal derivative (or the residual function which measures its deviation from the simple distribution appropriate to a completely infinite screen) is the result of applying the boundary condition to the space wave function. Utilizing the integral equation (whose solution is generally unobtainable), the diffracted spherical wave amplitude at large distances from the aperture is cast into a form which is stationary with respect to small variations (relative to the correct values) of the residual functions arising from a pair of incident waves. An homogeneous expression for the amplitude is exhibited wherein the part independent of the residual functions defines a Kirchoff approximation. The connection with another stationary form of the amplitude, involving a pair of aperture wave functions, is examined. A variational expression for the plane wave transmission cross section of the aperture is based on the amplitude observed in the direction of incidence. The variational formulation is applied for a wave incident normally on a circular aperture. By comparison with the exact results available for this problem, it appears that use of simple residual functions in the variational formulation yields approximate, yet accurate expressions for the diffracted amplitude and transmission cross section over a wide range of frequencies.

I. INTRODUCTION

IN a previous paper of the same title,[1] the diffraction of a scalar plane wave by an aperture in an infinite plane screen was described in terms of a variational principle. The viewpoint adopted in this formulation regards the aperture as a coupling surface of the half spaces on opposite sides of the screen. For a boundary condition of vanishing wave function on the screen, the amplitude of the diffracted spherical wave at large distances from the aperture is exhibited in a form which is stationary with respect to small variations (relative to the correct values) of the aperture fields arising from a pair of incident waves.

The purpose of this paper is to develop a second variational principle for the diffracted amplitude by considering the screen as an obstacle to the propagation of the incident wave through free space. With the same boundary condition as previously, a pair of discontinuities in normal derivative of the fields at the screen appear in the role of functions which render the variational expression stationary. (Such functions are analogous to the surface currents excited on a perfectly conducting screen by incident electromagnetic waves.)

For explicit construction of the second variational principle, it proves convenient to deal with the residual functions which measure the deviation of the discontinuities in normal derivative from the simple distributions appropriate to a completely infinite screen. This procedure leads directly to the desired spherical wave amplitude in the radiation field of the screen, as distinct from the plane wave part of the radiation field that exists even in the absence of the aperture.

The diffracted spherical wave amplitude is shown to be invariant with respect to reversal in the sense of excitation and observation along a pair of directions in space. With the assistance of this reciprocity relation, the amplitude is exhibited in a form which is stationary for small independent variations (relative to the correct values) of a pair of residual functions arising from excitation along the foregoing directions. Following a scale transformation of the residual functions, this relation is converted to a homogeneous form. A part of the diffracted amplitude, independent of the residual functions, is identified as the Kirchoff approximation for it is the result obtained by ignoring the influence of the aperture on the discontinuity in normal derivative of the wave function at the screen.

The plane wave transmission cross section of the aperture is related to the imaginary part of the spherical wave amplitude observed in the direction of incidence, and hence retains the stationary property. In the limit of vanishingly small wave-length, λ, compared to the aperture dimensions, the Kirchoff part alone contributes and the geometrical optics form of the cross section emerges. At long wave-lengths the cross section varies with λ^{-2} except for the correct residual functions, unlike the behavior of the earlier variational form of the cross section, where the λ^{-4} variation is obtained with any real aperture field (subject to the boundary condition at the rim of the screen). Thus the two variational principles are individually adapted to opposite extremes of wave-length, and their over-all compatibility indicates the departure from a correct solution.

The variational formulation developed below is applied in detail for a plane wave normally incident on a circular aperture. Numerical values of the

[1] H. Levine and J. Schwinger, Phys. Rev. **74**, 958 (1948); hereafter referred to as I.

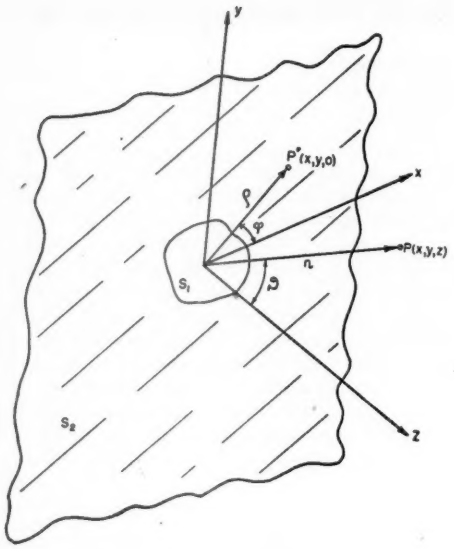

FIG. 1. Diffracting aperture in a plane screen.

transmission coefficient (transmission cross section/area of aperture) based on a relatively simple form of residual function are found to exhibit a high order of accuracy; it may also be noted that the Kirchoff procedure affords a reasonably satisfactory approximation.

II. INTEGRAL EQUATION FORMULATION FOR AN APERTURE OF ARBITRARY OPENING

We consider an infinitesimally thin plane screen S_2, of infinite extent, which is perforated by an aperture S_1. A rectangular coordinate system is chosen with origin at some point of the aperture, and oriented so that the screen lies in the x,y plane (Fig. 1).

A plane wave is incident on the screen in the half-space $z<0$, and it is desired to investigate the diffracted field. The incident wave, propagating in the direction ϑ', φ' (ϑ' measured from the positive direction of the z axis, and φ' from the positive direction of the x axis, in the x,y plane) is described by the scalar wave function

$$\phi^{\text{inc}}(\mathbf{r})=\exp(ik\mathbf{n}'\cdot\mathbf{r})=\exp[ik(x\sin\vartheta'\cos\varphi' +y\sin\vartheta'\sin\varphi'+z\cos\vartheta')], \quad (2.1)$$

where $\mathbf{n}'$ is a unit vector in the direction of propagation, $k=2\pi/\lambda$ is the free space propagation constant, and λ the corresponding wave-length. The harmonic time dependence $\exp(-i\omega t)$, $\omega=kc$, with c the velocity of wave propagation, is omitted throughout.

The wave function describing the complete (incident+diffracted) field satisfies the wave equation

$$(\nabla^2+k^2)\phi(\mathbf{r})=0 \quad (2.2)$$

at all points of space, and is subject to the prescribed boundary condition

$$\phi(\mathbf{r})=0, \quad \mathbf{r} \text{ on } S_2; \quad (2.3)$$

in addition, the wave function and its normal (i.e., z) derivative vary continuously on passing through the aperture.

Pursuant to a description of the screen as an obstacle imbedded in free space, we apply Green's second scalar identity,

$$\int[G(\mathbf{r}',\mathbf{r})(\nabla^{12}+k^2)\phi(\mathbf{r}') -\phi(\mathbf{r}')(\nabla'^2+k^2)G(\mathbf{r}',\mathbf{r})]d\tau'$$
$$=\int[G(\mathbf{r}',\mathbf{r})(\partial/\partial n')\phi(\mathbf{r}') -\phi(\mathbf{r}')(\partial/\partial n')G(\mathbf{r}',\mathbf{r})]dS', \quad (2.4)$$

to the wave function $\phi(\mathbf{r})$ and free space scalar Green's function,

$$G(\mathbf{r},\mathbf{r}')=\exp(ik|\mathbf{r}-\mathbf{r}'|)/4\pi|\mathbf{r}-\mathbf{r}'|=G(\mathbf{r}',\mathbf{r}), \quad (2.5)$$

within the domain bounded by the surfaces S_-, S_+ and parts of the respective faces of the screen (Fig. 2); the derivative is taken along the outward normal at each point of the bounding surface.

By virtue of (2) and the wave equation for the Green's function,

$$(\nabla^2+k^2)G(\mathbf{r},\mathbf{r}')=-\delta(\mathbf{r}-\mathbf{r}'), \quad (2.6)$$

where $\delta(\mathbf{r})$ is the three-dimensional Dirac delta function, the volume integral in (4) yields simply $\phi(\mathbf{r})$.

If the surface S_+ on the far side of the screen ($z>0$) is sufficiently remote, the wave and Green's functions there exhibit the behavior of spherical waves diverging from the aperture and field point $\mathbf{r}$, respectively, and the surface integral in (4) vanishes. Moreover, for a similarly disposed surface S_- on the near side of the screen ($z<0$), where the wave function describes incident and specularly reflected plane waves appropriate to a completely infinite screen (i.e., with no aperture), *viz.*:

$$\phi^{(0)}(\mathbf{r})=\phi^{\text{inc}}(x,y,z)-\phi^{\text{inc}}(x,y,-z),$$
$$\phi^{(0)}(x,y,0)=0, \quad (2.7)$$

in addition to a spherical wave diverging from the aperture, it is only $\phi^{(0)}(\mathbf{r})$ which contributes to the surface integral in (2.4). Thus, utilizing the boundary condition (2.3) and taking account of the oppositely directed normal derivatives at the two faces of the screen, we obtain for the wave function at an

arbitrary point in the enclosed region,

$$\phi(\mathbf{r})=\int_{S_-}[G(\mathbf{r},\mathbf{r}')(\partial/\partial n')\phi^{(0)}(\mathbf{r}') -\phi^{(0)}(\mathbf{r}')(\partial/\partial n')G(\mathbf{r},\mathbf{r}')]dS' +\int_{[S_2]}\Psi(\boldsymbol{\rho}')G(\mathbf{r};x',y',0)dS', \quad (2.8)$$

with

$$\Psi(\boldsymbol{\rho})=(\partial/\partial z)\phi(x,y,-0)-(\partial/\partial z)\phi(x,y,+0). \quad (2.9)$$

Here $\boldsymbol{\rho}$ denotes a position vector in the x,y plane, and $[S_2]$ that portion of the screen encompassed by the integration contour (ultimately all inclusive).

In the absence of an aperture, the result of applying Green's second scalar identity to the functions $\phi^{(0)}(\mathbf{r})$ and $G(\mathbf{r},\mathbf{r}')$ within the region bounded by S_- and the screen, is

$$\int_{S_-}[G(\mathbf{r},\mathbf{r}')(\partial/\partial n')\phi^{(0)}(\mathbf{r}') -\phi^{(0)}(\mathbf{r}')(\partial/\partial n')G(\mathbf{r},\mathbf{r}')]dS' +\int_{[S_2]}\Psi^{(0)}(\boldsymbol{\rho}')G(\mathbf{r};x',y',0)dS' +\int_{S_1}\Psi^{(0)}(\boldsymbol{\rho}')G(\mathbf{r};x',y',0)dS' =\phi^{(0)}(\mathbf{r}), \quad z<0, \quad =0, \quad z>0, \quad (2.10)$$

where, by (2.1), (2.7)

$$\phi^{(0)}(\mathbf{r})=2i\sin(kz\cos\vartheta')\exp(ik\mathbf{n}'\cdot\boldsymbol{\rho}),$$
$$\Psi^{(0)}(\boldsymbol{\rho})=(\partial/\partial z)\phi^{(0)}(x,y,-0) =2ik\cos\vartheta'\exp(ik\mathbf{n}'\cdot\boldsymbol{\rho}). \quad (2.11)$$

Hence, on subtracting (2.10) from (2.8), we obtain

$$\phi(\mathbf{r})=\begin{Bmatrix}\phi^{(+)}(\mathbf{r}),\ z>0\\ \phi^{(-)}(\mathbf{r}),\ z<0\end{Bmatrix}=\begin{Bmatrix}0\\ \phi^{(0)}(\mathbf{r})\end{Bmatrix} +\int_{S_2}[\Psi(\boldsymbol{\rho}')-\Psi^{(0)}(\boldsymbol{\rho}')]G(\mathbf{r};x',y',0)dS' -\int_{S_1}\Psi^{(0)}(\boldsymbol{\rho}')G(\mathbf{r};x',y',0)dS', \quad (2.12)$$

where integration over the entire screen is permissible, since $\Psi-\Psi^{(0)}$ vanishes at a point infinitely removed from the aperture. Introducing

$$\Psi(\boldsymbol{\rho})-\Psi^{(0)}(\boldsymbol{\rho})=2ik\cos\vartheta'\psi_{\mathbf{n}'}(\boldsymbol{\rho}) \quad (2.13)$$

(with dependence of $\psi_{\mathbf{n}'}$ on the direction of the incident plane wave indicated explicitly) and employing (2.11), Eq. (12) takes the form

$$\begin{Bmatrix}\phi^{(+)}(\mathbf{r})\\ \phi^{(-)}(\mathbf{r})\end{Bmatrix}=\begin{Bmatrix}0\\ \phi^{(0)}(\mathbf{r})\end{Bmatrix} +2ik\cos\vartheta'\left[\int_{S_2}\psi_{\mathbf{n}'}(\boldsymbol{\rho}')G(\mathbf{r};x',y',0)dS' -\int_{S_1}\exp(ik\mathbf{n}'\cdot\boldsymbol{\rho}')G(\mathbf{r};x',y',0)dS'\right]. \quad (2.14)$$

The wave functions $\phi^{(+)}$, $\phi^{(-)}$ in (14) are equal at any point of the aperture, since $\phi^{(0)}$ is an odd function of z and vanishes in the plane of the screen. Furthermore, with the Fourier integral representation of the Green's function (I, 2.5), it follows that

$$(\partial/\partial z)G(x,y,0;x',y',0) =\mp\frac{1}{8\pi^2}\int_{-\infty}^{\infty}\exp\{i[k_x(x-x')+k_y(y-y')]\}dk_xdk_y =\mp\tfrac{1}{4}\delta(x-x')\delta(y-y'),$$

where the upper and lower signs apply for $z\to+0$, $z\to-0$, respectively; thus, from (14)

$$\begin{Bmatrix}(\partial/\partial z)\phi^{(+)}(x,y,0)\\ (\partial/\partial z)\phi^{(-)}(x,y,0)\end{Bmatrix}=\begin{Bmatrix}0\\ 2ik\cos\vartheta'\exp(ik\mathbf{n}'\cdot\boldsymbol{\rho})\end{Bmatrix} \mp ik\cos\vartheta'\left[\int_{S_2}\psi_{\mathbf{n}'}(\boldsymbol{\rho}')\delta(x-x')\delta(y-y')dS' -\int_{S_1}\exp(ik\mathbf{n}'\cdot\boldsymbol{\rho}')\delta(x-x')\delta(y-y')dS'\right].$$

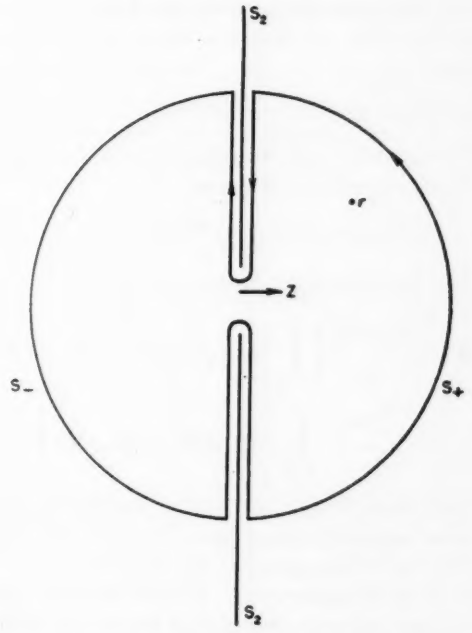

FIG. 2. Integration domain for Eq. (2.4)

Using familiar properties of the delta-function, we obtain

$$(\partial/\partial z)\phi^{(+)}(x, y, 0) = (\partial/\partial z)\phi^{(-)}(x, y, 0) = (\partial/\partial z)\phi^{\text{inc}}(x, y, 0), \quad \varrho \text{ in } S_1$$

for a point in the aperture (compare I, 2.14), and (after subtraction) the relation (2.13) for a point on the screen. Finally, by imposing the boundary condition (3) on either of the wave functions (14), we arrive at the integral equation

$$\int_{S_2} \psi_{\mathbf{n}'}(\varrho')G(\varrho, \varrho')dS' = \int_{S_1} \exp(ik\mathbf{n}'\cdot\varrho')G(\varrho, \varrho')dS', \quad \varrho \text{ on } S_2, \qquad G(\varrho, \varrho') = G(x, y, 0; x', y', 0), \tag{2.15}$$

to determine $\psi_{\mathbf{n}'}(\varrho)$ and thus, from (14), the wave function at any point of space.

According to (2.15), the projection of $\mathbf{n}'$ on the x,y plane distinguishes each function $\psi_{\mathbf{n}'}$ corresponding to a given direction of incidence. In particular, with excitation restricted to the half-space $z<0$, a reversal in the sign of $\mathbf{n}'$ implies an increase by π in the azimuthal angle φ'. By invoking the reflection symmetry with respect to the plane of the screen, this sign reversal can be ascribed to excitation in the direction opposite to $\mathbf{n}'$.

As in I, we shall confine our attention to the properties of the diffracted field at distances from the aperture large compared to its dimensions and the wave-length. Since a rigorous and explicit solution of the integral Eq. (2.15) is not generally feasible, the far field amplitude will be cast into a form which is insensitive to small deviations of the assumed solutions from the correct ones.

Inserting the asymptotic form of the Green's function

$$G(\mathbf{r}, \mathbf{r}') \simeq \exp(ik\{r-\mathbf{n}\cdot\mathbf{r}'\})/4\pi r, \quad r\to\infty \tag{2.16}$$

in (14), we obtain the transmitted field in the form of a diverging spherical wave,

$$\phi^{(+)}(\mathbf{r}) \simeq A(\mathbf{n}, \mathbf{n}')(e^{ikr}/r), \quad r\to\infty, \tag{2.17}$$

with the directionality factor

$$A(\mathbf{n}, \mathbf{n}') = \frac{ik\cos\vartheta'}{2\pi}\left[\int_{S_2} \psi_{\mathbf{n}'}(\varrho)\exp(-ik\mathbf{n}\cdot\varrho)dS - \int_{S_1} \exp(ik(\mathbf{n}'-\mathbf{n})\cdot\varrho)dS\right]. \tag{2.18}$$

It is clear from (2.14), (2.18) that an identical spherical wave appears along the direction obtained by reflecting $\mathbf{n}$ in the plane of the screen.

The transmission cross section of the aperture for a plane wave is calculated from the diffracted amplitude in the direction of incidence by the relation developed in I, namely,

$$\sigma(\mathbf{n}') = -(2\pi/k)ImA(\mathbf{n}', \mathbf{n}'). \tag{2.19}$$

III. VARIATIONAL PRINCIPLE FOR DIFFRACTED WAVE AMPLITUDE

Multiplying both sides of (2.15) by $\psi_{\mathbf{n}''}(\varrho)$ and integrating over the screen, we find

$$\int_{S_2} \psi_{\mathbf{n}'}(\varrho)G(\varrho, \varrho')\psi_{\mathbf{n}''}(\varrho')dSdS' = \int_{S_2} \psi_{\mathbf{n}''}(\varrho)dS\int_{S_1} G(\varrho, \varrho')\exp(ik\mathbf{n}'\cdot\varrho')dS' = \int_{S_2} \psi_{\mathbf{n}'}(\varrho)dS\int_{S_1} G(\varrho, \varrho')\exp(ik\mathbf{n}''\cdot\varrho')dS' \tag{3.1}$$

with recognition of the symmetry exhibited by the first term in $\mathbf{n}'$, $\mathbf{n}''$ (or the angular coordinates ϑ', φ' and ϑ'', φ''). Further, by invoking the additive nature of integration in the domains S_1, S_2, and with recourse to (2.15) once again, it follows that

$$\begin{aligned}
&\int_{S_2} \psi_{\mathbf{n}'}(\varrho)dS\int_{S_1} G(\varrho, \varrho')\exp(ik\mathbf{n}''\cdot\varrho')dS' \\
&= \int_{S_2} \psi_{\mathbf{n}'}(\varrho)dS\int_{S_1+S_2} G(\varrho, \varrho')\exp(ik\mathbf{n}''\cdot\varrho')dS' \\
&\quad - \int_{S_2} \psi_{\mathbf{n}'}(\varrho)dS\int_{S_2} G(\varrho, \varrho')\exp(ik\mathbf{n}''\cdot\varrho')dS' \\
&= \int_{S_2} \psi_{\mathbf{n}'}(\varrho)dS\int_{S_1+S_2} G(\varrho, \varrho')\exp(ik\mathbf{n}''\cdot\varrho')dS' \\
&\quad - \int_{S_1} \exp(ik\mathbf{n}'\cdot\varrho)dS\int_{S_2} G(\varrho, \varrho')\exp(ik\mathbf{n}''\cdot\varrho')dS' \\
&= \int_{S_2} \psi_{\mathbf{n}'}(\varrho)dS\int_{S_1+S_2} G(\varrho, \varrho')\exp(ik\mathbf{n}''\cdot\varrho')dS' \\
&\quad - \int_{S_1} \exp(ik\mathbf{n}'\cdot\varrho)dS\int_{S_1+S_2} G(\varrho, \varrho') \times\exp(ik\mathbf{n}''\cdot\varrho')dS' \\
&\quad + \int_{S_1} \exp(ik(\mathbf{n}'\cdot\varrho+\mathbf{n}''\cdot\varrho'))G(\varrho, \varrho')dSdS'.
\end{aligned} \tag{3.2}$$

The integration in S_1+S_2 is conveniently performed by use of the Fourier integral representation

$$G(\varrho, \varrho') = \frac{\exp(ik|\varrho-\varrho'|)}{4\pi|\varrho-\varrho'|} = \frac{i}{8\pi^2}\int_{-\infty}^{\infty} \frac{\exp[i\{k_x(x-x')+k_y(y-y')\}]}{(k^2-k_x^2-k_y^2)^{\frac{1}{2}}}dk_xdk_y, \qquad \arg(k^2-k_x^2-k_y^2)^{\frac{1}{2}} \geqslant 0; \tag{3.3}$$

thus

$$\int_{S_1+S_2} G(\varrho,\varrho')\exp(ik\mathbf{n}''\cdot\varrho')dS'$$
$$=\frac{i}{2}\int_{-\infty}^{\infty}\delta(k_x-kn_x'')\delta(k_y-kn_y'')$$
$$\times\frac{\exp[i\{k_xx+k_yy\}]}{(k^2-k_x^2-k_y^2)^{\frac{1}{2}}}dk_xdk_y=\frac{i\exp(ik\mathbf{n}''\cdot\varrho)}{2k|\cos\vartheta''|} \quad (3.4)$$

(where n_x'', n_y'' denote components of the vector $\mathbf{n}''$ along the x,y directions, respectively). Hence the relation (2) becomes

$$\int_{S_2}\psi_{\mathbf{n}'}(\varrho)dS\int_{S_1}G(\varrho,\varrho')\exp(ik\mathbf{n}''\cdot\varrho')dS'$$
$$=[i/2k|\cos\vartheta''|]\Big[\int_{S_2}\psi_{\mathbf{n}'}(\varrho)\exp(ik\mathbf{n}''\cdot\varrho)dS$$
$$-\int_{S_1}\exp(ik(\mathbf{n}'+\mathbf{n}'')\cdot\varrho)dS\Big]$$
$$+\int_{S_1}\exp(ik(\mathbf{n}'\cdot\varrho+\mathbf{n}''\cdot\varrho'))G(\varrho,\varrho')dSdS'$$

and from (3.1), (2.18),

$$\int_{S_2}\psi_{\mathbf{n}'}(\varrho)G(\varrho,\varrho')\psi_{-\mathbf{n}''}(\varrho')dSdS'$$
$$-\int_{S_2}\psi_{\mathbf{n}'}(\varrho)dS\int_{S_1}G(\varrho,\varrho')\exp(-ik\mathbf{n}''\cdot\varrho')dS'$$
$$-\int_{S_2}\psi_{-\mathbf{n}''}(\varrho)dS\int_{S_1}G(\varrho,\varrho')\exp(ik\mathbf{n}'\cdot\varrho')dS'$$
$$=-[\pi/k^2\cos\vartheta'\cos\vartheta'']$$
$$\times[A(\mathbf{n}'',\mathbf{n}')-A_K(\mathbf{n}'',\mathbf{n}')]$$
$$=-[\pi/k^2\cos\vartheta'\cos\vartheta'']$$
$$\times[A(-\mathbf{n}',-\mathbf{n}'')-A_K(-\mathbf{n}',-\mathbf{n}'')] \quad (3.5)$$

with

$$A_K(\mathbf{n}'',\mathbf{n}')=A_K(-\mathbf{n}',-\mathbf{n}'')$$
$$=-[k^2\cos\vartheta'\cos\vartheta''/\pi]$$
$$\times\int_{S_1}\exp(ik(\mathbf{n}'\cdot\varrho-\mathbf{n}''\cdot\varrho'))G(\varrho,\varrho')dSdS'. \quad (3.6)$$

The expressions (3.5), (3.6) apply for $\vartheta',\vartheta''<\pi/2$, since the absolute value signs have been discarded; the remaining amplitudes are readily obtained by means of the reflection symmetry in the plane of the screen. With omission of $\psi_{\mathbf{n}'}$, $\psi_{-\mathbf{n}''}$, or equivalently, on employing the wave functions appropriate to a completely infinite screen, the amplitudes A, A_K are identical. A_K may thus be described as a Kirchoff approximation for the diffracted amplitude, since it disregards the modification of the fields occasioned by the presence of an aperture. This Kirchoff approximation is to be distinguished from the more familiar type, in which aperture and incident fields are identified, with disregard for the presence of the screen.

Equality of the amplitudes $A(\mathbf{n}'',\mathbf{n}')$ and $A(-\mathbf{n}',-\mathbf{n}'')$ (or the corresponding Kirchoff amplitudes) describes a reciprocity condition for incidence and observation along a pair of directions in space.

On performing independent variations of $\psi_{\mathbf{n}'}$, $\psi_{-\mathbf{n}''}$ in (3.5), it is found that a stationary value of $A(\mathbf{n}'',\mathbf{n}')$ obtains, provided these functions obey integral equations of the form (2.15). If we introduce the scale transformations

$$\psi_{\mathbf{n}'}(\varrho)\rightarrow\alpha\psi_{\mathbf{n}'}(\varrho),\quad \psi_{-\mathbf{n}''}(\varrho)\rightarrow\beta\psi_{-\mathbf{n}''}(\varrho)$$

($\alpha=\beta=0$ for the Kirchoff approximation) and apply the stationary requirement to the determination of α,β, we arrive at a variational expression for $A(\mathbf{n}'',\mathbf{n}')$,

$$A(\mathbf{n}'',\mathbf{n}')=A_K(\mathbf{n}'',\mathbf{n}')+[k^2\cos\vartheta'\cos\vartheta''/\pi]$$
$$\times\frac{\Big(\int_{S_2}\psi_{\mathbf{n}'}(\varrho)dS\int_{S_1}G(\varrho,\varrho')\exp(-ik\mathbf{n}''\cdot\varrho')dS'\Big)\Big(\int_{S_2}\psi_{-\mathbf{n}''}(\varrho)dS\int_{S_1}G(\varrho,\varrho')\exp(ik\mathbf{n}'\cdot\varrho')dS'\Big)}{\int_{S_2}\psi_{\mathbf{n}'}(\varrho)G(\varrho,\varrho')\psi_{-\mathbf{n}''}(\varrho')dSdS'}, \quad (3.7)$$

which is homogeneous in $\psi_{\mathbf{n}'}$, $\psi_{-\mathbf{n}''}$.

A comparison of the two variational principles for the spherical wave amplitude is instructive; to this end, we recall the equations (I, 2.11, 2.12)

$$\phi^{(+)}(\mathbf{r})=\int_{S_1}\phi(\varrho')(\partial/\partial z')G(\mathbf{r};x',y',0)dS', \quad (3.8)$$

$$\phi^{(-)}(\mathbf{r})=\phi^{(0)}(\mathbf{r})-\int_{S_1}\phi(\varrho')(\partial/\partial z')G(\mathbf{r};x',y',0)dS', \quad (3.9)$$

for the wave function at any point of space in terms of its values in the aperture. In accord with (2.9), (2.13), we obtain on differentiating (3.8), (3.9),

$$\Psi(\varrho)-\Psi^{(0)}(\varrho)=2ik\cos\vartheta\psi_{\mathbf{n}}(\varrho)$$
$$=-2\int_{S_1}\phi_{\mathbf{n}}(\varrho')K(\varrho,\varrho')dS',$$

and hence

$$\psi_{\mathbf{n}}(\varrho)=(i/k\cos\vartheta)\int_{S_1}\phi_{\mathbf{n}}(\varrho')K(\varrho,\varrho')dS', \quad (3.10)$$

where

$$K(\varrho,\varrho')=(\partial/\partial z)(\partial/\partial z')G(x,y,0;x',y',0)$$
$$=K(\varrho',\varrho). \quad (3.11)$$

The relation (10) may be adopted as a general form of the residual function, to be evaluated with an assumed aperture field. If this be inserted in (3.5) and the resulting expression transformed after the fashion of (3.2)–(3.4), it turns out that

$$A(\mathbf{n}'',\mathbf{n}')=\frac{1}{4\pi}\Big[\int_{S_1}\phi_{\mathbf{n}'}(\varrho)K(\varrho,\varrho')\phi_{-\mathbf{n}''}(\varrho')dSdS'+ik\cos\vartheta'\int_{S_1}\phi_{-\mathbf{n}''}(\varrho)\exp(ik\mathbf{n}'\cdot\varrho)dS$$
$$+ik\cos\vartheta''\int_{S_1}\phi_{\mathbf{n}'}(\varrho)\exp(-ik\mathbf{n}''\cdot\varrho)dS\Big]-\frac{1}{\pi}\int_{S_1}\Big[\int_{S_1}\phi_{\mathbf{n}'}(\varrho'')K(\varrho'',\varrho)dS''$$
$$-ik\cos\vartheta'\exp(ik\mathbf{n}'\cdot\varrho)\Big]G(\varrho,\varrho')\Big[\int_{S_1}K(\varrho',\varrho''')\phi_{-\mathbf{n}''}(\varrho''')dS'''-ik\cos\vartheta''\exp(-ik\mathbf{n}''\cdot\varrho')\Big]dSdS'.$$

We observe that with aperture wave functions which satisfy the exact integral equation

$$\int_{S_1}\phi_{\mathbf{n}}(\varrho')K(\varrho,\varrho')dS'=ik\cos\vartheta\exp(ik\mathbf{n}\cdot\varrho),$$
$$\varrho \text{ on } S_1 \quad \text{(I, 2.9)}$$

(obtained by equating the z derivatives of (3.8), (3.9) in the aperture), only the first three terms in the preceding equation remain; more generally, on retaining just these terms, the amplitude $A(\mathbf{n}'',\mathbf{n}')$ is stationary with respect to variations relative to the exact aperture wave functions. Following a scale transformation of the trial wave functions, the resulting amplitude

$$\frac{1}{A(\mathbf{n}'',\mathbf{n}')}=\frac{(4\pi/k^2)\int_{S_1}\phi_{\mathbf{n}'}(\varrho)K(\varrho,\varrho')\phi_{-\mathbf{n}''}(\varrho')dSdS'}{\cos\vartheta'\cos\vartheta''\int_{S_1}\phi_{\mathbf{n}'}(\rho)\exp(-ik\mathbf{n}''\cdot\varrho)dS\int_{1}\phi_{-\mathbf{n}''}(\varrho)\exp(ik\mathbf{n}'\cdot\varrho)dS}, \quad \text{(I, 3.2)}$$

is identical with that derived from the variational principle in I. Thus, a practical measure of proximity to the correct solution is obtained from the over-all discrepancy in the two variational principles, following the use of assumed trial functions.

Combining (2.19) with (3.6), (3.7), the transmission cross section of the aperture for a plane wave incident in the direction $\mathbf{n}$ assumes the form

$$\sigma(\mathbf{n})=\sigma_K(\mathbf{n})-2k\cos^2\vartheta Im$$
$$\times\frac{\Big(\int_{S_2}\psi_{\mathbf{n}}(\varrho)dS\int_{S_1}G(\varrho,\varrho')\exp(-ik\mathbf{n}\cdot\varrho')dS'\Big)\Big(\int_{S_2}\psi_{-\mathbf{n}}(\varrho)dS\int_{S_1}G(\varrho,\varrho')\exp(ik\mathbf{n}\cdot\varrho')dS'\Big)}{\int_{S_2}\psi_{\mathbf{n}}(\varrho)G(\varrho,\varrho')\psi_{-\mathbf{n}}(\varrho')dSdS'}, \quad (3.12)$$

where

$$\sigma_K(\mathbf{n})=2k\cos^2\vartheta Im\int_{S_1}\exp\{ik\mathbf{n}\cdot(\varrho-\varrho')\}G(\varrho,\varrho')dSdS' \quad (3.13)$$

is the Kirchoff contribution.

To examine the behavior of the cross section at high frequencies, a convenient point of departure is the Fourier integral representation (3.3) of $G(\varrho,\varrho')$.

Thus

$$\int_{S_1} \exp\{ik\mathbf{n}\cdot(\varrho-\varrho')\}G(\varrho,\varrho')dSdS'$$
$$=(i/8\pi^2)\int_{-\infty}^{\infty}\int_{S_1}\exp[i\{\alpha(x-x')+\beta(y-y')\}]$$
$$\times[dk_xdk_y/(k^2-k_x^2-k_y^2)^{\frac{1}{2}}]dSdS',$$
$$\alpha=k_x+kn_x,\quad \beta=k_y+kn_y,$$

and, by virtue of the increasing oscillations of the exponential factor as $k\to\infty$, the integration variables x, y (or x', y') can be extended throughout the plane $z=0$, with the result

$$\int_{S_1}\exp\{ik\mathbf{n}\cdot(\varrho-\varrho')\}G(\varrho,\varrho')dSdS'$$
$$\simeq\frac{i}{2}\int_{-\infty}^{\infty}\int_{S_1}\exp[-i\{\alpha x'+\beta y'\}]\delta(\alpha)\delta(\beta)$$
$$\times[dk_xdk_y/(k^2-k_x^2-k_y^2)^{\frac{1}{2}}]dS'$$
$$=iS_1/2k\cos\vartheta,\quad k\to\infty,\qquad(3.14)$$

where S_1 is the area of the aperture.

Owing to the delta-function character of $G(\varrho,\varrho')$ in the limit of infinite frequency (cf. (3.3)), the second term in (12) tends to zero since the integration domains for the factors in its numerator are mutually exclusive. Thus, from (3.12)–(3.14),*

$$\sigma(\mathbf{n})\simeq\sigma_K(\mathbf{n})\simeq S_1\cos\vartheta,\quad k\to\infty,\qquad(3.15)$$

in which the last term contains the geometrical optics cross section, namely, the projected area of the aperture on a plane normal to the direction of the incident wave.

Although the cross section in the limit of infinite frequency is rigorously obtained independently of the residual functions, the previous considerations imply that deviations in this quantity are inherent for all other frequencies unless the correct residual functions are employed. In particular, with a choice of real, frequency independent residual functions $\psi(\varrho)$, unrelated to the direction of excitation, and use of the expansions

$$G(\varrho,\varrho')\doteqdot[1/4\pi|\varrho-\varrho'|]+[ik/4\pi]-\cdots,$$
$$\exp(\pm ik\mathbf{n}\cdot\varrho)\doteqdot 1\pm ik\mathbf{n}\cdot\varrho-\cdots,\quad k\to 0,$$

we find as the leading term in the frequency expansion of the cross section (12),

$$\sigma(\mathbf{n})=(k^2/2\pi)\cos^2\vartheta\left[S_1-\frac{\left(\int_{S_2}\psi(\varrho)dS\right)\left(\int_{S_2}\psi(\varrho)dS\int_{S_1}(dS'/|\varrho-\varrho'|)\right)}{\int_{S_2}(\psi(\varrho)\psi(\varrho')/|\varrho-\varrho'|)dSdS'}\right]^2,\quad k\to 0.\qquad(3.16)$$

The cross section (3.16) departs from the k^4 behavior characteristic of low frequencies, although it embodies the correct angular dependence (compare I, 3.7). Nevertheless, as shown in a later example, these low frequency deviations may prove insignificant when viewed on a scale appropriate to the over-all frequency variation of the cross section.

IV. DIFFRACTION BY A CIRCULAR APERTURE

To illustrate the utility of the variational formulation, we describe an application for the case of normal incidence of a plane wave on a circular aperture. We calculate, in particular, the transmission coefficient of the aperture as a function of the characteristic parameter, $ka=2\pi$(radius of aperture/wave-length).

From (3.12), (3.13) the transmission coefficient for normal incidence on an arbitrary aperture becomes

$$t=\sigma(0)/S_1=t_K-[2k/S_1]Im\times\frac{\left(\int_{S_2}\psi(\varrho)dS\int_{S_1}G(\varrho,\varrho')dS'\right)^2}{\int_{S_2}\psi(\varrho)G(\varrho,\varrho')\psi(\varrho')dSdS'},\qquad(4.1)$$

$$t_K=(2k/S_1)Im\int_{S_1}G(\varrho,\varrho')dSdS',\qquad(4.2)$$

involving the single residual function $\psi(\varrho)$ (omitting subscript) which arises from plane wave excitation on opposite sides of the screen.

For a circular domain S_1, it is convenient to introduce polar coordinates ρ, φ in the plane of the aperture, with origin at its center, whence $G(\varrho,\varrho')=G(\rho,\varphi;\rho',\varphi')$ and $\psi(\varrho)=\psi(\rho)$ is a func-

* Observe that this result follows from (2.18), (2.19) with omission of the residual function.

tion only of the radial coordinate. The Kirchoff transmission coefficient t_K is readily evaluated in this case with the aid of the integral representation (see I, 4.12),

$$G(\rho, \varphi; \rho', \varphi') = \frac{1}{4\pi}\int_0^\infty J_0(\zeta R)\frac{\zeta d\zeta}{(\zeta^2-k^2)^{\frac{1}{2}}},$$

$$R=(\rho^2+\rho'^2-2\rho\rho'\cos(\varphi-\varphi'))^{\frac{1}{2}}, \quad (4.3)$$

where J_0 denotes the zero-order Bessel function. The integration contour in (4.3) avoids a singularity at $\zeta=k$ by an indentation below the singular point, and $\arg(\zeta^2-k^2)^{\frac{1}{2}}=0$, $\zeta>k$; $=-\pi/2$, $\zeta<k$. Thus, employing the Bessel function addition theorem

$$J_0(\zeta R)=\sum_{n=0}^{\infty}(2-\delta_{0n})J_n(\zeta\rho)J_n(\zeta\rho')\cos n(\varphi-\varphi'),$$

$$\delta_{pq}=\begin{matrix}0, & p\neq q\\ 1, & p=q\end{matrix} \quad (4.4)$$

it follows that

$$t_K=(2k/\pi a^2)\,Im\int_{S_1}G(\rho, \varphi; \rho', \varphi')\rho d\rho d\varphi\rho' d\rho' d\varphi'$$

$$=(2k/a^2)\,Im\int_0^\infty \zeta(\zeta^2-k^2)^{-\frac{1}{2}}d\zeta \times\left(\int_0^a \rho J_0(\zeta\rho)d\rho\right)^2.$$

Extracting the imaginary part of the latter expression and performing the ρ-integration, we find after a change of variable,

$$t_K=2\int_0^1(1-v^2)^{-\frac{1}{2}}J_1^2(kav)(dv/v), \quad (4.5)$$

whence (see appendix)

$$\begin{aligned}t_K&=1-(1/ka)J_1(2ka)\\ &\simeq\tfrac{1}{2}(ka)^2, \quad ka\ll 1,\\ &\simeq 1, \quad ka\gg 1.\end{aligned} \quad (4.6)$$

Numerical values of t_K are given in Fig. 3, for the interval $0<ka<10$, together with exact values of the transmission coefficient calculated by Bouwkamp (I, reference 5). A comparison of this Kirchoff approximation with one based on a constant aperture field (see I, Fig. 2) reveals that both approach the value unity at high frequencies and possess a k^2 behavior at low frequencies. The latter approximation, however, is distinctly less accurate for intermediate frequencies, failing to take values in excess of unity and exhibit characteristic oscillations of the diffraction curve.

We consider next a more refined approximation to the transmission coefficient, deduced from the variational expression (1). A simple choice of frequency independent residual function is

$$\psi(\rho)=(a/\rho)^3(1-(a/\rho)^2)^{-\frac{1}{2}}, \quad (4.7)$$

featuring a characteristic (low frequency) singularity at the rim of the screen and decreasing with sufficient rapidity therefrom to ensure integrability over the entire screen. The integrals in the second term of (4.1) are again simplified with the aid of (4.3), (4.4). Thus

$$\int_{S_2}\psi(\rho)\rho d\rho d\varphi\int_{S_1}G(\rho, \varphi; \rho', \varphi')\rho' d\rho' d\varphi'$$

$$=\pi\int_0^\infty \zeta(\zeta^2-k^2)^{-\frac{1}{2}}d\zeta\left(\int_a^\infty (a/\rho)^3(1-(a/\rho)^2)^{-\frac{1}{2}} \times\rho J_0(\zeta\rho)d\rho\right)\left(\int_0^a \rho' J_0(\zeta\rho')d\rho'\right)$$

$$=\pi a^3\int_0^\infty(\zeta^2-k^2)^{-\frac{1}{2}}J_1(\zeta a)d\zeta \times\int_1^\infty(x^2-1)^{-\frac{1}{2}}J_0(\zeta ax)(dx/x).$$

To perform the x integration, we consider

$$F(\xi)=\int_1^\infty J_0(\xi x)(x^2-1)^{-\frac{1}{2}}(dx/x), \quad F(0)=\pi/2$$

and observe that[2]

$$dF/d\xi=-\int_1^\infty J_1(\xi x)(x^2-1)^{-\frac{1}{2}}dx=-\sin\xi/\xi,$$

whence

$$F(\xi)=(\pi/2)-\int_0^\xi(\sin x/x)dx=(\pi/2)-Si\,\xi=si\,\xi,$$

where Si denotes the sine integral.

Consequently,

$$\int_{S_2}\psi(\rho)\rho d\rho d\varphi\int_{S_1}G(\rho, \varphi; \rho', \varphi')\rho' d\rho' d\varphi' =\pi a^3(R_1(ka)+iI_1(ka)), \quad (4.8)$$

with

$$I_1(\alpha)=\int_0^\alpha J_1(x)(\alpha^2-x^2)^{-\frac{1}{2}}sixdx,$$

$$R_1(\alpha)=\int_\alpha^\infty J_1(x)(x^2-\alpha^2)^{-\frac{1}{2}}sixdx. \quad (4.9)$$

[2] G. N. Watson, *A Treatise on the Theory of Bessel Functions* (Cambridge University Press, London, 1945), p. 417.

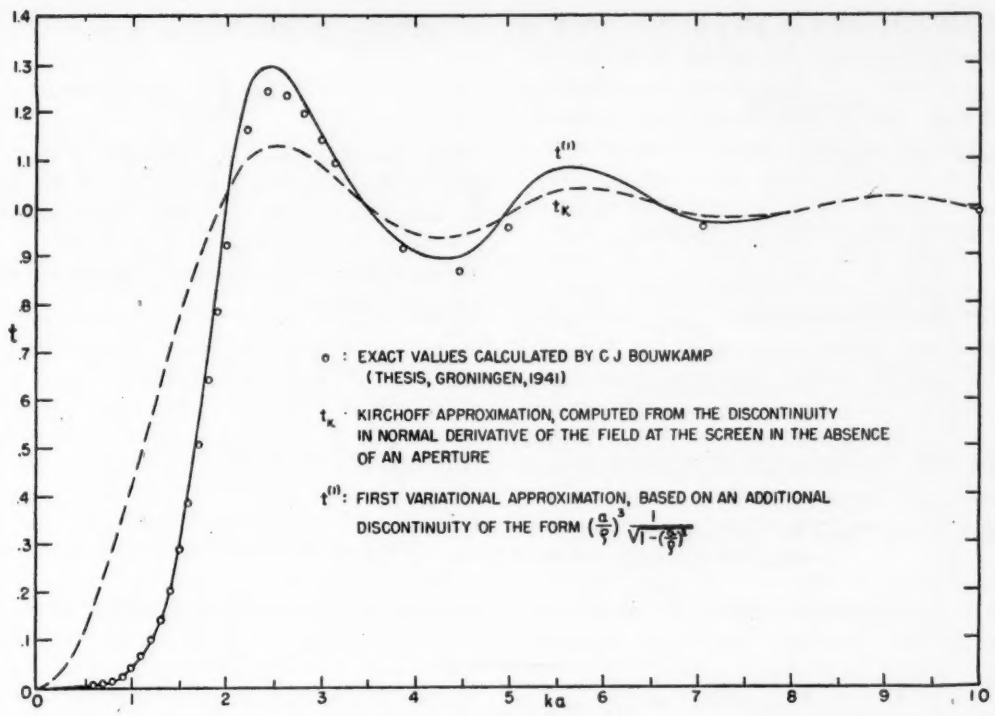
t
ka
$t^{(1)}$
t_K
o : EXACT VALUES CALCULATED BY C J BOUWKAMP (THESIS, GRONINGEN, 1941)
t_K : KIRCHOFF APPROXIMATION, COMPUTED FROM THE DISCONTINUITY IN NORMAL DERIVATIVE OF THE FIELD AT THE SCREEN IN THE ABSENCE OF AN APERTURE
$t^{(1)}$: FIRST VARIATIONAL APPROXIMATION, BASED ON AN ADDITIONAL DISCONTINUITY OF THE FORM $(\frac{a}{\rho})^3 \frac{1}{\sqrt{1-(\frac{a}{\rho})^2}}$

FIG. 3. Transmission coefficient of circular aperture for normally incident plane waves, as a function of the parameter $ka=2\pi$ (radius of aperture/wave-length). Scalar wave function assumed to vanish on the screen.

In a similar fashion, we obtain

$$\int_{S_2} \psi(\rho)G(\rho,\varphi;\rho',\varphi')\psi(\rho')\rho d\rho d\varphi \rho' d\rho' d\varphi' = \pi a^3(R_2(ka)+iI_2(ka)), \quad (4.10)$$

with

$$I_2(\alpha)=\int_0^\alpha x(\alpha^2-x^2)^{-\frac{1}{2}}si^2x dx,$$
$$R_2(\alpha)=\int_\alpha^\infty x(x^2-\alpha^2)^{-\frac{1}{2}}si^2x dx. \quad (4.11)$$

The result of inserting (4.6), (4.8), (4.10) in (4.1) yields as a first variational approximation to the transmission coefficient,

$$t^{(1)}=1-[J_1(2ka)/ka] -2ka[(2I_1R_1R_2-I_2(R_1^2-I_1^2))/(R_2^2+I_2^2)], \quad (4.12)$$

in which the argument, ka, of the functions I_1, I_2, R_1, R_2 is omitted. The values of $t^{(1)}$ presented in Fig. 3 are based on numerical integrations of (4.9), (4.11), with appropriate modifications for the singular point. A very accurate low frequency behavior is exhibited therein, although considerations of the previous section imply some residual k^2 dependence in $t^{(1)}$. We have, in fact,

$$\left.\begin{aligned} &I_1(\alpha)\doteqdot \pi\alpha/4, \quad I_2(\alpha)\doteqdot \pi^2\alpha/4 \\ &R_1(\alpha)\doteqdot \int_0^\infty J_1(x)six(dx/x)=(\pi/2)-1 \\ &R_2(\alpha)\doteqdot \int_0^\infty si^2x dx=\pi/2 \end{aligned}\right\} \alpha\to 0,$$

whence, from (4.12),

$$t^{(1)}\doteqdot (1/2)(\pi-3)^2(ka)^2=0.010(ka)^2, \quad ka\to 0. \quad (4.13)$$

(The same result is obtained from (3.16) for the case of normal incidence.) We may note that if the radical is omitted in (4.7), the coefficient of (4.13) is replaced by 0.041. From the over-all agreement of the end results in the two variational formulations, we may infer their proximity to that of an exact solution, quite apart from Bouwkamp's work.

The construction of analogous variational principles for the diffraction of electromagnetic waves by an aperture in a perfectly conducting screen will appear in a forthcoming paper.

The assistance of Mrs. D. Abkowitz with numerical calculations is gratefully acknowledged.

This work was supported in part by the Office of Naval Research Contract N5-ori-76, T.O.I.

APPENDIX

To evaluate the integral

$$I=\int_0^1 (1-v^2)^{-\frac{1}{2}}J_1^2(\alpha v)(dv/v),$$

we introduce the representation

$$J_1^2(z)=(1/\pi)\int_0^\pi J_2(2z\sin\vartheta)d\vartheta$$

and obtain, with the change of variable $v=\sin\varphi$,

$$I=(1/2\pi)\int_0^\pi \sin^{-1}\varphi d\varphi\int_0^\pi J_2(2\alpha\sin\vartheta\sin\varphi)d\vartheta.$$

Regarding ϑ, φ as the polar angles of a point on a unit sphere, we may write

$$I=(1/2\pi)\int_{x\geq 0} x^{-1}J_2(2\alpha x)d\omega,$$

where $x=\sin\vartheta\sin\varphi$, $d\omega=\sin\vartheta d\vartheta d\varphi$, and the integration extends over the surface of the hemisphere on which x is positive. The replacement of x by $z(=\cos\vartheta)$ corresponds to a rotation of the coordinate system and does not affect the value of the integral. Hence

$$I=(1/2\pi)\int_{z\geq 0} z^{-1}J_2(2\alpha z)d\omega$$

$$=\int_0^1 \mu^{-1}J_2(2\alpha\mu)d\mu$$

$$=-\int_0^1 d(J_1(2\alpha\mu)/2\alpha\mu)=\tfrac{1}{2}[1-(J_1(2\alpha)/\alpha)],$$

which allows the verification of Eq. (4.6) in the text.

PHYSICAL REVIEW VOLUME 75, NUMBER 9 MAY 1, 1949

The Energy Spectrum of the Decay Particles and the Mass and Spin of the Mesotron*

ROBERT B. LEIGHTON, CARL D. ANDERSON, AND AARON J. SERIFF
California Institute of Technology, Pasadena, California

(Received March 11, 1949)

Energy values determined from curvature measurements of 75 cloud-chamber tracks of decay particles of cosmic-ray mesotrons at sea level, in a magnetic field of 7250 gauss, are here reported. The observed spectrum extends from 9 Mev to 55 Mev with an apparently continuous distribution of intermediate energy values and a mean energy of 34 Mev. The shape of the spectrum and the value of its upper limit are strong evidence that the mesotron disintegrates into an electron and two neutrinos. It is concluded that the mesotron has half-integral spin. The value of the observed upper limit of the energy spectrum corresponds to a mass value of the mesotron equal to 217±4 electron masses.

I. INTRODUCTION

MEASUREMENTS of the energy of the particles resulting from the decay of mesotrons have previously been made in three ways. In a very few cases, the energies have been determined directly by measurement of the curvature of cloud-chamber tracks of the decay particles in a magnetic field.[1] In other experiments, the energies of the decay particles have been inferred from measurement of their absorption in various materials,[2] and recently, from measurement of their scattering in photographic emulsions.[3] The very small number of cases available for measurement, and the difficulty in making precise energy measurements, have made it impossible so far to distinguish between a continuous spectrum of energies and two or three discrete energies for the decay particles. Thus, the basic nature of the spectrum has so far not been established.

The measurements of the energies of decay particles that are here reported were made on 75 cases obtained in a cloud chamber operated in a magnetic field. The precision of the measurements and the number of cases provide strong evidence for a continuous decay spectrum, and yield some information as to its shape.

* Assisted by the joint program of the ONR and AEC.

[1] (a) Adams, Anderson, Lloyd, and Rau, Phys. Rev. **72**, 724 (1947); (b) Adams, Anderson, Lloyd, Rau, and Saxena, Rev. Mod. Phys. **20**, 344 (1948); (c) R. W. Thompson, Phys. Rev. **74**, 490 (1948).

[2] Fowler, Cool, and Street, Phys. Rev. **74**, 101 (1948); Zar, Hershkowitz, and Berezin, Phys. Rev. **74**, 111 (1948); J. Steinberger, Phys. Rev. **74**, 500 (1948); E. P. Hincks and B. Pontecorvo, Phys. Rev. **74**, 697 (1948); M. H. Shamos and A. Russek, Phys. Rev. **74**, 1545 (1948); Kan-Chang Wand and S. B. Jones, Phys. Rev. **74**, 1547 (1948).

[3] Brown, Camerini, Fowler, Muirhead, Powell, and Ritson, Nature **163**, 47 (1949).

Preliminary results of the present experiments have been reported.[4]

II. APPARATUS

Tracks were photographed in a cloud chamber of 30-cm inside diameter and 11-cm depth, operating in a magnetic field of 7250 gauss. The chamber was filled with argon to an absolute pressure of 1.25 atmospheres; a mixture of 35 percent water and 65 percent ethyl alcohol was used, giving an expansion ratio of 1.08. The gross weight of the magnet is 3300 pounds and it consumes a power of 10 kw. The cloud chamber is of the freely falling type.[5] This type of cloud chamber is employed in order to obtain a stronger and more uniform magnetic field for a given power consumption and magnet weight, to simplify the illumination, and to study the characteristics of a freely falling chamber with respect to track distortions arising from convection currents in the gas. In the present apparatus, the cloud chamber falls freely for a distance of 45 cm between the time the particle enters the chamber and the time the photograph is made. The tracks are illuminated by light projected from the rear of the cloud chamber through the front and rear walls which consist of glass plates. Four condensers, each of 23 μf charged to 1500 volts, are discharged through four FT-422 (General Electric Company) lamps to provide the illumination, and stereoscopic photographs are made on linagraph orthofilm with a lens setting of $f/14$. By means of a thermostated water jacket, all portions of the cloud chamber are maintained at constant temperature to within ± 0.1°C.

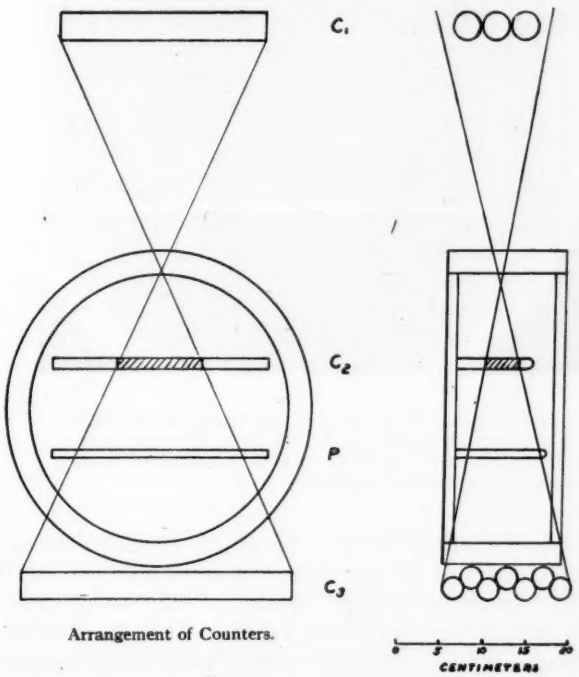

FIG. 1. Schematic diagram of cloud chamber and arrangement of Geiger counters.

The disposition of the Geiger counters which control the chamber is shown in Fig. 1. A lead absorber of 10-cm thickness has been placed directly below the upper coincidence tray. The chamber is actuated when a coincidence occurs between a counter in the tray C_1 above the chamber, and the counter C_2 mounted inside the chamber, if this coincidence is not accompanied by the discharge of a counter in the lower tray C_3. In this way the relative yield of slow particles, which stop inside the chamber, is increased. The total counting rate is approximately ten per hour.

The counter C_2 inside the chamber is rectangular in shape, having flat top and bottom surfaces consisting of copper sheet of 0.87-mm uniform thickness. The counter is mounted inside a flat copper jacket whose wall thickness is 0.63 mm. The counter also acts as an absorber for the determination of the mass of the mesotron by measurements of its momentum before and after it traverses the 3.0 mm of copper in the counter and jacket. A carbon plate P, 2.0 g/cm^2 in thickness, is mounted in the lower part of the chamber and provides an additional absorber for mass determinations and for the observation of decay particles.

III. EXPERIMENTAL RESULTS

Out of a total of 15,000 photographs, 75 photographs were obtained which show slow mesotrons which are observed to produce decay particles whose tracks are suitable for measurement. In these cases the mesotron stops either in the gas of the chamber, in the counter C_2 inside the chamber, in the carbon plate, or in the Bakelite or glass walls of the chamber. On the basis of evidence presented in Section IV of this paper, the decay particles are assumed to be electrons. Figures 2 and 3 are examples of electrons produced in the decay of mesotrons. The energy of the electron was determined in each case from measurement of the track curvature in the magnetic field. Each energy measurement was corrected for the angle between the electron track and the magnetic field, and for the energy lost by the electron before it appeared in the cloud chamber. The latter correction was made by calculating the distance of penetration of the incoming mesotron into the absorber, using for this purpose the momentum of the mesotron as determined from the observed curvature of its track, and assuming that the mass of the mesotron in each case is 220 m_e (m_e=electron mass); then, with the

[4] Leighton, Anderson, and Seriff, Phys. Rev. **75**, 1466 (1949). See also: R. W. Thompson, Phys. Rev. **75**, 1279 *et seq.* (1949); J. Steinberger, Phys. Rev. **75**, 1279 *et seq.* (1949).

[5] C. T. R. Wilson and J. G. Wilson, Proc. Roy. Soc. **148A**, 523 (1935).

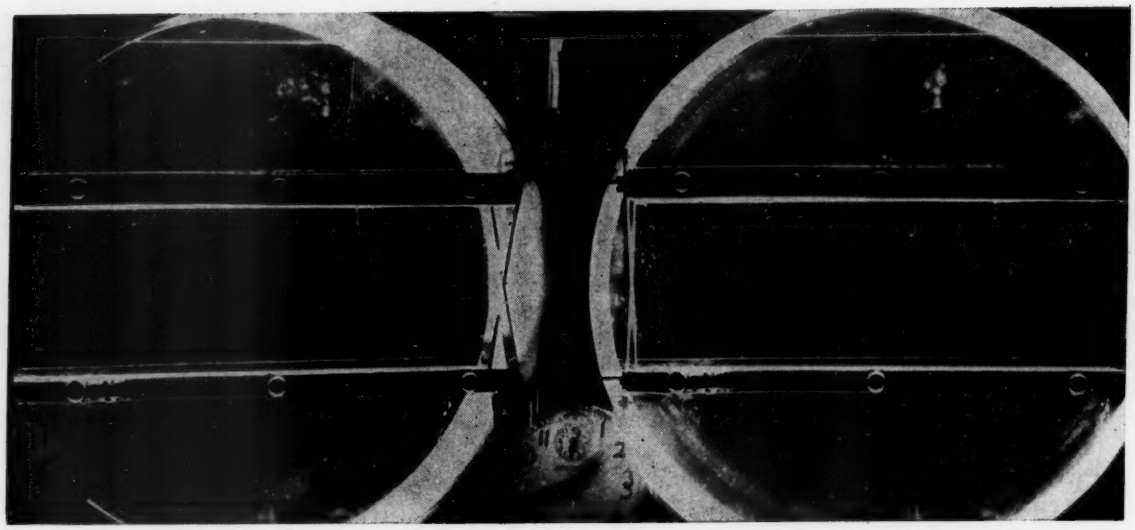

FIG. 2. A mesotron of positive charge passes downward through the counter in the cloud chamber, comes to rest in the carbon plate, and produces a decay electron whose energy, after correction for energy loss in the plate is 37 ± 1.5 Mev. The momentum of the mesotron upon entering the carbon plate is 72 Mev/c. A magnetic field of 7250 gauss, directed toward the observer, is present. Two stereoscopic views are shown.

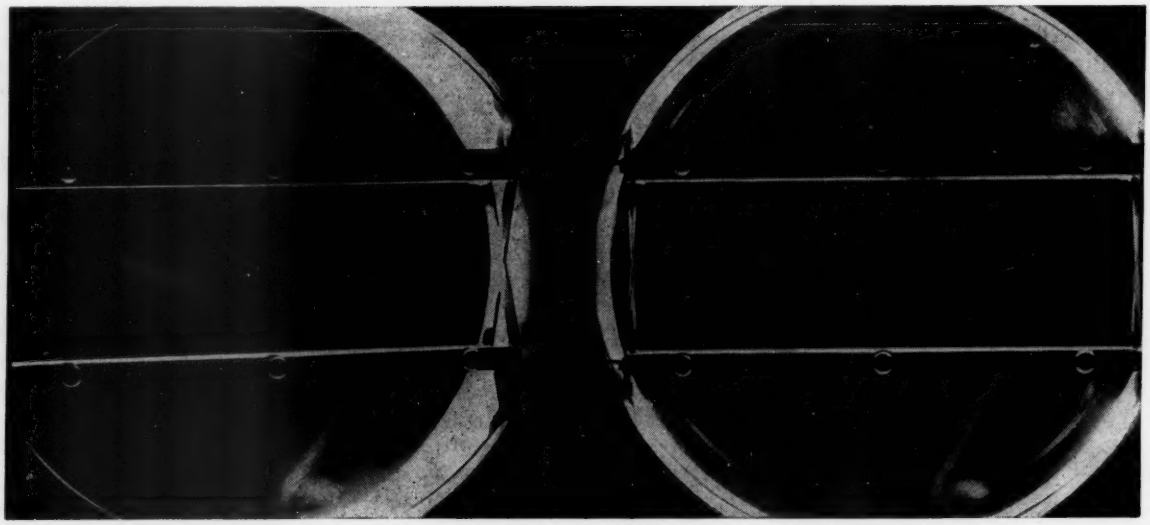

FIG. 3. A mesotron of negative charge passes through the counter in the cloud chamber and comes to rest in the gas (argon). A decay electron of 13.0 ± 1 Mev is produced. The decay electron is projected in a direction almost normal to the front glass of the cloud chamber, thus producing only a short track. The increase in ionization and the scattering of the mesotron near the end of its range is apparent in the photograph.

aid of stereoscopic observation of the tracks, the thickness of material traversed by the electron and the corresponding loss in energy of the electron were determined. The largest of these corrections is 11 Mev, and in the great majority of cases, the corrections are only 2 to 5 Mev. Since these corrections could be made with considerable accuracy, the error they introduce into the final energy of the decay electron is only 1 to 2 Mev.

It is possible that electrons of very low energy may have escaped detection by their failure to emerge from the walls of the chamber or from the carbon plate. However, the effect of such cases on the observed energy distribution should be small, and should be limited almost wholly to electrons of energy less than about 10 Mev. It is also possible that electrons of high energy may have escaped detection by entering the bank of anticoincidence counters below the cloud chamber. The combined thickness of the lower wall of the cloud chamber, and the anticoincidence counter wall is about 7 g/cm², which corresponds to the total range of an electron of about 15 Mev. Geometrical considerations, which include the effect of the curvature of the electron

TABLE I. Energies of decay electrons. List of observed decay electrons arranged in order of increasing energy. The sign of charge is indicated and the region of the chamber in which the decay occurred.

Sign of charge	Material	Energy in Mev
+	Carbon	9.0±2.0
+	Carbon	11.0±1.5
−	Carbon	11.8±0.5
+	Carbon	12.5±2.0
−	Gas (argon)	13.0±1.0
+	Bakelite	16.0±3.0
+	Carbon	17.0±1.0
−	Carbon	18.0±1.0
+	Copper	18.0±1.0
+	Carbon	19.0±1.0
−	Carbon	20.5±1.0
−	Copper	21.0±2.0
−	Bakelite	21.5±0.5
+	Bakelite	22.0±1.0
+	Bakelite	22.5±2.0
+	Copper	23.0±5.0
+	Bakelite	24.0±2.0
+	Carbon	25.5±2.0
−	Bakelite	27.0±2.0
+	Glass	27.5±1.5
−	Carbon	27.5±1.5
−	Glass	28.0±3.0
+	Copper	28.5±3.5
+	Carbon	29.0±1.0
−	Carbon	29.0±2.0
−	Carbon	29.0±6.0
+	Brass	30.0±1.0
+	Bakelite	30.0±1.0
−	Carbon	30.5±1.5
+	Copper	31.0±4.0
+	Bakelite	31.5±2.0
+	Carbon	32.5±1.5
+	Copper	32.5±1.5
+	Copper	33.0±3.0
−	Carbon	34.0±2.0
+	Carbon	35.0±1.5
−	Carbon	35.0±3.0
−	Carbon	36.0±2.0
−	Carbon	36.0±2.0
+	Carbon	36.5±2.0
+	Carbon	37.0±1.5
−	Carbon	37.0±4.0
−	Copper	38.0±5.0
−	Copper	38.5±3.0
+	Glass	38.5±5.0
+	Glass	38.5±5.0
+	Carbon	39.0±2.0
+	Copper	39.0±4.0
−	Glass	39.0±4.0
−	Carbon	40.0±2.0
+	Copper	40.0±2.0
+	Carbon	40.0±2.0
−	Carbon	40.0±4.0
−	Glass	41.0±1.5
+	Carbon	41.0±1.5
+	Carbon	41.0±2.0
−	Carbon	42.0±3.0
−	Carbon	43.0±2.0
−	Carbon	43.0±3.0
+	Bakelite	43.0±4.0
−	Carbon	43.0±4.0
+	Carbon	43.5±2.0
+	Carbon	44.0±1.5
+	Carbon	45.5±1.0
+	Carbon	45.5±3.0
+	Bakelite	46.5±3.0
−	Carbon	46.5±3.0
+	Carbon	47.0±2.0
−	Carbon	48.5±2.5
−	Carbon	51.5±2.0
−	Glass	52.0±2.0
−	Copper	52.0±4.0
−	Carbon	52.5±2.0
−	Bakelite	53.0±2.0
+	Bakelite or brass	54.9±1.0

trajectories, indicate, however, that not more than 10 percent of the electrons should have escaped detection in this way.

In Table I are listed the energies of all the decay electrons observed. The estimated uncertainties in the energy values, the sign of charge, and the material in which the mesotron decayed are also given.

It will be noted that in the case of mesotrons which decay in carbon and Bakelite, positive and negative electrons occur in almost equal numbers, while positive electrons predominate when the mesotron decays in copper. The average energy of all the decay electrons is 34 Mev.

In Fig. 4 is shown the integral distribution of the observed energies of the decay electrons, where the ordinate of each point corresponds to the total number of decay electrons having an energy less than, or equal to, the energy indicated by the abscissa.

In Fig. 5 is shown the differential energy spectrum where each point represents the observed number of electrons per energy interval of 10 Mev. Points corresponding to two sets of overlapping energy intervals, displaced from one another by 5 Mev, are plotted.

The energy spectrum of mesotron decay electrons may be compared with the distribution found in the case of nuclear β-decay. In the case of mesotron decay, the most probable electron energy is about 40 Mev, which corresponds to about three-fourths of the observed maximum energy, whereas the most probable energy in the case of nuclear β-decay is usually about equal to, or even less than, one-half of the maximum energy. The present data are not sufficient to establish the behavior of the curve at the upper and lower energy limits. The relatively large number of cases observed in the vicinity of the upper energy limit, however, indicates that the energy spectrum of mesotron decay electrons falls to zero at the upper energy limit more abruptly than does the spectrum of nuclear β-particles.

In many cases, the curvature in the magnetic field and, therefore, the momentum of the incoming mesotron was measured before and after it traversed the known amount of material represented by either the flat counter or the carbon plate in the chamber. Computation of the mass of the mesotron from

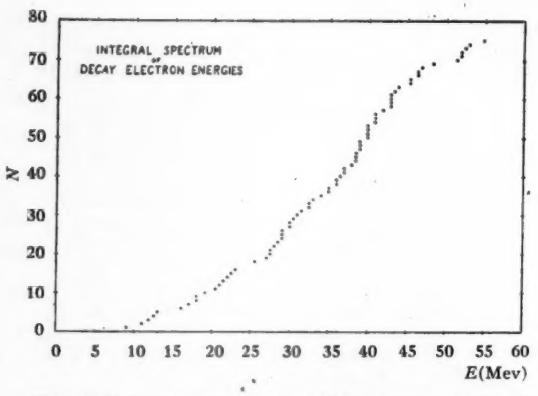

FIG. 4. Integral distribution of the energy of mesotron decay electrons.

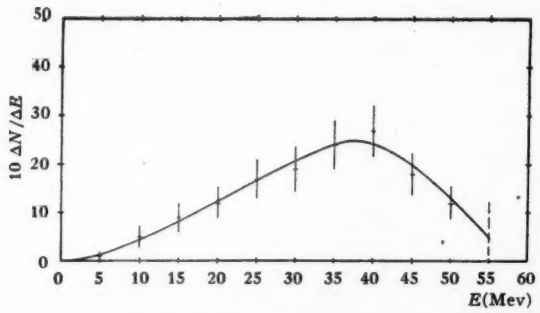

FIG. 5. Energy spectrum of mesotron decay electrons. Each point represents the number of electrons per energy interval of 10 Mev. The vertical lines indicate the expected statistical spread. A smooth curve is drawn through the observed points.

these data lead to values usually ranging from about 175 to 300 m_e. The effects of gas distortions, the short length of track available for measurement, and the small curvature of the tracks did not permit the rather high precision of measurement needed to obtain mass values of small uncertainty. The observed mass values, however, are not inconsistent with a unique mass of about 220 m_e.

IV. THE DECAY PRODUCTS OF THE MESOTRON

It has been assumed throughout this paper that the observed ionizing decay particle is an electron. This, of course, has not actually been proved. It is possible, however, to estimate the charge and to set an upper limit to the mass of the particle. Visual estimates of the minimum ionization of the decay particles indicate that their charge is certainly less than twice that of an electron. In one photograph the decay particle was deflected by the magnetic field so that it made four traversals of the carbon plate before coming to rest within the plate. The successive values of the momentum of this particle, after each traversal of the plate, were measured. From these momenta and the corresponding amount of carbon traversed, it is possible to set an upper limit to the mass of the decay particle equal to 15 m_e. Comparison with its own ionization at higher momenta, and with the ionization of the 90-Mev/c mesotron, gave 1.5 times minimum as an upper limit for the ionization of the decay particle, when its momentum was 5.5 Mev/c. This leads to a value of 10 m_e for the upper limit of its mass. The data are therefore wholly consistent with the assumption that the charged particle is an electron.[6]

Before any measurements had been made of the energy of the decay electrons, it was generally assumed that in the decay process an electron and a single neutrino are formed. If momentum and energy are conserved in the decay process, one would then expect to find decay electrons of a discrete energy equal to about 55 Mev for a mesotron whose mass is 220 m_e. The first accurate measurements,[7] however, of the energy of mesotron decay electrons consisted of two cases in each of which the energy of the decay electron was only 25 Mev, thus ruling out this hypothesis. The new data here reported serve to place further restrictions on the alternative modes of decay suggested at that time, and indeed, only one of these is entirely consistent with the present data; i.e., a decay resulting in the production of an electron and two neutral particles of very low mass.

If one excludes the possibility that the mesotron has a variable mass,[**] then, on the basis of conservation of energy and momentum, the observed broad energy spectrum is inconsistent with any mode of decay which results in the production of only two particles of discrete mass, e.g., an electron and neutrino, or an electron and a neutral mesotron. If we assume, therefore, that an electron and two neutral particles are produced, it is possible to compute an upper limit to the sum of the masses of the two neutral particles from the observed upper limit of the decay spectrum on the basis of the conservation laws. Assuming the mass of the mesotron to be 216 ± 4 m_e,[8] and taking the observed upper limit of the energies of the decay electrons to be 55 ± 1 Mev, one finds that the data are consistent within the given errors only with the emission of particles whose added masses are less than 30 m_e. The fact that the production of energetic photons is not observed in mesotron decay[9] leaves open only

[6] See also J. C. Fletcher and H. K. Forster, Phys. Rev. **75**, 204 (1949); E. P. Hincks and B. Pontecorvo, Phys. Rev. **75**, 698 (1949).

[7] See reference 1, (a) and (b).

[**] In several instances, both the mass of the mesotron and the energy of its decay electron were measured with sufficient precision to show that these quantities do not bear the relationship to one another to be expected on the basis of the conservation laws, if the mesotron decays simply into an electron and a single neutrino.

[8] A. S. Bishop, Phys. Rev. **75**, 1468A (1949).

[9] R. D. Sard and E. J. Althaus, Phys. Rev. **75**, 1251 (1948); E. P. Hincks and B. Pontecorvo, Phys. Rev. **73**, 257 (1948); O. Piccioni, Phys. Rev. **74**, 1754 (1948).

the possibility that the neutral particles are neutrinos or other neutral particles of low mass. In terms of generally accepted particles, the simplest decay process is thus one which results in the production of an electron and two neutrinos.

On the other hand, if the neutral particles have rest masses which are actually zero, then the mass of the mesotron, calculated from the upper limit of the energy spectrum, is equal to $217\pm4\ m_e$. Within experimental uncertainty this value is equal to the values, $216\pm4\ m_e$[8] and $215\pm4\ m_e$,[10] determined by other methods, and is in satisfactory agreement with 220 ± 35 Mev, the only mass measurement previously reported from this laboratory.[11]

The observed shape of the energy distribution curve and the observed average electron energy provide further support to the assumption that the decay results in the production of three particles and not more than three; for if the decay results in the production of three particles whose proper energy is small compared with the total available energy, and if the three particles play symmetrical roles in the decay process, then each particle should receive an average energy approximately equal to one-third of the total available energy or two-thirds of the maximum electron energy. Two-thirds of the maximum observed electron energy (55 Mev) is 37 Mev, which is in satisfactory agreement with the observed value of 34 Mev for the average decay electron energy. A decay resulting in the production of four or more particles seems unlikely as the average energy then to be expected would be 27.5 Mev or less.

If one adopts the view indicated above, that the decay of the mesotron results in the production of an electron and two neutrinos, $\mu^{\pm}\rightarrow e^{\pm}+2\nu$, then, in order that spin may be conserved in the decay, the spin assigned to the mesotron must be half-integral.

Electron energy distributions have been computed recently for several different types of fields.[12] In some cases these are in good qualitative agreement with the observed spectrum, but more data will be needed for a precise comparison.

We wish to acknowledge the assistance of Dr. E. W. Cowan who provided the counter circuits, and of Mr. Robert C. Hsiao who shared in the operation of the equipment and in the measurements.

[10] J. G. Rettallack and R. B. Brode, Phys. Rev., in press.
[11] S. H. Neddermeyer and C. D. Anderson, Rev. Mod. Phys. 11, 201 (1939).
[12] J. Tiomno and J. A. Wheeler, Rev. Mod. Phys. 21, 144 (1949).

Letters to the Editor

PUBLICATION of brief reports of important discoveries in physics may be secured by addressing them to this department. The closing date for this department is five weeks prior to the date of issue. No proof will be sent to the authors. The Board of Editors does not hold itself responsible for the opinions expressed by the correspondents. Communications should not exceed 600 words in length.

Some Possible Rare Stable Isotopes*

HENRY E. DUCKWORTH
Scott Laboratory, Wesleyan University, Middletown, Connecticut
March 22, 1949

SINCE the current data on stable isotopic species are so well authenticated it should be possible to assume the existence of empirical relationships between existent stable nuclei and deduce therefrom the existence of unobserved isotopes. Such unobserved isotopes must be expected to be rare. An examination of a table of isotopes shows that most of the rare species occur among elements of even atomic number. Also, among the heavier members of this group, there is considerable symmetry in the location of the rare isotopes. With the exception of neodymium, the rarer isotopes of the even-numbered elements from ruthenium ($Z=44$) to lead ($Z=82$) are among the lighter isotopes. Thus, in a search for rare isotopic species, the region occupied by the lighter isotopes of heavy elements of even atomic number is a promising one.

In Fig. 1 the atomic masses of the lightest known isotopes of the even-numbered elements from palladium ($Z=46$) to lead ($Z=82$) are plotted against the respective atomic numbers. From cadmium ($Z=48$) through neodymium ($Z=60$) there is a linear relationship for six of the seven elements, tellurium ($Z=52$) being the exception. Similarly, beginning with samarium ($Z=62$) and ending with tungsten ($Z=74$), another group of seven, there is a second linear relationship in which gadolinium ($Z=78$) is the exception. The physical interpretation of such linear stability curves will be clear: if A be the lowest stable mass associated with a particular Z, the lightest stable configuration belonging to the element $Z+2$ is that which has a mass $A+6$. In other words it is formed from (A, Z) by the addition of 2 protons and 4 neutrons.

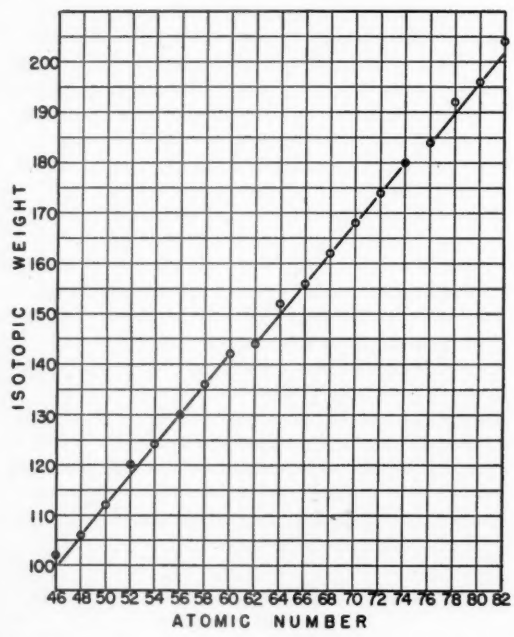

FIG. 1. The atomic masses of the lightest known isotopes of the even-numbered elements from palladium ($Z=46$) to lead ($Z=82$) are plotted against the respective atomic numbers.

Each of the three exceptional elements would be reconciled to its respective group if it possessed an isotope mass two units lighter than the lightest now known. Since such a mass difference between lightest and next-to-lightest isotopes is found for almost all the elements of even-atomic number, this requirement offers no barrier to the existence of such unobserved species. Furthermore, Seaborg and Perlman[1] in their 1948 Table of Isotopes list no radioactive isotopes of Gd^{150} and Pt^{190} and give for Te^{118} only a "probable" one. Although the existence of such radioactive isotopes would not preclude the possibility of stable isomers, their absence heightens it. Finally, a survey of the literature indicates that the search for these particular isotopes has not been notably intensive. From Dempster's[2] photograph showing Te^{120}, Te^{118} is estimated to exist to less than one part in 6000. Gd^{150} is given by Hess[3] as less than one part in 20,000. There is nothing in the literature upon which to base an estimate of the abundance of Pt^{190} other than that it is less abundant than Pt^{192} which is 0.78 percent.

Since the existence of Te^{118}, Gd^{150}, and Pt^{190} would lead to a rather high degree of symmetry in the stability curve and since there is evidence to disprove the existence of none of them, a search for these species appears to be a promising endeavor. The following letter describes the first fruits of such a search.

It should be pointed out that the scheme would still be served if tungsten were found to have a stable isotope at mass 178, then hafnium ($Z=72$) one at mass 172, and so on. Also a lead isotope may exist at mass 202 and a palladium isotope at mass 100. Such species should be kept in mind as possible stable forms.

* This letter is based on work done at Wesleyan University under Contract AT (30-1)-451 with the AEC.
[1] G. T. Seaborg and I. Perlman, Rev. Mod. Phys. **20**, 585 (1948).
[2] A. J. Dempster, Phys. Rev. **50**, 186 (1936).
[3] D. C. Hess, Jr., Phys. Rev. **74**, 773 (1948).

A New Stable Isotope of Platinum*

HENRY E. DUCKWORTH, ROBERT F. BLACK, AND RICHARD F. WOODCOCK
Scott Laboratory, Wesleyan University, Middletown, Connecticut
March 22, 1949

THE first successful mass analysis of platinum was made by Dempster[1] in 1935 using his double-focusing mass spectrograph. The platinum ions were produced in a high frequency spark between electrodes of a platinum-rhodium alloy and isotopes were found at mass numbers 192, 194, 195, 196, and 198. Accurate electrical measurements of the isotopic abundances have since been made by Sampson and Bleakney[2] and by Inghram, Hess, and Hayden,[3] the latter giving the abundance of the faintest isotope, Pt^{192}, as 0.78 percent.

Guided by the principles outlined in the preceding letter, the authors have employed an ion source and double-focusing mass spectrograph similar to Dempster's in a search for Pt^{190}. With a spark between a platinum-iridium and a copper electrode, a faint line appeared at mass 190 after an exposure of three hours. The electrodes were replaced by pure platinum electrodes (99.999 percent purity obtained from Sigmund Cohn of New York). With an hour's exposure the faint 190 appeared. Similarly with two platinum electrodes of commercial purity (obtained from the J. M. Ney Company of Hartford) the line at 190 was clearly visible after an hour's

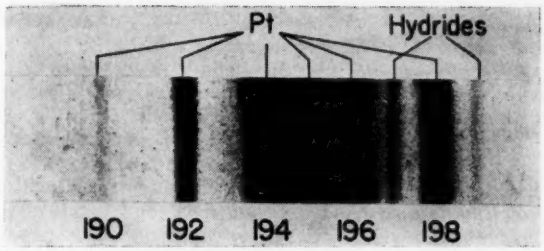

FIG. 1. Mass spectrum of platinum.

exposure. Figure 1 is a reproduction of one of the mass spectra taken with commercial platinum electrodes. As nearly as can be judged from microphotometric traces, the ratio 190/192 is independent of the type of platinum used.

In concluding that the faint 190 is due to platinum, rather than to an impurity, the authors have been influenced by the following additional arguments. The fact that the faint line appears at a mass less than the known platinum isotopes precludes the possibility of its being a hydride, as are the lines at 197 and 199 in Fig. 1. It cannot be the stable isotope of osmium at mass 190 since this has an abundance of 26.4 percent and would have been accompanied by the 16.1 percent abundant Os^{189}. It is possible for particles of mass 95 to reach the 190 position by passing through the accelerating field and electrostatic analyzer as doubly-charged ions and losing one charge before entering the magnetic analyzer. In such a case the 15.7 percent abundant Mo^{95} would have been accompanied by the 9.12 percent abundant Mo^{94} at mass 188. Thus it seems clear that the line is a faint isotope of platinum.

An approximate measure of the abundance was obtained by making short exposures on which the intensity of the 0.78 percent Pt^{192} could be compared with the intensity of the 190 on the long exposures. Comparisons were made on five plates and give for the abundance of Pt^{190} the values 0.0052 percent, 0.0056 percent, 0.0046 percent, 0.0060 percent, and 0.0088 percent. The average of these values is 0.006 percent and is probably accurate to 20 percent, the inaccuracy arising from the unsteadiness of the spark.

The authors wish to thank Mr. Clifford Geiselbreth for his excellent machining of many essential parts and Dr. Richard Clarke for the use of the recording microphotometer.

* This letter is based on work done at Wesleyan University under Contract AT (30-1)-451 with the AEC.
[1] A. J. Dempster, Nature **135**, 993 (1935).
[2] Milo B. Sampson and Walter Bleakney, Phys. Rev. **50**, 732 (1936).
[3] M. G. Inghram, D. C. Hess, Jr., and R. J. Hayden, Plutonium Project Report ANL-4082, (Nov. 1947), p. 5.

Decay of Scintillations in Calcium Fluoride Crystals*

W. J. MACINTYRE
Sloane Physics Laboratory, Yale University, New Haven, Connecticut
March 18, 1949

IT has been estimated[1] that the inorganic phosphors have a decay time greater than 0.2 microsecond with the possible exception of fluorites. The decay of the scintillations of a calcium fluoride crystal has been measured by a delayed coincidence method in which data on the scintillations of a crystal are obtained as a function of time. This method is based on a delayed coincidence counting of the pulse of a proportional counter activated by a beta-particle with the pulse of an electron multiplier tube detecting the scintillation from the crystal activated by the same particle.

The experimental procedure utilizes a beam of beta-particles from P^{32} which penetrates the proportional counter and impinges on the scintillation phosphor. As the pulse from the channel of the proportional counter is delayed by a variable delay line, coincidences are obtained as a function of line length which can be directly calibrated in units of time. Provided the pulse from the proportional counter is appreciably faster than the pulse from the scintillation phosphor channel, the resulting variation of coincidences per unit time with time shows the decay of the scintillations. The variable delay is introduced by means of seventy-ohm coaxial cable (RG 11/u) calibrated to desired lengths.

The proportional counter used has a resolving time of 2.8×10^{-8} second and works into a cathode follower and amplifier of 23 megacycles/sec. band widths.[2] The scintillations of the phosphor were detected by a 931A electron multiplier tube working into a similar cathode follower and amplifier.

Figure 1 shows the variations of the coincidences with time delay, the data taken with the phosphor at dry ice temperature. The selection of the zero point is arbitrary since the amplifiers and associated circuits are not of equal natural delay. For comparison, curves of both naphthalene and calcium fluoride crystals are shown. The fast rise time is seen to be the same in both cases and shows the limitations of the time variation that may be detected as imposed by circuit band width, variation in pulse formation, or other broadening factors.

Following the analysis of Van Name[3] for coincidences between a pulse fixed in time and a pulse from an exponential decay process, it is known that for values of delay greater than the pulse half-width distribution, the coincidences are directly proportional to $e^{-\lambda D}$ where D is the delay time and λ is the decay constant.

For this analysis the logarithm of the coincidences was plotted against time, giving a reasonably straight line with a half-life of 15×10^{-8} second. The corresponding value for the leading edge of the curve is 1.4×10^{-8} second. This time is shown by the dotted curve in Fig. 1, which was drawn by reflecting the leading edge of the naphthalene curve about its zero point.

Similar analysis for the naphthalene curve indicates a value of the order of magnitude of 3.3×10^{-8} second but this is too close to the limitations of the circuit to ascribe much value to the estimate.

Figure 2 shows similar measurements for the calcium fluoride crystal taken at room temperature. The variation of 100°C has resulted in no change of decay time of sufficient

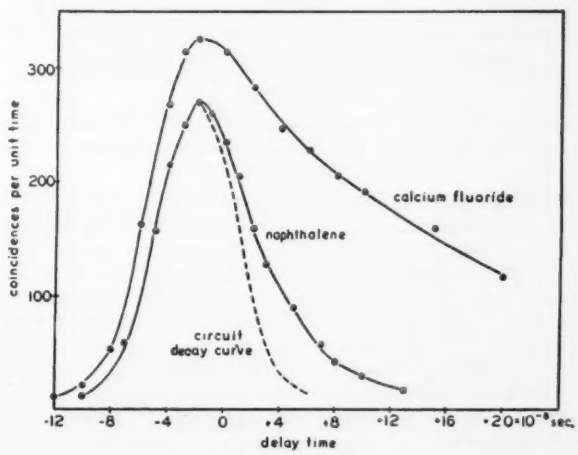

FIG. 1. Coincidence rate *versus* delay curve for calcium fluoride and naphthalene scintillations. The dotted curve refers to circuit decay time obtained by plotting a symmetrical curve with decay constant equal to that of the leading edge. Data taken at dry ice temperature.

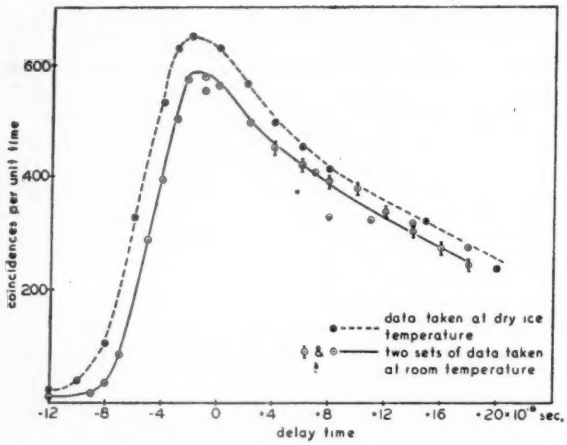

FIG. 2. Comparison of coincidence rate *versus* delay curve for calcium fluoride scintillations taken at room temperature and at dry ice temperature. Note similar decay rates within the accuracy range of the equipment.

magnitude to be detected by this equipment. Plotting of this decay section of the curve shows the half-life to be still in the range of $14\text{–}16\times10^{-8}$ second.

The apparent temperature independence together with the magnitude of the decay time indicate several possibilities: (a) the process of emission may be a straight radiative transition of a slightly forbidden state; (b) if the process is one of electron migration the barrier would be small, say of the order of a few hundredths of an electron volt with the tunnel effect being large in relation to overcoming the barrier; (c) the process may be twofold, with fast electron migration preceding radiative transition.

The writer wishes to express his thanks to Professor E. C. Pollard for valuable discussions throughout, to Professor H. L. Schultz for discussion of coincidence counting techniques and circuits involved, and to Dr. R. B. Setlow for suggestions on interpretation. Thanks are also due Mr. J. A. Rich for loan of the naphthalene and calcium fluoride crystals.

* Assisted by the joint program of the ONR and the AEC.

[1] Conference on Scintillation Counters and Crystal Counters, University of Rochester, Rochester, New York, July 1948.

[2] H. L. Schultz, *High Speed Counters and Short Pulse Techniques* (Brookhaven Conference Report, August 1947), p. 35.

[3] F. W. Van Name, Phys. Rev. 75, 102 (1949).

Anomalous Behavior of the Dielectric Constant of a Ferromagnetic Ferrite at the Magnetic Curie Point

FRANK G. BROCKMAN, P. H. DOWLING, AND WALTER G. STENECK
Philips Laboratories, Inc., Irvington-on-Hudson, New York
March 14, 1949

IN the discussion following our papers "Magnetic Properties of a Ferromagnetic Ferrite," presented at the 1948 Annual Meeting of the American Physical Society, we showed the lantern slide reproduced here. This represents the effective dielectric constant, as a function of temperature, measured at 10,000 c.p.s. on a block of a commercial ferromagnetic ferrite (Ferroxcube III) provided with evaporated gold electrodes. Direct current measurements of the resistivity of the block were made at the same time and show, in the same temperature interval, only the variation with temperature expected of semiconductors.

At that time we thought that the almost discontinuous course of the dielectric constant *versus* temperature curve at the magnetic Curie point might be some indication of the fundamental character of the dielectric behavior, perhaps related to a coupling of the electric and magnetic dipoles.

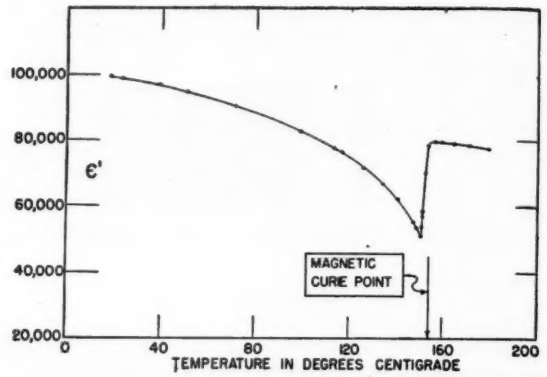

FIG. 1. Real part of dielectric constant *vs.* temperature.

We have found, however, that the behavior of the dielectric constant at the magnetic Curie point can be described on the basis of straightforward electromagnetic theory. The decrease in the measured dielectric constant between room temperature and the Curie point is due principally to the increasing ohmic conductivity in this region. The sudden rise at the Curie point follows from the collapse of the permeability. Differences between the experimental and calculated curves indicate that the actual dielectric constant decreases slowly with increasing temperature throughout the entire region.

A paper covering in more detail our work on the dielectric and magnetic properties of a ferromagnetic ferrite is in preparation for submission to the Physical Review.

Divergences in Field Theory

K. M. CASE
The Institute for Advanced Study, Princeton, New Jersey
March 17, 1949

THE considerable advances which have recently been achieved in quantum electrodynamics have been based on the twin concepts of charge and mass renormalization. Thus it has been found that the divergences that occur as a result of the interaction between electron and electromagnetic fields are due to terms which, if finite, would be interpreted as changing the mechanical mass and charge of the electron to the empirically observed values. On separating out the additional mass and charge terms, it has been found that the present form of electrodynamics gives finite and unambiguous predictions with at least reasonably close agreement with experiment.

The question immediately arises as to whether the use of these concepts is sufficient to remove the divergences of other current or proposed forms of quantum field theories, or if their success is an accident peculiar to electrodynamics. Offhand, one would say that the latter is obviously the answer. The divergences encountered with a Dirac electron interacting with the electromagnetic field are particularly weak. While it would seem not unreasonable that the removal of two infinite quantities would render electrodynamics convergent, the success of this procedure in theories with much stronger divergences is *a priori* rather unlikely. Surprisingly, it has been found that the utilization of the renormalization ideas does give convergent results for the scalar and pseudoscalar meson theories (even with dipole coupling) and for the scalar electron interacting with the electromagnetic field. This might tend to support the view that all the divergences of the

customary field theories have been isolated and put into an innocuous form.

A more critical test of this hypothesis is the vector meson theory with tensor coupling between mesons and nucleons. Here the divergences are most acute. We have made calculations with this theory using the new covariant methods.[1] Particular care was taken to consider all effects of renormalization of charge and of both the nucleon and meson mass. It was found that there are additional divergences beyond those in mass and charge. Thus, the anomalous neutron and proton moments were found to be logarithmically infinite. Similar results were found for the velocity independent neutron-electron interaction and the corrections to the interaction of a proton with a fixed external field. In addition, vacuum polarization phenomena gave rise to an infinite dipole density distribution with zero total dipole moment. It is interesting that the analog of the latter term in electrodynamics gives rise to the usual charge renormalization. In the present theory this term, if finite, would not renormalize the electric charge and so would not give different proton and electron charges.

Two conclusions follow: The first is that new methods must be developed before the vector meson theory with tensor coupling can be used for calculations. The second follows from the fact that the above divergences were not a consequence of the finite meson mass. The same lack of convergence is contained in a phenomenological description of the anomalous neutron, proton, or electron moments by means of a Pauli type magnetic moment term.

From this work we can state that mass and charge renormalization do not completely encompass the divergences of field theory. New developments would be required to enable us to use vector mesons as a supplement to the pseudoscalar theory. Recent calculations with the latter have given rather unsatisfactory results. In fact, if the recently proposed experiment of Wentzel should show the π-meson to have spin one, we could be sure of our inability to treat the nuclear force problem by present methods.

It is a pleasure to acknowledge a very helpful discussion with Professor J. R. Oppenheimer and Dr. A. Pais.

This work was supported by a grant-in-aid from the AEC to the Institute for Advanced Study.

[1] In a footnote, Luttinger states that Villars has previously found that tensor coupling yields infinite magnetic moments. Since the method of this calculation was not indicated, it was thought advisable to repeat the calculation explicitly, using the renormalizations and the covariant formalism. J. M. Luttinger, Helv. Phys. Acta **XXI**, 483 (1948).

On Meteor Speed Measurements by the Radio Doppler Method at Low Frequencies*

D. D. CHERRY AND C. S. SHYMAN
Department of Electrical Engineering, Stanford University, Stanford University, California
February 14, 1949

IT has been shown[1] that meteor speeds can be determined with good accuracy at 30 megacycles from a recording of the Doppler whistle produced when continuous-wave radio energy reflected from the nose of a meteoric ion trail is combined with a portion of the transmitted signal. The question has been raised as to whether the same accuracy can be obtained by this method at lower frequencies in view of Pierce's suggestion[2] that the echo from an ion column at these frequencies might be more indicative of the rate of growth of the column than of the velocity of the meteoric particle.

During the Geminid shower of December 11, 1948, simultaneous radio Doppler speed measurements were made at 30.66 and 12.8625 megacycles between 0400 and 0700 P.S.T. The velocities of twenty meteors were obtained at both frequencies. Figure 1 shows a plot of the velocity of each meteor

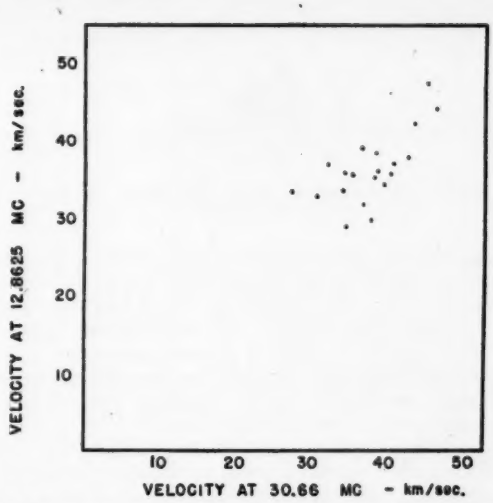

FIG. 1. Correlation of velocities measured at 12.8625 Mc and 30.66 Mc.

as measured at 12.8625 megacycles, *versus* the velocity as measured at 30.66 megacycles.

When a line through the origin was fitted to the points by the method of least squares, the slope was found to be 1.015. The correlation coefficient of the points was 0.97. It, accordingly, appears that radiofrequency is not a factor in the Doppler velocity measurement.

A simplified technique was used to obtain the slope of the whistle-pitch *versus* time-curve from which velocity is calculated. In the earlier experiments[1] the meteor whistles had been recorded on a magnetic tape and then transcribed by a moving-film oscillograph; in this test the intermediate step was eliminated. A Brush "penmotor" direct-inking magnetic oscillograph—which operates very satisfactorily with inexpensive adding machine paper as the recording medium—was connected to the output of the radio receivers. Since the frequency response of this instrument extends up to 120 c.p.s., it is possible to record four or five cycles of the whistle of a 35-km/sec. meteor at a radiofrequency of 30 megacycles—or an 85-km/sec. meteor at 12 megacycles—before the pitch falls to zero. This number of points has been found to be sufficient to establish the slope of the whistle-pitch curve. While the accuracy of this recording technique is somewhat less than the other, its simplicity is very attractive. Meteor velocity measurements may thus be made with a minimum of equipment.

Figure 2 is a plot of the velocities of all the meteors whose speed was recorded during the test.

As in reference 1, an effort was made to establish which of the recorded meteors belonged to the shower. The relationship between their direction and range was compared with the approximate relationship which must be satisfied by shower meteors having a given radiant and producing reflections within a relatively narrow range of altitudes centered about 100 km. In this test the azimuth of the reflections was obtained by means of an instantaneous radio direction-finder.

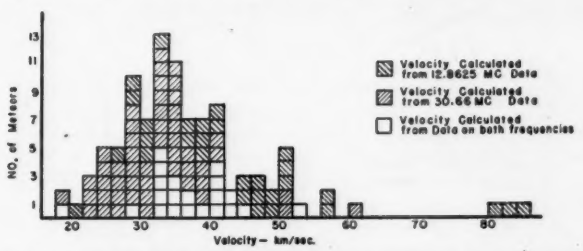

FIG. 2. Velocities of all meteors whose speed was recorded during the test.

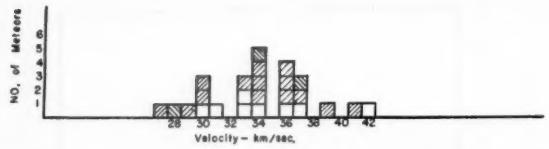

FIG. 3. Meteors whose direction, range, and velocity are correct to be Geminid shower meteors.

Meteors having azimuths and ranges satisfying the above requirement, and having velocities between 27 and 43 km/sec., were classified as possible Geminids. Their speeds are plotted in Fig. 3. The mean velocity was 34.8 km/sec. (standard deviation 3.7 km/sec.) which is in good agreement with the Geminid velocities of 34.7 km/sec. obtained photographically by Whipple,[3] and 34.4 km/sec. obtained using diffraction radar techniques by Ellyett and Davies.[4]

The work described in this letter was carried out by the Meteor Ionization Research group at Stanford University.

* This work sponsored jointly by the ONR and the U. S. Army Signal Corps.

[1] L. A. Manning, O. G. Villard, Jr., and A. M. Peterson, J. App. Phys. to be published.
[2] J. A. Pierce, Phys. Rev. **71**, 88–92 (1947).
[3] F. L. Whipple, Proc. Am. Phil. Soc. **91**, 189 (1947).
[4] C. D. Ellyett and J. G. Davies, Nature **161**, 596 (1948).

Beta-Ray Spectrum of K^{40}

DAVID E. ALBURGER
*Brookhaven National Laboratory, Upton, New York**
March 7, 1949

THE mass 40 isotope of potassium is known to decay by beta-ray emission to Ca^{40}, and by electron capture to A^{40}, with a total half-life of about 4×10^8 years. A gamma-ray of 1.5 Mev is thought to be associated with the electron capture process, since beta-gamma-coincidences have not been found.[1] The maximum beta-ray energy has generally been observed to be 1.3–1.5 Mev[2–5] although a value of 1.7 Mev has been reported.[6]

Aside from the geological significance of the decay rates and energies, the nature of the beta-ray distribution is of considerable interest. A measurement has shown[7] the spin of the K^{40} nucleus to be four, while the "even-even" Ca^{40} is usually assumed to be zero. The long life and moderately high beta-ray energy are consistent with a large spin change. The shape of the spectrum should therefore correspond to a highly forbidden transition, and its determination might well afford a test of present theories.

Electron spectrometer measurements have been made difficult by the low specific activity of potassium, due in part to the natural K^{40} abundance of only 0.012 percent. Dželepow, Kopjova, and Vorobjov[4] used a six-section semicircular focusing spectrometer and measured the beta-ray distribution from sources of $K_2C_2O_4$, 69 mg/cm² thick. Their curve had an upper energy limit at 1.35 ± 0.05 Mev and was said to be of the allowed shape.

The 100-fold enrichment of potassium in the K^{40} isotope to 1.2 percent has recently been achieved.[8] This communication reports the results of a lens spectrometer measurement of the beta-ray distribution from such an enriched sample.

The instrument used was recently constructed at this laboratory. It is a conventional magnetic lens spectrometer[9] designed for a variety of applications up to electron energies of 10 Mev. The four-section 850-lb. copper coil is water-cooled, and at the maximum energy setting dissipates 12 kw. A 10-in. i.d. brass vacuum chamber 48 in. long is normally used.

For the present application, relatively high solid angle was achieved by use of a 24-in. chamber lined on the inside with aluminum, and by employing only the outer two coil sections having a separation of 5.5 in. From an estimate of the electron trajectories, the solid angle appeared to be between 6 and 9 percent of 4π. A measurement of the photoelectron line produced in a 0.001-in. thick uranium foil by annihilation quanta gave a resolution figure of about 15 percent (full width at half maximum) under these conditions.

The source holder consisted of a Plexiglas cup having a cavity 1 in. deep and 1 in. in diameter, and with a sheet of mica 4 mg/cm² thick attached at the rim. 74 mg of enriched KCl were crystallized on a 4-cm² central area of the mica.

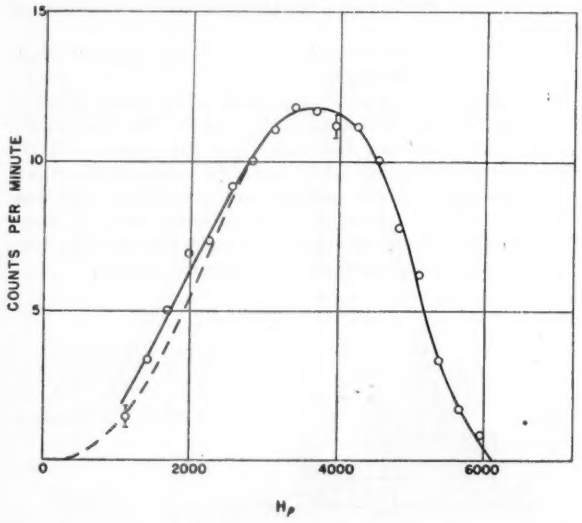

FIG. 1. Beta-ray intensity distribution from K^{40}. The dashed curve corresponds to a linear Fermi plot.

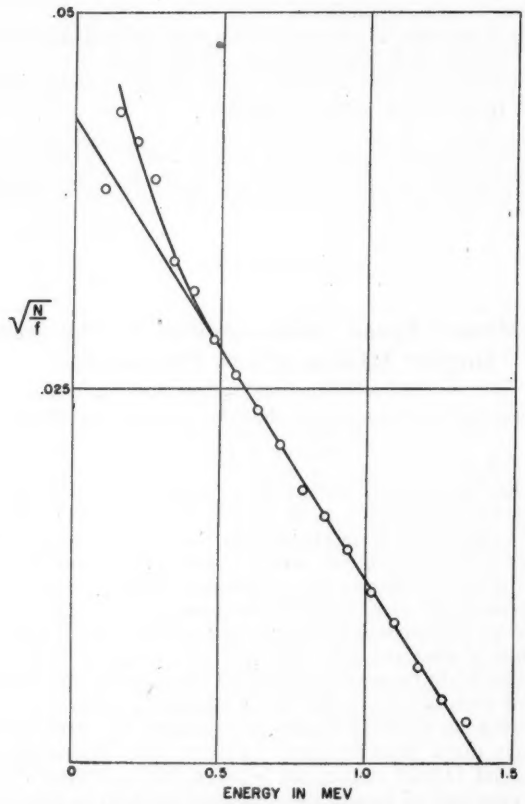

FIG. 2. Fermi plot of the K^{40} beta-ray spectrum.

Because of non-uniform crystallization, the source thickness appeared to be greater than 18.5 mg/cm² at some points. Both by measurement with an end-window counter, and from a calculation using a published value of the beta-ray decay constant, the strength of the sample was found to be about 0.002 μC.

Figure 1 shows the beta-ray intensity distribution plotted against momentum in gauss-cm. The curve has a maximum of 11.8 counts per minute against a background of 18.3 per minute. A Fermi plot taken from the experimental points is shown in Fig. 2. This is linear above 450 kev, and gives an end-point energy of 1.40±0.03 Mev. Calibration was taken from the Fermi plot of P^{32} beta-rays measured under identical conditions except for source thickness. An upper energy limit of 1.71 Mev[10] was assumed for the phosphorus beta-rays. The annihilation quantum photoelectron line, previously mentioned, gave the same calibration figure within 1 percent.

The theoretical intensity distribution for K^{40}, corresponding to a Fermi plot linear over the entire range, is indicated in Fig. 1 by a dashed line. The point at 1130 gauss-cm (103 kev) is probably low because of absorption in the 3-mg/cm² counter window. The area under the experimental curve shows an excess of about 4 percent over the theoretical distribution.

The Fermi plot for P^{32} was also linear down to 500 kev and had a deviation of about the same shape and magnitude as in Fig. 2 for K^{40}. This would indicate that in both cases the excess of low energy electrons is mainly due to scattering which is difficult to eliminate under conditions of large solid angle and low resolution. It is therefore probable that the true K^{40} beta-ray Fermi plot would follow a straight line to considerably lower energies than observed here.

The author is indebted to Dr. L. B. Borst for arranging the loan of the material from the Stable Isotopes Division of the AEC and for mounting the source. Thanks are also due Dr. T. Lauritsen who made valuable suggestions for the use of the lens spectrometer in this application.

* Research carried out under contract with the AEC.
[1] Meyers, Schwachheim, and deSouza Santos, Phys. Rev. 71, 908 (1947).
[2] O. Hirzel and H. Wäffler, Phys. Rev. 74, 1553 (1948).
[3] W. J. Henderson, Phys. Rev. 71, 323 (1947).
[4] Dželepow, Kopjova, and Vorobjov, Phys. Rev. 69, 538 (1946).
[5] J. J. Floyd and L. B. Borst, Phys. Rev. 75, 1106 (1949).
[6] S. Franchetti and M. Giovanozzi, Phys. Rev. 74, 102 (1948).
[7] J. R. Zacharias, Phys. Rev. 60, 168 (1941).
[8] Carbide and Carbon Chemicals Company, Oak Ridge, Tennessee.
[9] Deutsch, Elliott, and Evans, Rev. Sci. Inst. 15, 178 (1944).
[10] K. Siegbahn, Phys. Rev. 70, 127 (1946).

Microwave Magnetic Resonance Absorption in a Nickel Salt near 1.25 Cm

A. N. Holden, C. Kittel, and W. A. Yager
Bell Telephone Laboratories, Murray Hill, New Jersey
March 22, 1949

Magnetic resonance absorption at a frequency of 24,446 mc/sec. was observed in a crystal of nickel fluosilicate ($NiSiF_6 \cdot 6H_2O$) at room temperature as a function of the static magnetic field applied in directions parallel and perpendicular to the optic axis. The microwave technique enables a direct determination of values of the ground state splitting δ and splitting factor g, quantities previously inferred[1] from measurements of Becquerel and van den Handel[2] on the magneto-optic effect in this salt, and also from susceptibility measurements on other nickel salts.[3]

Our results are plotted in Fig. 1. For $H \parallel$ axis, we find $\delta = 0.52$ cm^{-1}, $g = 2.36$; for $H \perp$ axis, $\delta = 0.49$ cm^{-1} and $g = 2.29$. The differences between these values are probably within the over-all experimental error. These values, which are for room temperature, may be compared with $g = 2.252$ and $\delta = 0.301$ cm^{-1} at liquid He temperatures, as calculated by Becquerel and Opechowski[1] from the measured Verdet constant. Schlapp and Penney[4] show that $g = 2(1 - 2\lambda/5qD)$, where λ is the spin-orbit coupling constant and is equal to -335 cm^{-1} from spectroscopic data for the Ni^{++} ion; qD is the cubic field constant. Microwave measurements recently reported by the Oxford group[4] give $\delta = 0.32$ cm^{-1} at 195°K, 0.17 cm^{-1} at 90°K, and 0.12 cm^{-1} at 20°K.

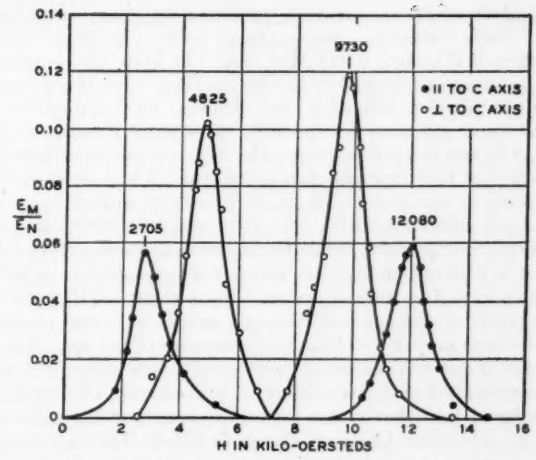

FIG. 1. Magnetic resonance absorption in $NiSiF_6 \cdot 6H_2O$ at 24,446 mc/sec. Vertical axis is ratio of (magnetic energy loss in sample) to (total non-magnetic energy loss in cavity and sample). Results are shown for two crystal orientations, parallel and perpendicular to the static field.

The free Ni^{++} ions is in a ^3F state; in the cubic electric field of the surrounding octahedron of water molecules, the non-degenerate orbital level Γ_2 is lowest. The threefold spin degeneracy of the ground level is partly lifted by the combined action of spin-orbit coupling and a small trigonal component of the crystal field. The relation between field strength and absorption frequency may be understood approximately by a "symbolic" method; namely, by considering the behavior of a level with $L = 1$ in a cylindrical electric potential ($V = A[x^2 + y^2 - 2z^2]$) and in a magnetic field H. We thus treat only three states, instead of the 21 states of the complete problem; the validity of this procedure is a consequence of group theory.

For $H \parallel$ axis, the three eigenvalues are $E_1 = g\mu_B H$; $E_2 = -g\mu_B H$; $E_3 = \delta$; and the allowed transitions satisfy $g\mu_B H_{\parallel} = h\eta \pm \delta$. For $H \perp$ axis, $E_1 = 0$; $E_{2,3} = (\delta/2) \mp [(\delta/2)^2 + (g\mu_B H)^2]^{\frac{1}{2}}$, which in the limit of $g\mu_B H \gg \delta$ gives $g\mu_B H = h\nu \pm \delta/2$.

We wish to thank Dr. Conyers Herring for a profitable discussion, and F. R. Merritt and J. Andrus for valuable experimental assistance.

[1] J. Becquerel and W. Opechowski, Physica 6, 1039–1056 (1939).
[2] J. Becquerel and J. van den Handel, Physica 6, 1034–1038 (1939).
[3] R. Schlapp and W. G. Penney, Phys. Rev. 42, 666–686 (1932).
[4] Bagguley, Bleaney, Griffiths, Penrose, and Plumpton, Proc. Phys. Soc. 61, 551–561 (1948).

The Decay of Co^{55}

Martin Deutsch* and Arne Hedgran
Nobel Institute for Physics, Stockholm, Sweden
March 14, 1949

The decay of Co^{55} (18.2 hr.) has been studied by means of a large double focusing spectrometer[1] and by coincidence experiments. Samples were prepared by deuteron bombardment of iron. The cobalt was separated chemically. Small corrections for the radiations of the longer lived cobalt isotopes were made where necessary. The positron spectrum was found to be complex. There are two components[2] with maximum energies of 1.50 Mev and 1.01 Mev and about equal abundance. Another softer component of low abundance is possible. The

secondary electron spectrum produced by the γ-rays in a thin lead converter shows three nuclear gamma-rays of energies 0.477 Mev, 0.935 Mev, and 1.41 Mev. By comparing the number of photoelectrons due to these with those due to the annihilation radiation, we estimate the abundances of these three gamma-rays (in order of increasing energy) to be 0.3, 1.4, and 0.3 per positron. The negative electron spectrum consists of four internal conversion lines. Three of these correspond to the above gamma-rays and the intensities of the lines are about 7.4×10^{-4}, 5.4×10^{-4}, and 3.5×10^{-5} conversion electron per positron, in order of increasing energy. In addition, a conversion line was found corresponding to a 0.095-Mev γ-ray. The intensity of this line is about 1×10^{-3} electron per positron. Coincidences between gamma-rays and positrons of definite energies (selected in a magnetic-lens spectrometer designed for coincidence experiments[3]) were measured using copper-walled and gold-walled G-M counters. The combined results of the experiments lead us to conclude that the main decay scheme of Co^{55} is as shown in Fig. 1. The two positron

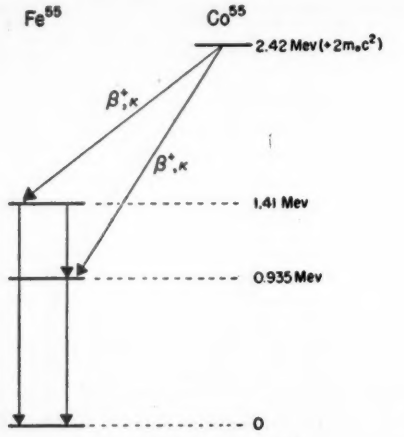

FIG. 1. Decay scheme of Co^{55}.

transitions are of approximately equal intensity. The same is true for the 0.477-Mev and 1.41-Mev gamma-rays. If our estimate of the intensities of the several gamma-rays compared with the number of positrons is correct, orbital electron capture is considerably more probable than expected theoretically for allowed transitions, particularly in the case of the transition to the 0.935-Mev level. The significance of the 0.095-Mev gamma-ray is not yet understood, but its intensity must be quite low. A more complete report on these experiments will be submitted for publication in the Arkiv for Matematik Astronomi och Fysik.

We wish to express our gratitude to Professor Manne Siegbahn and the Swedish Academy of Science for the generous hospitality extended to one of us (M.D.), and to the staff of the Nobel Institute for their friendly cooperation.

* On leave from Massachusetts Institute of Technology, Cambridge, Massachusetts.
[1] Siegnahn, Svartholm, and Hedgran (to be published).
[2] J. L. Lawson, Phys. Rev. 56, 131 (1939).
[3] K. Siegbahn and A. Johanson, Arkiv f. Mat. Astr. Fys., 34A, No. 10 (1946).

Electron-Neutrino Correlation in Heavy Elements*

M. E. ROSE
Oak Ridge National Laboratory, Oak Ridge, Tennessee
March 14, 1949

THE electron-neutrino correlation for both allowed and first forbidden transitions has been discussed by Hamilton.[1] For allowed transitions the correlation function is

$$F(\theta)=1+n\beta\cos\theta, \quad (1)$$

where θ is the angle between electron and neutrino directions, $\beta=v/c$ and $n=-1$ for scalar and pseudoscalar, $\frac{1}{3}$ for tensor $(G-T)$, $-\frac{1}{3}$ for axial vector and 1 for polar vector (Fermi) interactions. Since (1) assumes plane wave electrons ($Z=0$) it is of interest to consider the effect of the Coulomb field[2] in order to determine whether or not the consequent change in the factor n may be as large as a factor 3. In the following we consider only allowed transitions.

For this purpose the following approximative calculation has been performed. A Dirac plane wave corresponding to a z-component of spin equal to $\frac{1}{2}$ can be expanded in terms of a representation in which j^2 and j_z, where j is the total angular momentum, are diagonal. This gives

$$\psi_{\frac{1}{2}}{}^{(0)}(\theta,\phi)=\text{const.}\sum_{l,m} i^l(2l+1)^{-\frac{1}{2}}Y_l{}^{m*}(\theta,\phi) \times[(l-m)^{\frac{1}{2}}u_{lm}{}^{(-)}-(l+m+1)^{\frac{1}{2}}u_{lm}{}^{(+)}], \quad (2)$$

where θ, ϕ are the polar and azimuth angles of the direction of motion of the electron, $Y_l{}^m$ a normalized spherical harmonic and $u^{(\pm)}$ are spherical free particle wave functions for $j=l\pm\frac{1}{2}$. The superscript (0) indicates $Z=0$. For z-component of spin equal to $-\frac{1}{2}$ the corresponding expansion can be obtained from (2) by applying the usual operator which converts $\psi_{\frac{1}{2}}{}^{(0)}$ to $\psi_{-\frac{1}{2}}{}^{(0)}$. Of course, in (2) we can set $\theta=0$ and therefore $m=0$. We now use the same unitary transformation for the Coulomb field. That is, the wave functions used for the electron are given by (2) with $u_{lm}{}^{(\pm)}$ identified with solutions for the Dirac Coulomb field in the representation j^2, j_z diagonal. This approximation can be justified if the effect of the Coulomb field is small.

For allowed transitions we need only the terms $j=\frac{1}{2}$, $l=0$, 1 corresponding to $s_{\frac{1}{2}}$ and $p_{\frac{1}{2}}$ electrons. The correlation function then has the form (1) with n replaced by nf where f, which is independent of the type of interaction, is given by

$$f=\tfrac{1}{3}[1+2(1-\alpha^2Z^2)^{\frac{1}{2}}](1+\alpha^2Z^2/p^2)^{\frac{1}{2}}. \quad (3)$$

In (3) α is the fine structure constant and p is the electron momentum in units mc. Averaging (3) over a typical energy distribution for allowed transitions we find that even for an element as heavy as Pb, the value of $\langle\beta f\rangle_{Av}$ differs from $\langle\beta\rangle_{Av}$ by about 20 percent. Therefore one may safely disregard effects of the Coulomb field in comparing theory and experiment for the purpose of distinguishing between the various forms of the beta-interaction.

* This document is based on work performed under Contract No. W-7405-eng-26 for the AEC at the Oak Ridge National Laboratory.
[1] D. R. Hamilton, Phys. Rev. 71, 456 (1947).
[2] Obviously, no significant effect from the Coulomb field would be expected in an experiment like that of J. S. Allen *et al.*, Phys. Rev. 75, 570 (1949), in which He^4 was used. However, the question of the Coulomb field might arise in the case of Y^{90} used in the measurements of C. W. Sherwin, Phys. Rev. 73, 1173 (1948).

A Possible Experimental Verification of the Statistics of He^3

D. TER HAAR
Department of Physics, Purdue University, Lafayette, Indiana
March 18, 1949

IN principle it is possible to determine whether He^4 obeys Fermi-Dirac or Bose-Einstein statistics by measuring the second virial coefficient B. J. de Boer,[1] and Massey and Buckingham[2] have calculated B starting from a field of force determined by measurements at high temperatures. It turns out that the $BT^{\frac{1}{2}}$ curve (T: temperature) as a function of temperature shows a maximum at about 0.8°K if He^4 obeys Bose-Einstein statistics but that there is no such maximum if He^4 should obey Fermi-Dirac statistics. A difference between

the two statistics becomes discernible at about 1.7 to 1.8°K. The vapor pressure of He^4 is then, however, of the order of 1 cm Hg or less and it becomes extremely difficult to measure B accurately. Kistemaker[3] has made measurements down to 1.8°K but the uncertainty of his B at the lowest temperature at which he measured is too high so that it is impossible to make an experimental verification of the fact that He^4 obeys Bose-Einstein statistics.

For He^3 the situation is, however, much more favorable. Due to its smaller mass, quantum effects will be more pronounced and its vapor pressure will be much higher. Indeed, as far as the vapor pressure is concerned, the theoretical predictions of J. de Boer and Lunbeck[4] were completely borne out by the experiments of Sydoriak, Grilly and Hammel.[5] At 1.2°K the vapor pressure of He^3 is still 2 cm Hg and it should therefore be possible to measure B down to about 1.2°K. The amount of He^3 needed for these measurements is not too large, even not in view of the scarcity of the light helium isotope in a pure state. Kistemaker[3] used about 200 cc S.T.P. which is about ten times as much as the 20 cc S.T.P. used by Sydoriak, Grilly and Hammel[5] in their experiments.

In order to get a rough check as to the influence of the smaller mass on the behavior of the $BT^{\frac{1}{2}}$ curve, we have calculated B as a function of T for low temperatures, using the hard sphere model.[1,6] Using the same radius for mass 3 and for mass 4, and assuming both times Bose-Einstein statistic it turns out that the maximum in the curve for mass 3 was shifted to a temperature about one third higher than in the case of mass 4. Calculations using the correct field of force are now in progress, but it seems safe to conclude that, indeed, for the case of He^3 the second virial coefficient can show us whether or not He^3 really obeys Fermi-Dirac statistics.

[1] J. de Boer, Thesis (Amsterdam, 1940); J. de Boer and A. Michels, Physica 6, 409 (1939).
[2] H. S. W. Massey and R. A. Buckingham, Proc. Roy. Soc. (London) A168, 378 (1938).
[3] J. Kistemaker, Thesis (Leiden, 1945); J. Kistemaker and W. H. Keesom, Physica 12, 227 (1946).
[4] J. de Boer and R. J. Lunbeck, Physica 14, 510 (1948).
[5] Sydoriak, Grilly, and Hammel, Phys. Rev. 75, 303 (1949).
[6] G. E. Uhlenbeck and E. Beth, Physica 3, 729 (1936).

Determination of the Potential from the Asymptotic Phase

NORMAN LEVINSON*
Mathematics Institute, Copenhagen, Denmark
March 14, 1949

AS V. Bargmann has shown,[1] problems concerning the determination of the potential from the asymptotic phase require a mathematically rigorous treatment since heuristic processes lacking in rigor have led to erroneous results. By methods developed in a paper to appear shortly in the Det Kgl Danske Videnskabernes Selskab (where the case $l=0$ is taken up) it is possible to show that the solution $y(x,\lambda)$ of

$$y''+\left(\lambda^2-\frac{l(l+1)}{x^2}-V(x)\right)y=0$$

with boundary condition $y(x,\lambda)/x^{l+1}\to 1$ as $x\to+0$, exists if $\int_0^\infty x|V(x)|dx<\infty$. Moreover for any $\lambda>0$, as $x\to\infty$, it is the case that

$$y(x,\lambda)\sim(A(\lambda)/\lambda^{l+1})\sin(\lambda x-\tfrac{1}{2}l\pi-\phi(\lambda)).$$

The function $\phi(\lambda)$ is called the asymptotic phase. If $l(l+1)/x^2+V(x)\geqq 0$, then $\phi(\lambda)$ determines $V(x)$ uniquely. It is also the case that $\log A(\lambda)$ and $\phi(\lambda)$ are conjugate functions.

* John Simon Guggenheim Memorial Fellow on leave from the Massachusetts Institute of Technology, Cambridge, Massachusetts.
[1] V. Bargmann, Phys. Rev. 75, 301 (1949).

On the Beta-Particle Spectrum from the Decay of Radium E*

ARTHUR WALTNER
North Carolina State College of Engineering, Raleigh, North Carolina
AND
F. T. ROGERS, JR.
U. S. Naval Ordnance Test Station, Inyokern, California
March 17, 1949

SEVERAL investigations have now been made of that portion of the energy-distribution of beta-particles from the decay of $RaE(_{83}Bi^{210})$, which lies at quite small energies. H. O. W. Richardson seems to have made the first[1] by observing tracks from active sources on various thin supports in a cloud chamber, and making calculated allowances for back-scattering and absorption. The points plotted in Fig. 1 show the differential distribution (here called (A)) obtained[2] by Richardson. Somewhat later C. B. Madsen made an investigation[3] of this spectrum, using active deposits on collodium supports (0.2μ thick), and giving careful attention to the reduction of scattering in the analyzer; to correct for the effects of the source-support, he used an empirical relation suggested by the measurements of Flammersfeld:[4]

$$\log I_{\text{support}}=a-bE,$$

where a and b are constants. Dr. Madsen writes that his results, shown by curve (B) in Fig. 1, seem to be in good agreement with our earlier observations.[5]

Curve (C) in Fig. 1 shows the distribution which we have recently obtained from observations of beta-particle tracks from a vapor of $Bi^{210}(CH_3)_3$ in a cloud chamber. Professor Richardson writes that Mrs. A. Leigh-Smith and he considered this method some years ago. In our observations 131 tracks were photographed non-stereoscopically and measured by the method of Petrova.[6] Corrections were applied to reduce the errors of projections and to allow for the change of effective solid angle with track-length. The conversion to energy as the independent variable, was effected with the best available composite relations of energy and of stopping power to range for particles of low energy.

There is a significant measure of general agreement between the three sets of data shown in Fig. 1, possibly strengthened by the fact (based on the coherence of curve (B) with our earlier results) that data (A) and curve (B) may be undercorrected for the effects of the source-supports. Thus it appears: (1) that the maximum of intensity in the observed spectrum of beta-particle energies from RaE lies at a rather low energy (~30 kev, more or less); and (2) that the intensity

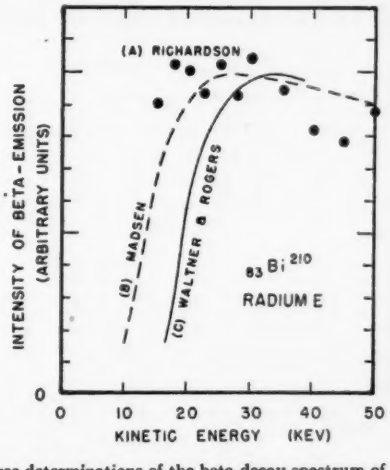

FIG. 1. Three determinations of the beta-decay spectrum of RaE at very low energies, normalized to approximately the same maximum intensity. See text for references.

in this observed spectrum drops off sharply at lower energies, apparently to quite small values. It is impossible to overemphasize the need for further investigations of this spectrum, for these conclusions appear to stand in contradiction of the modern theories of beta-decay.

* The new data reported here, shown as curve (*C*) in Fig. 1, were obtained in 1948 in the research laboratories of The University of North Carolina in Chapel Hill.

[1] H. O. W. Richardson, Proc. Roy. Soc. **147A**, 442 (1934).

[2] The investigations of Flammersfeld (reference 4) and of G. J. Neary (Proc. Roy. Soc. **175A**, 71 (1940)), though not directed entirely toward the low-energy spectrum, yielded distributions which had positive derivatives at these energies.

[3] C. B. Madsen, Acta Jutlandica Aarskrift for Aarhus Universitet **XV**, 1 (1942).

[4] A. Flammersfeld, Zeits. f. Physik **112**, 727 (1939).

[5] Arthur Waltner and F. T. Rogers, Jr., Phys. Rev. **74**, 699 (1948).

[6] J. Petrova, Zeits. f. Physik **55**, 628 (1929).

Measurement of Particle Energies with Scintillation Counters

G. F. J. Garlick and R. A. Fatehally
University of Birmingham, England
March 14, 1949

In a recent paper Kallmann[1] has shown that single crystals of cadmium sulphide, used with a photo-multiplier to detect single α-particles, give output pulses of fairly uniform size from α-particles of a given energy. Such crystals emit red luminescence which matches the spectral response of the photo-multiplier used by Kallmann. We have found that similar uniformity of pulse heights is obtained when small ($1\times1\times1.5$ mm) crystals of natural, transparent scheelite are used as α-particle detectors in conjunction with photo-multipliers having an antimony-caesium cathode. Figure 1 gives the "integrated bias" curve for pulses caused by α-particles of 4.5-Mev energy, and also the pulse height distribution curve derived from it. A considerable spread of pulse heights is shown which is not accounted for by scattering and straggling of the incident particles. Removal of the spherical concave mirror, used in the system for collecting a large amount of the emitted light, does not alter the form of the "bias" curve to any marked extent. Similar "bias" curves were obtained for the scintillations produced in small single crystals of naphthalene activated by anthracene or by stilbene. We find that the average pulse height is approximately proportional to the energy of the incident particles. The rise in counting rate shown at low bias values is the result of multiple counting and is not present for crystals having a much more rapid decay of luminescence than scheelite (3 μsec.).

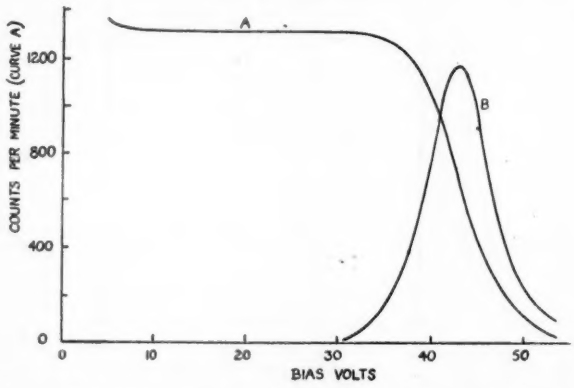

FIG. 1. Bias curves for multiplier output pulses due to scintillations in scheelite crystal bombarded by α-particles of 4.5-Mev energy. *A* is integrated bias curve; *B* is pulse height distribution curve derived from *A*.

Other observations would appear to be of interest here. We have found that stilbene functions as an efficient activator in naphthalene crystals in a similar manner to anthracene, but gives output pulses of about twice the magnitude of those from anthracene-activated crystals. We find also that for both these phosphors, as well as for such inorganic phosphors as zinc oxide, silver-activated zinc sulphide, lead-activated barium sulphate, and synthetic and natural scheelite, there are no marked differences in maximum pulse heights due to α-particles and γ-rays, if these are of equivalent energies. These results are contrary to those reported by Kallmann.[2]

[1] H. Kallmann, Phys. Rev. **75**, 623 (1949).

[2] H. Kallmann, Research **2**, 62 (1949).

Beta-Decay Spectrum of Ag^{110}

Werner S. Emmerich and J. D. Kurbatov
Ohio State University, Columbus, Ohio
March 16, 1949

The disintegration of Ag^{110} has been studied previously by several authors.[1-3] Of the two modes of disintegration into stable isobars, Pd^{110} and Cd^{110}, the disintegration by electron emission into Cd^{110} is well substantiated.[2] The maximum energy of the beta-spectrum was found to be 0.59 Mev. It was reported that the beta-spectrum is complex with more than half of the disintegration electrons absorbed by 2 mg cm^{-2} of aluminum.[1] The first mode of disintegration, into Pd^{110}, has not been studied as yet either with regard to positron emission or to orbital electron capture. Several gamma-rays, of energies 0.66 Mev −44 percent, 0.90 Mev −47 percent partially converted and 1.40 Mev −9 percent have been found. In the most recent publication a converted gamma-ray of 114 kev has been reported.[3]

In the present work the disintegration of Ag^{110} into the isobars Cd^{110} and Pd^{110} was studied by means of a cloud chamber since disintegration into Pd^{110} by emission of positrons *a priori* could not be excluded.

The silver 110 of high specific activity was obtained from Oak Ridge National Laboratory, AEC. It was purified and mounted in the center of a cloud chamber on zapon film. Pictures of tracks were taken with and without magnetic field applied. The first series of tracks were photographed in air with a field of 372.5 gauss. The distribution of electrons *vs.* energies showed: (a) the existence of converted electrons corresponding to the gamma-rays of Ag^{110}, and (b) electrons of a continuous spectrum.

The Kurie plot produced a straight line in the energy range from 150 kev to 550 kev with upper limit about 0.59 Mev. The presence of converted electron groups limited observation of a continuous spectrum in a cloud chamber.

Several single positrons and pairs were found. The upper ratio of number of positrons, for which pairs could not be established, to the number of the electrons of the continuous spectrum did not exceed 0.2 percent. The experimental data obtained allowed the conclusion that there is no positron disintegration in Ag^{110} with branching ratio β^+/β^- higher than 0.2 percent.

The second series of tracks were photographed in helium with a field of 149 gauss. The subtraction of the 0.59-Mev continuous spectrum and recalculations for a second Kurie plot produced evidence for the existence of a continuous spectrum of electrons with upper energy 90 ± 10 kev. Independently it has been found that the electrons of the 90 ± 10-kev spectrum are in coincidence with gamma-rays.[4] The electron groups in the energy interval 90–150 kev were not sufficiently resolved.

It has been shown recently that excess of low energy electrons in Kurie plots very often are due to imperfect mounting.[5]

Conversely, with proper mounting the abundance of low energy electrons may be due to additional spectra as is the case with Ag^{110}.

The authors are indebted to Professor Edward Mack, Jr. for his support of this research.

It is a pleasure to express our gratitude to the Ohio State University Development Fund for grants for research equipment.

[1] Martin Deutsch, Phys. Rev. **72**, 527 (1947).
[2] Waldo Rall and Roger G. Wilkinson, Phys. Rev. **71**, 321 (1947).
[3] J. M. Cork, R. G. Shreffler, and C. M. Fowler, Phys. Rev. **74**, 1657 (1948).
[4] Fu-Chun Yu, Lin-Cheng Cheng, and J. D. Kurbatov, Phys. Rev. **75**, 1279 *et seq* (1949).
[5] R. D. Albert and C. S. Wu, Phys. Rev. **74**, 847 (1948).

The Hyperfine Structure of the Ground Term of Hydrogen

G. Breit and R. E. Meyerott
Yale University, New Haven, Connecticut*
March 23, 1949

REFERENCES to a paper[1] by the authors on the hyperfine structure of hydrogen indicate that the results are understood to have a higher accuracy than they do. The present note is intended as an addendum to the paper with the object of stating the limitations more clearly. The Hamiltonian contains a term called Y in the paper referred to, which contains products of Dirac's α-matrices. This term is responsible for the hyperfine structure. The employment of its expectation value in order to obtain an additive correction to the energy is the apparent limit of its applicability. The wave function by means of which the expectation value is calculated is obtained from Eq. (2) in reference 1 which is not accurate to relative order v^2/c^2 where v is the electron velocity. The expectation value of Y cannot be expected to be accurate to relative order v^2/c^2 except by accident. Therefore no claims for the correctness of the relativistic terms in the correction to hyperfine structure involving m/M can be made. The reason for reporting on the results of the calculations which gave such effects was that the relativistic effects which have been calculated can be expected to have a bearing on the actual corrections. No certain method of obtaining these appears to be available.

It should also be mentioned that in the first of the two Eqs. (3.1) an approximation has been made. This is immaterial for the hyperfine structure terms of relative order m/M and it does not affect the relativistic corrections to these terms in a qualitative way.

The hyperfine structure appears in the calculation as a relativistic effect. The relativistic corrections to it remain uncertain because the Hamiltonian does not determine the wave function with the required accuracy.

* Assisted by ONR.
[1] G. Breit and R. E. Meyerott, Phys. Rev. **72**, 1023 (1947).

On the Decay of K^{40}

E. L. Fireman*
Palmer Physical Laboratory, Princeton University, Princeton, New Jersey
March 21, 1949

AN interesting feature of the K^{40} decay is the evidence for electron capture[1–5] and no evidence for positron emission.[6] The purpose of this note is to point out several consequences of this fact.

The consequences are: (1) a determination of an upper limit to the $A^{40}-K^{40}$ mass difference, (2) the possibility of observing positrons from K^{40} if estimates[1–3] of the K capture are correct, and (3) a determination of the ratio of the nuclear matrix elements for the A- and Ca-transitions.

The ratio of positron emission to electron capture is independent of the nuclear matrix elements to a large extent** and should, therefore, give a reliable estimate of the mass difference. If the expressions for forbidden β-transitions[7,8] are used, the ratio of positron emission to electron capture under the third forbidden axial vector or tensor interactions and $Z=19$ is

$$\lambda^{\beta^+}/\lambda^e=\frac{0.450\eta^{6\frac{1}{2}}}{(\eta+2)^3}[0.0676+1.25\eta+8.48\eta^2+12.5\eta^3+1.74\eta^4+0.079\eta^5],$$

where $\eta=\Delta M-2$ and ΔM is the atomic mass difference in units of the mass of the electron. The mass difference obtained by use of this expression and from the expressions arising from various fourth forbidden interactions are practically identical.

Table I gives the $A^{40}-K^{40}$ atomic mass difference as a function of the ratio of positron emission to electron capture. If the experimental values[1–3] $\lambda^{\beta^-}/\lambda^e=\frac{1}{2}$ and $\lambda^{\beta^+}/\lambda^{\beta^-}<0.01$ are used,[6] then $\lambda^{\beta^+}/\lambda^e<0.005$ and the $A^{40}-K^{40}$ mass difference is less than 1.6 Mev.

TABLE I. $A^{40}-K^{40}$ atomic mass differences.

$\Delta M(mc^2)$	0–2	3.00	3.25	3.50	3.75	4.00	4.25
$\lambda^{\beta^+}/\lambda^e$	0	0.00165	0.00675	0.0203	0.0494	0.104	0.195

The experiments on the K^{40} β^--energy endpoint require that the 1.55 Mev γ-ray be placed on the A^{40} side of the decay scheme. If experiments of references 1 to 3 are correct there are approximately fifteen K captures to one γ-ray so that most of the K captures go to the ground state. This would lead to the conclusion that there is one positron to every two hundred and fifty electrons. The probability for positrons from the internal pair creation of the γ-ray or β-ray is much smaller.

If one uses the value of the $\lambda^{\beta^-}/\lambda^e$ ratio, the corresponding upper limit to the $K^{40}-A^{40}$ mass difference, and β^--energy endpoint, one can estimate the ratio of the $(K^{40}-A^{40})$ to $(K^{40}-Ca^{40})$ nuclear matrix element. These are

$$\left(\frac{|Q_{K-A}|^2}{|Q_{K-Ca}|^2}\right)=50,\quad \left(\frac{|Q_{K-A}|^2}{|Q_{K-Ca}|^2}\right)=\tfrac{1}{2},$$

$$\lambda^{\beta^-}/\lambda^e=\tfrac{1}{2},\quad \lambda^{\beta^-}/\lambda^e=10,$$

$$E_{\beta^-}=1.4\text{ Mev},\quad E_{\beta^-}=1.4\text{ Mev}.$$

If the higher value of $\lambda^{\beta^-}/\lambda^e$ is approximately correct, it would indicate that the A^{40} and Ca^{40} nuclear states are very similar and probably have the same parity. However, the lower value of $\lambda^{\beta^-}/\lambda^e$ has more experimental support.

The author wishes to thank Professor E. P. Wigner for several stimulating discussions.

* AEC post-doctoral fellow.
** This ratio is completely independent of the nuclear matrix element for the third forbidden tensor and axial vector interaction and the fourth forbidden scalar, axial vector and pseudoscalar interactions. For the other fourth forbidden interactions and the various linear combinations, the $\lambda^{\beta^+}/\lambda^e$ ratio involves the ratio of certain matrix elements between the same initial and final states. These can be estimated fairly well.

[1] F. C. Thompson and S. Rowlands, Nature **152**, 103 (1943).
[2] E. Bleuler and M. Gabriel, Helv. Phys. Acta **20**, 67 (1947).
[3] L. Ahrens and R. D. Evans, Phys. Rev. **74**, 279 (1948).
[4] L. T. Aldrich and A. O. Nier, Phys. Rev. **74**, 876 (1948).
[5] H. F. Suess, Phys. Rev. **73**, 1209 (1948).
[6] Bothe and Flammersfeld, Naturwis. **29**, 194 (1941).
[7] Eugene Greuling, Phys. Rev. **61**, 568 (1942).
[8] W. Goode, D. Peaslee, and M. Deutch, Phys. Rev. **69**, 313 (1946).

On the Maximum β-Energy Release in Tritium*

L. SLACK, G. E. OWEN, AND H. PRIMAKOFF
Washington University, St. Louis, Missouri
March 10, 1949

SOME time ago (1947) Konopinski emphasized that the then existing data on the half-life and the maximum β-energy release in H^3 implied a "degree of allowedness" for it much greater than that for the supposedly equally allowed He^6 spectrum:[1]

$$|M|^2 \text{ ft.} = 900 \text{ for } H^3, \quad |M|^2 \text{ ft.} = 5760 \text{ for } He^6.$$

More recently Bowers and Rosen[2] have pointed out that work by Curran *et al.*[3] and by Novick[4] (maximum β-energy release of 16.9 ± 0.3 kev; half-life of 12 years) greatly minimize the above discrepancy, while the yet unpublished maximum β-energy value of Pontecorvo obtained with a proportional counter, 18.5 kev (quoted in Seaborg),[5] practically removes it (see below).

We wish to remark in the present note that the accurate calorimetric determination of the average β-energy release in H^3, 5.69 ± 0.06 kev, just published by Jenks *et al.*[6] enables an equally accurate determination of the maximum β-energy release which, moreover, turns out to be in excellent agreement with Pontecorvo's. Thus, suppose the tritium spectrum is Fermi allowed; one then has:[7]

$$5.69 \pm 0.06 \text{ kev} = \text{average } \beta\text{-energy release} \equiv \langle(\epsilon-1)\rangle_{Av} = \frac{\int_1^{\epsilon_{max}} \frac{2\pi Z}{137}\frac{\epsilon}{(\epsilon^2-1)^{\frac{1}{2}}}\left\{1-\exp\left(-\frac{2\pi Z}{137}\frac{\epsilon}{(\epsilon^2-1)^{\frac{1}{2}}}\right)\right\}^{-1}(\epsilon^2-1)^{\frac{1}{2}}\epsilon(\epsilon_{max}-\epsilon)^2(\epsilon-1)d\epsilon}{\int^{\epsilon_{max}} \frac{2\pi Z}{137}\frac{\epsilon}{(\epsilon^2-1)^{\frac{1}{2}}}\left\{1-\exp\left(-\frac{2\pi Z}{137}\frac{\epsilon}{(\epsilon^2-1)^{\frac{1}{2}}}\right)\right\}^{-1}(\epsilon^2-1)^{\frac{1}{2}}\epsilon(\epsilon_{max}-\epsilon)^2 d\epsilon} \quad (1)$$

where ϵ = kinetic + rest energy of the emitted β-particle (in units of its rest energy), ϵ_{max} = maximum kinetic + rest energy of the emitted β-particle, and Z = nuclear charge of the daughter element = 2. Numerical integration and interpolation in Eq. (1) gives (see Fig. 1):

$$\epsilon_{max} - 1 = (3.64 \pm 0.04) \times 10^{-2} = 18.6 \pm 0.2 \text{ kev},$$

the discrepancy with Pontecorvo's value being well within experimental error. A comparison of the "degrees of allowedness" of H^3 and He^6 (calculated with the above $(\epsilon_{max})_{H^3}$, with an H^3 half-life of 12.46 years,[6] and with more recent values of the half-life and maximum β-energy release of He^6: 0.89 sec.[8], $(\epsilon_{max})_{He^6} = 3.5 \pm 0.6$ Mev[8]) yields:

$$|M|^2 \text{ ft.} = 3360 \pm 200 \text{ for } H^3,$$
$$|M|^2 \text{ ft.} = 6300 \pm 3000 \text{ for } He^6.$$

Complete consistency is thereby established between the last quoted H^3 and He^6 measurements and between the application of the Gamow-Teller selection rules to these two simplest of the β-active nuclei.

In conclusion it may be pointed out that if we had (incorrectly) used the value $Z = 1$, appropriate to the parent nucleus, in the Coulomb factor of the β-energy distribution in the integral, we would have obtained the (incorrect) maximum β-energy release: 17.8 ± 0.2 kev. The error made in using $Z = 1$ instead of $Z = 2$ is also appreciable in the Kurie plot of the β-spectrum; below we append a Kurie plot of an H^3 β-distribution actually obeying the Fermi allowed shape with $Z = 2$ (curve A, Fig. 2); the same distribution is then plotted with use of a Coulomb factor appropriate to $Z = 1$ (curve B, Fig. 2).

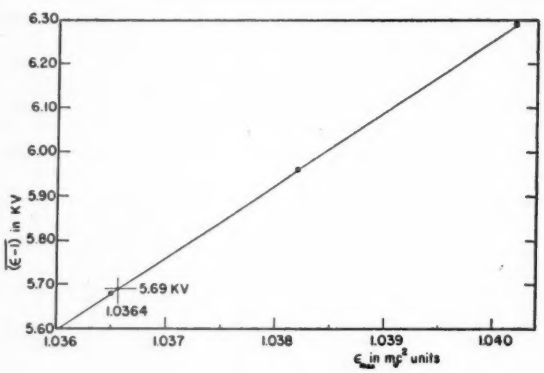

FIG. 1.

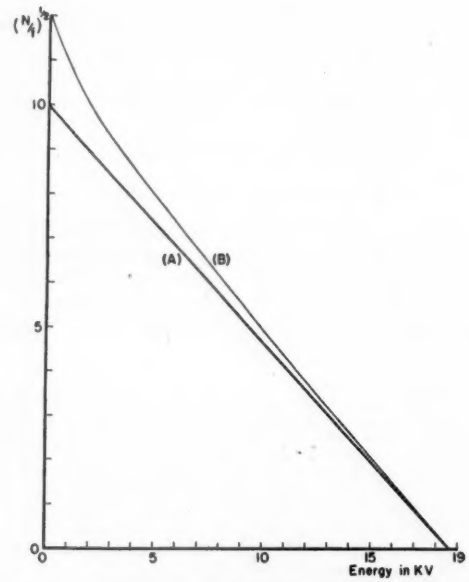

FIG. 2. A: Kurie plot for an H^3 β-distribution with $Z = 2$. B: Plot of the same distribution with Coulomb factor appropriate to $Z = 1$.

* Assisted by the joint program of the ONR and the AEC.
[1] E. J. Konopinski, Phys. Rev. **72**, 518 (1947).
[2] W. A. Bowers and N. Rosen, Phys. Rev. **75**, 523 (1949).
[3] S. C. Curran, J. Angus, and A. L. Cockcroft, Nature **162**, 302 (1948).
[4] A. Novick, Phys. Rev. **72**, 972 (1947).
[5] G. T. Seaborg, Rev. Mod. Phys. **20**, 585 (1948).
[6] G. H. Jenks, J. A. Ghormley, and F. H. Sweeton, Phys. Rev. **75**, 701 (1949).
[7] The use of the non-relativistic Coulomb factor in the Fermi allowed distribution function in Eq. (1) introduces a negligible error.
[8] H. S. Sommers and R. Sherr, Phys. Rev. **69**, 21 (1946).

Neutron and Proton Binding Energies in the Region of Lead*

KATHARINE WAY**
Oak Ridge National Laboratory, Oak Ridge, Tennessee
March 18, 1949

THE maxima in α-particle decay energies for mass numbers 210–215 recently emphasized by Perlman, Ghiorso, and Seaborg[1] can be looked at in terms of neutron

and proton energies and, when thus interpreted, reveal rather sharp discontinuities in these bindings at proton number 82 and neutron number 126. The numbers 82 and 126 are two of the "magic" numbers connected with marked nuclear stability on which attention has been focused by M. G. Mayer.[2] If one considers these "magic" numbers as numbers for which neutron or proton shells are closed, one would expect unusually high binding energies for the 82nd, 81st, etc., proton and for the 126th, 125th, etc., neutron and unusually small bindings for protons with number slightly greater than 82 and neutrons with number slightly greater than 126. As the new shells fill up, the binding energies should gradually return to "normal."

The binding energy of four neutrons to certain heavy nuclei can be found with a good deal of accuracy from known α- and β-decay energies. Thus the binding energy of four neutrons to U^{234} is equal to {mass (U^{234})+mass $(4n$'s$)$ −mass (U^{238})} or {mass $(4n$'s$)$−mass $(He^4)-E_\alpha(U^{238})-E_\beta(UX_1)-E_\beta(UX_2)-E_{recoil}$} which equals[3,4] {29.64−4.18 −0.20−2.32−0.07} or 22.9 Mev. The binding energy of four neutrons to Pb^{208} turns out by a similar calculation to be only 17.6 Mev using $E_\beta(ThB)=0.88$ Mev, $E_\beta(ThC)=2.20$ Mev, and $E_\alpha(ThC')=8.78$ Mev. The Bohr-Wheeler[5] liquid drop model with the semiempirical constants given by them gives 22.8 Mev for the binding of 4 neutrons to U^{234}. However, for the Pb^{208} value the Bohr-Wheeler model gives again 22.8 Mev in marked disagreement with the 17.6 Mev now found from decay energies.

If one neutron binding energy in each of the four naturally radioactive families is known, a whole series of additional binding energies can be calculated from the information now available on α- and β-decay energies. In the case of α-decay

$$B_n(A-4, Z-2)=B_n(A, Z)-E_{\alpha 1}-E_{\alpha 2},$$

where $B_n(A, Z)$ is the binding energy of a neutron to a nucleus with mass A and charge Z, and where $E_{\alpha 1}$ and $E_{\alpha 2}$ are the disintegration energies associated with the emission of α-particles from the nuclei (A, Z) and $(A+1, Z)$, respectively. A similar relation holds for β-decay.

Since no measurements of neutron binding energies in the very heavy region are available, the four individual values for U^{234}, U^{235}, U^{236}, and U^{237} given by the Bohr-Wheeler model have been taken as starting points. The sum of these four binding energies as already pointed out, agrees very well with the latest measurements of α- and β-decay energies and there seems at present no reason to believe that shell structure plays an important part in nuclear binding in the uranium region.

Proceeding in steps by means of decay energies the neutron and proton binding energies in the region of the two magic numbers 82 and 126 have been calculated. The results are in doubt not only because of inaccuracy in the binding energies taken as starting points but also because of uncertainties in some of the disintegration energies, especially those for β-decay where decay schemes are often in some doubt. Some checks were possible from stability considerations and cycle calculations but in some cases it was necessary to depend on cycle calculations entirely. Such a calculation is one in which a value is found by requiring disintegration energies leading from the same initial to the same final nucleus to be equal.

Table I shows the results. Here the value 7.1 in the first row is the binding energy in Mev of the 126th neutron to a nucleus containing 81 protons and 125 neutrons, while the value 7.8 in the second row gives the binding energy of the 82nd proton to the same nucleus. The values found support the shell picture since unusually high binding energies are observed just before and unusually small ones just after the completion of the shells at neutron number 126 and proton number 82. The nucleus Pb^{208} containing both 82 protons and 126 neutrons is seen to act like a core, additional neutrons and protons being bound to it by approximately equal amounts.

TABLE I. Neutron and proton binding energies.

Z \ N	124	125	126	127	128	129	130	131	
Tl_{81}			7.1	3.5	4.7	4.0(?)			
Pb_{82}	6.9	7.8	7.7	7.7	8.5(?)				
			7.0	3.5	5.5	4.0	4.6		
Bi_{83}			*	3.5	4.9	4.6	4.8		
				4.9	5.3	4.1	4.9	4.3	
Po_{84}			5.3	5.2	5.6	5.4	6.7	6.7	
				4.8	5.7	4.0	6.2	4.3	5.3
At_{85}								4.9	5.5

* Experimental value of 7.45±0.2 just reported by McElhinney *et al.*, Phys. Rev. 75, 542 (1949).

Results rather similar to those of Table I were found by Berthelot[6] in 1942 from data on the disintegration energies of Pb, Bi, and Po isotopes only.

* This document is based on work performed under contract W-7405-eng-26 for AEC at the Oak Ridge National Laboratory.

** Present address: National Bureau of Standards, Washington, D. C.

[1] I. Perlman, A. Ghiorso, and G. T. Seaborg, Phys. Rev. 74, 1730 (1948).
[2] Maria G. Mayer, Phys. Rev. 74, 235 (1948).
[3] H. Bradt and P. Sherrer, Helv. Phys. Acta 19, 307 (1946); Phys. Rev. 71, 141 (1947).
[4] H. Bradt, Nucleonics (May 1948), Part 2.
[5] N. Bohr and J. A. Wheeler, Phys. Rev. 56, 426 (1939).
[6] A. Berthelot, J. de phys. et rad. (VIII) 3, 17 (1942).

Erratum: On the Application of Heisenberg's Theory of *S*-Matrix to the Problems of Resonance Scattering and Reactions in Nuclear Physics

[Phys. Rev. 74, 131 (1948)]

NING HU*
Universitetets Institut for Teoretisk Fysik, Copenhagen, Denmark

IT should be pointed out, first, that the one-level formula (52) is not different from the one given in literature. The difference in form is only due to the fact that in (52) the true level W_S and true width γ_S are used, while in the usual formulation W_S and γ_S are defined differently. Second, the parameters α and β of Section 4 should in general cases be considered as functions of $k_A^{(0)}$ and $k_C^{(0)}$. No demand on the analytical nature of α and β can be made by the present treatment. In fact they are not analytic according to the treatment of Wigner and Eisenbud.[1] Third, the present author was not aware of several papers by Professor Wigner and others[1] which give many far reaching results. Therefore he is anxious to withdraw the last sentence in the Introduction of his paper.

* Now at Laboratory of Nuclear Studies, Cornell University, Ithaca, New York.

[1] E. P. Wigner and L. Eisenbud, Phys. Rev. 72, 29 (1947); E. P. Wigner, Phys. Rev. 73, 1002 (1948); G. Goertzel, Phys. Rev. 73, 1463 (1948).

Erratum: Second-Order Stark Effect of Methyl Chloride

[Phys. Rev. 75, 889 (1949)]

ROBERT KARPLUS AND A. HARRY SHARBAUGH
General Electric Research Laboratory, Schenectady, New York

BECAUSE of an error in reducing the data, the field strengths of Fig. 1 should all be reduced by the factor 0.91. Using the corrected field strengths, the value of the dipole moment for methyl chloride becomes $\mu_0=1.87\pm0.03$ Debye units, which is in agreement with 1.86D given by Smyth.[1]

[1] C. P. Smyth, *Dielectric Constant and Molecular Structure* (Reinhold Publishing Company, New York, 1931).

The Hydrogen Sulfide Bands at 10,200 cm^{-1} *

HAROLD R. GRADY** AND PAÚL C. CROSS
Metcalf Chemical Laboratories, Brown University, Providence, Rhode Island
AND
GILBERT W. KING
Arthur D. Little, Inc., Cambridge, Massachusetts
March 22, 1949

APPROXIMATELY ninety absorption lines have been measured in the region 10,070 cm^{-1} to 10,270 cm^{-1} using a 21-foot grating (15,000 lines per inch) and a path of 220 ft. of H_2S at 0.75 atmosphere pressure. The high frequency portion of this region also contains a number of atmospheric water vapor lines.

Essentially all these lines are assigned as water lines or as transitions in one (or both) of two bands at $\nu_0=10{,}194.48$ cm^{-1} and $\nu_0=10{,}188.25$ cm^{-1}, respectively. The selection rules correspond in the first band to the electric moment along the axis of least inertia, perpendicular to the symmetry axis and, in the second band, along the axis of intermediate inertia, parallel to the symmetry axis. The constants are tabulated (see Table I)

TABLE I. Constants for the H_2S molecule.

ν_0	0.00	9911.05	10188.25	10194.48 cm^{-1}
a	10.373	9.883	9.605	9.698
b	8.991	8.340	8.560	8.466
c	4.732	4.474	4.477	4.490
I_a	2.698	2.832	2.914	2.886×10^{-40} g cm^2
I_b	3.113	3.356	3.269	3.306
I_c	5.914	6.255	6.251	6.233
Δ	0.103	0.067	0.068	0.041

together with those derived from the 9911.05 cm^{-1} band,[1,2] recalculated using $h/8\pi^2c=27.98_{65}\times10^{-40}$ g cm.

In the table, $\Delta=I_c-I_a-I_b$ and the inertial constants a, b, c were determined by least squares after applying a first-order classical correction for centrifugal distortion.[1] The 9911 and 10,194 bands are probably the $(\nu_a\nu_b\nu_b)=(130)$ and (310) bands, considerably mixed by resonance.[3] The 10,188 band is believed to correspond approximately to the (400) band, also possibly involved in resonance. Since the absorption in this band is much weaker than in the other band, the upper state constants are not as well established as are those given for the 10,194 band.

The previous report[1] of a new band at about 10,100 cm^{-1} was an erroneous conclusion based on the observed spacing in this region as about that expected in an R-branch near the band center. This spacing is now established as due to the interspersed P-branches of the two new bands reported here.

* This work was supported in part by the Office of Naval Research Contract N6ori-88 Task I.
** Arthur D. Little Fellow in chemistry.
[1] P. C. Cross, Phys. Rev. **47**, 7 (1935).
[2] B. L. Crawford and P. C. Cross, J. Chem. Phys. **5**, 621 (1937).
[3] B. T. Darling and D. M. Dennison, Phys. Rev. **57**, 128 (1940).

On the Anomalous Line-Shapes in the Ammonia Inversion Spectrum at High Pressures

P. W. ANDERSON*, **
Harvard University, Cambridge, Massachusetts
March 17, 1949

THE purpose of this letter is to suggest a qualitative, rather than rigorous, explanation of the magnitude and direction of the observed anomalies in line-shapes in the ammonia inversion spectrum.[1-4] At high pressures the line is found to be much narrower than would be expected on the standard theory, and is shifted strongly to lower frequencies. It appears that these effects can be explained on the basis of simple permanent dipole interaction of two ammonia molecules, without bringing in the complicated effects suggested by some authors.[1,2,4]

We limit ourselves to the statistical type of theory, in which the perturbed energy of the levels of interest for two molecules fixed relative to each other is computed as a function of the intermolecular distance r, and then suitably averaged over all r to obtain the line-shape. One can think of our results in terms of a single molecule in a varying electric field. In weak fields the "proper linear combinations" of wave functions are $\psi_+=(\psi_{+K}+\psi_{-K})(1/\sqrt{2})$ and $\psi_-=(\psi_{+K}-\psi_{-K})(1/\sqrt{2})$, where ψ_{+K} and ψ_{-K} are the "single-ended" wave functions in which the N atom is thought of as on one side or the other of the potential barrier formed by the triangle of H atoms. The perturbation is second order and small (not true in the case of two atoms), and the selection rule is $\psi_+\leftrightarrow\psi_-$ only.

On the other hand, under a strong electric field, such that the perturbation, $\mathbf{p}\cdot\mathbf{E}$, is greater than the inversion splitting ΔE, the inversion is completely broken down by the external perturbation, and the right linear combinations are ψ_{+K} and ψ_{-K}. Here the selection rule is $+K\nleftrightarrow-K$, so that the only allowed radiation is composed of jumps in magnetic quantum number of one, small in frequency relative to the $\pm K$ splitting. It seems clear that such a change in selection rules can account both for the shift and the narrowing of the observed line.

An exact solution of the secular equation, simplified by ignoring the m-dependence of all quantities, and thus by using an unperturbed wave functions the products $\psi_\pm(1)\psi_\pm(2)$, shows that the same considerations apply in this more complicated case, except that the degenerate pair of levels $\psi_+(1)\psi_-(2)$ and $\psi_-(1)\psi_+(2)$ always undergo a first-order perturbation. The perturbing energy is the simple first-order interaction of two dipoles

$$H=\frac{1}{r^3}\left[\mathbf{p}_1\cdot\mathbf{p}_2-\frac{3(\mathbf{p}_1\cdot\mathbf{r})(\mathbf{p}_2\cdot\mathbf{r})}{r^2}\right].$$

The observed anomaly has become pronounced at atmospheric pressure. At this pressure it is easy to show that the molecules are within distances such that $H(r)\geq\Delta E$ for a large percentage (perhaps 50 percent) of the time. In this case one would suspect that the effect here discussed is quite strong since the molecules spend a large percentage of their time in the region where the strong field solution has some validity. Then one would expect a shift toward zero frequency and a narrowing of the line of much the same order of magnitude as is observed. A quantitative check must, of course, await a theory which reconciles the impact theory with the statistical theory used here, and in addition a complete statistical theory which sets up the rigorous secular equation and averages the result properly over all r, taking into account selection rules.

* Now at Bell Telephone Laboratories, Inc.
** National Research Council Predoctoral Fellow.
[1] Bleaney and Penrose, Proc. Phys. Soc. (London) **60**, 83 (1948).
[2] Bleaney and Loubser, Nature **161**, 523 (1948).
[3] DeForest F. Smith, Phys. Rev. **74**, 506 (1948).
[4] I. Weingarten, unpublished Thesis, Columbia University, New York, 1948.

Interaction Hamiltonian for Photon, Meson, and Nucleon Fields

GEORGE J. YEVICK
Stevens Institute of Technology, Hoboken, New Jersey
January 10, 1949

USING the methods developed by Tomonaga and collaborators, we have obtained the Hamiltonian for vector mesons interacting simultaneously with nucleons and with the electromagnetic field. The method is the same as that of

Kanesawa and Tomonaga, who first applied it to photon-scalar meson interaction[1] and then to the photon-vector meson system.[2] The invariant interaction Hamiltonian satisfies the condition of integrability (A):

$$[H_P[\sigma], H_{P'}[\sigma]]+\frac{\hbar}{i}\left\{\frac{\delta H_{P'}[\sigma]}{\delta\sigma_P}-\frac{\delta H_P[\sigma]}{\delta\sigma_{P'}}\right\}=0, \quad \text{(A)}$$

where x'_P is space-like separated from x_P. In view of the probable lack of availability of the Prog. Theo. Phys. journal, we shall summarize the Kanesawa-Tomonaga procedure very briefly. One computes the total Hamiltonian, subtracts off the Hamiltonian without interaction, and obtains the interaction part of the Hamiltonian. One makes the contact transformation on this to the uncoupled field situation. The resulting Hamiltonian is usually not an invariant. In going to the Tomonaga relativistic wave equation, one adds on to this a part depending on the normal to the space-like surface which causes the Hamiltonian to satisfy condition (A) and also makes it an invariant. Thus, for the photon-vector meson-nucleon system we get the following:

$$H=H_{np}+H_{mp}+H_{1nm}+H_{2nm}+H_{1nmp}+H_{2nmp}+H_{1n}+H_{2n},$$

where

$$H_{np}=-i\epsilon\bar{\psi}\gamma^\mu\tau_\rho\psi A_\mu,$$

$$H_{mp}=i\epsilon/2(G_{\mu\nu}U_{\mu\nu}-U_{\mu\nu}G_{\mu\nu})-\tfrac{1}{2}(i\epsilon)^2(G_{\mu\nu}{}^*G_{\mu\nu}+2G_{\mu\nu}{}^*G_{\mu\sigma}N_\nu N_\sigma)-[(i\epsilon)^2/\mu^2]A_\mu A_\nu U_{\mu\lambda}U_{\nu\rho}{}^*N_\lambda N_\rho,$$

$$H_{1nm}=f_1J_\mu\phi_\mu+f_1{}^*J_\mu{}^*\phi_\mu{}^*,$$

$$H_{2nm}=(f_2/2)S_{\mu\nu}U_{\mu\nu}+(f_2{}^*/2)S_{\mu\nu}{}^*U_{\mu\nu}{}^*,$$

$$H_{1nmp}=(i\epsilon/\mu^2)f_1(A_\lambda U_{\lambda\mu}N_\mu)(J_\nu N_\nu)-(i\epsilon/\mu^2)f_1{}^*(A_\lambda U_{\lambda\mu}{}^*N_\mu)(J_\nu{}^*N_\nu),$$

$$H_{2nmp}=-(i\epsilon/2)f_2(S_{\mu\nu}G_{\mu\nu}+2S_{\mu\nu}G_{\mu\sigma}N_\nu N_\sigma+(i\epsilon/2)f_2{}^*(S_{\mu\nu}{}^*G_{\mu\nu}{}^*+2S_{\mu\nu}{}^*G_{\mu\sigma}{}^*N_\nu N_\sigma),$$

$$H_{1n}=(f_1f_1{}^*/\mu^2)(J_\mu{}^*N_\mu)(J_\nu N_\nu),$$

$$H_{2n}=(f_2f_2{}^*/2)S_{\mu\nu}{}^*(S_{\mu\sigma}-S_{\sigma\mu})N_\nu N_\sigma,$$

and where we define

$$J_\mu\equiv\bar{\psi}\gamma^\mu\tau_{PN}\psi,$$

$$S_{\mu\nu}\equiv\bar{\psi}\gamma^\mu\gamma^\nu\tau_{PN}\psi,$$

$$G_{\mu\nu}\equiv A_\mu\phi_\nu-A_\nu\phi_\mu,$$

$$U_{\mu\nu}\equiv\partial\phi_\nu/\partial x_\mu-\partial\phi_\mu/\partial x_\nu,$$

and where A_ν is the photon field; ϕ_ν the meson field; and ψ the nucleon field. The H_{nmp} terms constitute the new contributions in as much as H_{mp} was first obtained by Kanesawa and Tomonaga[2] while $H_{1nm}+H_{2nm}+H_{1n}+H_{2n}$ by Miyamoto[3] with the δ-type terms expressed differently. In deriving H we used the Proca formalism for the meson field. On the other hand, Miyamoto in considering the nucleon-meson interaction used in the Stuckleberg formulation[4] employing two auxiliary fields. Preliminary calculations revealed no simple way of including the photon interaction into the Stuckleberg procedure.[4]

For completeness' sake we give the photon-scalar meson-nucleon interaction Hamiltonian:

$$H=H_{np}+H_{mp}+H_{1nm}+H_{2nm}+H_{2nmp}+H_{2n},$$

where

$$H_{np}=-i\epsilon\bar{\psi}\gamma^\mu\tau_\rho\psi A_\mu,$$

$$H_{mp}=-i\epsilon A_\mu\left(\phi^*\frac{\partial\phi}{\partial x_\mu}-\frac{\partial\phi^*}{\partial x_\mu}\phi\right)-(i\epsilon)^2(A_\mu{}^2-(A_\mu N_\mu)^2)\phi^*\phi,$$

$$H_{1nm}=f_1\bar{\psi}\tau_{PN}\psi\phi+f_1{}^*\bar{\psi}\tau_{NP}\psi\phi^*,$$

$$H_{2nm}=f_2\bar{\psi}\gamma^\mu\tau_{PN}\psi\frac{\partial\phi}{\partial x_\mu}+f_2{}^*\bar{\psi}\gamma^\mu\tau_{NP}\psi\frac{\partial\phi^*}{\partial x_\mu},$$

$$H_{2nmp}=-i\epsilon f_2\{\bar{\psi}\gamma^\mu\tau_{PN}\psi A_\mu\phi+\bar{\psi}\gamma^\mu\tau_{PN}\psi N_\mu A_\nu N^\nu\phi\}+i\epsilon f_2{}^*\{\bar{\psi}\gamma^\mu\tau_{NP}\psi A_\mu\phi^*+\bar{\psi}\gamma^\mu\tau_{NP}\psi N_\mu A_\lambda N_\lambda\phi^*\},$$

$$H_{2n}=f_2f_2{}^*(\bar{\psi}\gamma^\mu\tau_{NP}\psi)N_\mu(\bar{\psi}\gamma^\lambda\tau_{PN}\psi)N_\lambda.$$

H_{mp} is to be found in reference 1 and $H_{1nm}+H_{2nm}+H_{2n}$ in reference 3.

[1] Kanesawa and Tomonaga, Prog. Theo. Phys. 3, 1 (1948).
[2] Kanesawa and Tomonaga, Prog. Theo. Phys. 3, 101 (1948).
[3] Miyamoto, Prog. Theo. Phys. 3, 124 (1948).
[4] Stuckleberg, Helv. Phys. Acta. 11, 225, 299 (1938).
[4] Another aspect which requires more investigation is the utilization of Kemmer's linear formulation. The problem here is the role of the auxiliary conditions.

Erratum and Addendum: Domain Interactions in the Theory of Ferromagnetic Resonance

[Phys. Rev. 75, 893 (1949)]

GEORGE T. RADO
Naval Research Laboratory, Washington, D. C.
March 22, 1949

BECAUSE of typographical errors, Eq. (2) of this Letter to the Editor appeared incorrectly. The correct equation is:

$$P=1+\frac{1}{2(r+1)}+\frac{1}{2(r+1)^2}\left[\frac{r+1}{r}\right]^{\frac{1}{2}}\tanh^{-1}\left[\frac{r}{r+1}\right]^{\frac{1}{2}}. \quad (2)$$

This change does not affect any of the calculations or statements of the previous letter (to be referred to as A).

It seems appropriate to emphasize at this time that (as noted in A) the use of Eq. (1) of A for the local field H' *assumes* the validity of a $1/H^2$ law for the approach to technical saturation. The proposed theory is, therefore, particularly applicable to pure nickel[1] carefully annealed in pure hydrogen and to alloys of high nickel content (e.g., Supermalloy). In the case of iron,[2] on the other hand, the law of approach in the fields of interest ($\approx 10^3$ oersteds) is often of the $1/H$ type; for this reason the resonance data for iron were not considered in A.

In a recent experiment Yager and Merritt[3] found that in the particular case of a certain Heusler alloy the Landé g-factor calculated from their microwave resonance data on the basis of Kittel's theory (i.e., by neglecting domain interactions) agrees essentially with Barnett's experimental g-value. This result may well be due to the failure of the $1/H^2$ law of approach to saturation. The details of this problem will be discussed at a later date.

Note Added in Proof: In paper *A* the author used and cited L. Néel's formula (J. de phys. et rad. [VIII] 9, 193 (1948)) for the approach to saturation. It has since come to his attention that this formula was also derived by T. Holstein and H. Primakoff, Phys. Rev. 59, 388 (1941), Eq. (25).

[1] L. Néel, J. de phys. et rad. [VIII] 9, 193 (1948). In this paper Néel provides experimental confirmation (for nickel) for his $1/H^2$ law of approach to saturation.
[2] L. Néel, J. de phys. et rad. [VIII] 9, 184 (1948). In this paper Néel provides experimental confirmation (for iron) for his $1/H$ law of approach to saturation.
[3] W. A. Yager and F. R. Merritt, Phys. Rev. 75, 318 (1949). This paper appeared after paper A had been submitted for publication.

Cosmic-Ray Induced Nuclear Stars at High Altitudes*

P. FREIER, E. P. NEY, AND F. OPPENHEIMER
University of Minnesota, Minneapolis, Minnesota
March 23, 1949

WE have tabulated the rate of nuclear star formation in Ilford C2 emulsions sent aloft by General Mills balloons in Minnesota under various conditions. The results are summarized in Table I. We believe that the result will be

TABLE I. Number of stars/cm³ of emulsion/day.

	Small Stacks ¾″×2″×4″			Large Stack 4″×4″×10″ Based on time above 30,000 feet			
	Average of 4 flights based on total time above 30,000 feet	Ascent and descent to 70,000 feet	Average of 4 flights corrected for ascent and descent time	Under 0–12 g/cm² of glass	Under 12–25 g/cm² of glass	Under 25–37 g/cm² of glass	Under 37–50 g/cm² of glass
Average time per flight	5.8 hrs.	2.25 hrs.	4.1 hrs.	5.8 hrs.*	5.8 hrs.*	5.8 hrs.*	5.8 hrs.*
Residual atmosphere	300−14 g/cm²	300−50 g/cm²	24−14 g/cm²	300−13* g/cm²	300−13* g/cm²	300−13* g/cm²	300−13* g/cm²
3, 4, 5 prongs	630±30	1260±120	320±60	770±50	1140±70	1240±90	1050±70
6, 7, 8, 9 prongs	320±20	350±60	300±50	370±40	480±50	460±60	480±50
≧10 prongs	240±20	260±50	250±25	320±35	270±35	280±45	320±40
Total	1190±40	1870±140	880±90	1460±70	1890±90	1980±120	1850±100
Observed σ-stars	$\frac{12}{924}$=1.3%	$\frac{1}{171}$=0.6%		$\frac{9}{402}$=2.2%	$\frac{24}{417}$=5.8%	$\frac{19}{287}$=6.6%	$\frac{13}{371}$=3.5%
Observed total stars of ≧2 prongs							

* This stack spent 5.8 hours above 30,000 feet (300 g/cm²), 4.6 hours above 70,000 feet (50 g/cm²), and 4 hours above 93,000 feet (15 g/cm²).

of interest to others primarily because of the evidence for a strong maximum in the rate of star production below 70,000 feet.

The data for high altitude have been derived from four flights, each of which spent about four hours at altitudes varying from 14 to 24 g/cm². The emulsions in these flights were in stacks 2″×4″×¾″ under negligible local material. The data from the four flights have been combined, as the differences between them were disguised by statistical fluctuations.

We made one flight which rose to 50 g/cm² (70,000 feet) and then dropped the load by parachute. Since the rise and fall time for this flight (about 2¼ hours) was similar to the rise and fall time on the higher altitude flights, we have been able to subtract the number of stars during ascent and descent from the high altitude flights, and have thus been able to calculate the average rate of star formation at altitudes between 24 and 14 g/cm² and altitudes between 50 and 300 g/cm². The results are shown in Table I, columns 2 and 3, and clearly show the transition effect for small stars in the atmosphere. We have excluded the portion of the flights spent below 30,000 feet in calculating rates.

In addition to the flights with the small stacks (2″×4″×¾″) we have made one flight at the same latitude (56° N magnetic) with a large stack 4″×4″×10″. The plane of the emulsion and the 10″ dimension were vertical. This flight remained above 15 g/cm² for about four hours. We have no way of correcting this flight for the ascent and descent, and, therefore, the top plates should be compared with rates shown in column I of Table I. We have, however, been able to observe the transition effect in this stack as well as compare the rate of star formation under air and glass.

Inspection of Table I leads to the following observations:

1. The rate of small star production at high altitudes is only about ¼ the rate at intermediate altitudes.

2. The rate of small star production in the large stack at high altitude (where it spent most time) is approximately equal to the rate of small star production in the "free atmosphere" (small stack) at intermediate altitudes.

3. The rate of large star production (≧10 prongs) is not appreciably affected by thickness of matter up to 50 g/cm².

4. The rate of small star production in the stack saturates at a thickness of glass of about 18 g/cm².

5. The ratio of slow meson σ-stars to all stars is roughly five times greater in the dense matter of the large stack than in the free atmosphere, even under the same total matter.

The increased rate of production of σ-stars in the large stack shows the effect of the meson lifetime. The approximate equality of the rate of production of small stars in the small stack at intermediate altitudes and the large stack under an equivalent thickness of glass indicate that these small stars are not produced by a particle with a lifetime less than 10^{-6} second. It therefore seems plausible that these small stars are made by secondary nucleons.

Our data are consistent with the conclusion that the primaries themselves generate a negligible number of small stars since the relatively few small stars made at high altitudes can be accounted for by the fraction of the primary radiation that, because of its obliquity, has traversed at least 60 g/cm². If one assumes that at high altitudes the stars with 10 or more prongs are made by primaries interacting with the iodine, bromine and silver in the emulsion, one can calculate the cross section for star production. If we assume the proton flux to be 0.12/cm²/sec./ster., then the cross section is 0.15×10^{-24} cm². This value is about 1/10 the average nuclear area of the I, Br, and Ag. The proton flux may well be higher at these latitudes than at White Sands, New Mexico. However, even a value of 1/20 the nuclear area would appear to be rather high collision cross section for the transfer and sharing of energy to produce a ten-prong star. The mechanism of large star formation may well involve the production within the nucleus of a shower of mesons and the subsequent interaction of these mesons with the other nucleons.

It is difficult to understand the rapid saturation of the transition effect for the production of small star-producing secondaries in glass. If the small stars are produced by secondary neutrons as well as by charged particles, one would expect the rate of star production to increase down to depths comparable with the mean free path of the secondary neutrons. It is possible, however, that the rapid saturation of the small star transition effect arises because of a very rapid decrease of the cross section for star production with energy. Such a rapid decrease has been observed by E. Gardner[1] for the stars produced by several hundred Mev α-particles from the Berkeley cyclotron.

* Assisted by the joint program of ONR and AEC.

[1] E. Gardner, Phys. Rev. 75, 379 (1949).

On the Intuitive Approach to the Spectrum of a Wave Equation

PHILIP HARTMAN AND AUREL WINTNER
Department of Mathematics, The Johns Hopkins University, Baltimore, Maryland

January 19, 1949

LET $f(s)$, where $0\leqq s<\infty$, be a real-valued, continuous function which is not too unbounded when $s\to\infty$. For instance, let $|f(s)|<\text{const}$. Under this assumption, it is

known[1] that for no value of the real parameter λ will the differential equation

$$\varphi''+(f(s)+\lambda)\varphi=0 \tag{1}$$

be such as to possess only solutions satisfying

$$\int_0^\infty |\varphi(s)|^2 ds<\infty. \tag{2}$$

In other words, if $\varphi=\varphi_1(s)$ and $\varphi=\varphi_2(s)$ are two linearly independent solutions of Eq. (1) for some λ, then at least one of the functions φ_1, φ_2 will violate condition (2). This means that Eq. (1) and any homogeneous, linear boundary condition at $s=0$ (such as $\varphi(0)=0$ or $\varphi'(0)=0$) will *determine* an eigenvalue problem. This will, in particular, be the case if the potential $f(s)$ tends to a finite limit when $s\to\infty$.

The latter particular case of the restriction $|f(s)|<$const. can be assumed in the form

$$\lim_{s\to\infty} f(s)=0. \tag{3}$$

In this case, it can be expected, and recently it was proved,[2] that the spectrum contains every point of the half-line $0\leqq\lambda<\infty$.

In order to simplify the manner of speaking, let the "essential spectrum" of a differential Eq. (1) be defined as follows: A λ-value is in the essential spectrum if it is in the spectrum of *every* boundary condition assigned at $s=0$. In this terminology, the fact mentioned before can be expressed by saying that every point of the half-line $0\leqq\lambda<\infty$ is in the essential spectrum of Eq. (1) if the potential satisfies condition (3).

It was emphasized in a previous note[3] that an exact definition of the notion of a spectrum cannot be reduced to heuristic ideas. It will be shown below that intuitive notions on the spectrum are capable of leading to results which prove to be wrong.

First, an intuitive approach to the notion of a spectrum leads to the following definition:[4] A λ-value is in the spectrum (for *some* boundary condition assigned at $s=0$) if and only if the corresponding Eq. (1) has a solution $\varphi=\varphi(s)$ which remains bounded

$$|\varphi(s)|<\text{const. when } s\to\infty \tag{4}$$

(but is not the trivial solution, $\varphi(s)\equiv 0$). This definition clearly implies that a given λ cannot be in the essential spectrum unless the corresponding Eq. (1) has a solution $\varphi(s)$ satisfying condition (4). It is assumed, of course, that $f(s)$ is subject to some reasonable restriction when $s\to\infty$, such as the restriction mentioned before Eq. (1).

This restriction is surely satisfied if $f(s)$ is such as to satisfy condition (3). Since the latter condition assures that every point of the half-line $0\leqq\lambda<\infty$ is in the essential spectrum, there results the following assertion: If $f(s)$ is subject to condition (3), then there cannot exist a positive λ-value corresponding to which Eq. (1) fails to possess *some* solution satisfying condition (4). The truth of this assertion was deduced from the customary intuitive definition of a spectrum. Hence, if the assertion deduced will turn out to be false, it will follow that the intuitive definition must in general be discarded.

Accordingly, it is sufficient to ascertain that, if $f(s)$ is a real-valued, continuous function satisfying assumption (3), and if λ has a positive value, say $\lambda=1$, then *all* solutions of the corresponding differential Eq. (1), that is, of

$$\varphi''+(f(s)+1)\varphi=0, \tag{5}$$

can be such as to violate condition (4). But the existence of such an $f(s)$ is assured by the method of construction applied in an earlier paper.[5] In fact, the detailed construction given in that paper implies that such an $f(s)$ results by placing

$$f(s)=3\chi(s)\sin s-\chi^2(s)\cos^2 s-\chi'(s)\cos s,$$

if $\chi(s)$ is defined by

$$\chi(s)=s^{-\frac{1}{4}}(\cos s)\cos(\log s)$$

for $1\leqq s<\infty$ (and arbitrarily for $0\leqq s<1$, with the only restriction that $\chi'(s)=d\chi(s)/ds$ exists and is continuous for $0\leqq s\leqq 1$ also).

[1] H. Weyl, Math. Annalen **68**, 238 (1910).
[2] P. Hartman, Am. J. Math. **71**, 71 (1949).
[3] A. Wintner, Phys. Rev. **72**, 81 (1947).
[4] See, for instance, L. Pauling and E. B. Wilson, *Introduction to Quantum Mechanics* (McGraw-Hill Book Company, Inc., New York, 1935), p. 58, or H. A. Kramers, *Die Grundlagen der Quantentheorie* (1938), end of first paragraph on p. 72.
[5] A. Wintner, Am. J. Math. **68**, 385–397 (1946). An $f(s)$ of the type desired above results by choosing $\lambda=0$ and $\mu=\infty$ on p. 396 and then proceeding as on the bottom of p. 396 and the top of p. 397. For details, see Theorem (i) in a paper of the authors, to appear shortly in the Am. J. Math.

Nuclear Quadrupole Effects in the Microwave Spectrum of the Asymmetric Top Molecule, Vinyl Chloride*

J. H. GOLDSTEIN** AND J. K. BRAGG***
Mallinckrodt Chemical Laboratory, Harvard University, Cambridge, Massachusetts
February 28, 1949

THE study of nuclear quadrupole effects in molecular spectra has heretofore been confined to linear and symmetric top molecules. The theory of these effects has recently been extended to asymmetric tops by Bragg.[1] This communication is a preliminary report of the analysis of the observed hyperfine structure in the microwave spectrum of the asymmetric top vinyl chloride (C_2H_3Cl) with the aid of the first-order theory.

Table I gives the principal lines in the K-band spectrum of vinyl chloride and the frequencies corrected for quadrupole shift, together with the values of the rotational constants and the asymmetry parameter κ derived from them. The transitions are designated in the notation of King, Hainer, and Cross,[2] and the listed frequencies are those of the principal component of each multiplet.

The transitions were identified on the basis of an assumed planar model for the molecule, and were verified by measurement of Stark effect, relative intensities, temperature coefficient of intensity, and isotopic shift. The rotational constants were calculated from the corrected $1_{10}\to 2_{11}$ and $1_{11}\to 2_{12}$ frequencies using the Mecke sum rules,[3] and κ was evaluated on the assumption of planarity. From these results, the predicted frequencies for the $1_{01}\to 2_{02}$ transitions are 22,946.3 Mc and 22,485.3 Mc for $C_2H_3Cl^{35}$ and $C_2H_3Cl^{37}$, respectively. The close agreement of these values with the observed frequencies indicates that the deviation from planarity is very small.

The first-order quadrupole interaction energy was calculated from the expression:

$$E_Q=\frac{2}{2J+1}\left[\frac{\frac{3}{4}C(C+1)-I(I+1)J(J+1)}{2I(2I-1)(2J-1)(2J+3)}\right]\sum_{\tau'}\{\chi_{aa}(\lambda^a_{J\tau;J\tau'}-\lambda^c_{J\tau;J\tau'})+\chi_{bb}(\lambda^b_{J\tau;J\tau'}-\lambda^c_{J\tau;J\tau'})\}, \tag{1}$$

where $C=F(F+1)-I(I+1)-J(J+1)$, χ_{aa} and χ_{bb} are the two parameters of the problem, defined by $\chi_{aa}=eQ(\partial^2V/\partial a^2)$ and $\chi_{bb}=eQ(\partial^2V/\partial b^2)$, a and b being the principal axes of least and intermediate moment of inertia, respectively; Q is the nuclear quadrupole moment; and $\partial^2V/\partial_a{}^2$ and $\partial^2V/\partial_b{}^2$ are components of the molecular electric field gradient at the chlorine nucleus. The quantities $\lambda^a_{J\tau;J\tau'}$, etc., are the line strengths, tabulated by Cross, Hainer, and King[2] for the

transition $J_\tau \rightarrow J_{\tau'}$ appropriate to the given value of κ, and for a component of dipole moment parallel to the axis indicated by the superscript. The values of χ_{aa} and χ_{bb}, determined by a least square fit of two of the well resolved transitions of $C_2H_3Cl^{35}$ are given in Table II.

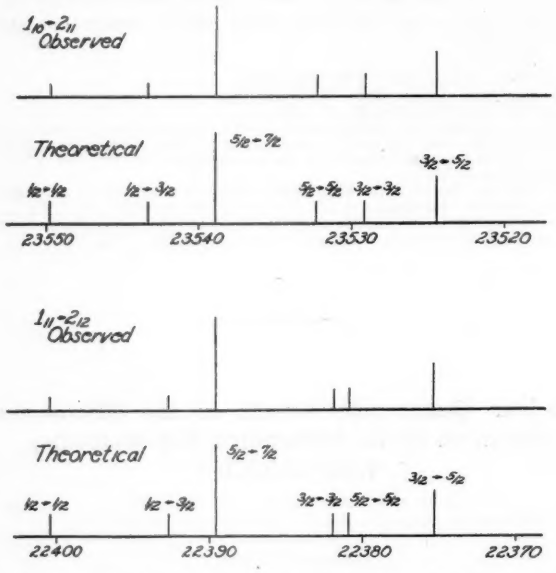

FIG. 1. Comparison of observed and calculated hyperfine structures.

A comparison of the observed hyperfine structures with those calculated from the values of χ_{aa} and χ_{bb} given in columns I and II of Table II is shown in Fig. 1. The indicated intensities are only approximate. The two weak components corresponding to $\Delta F=-1$ were not observed. Analysis of the structure of the $1_{01}\rightarrow 2_{02}$ transition gave a value of -57 ± 1 Mc for χ_{aa}, using for χ_{bb} the average given in Table II.

TABLE I. *K*-band spectrum and rotational constants of vinyl chloride.

Transition	$C_2H_3Cl^{35}$ Observed	$C_2H_3Cl^{35}$ Corr. for quad. effect	$C_2H_3Cl^{37}$ Observed	$C_2H_3Cl^{37}$ Corr. for quad. effect
$1_{01}\rightarrow 2_{02}$	22,946.9 Mc	22,945.7 Mc	22,485.9 Mc	22,485.0 Mc
$1_{10}\rightarrow 2_{11}$	23,538.9	23,535.6	23,055.0	23,052.4
$1_{11}\rightarrow 2_{12}$	22,369.6	22,366.2	21,930.2	21,927.5
B, Mc		6030.5		5903.7
C, Mc		5445.2		5341.3
κ		−0.9769		−0.9779

TABLE II. Values of the quadrupole coupling parameters χ_{aa} and χ_{bb}.

	I $1_{10}\rightarrow 2_{11}$	II $1_{11}\rightarrow 2_{12}$	III Average
χ_{aa} Mc	−57.6	−57.2	−57.4
χ_{bb} Mc	26.1	26.3	26.2

The value of χ_{zz}, the quadrupole coupling constant along the C−Cl bond calculated from the above data and assuming an axially symmetric bond is −62 Mc. However, the assumption of axial symmetry leads to an unreasonable angle of orientation of the bond in the principal axis system, and would, moreover, not be expected if appreciable double bond character is present. Alternately, the assumption that the C−Cl bond is a principal axis of the χ-dyadic, at an inclination of about 20° to the a axis, as determined from the moments of inertia, leads to a value of −67 Mc for χ_{zz}. The calculations indicate that the value of χ_{zz} probably lies between −62 and −70 Mc.

Acknowledgment is due to Professor E. Bright Wilson, Jr., for his encouragement and advice, and to Mr. Kenneth B. McAfee for his valuable assistance in resolving the hyperfine structures described above.

* This work was supported by the Navy Department through Contract N5ori-76, Task Order V, ONR.
** National Research Council Predoctoral Fellow.
*** Present address: Department of Chemistry, Cornell University, Ithaca, New York.

[1] J. K. Bragg, Phys. Rev. **74**, 533 (1948).
[2] P. C. Cross, R. M. Hainer, and G. W. King, J. Chem. Phys. **12**, 210 (1944).
[3] G. Herzberg, *Infrared and Raman Spectra* (D. Van Nostrand Company, Inc., New York, 1945), p. 50.

On the Decay of Isotropic Turbulence

S. CHANDRASEKHAR
Yerkes Observatory, University of Chicago, Williams Bay, Wisconsin
February 25, 1949

IN a recent paper Heisenberg[1] has discussed the decay of isotropic turbulence on the basis of the equation

$$-\frac{\partial}{\partial t}\int_0^k F(k,t)dk=2\left\{\frac{\mu}{\rho}+\kappa\int_k^\infty\left(\frac{F(k,t)}{k^3}\right)^{\frac{1}{2}}dk\right\}\int_0^k F(k,t)k^2dk, \quad (1)$$

where $F(k,t)$ represents the spectrum of turbulence at time t, μ the viscosity, ρ the density and κ a pure number of order unity. Heisenberg has pointed out that Eq. (1) admits solutions of the form

$$F(k,t)=t^{-\frac{1}{2}}f(k\sqrt{t}), \quad (2)$$

where $f(x)$ satisfies the integral equation

$$\int_0^x f(x)dx-\tfrac{1}{2}xf(x)=2\left\{\frac{\mu}{\rho}+\kappa\int_x^\infty\left(\frac{f(x)}{x^3}\right)^{\frac{1}{2}}dx\right\}\int_0^x f(x)x^2dx. \quad (3)$$

Heisenberg justifies the similarity hypothesis (2) on dimensional grounds.

Now from Eq. (3) it readily follows that

$$f(x)\rightarrow\text{constant}\times x \quad \text{as} \quad x\rightarrow 0. \quad (4)$$

Heisenberg, further, states that for $\mu=0$, $f(x)\sim$constant $\times x^{-5/3}$ (i.e., the stationary Kolmogoroff spectrum) for $x\rightarrow\infty$, and that for $\mu\rightarrow\infty$ (i.e., for small Reynolds numbers) $f(x)\rightarrow$constant$\times x^{-7}$ for $x\rightarrow\infty$. It does not seem that the latter statement concerning the solution of Eq. (3) is correct. For letting

$$g=\kappa^2x^3f(x) \quad \text{and} \quad y=\kappa^2\int_0^x f(x)x^2dx, \quad (5)$$

we can show that g as a function of y satisfies the second-order differential equation

$$g^{\frac{1}{2}}g''+2y(4+g')+2g^{\frac{1}{2}}(4-g')-8g=0, \quad (6)$$

where primes denote differentiation with respect to y.

The requirement that $f(x)\rightarrow$constant$\times x$ as $x\rightarrow 0$ now implies that $g(y)$ is tangential to the line $g=4y$ at $y=0$. From Eq. (6) it now follows that there is a one-parametric family of solutions which have this property: indeed, the asymptotic behavior of these solutions at the origin is given by

$$g=4y+y^{\frac{1}{2}}\left(a+\frac{4}{3}\log y\right)+O(y^2\log^2 y), \quad (7)$$

where a is an arbitrary constant. The constant a is related to μ/ρ of Eq. (3) by

$$\mu/c\rho=\tfrac{1}{6}-0.375a-\lim_{\substack{x\rightarrow 0\\ y\rightarrow 0}}\left(\int_x^\infty (g)^{\frac{1}{2}}\frac{dx}{x^2}+\tfrac{1}{2}\log y\right), \quad (8)$$

where c is a constant; also, in evaluating the integral on the

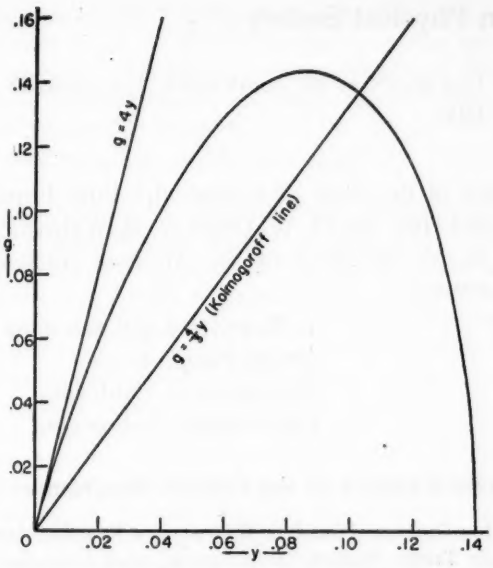

FIG. 1. The solution of Eq. (6) for the case $a=0$.

right-hand side the constant of integration in the equation (cf. Eq. (5))

$$\log x=\int^{y} dy/g(y)+\text{constant}, \tag{9}$$

is to be so adjusted that $y\to x^4$ as $x\to 0$. The limit on the right-hand side of Eq. (8) exists: the logarithmic divergence of the integral as $x\to 0$ exactly canceling the term $\frac{1}{4}\log y$.

The quantity $\mu/c\rho$ in Eq. (8) is essentially the reciprocal of the Reynolds number.

A discussion of Eq. (6) shows that the physical solutions which start tangentially to the line $g=4y$ have a single maximum and reach the y axis for a finite y with the behavior

$$g(y)\sim[6y_0(y-y_0)]^{\frac{1}{2}}. \tag{10}$$

A direct numerical integration of Eq. (6) illustrating this behavior of the solutions is shown in Fig. 1.

Since the solution curves cut the y axis for a finite y, it follows that the range of x is also finite and that there exists an $x_{\max}$ for which $f(x)=0$. This means that whenever the Reynolds number is finite, there is always a minimum size to the eddies, during the process of decay: and that this minimum size grows with time like $(t)^{\frac{1}{2}}$. However, when the Reynolds number becomes infinite this minimum size tends to zero. It would seem that in this latter case the solution curve becomes asymptotic to the Kolmogoroff line $g=4y/3$; for Eq. (6) admits a solution of the form $(y\to\infty)$,

$$g=(4/3)y[1+(8/7\sqrt{3})y^{-\frac{1}{2}}+4/63+O(y^{-1})]. \tag{11}$$

A more detailed discussion of Eq. (6) with tables of solutions, will be published elsewhere.

[1] W. Heisenberg, Proc. Roy. Soc. **A195**, 402 (1948).

Proceedings of the American Physical Society

MINUTES OF THE MEETING AT THE UNIVERSITY OF CALIFORNIA, AT BERKELEY, CALIFORNIA
FEBRUARY 3–5, 1949

THE 290th meeting of the American Physical Society was held at the University of California, Berkeley, on February 3–5, 1949. There were at least 200 members of the Society at the meeting, and the attendance at the various sessions varied up to a maximum of about 400. From the point of view of the number of papers presented, this was the largest meeting of the Society ever held on the Pacific Coast. The new University Cafeteria provided excellent service for luncheon and the local arrangements were excellent in every way. The various sessions were presided over by Professors R. T. Birge, R. B. Brode, J. W. Ellis, F. A. Jenkins, and J. Kaplan, of the University of California; Professors C. D. Anderson and W. A. Fowler of the California Institute of Technology, and Professor M. L. Pool of the Ohio State University.

The invited paper by Dr. Frederick Bedell was read by Professor R. T. Birge, because of the absence of Dr. Bedell. In addition to the invited papers which are listed below, it was possible to present all of the papers on the supplementary program, as well as three post-deadline papers. These were "Neutron-Proton Mass Difference from the $D-D$ Reactions" by F. A. Jenkins, A. V. Tollestrup, W. A. Fowler, and C. C. Lauritsen; "Quantization of Magnetic Flux," by L. Onsager of Yale University; and "Comparison of the Flow of Isotopically Pure Liquid He^3 and He^4," by D. W. Osborne, B. Weinstock, and B. M. Abraham of the Argonne National Laboratory.

J. KAPLAN, *Local Secretary for the Pacific Coast*
University of California,
Los Angeles, California.

Invited Papers on the General Programme

A New Concept of Catalytic Hydrocarbon Reactions from Isotopic Tracer Studies. OTTO BEECK, *Shell Development Company, Emeryville, California.* (40 min.)

Spectroscopic Determination of Molecular Structure. R. ROBERT BRATTAIN, *Shell Development Company, Emeryville, California.* (30 min.)

Nuclear Reactions Produced by High Energy Neutrons. G. F. CHEW AND M. L. GOLDBERGER, *Radiation Laboratory, University of California, Berkeley.* (30 min.)

Cloud-Chamber Analysis of the Particles Coming from Carbon when Bombarded by 90-Mev Neutrons. WILSON M. POWELL, *Radiation Laboratory, University of California, Berkeley.*

What Led to the Founding of the American Physical Society. FREDERICK BEDELL, *Pasadena, California.* (30 min.)

Recent Experimental Work at the Radiation Laboratory. ROBERT THORNTON, *Radiation Laboratory, University of California, Berkeley.* (30 min.)

Certain Principles Governing Mechanisms of Electrical Discharges Derived from Corona Studies. L. B. LOEB, *University of California, Berkeley.* (30 min.)

Contributed Papers

A1. Rupture Strength of Benzene.* J. J. DONOGHUE, E. GERJUOY, AND R. E. VOLLRATH, *University of Southern California.*—Observations have been made by the centrifuge method[1] of the rupture strength of outgassed samples of benzene sealed in Pyrex glass tubes. The equilibrium air pressure ranged from 1 to 10^{-5} cm Hg. In general, highly outgassed samples attained a strength so high that the tube was shattered by the shock of rupture. The maximum strength observed was 82 atmospheres. Increasing the equilibrium air pressure decreased the rupture strength and increased the variability. Very reproducible results have been obtained on some highly outgassed samples. The reproducibility is improved by careful temperature control.

* Work supported by the ONR.

[1] J. J. Donoghue, E. Gerjuoy, and R. E. Vollrath, Phys. Rev. 73, 538(A) (1948).

A2. Relative Electrodynamics. F. W. WARBURTON, *University of Redlands.*—The reciprocal force equation[1] with the choice of parameter $A=\frac{1}{2}$ describes an apparent transverse mass for an electron moving in a circular path. This value also predicts a magnetic moment of 0.001147 Bohr magneton for a stable tripole electron. As the force on any charge exerted by a moving electron is, on this basis, a function of the latter's velocity, an electrical conductor can be in mechanical equilibrium only when it is not electrostatically neutral. In copper, for example, one atom in three or four should lack an electron. This mechanism of unequal force of a high speed electron and a slower proton on a negative ion, and its prediction of thermal electron emission as well as its suggestions for cosmic-ray emission, are discussed. The propagation equations for the scalar and vector potentials, when developed on the relative basis, are less subjective than the Maxwell equations.

They involve the time derivative of the distance from the emitting dipole to the receiving electron, rather than the classical relative velocity of source and stationary observer. Plane wave solutions in the forms, $\phi_0(t+r/(c-v_r))$ and $\phi_0(t-r/(c+v_r))$, are studied.

[1] F. W. Warburton, Phys. Rev. **69**, 40 (1946).

A3. Quantum-Theory Restrictions on the General Theory of Relativity. M. F. M. OSBORNE, *Naval Research Laboratory, Washington, D. C.*—The limitations set by the uncertainty principle on the measurement of the curvature of space are determined by passing a small test particle around a geodesic triangle. In measuring the curvature of space around a Schwarzchild-solution particle of finite size and physically realized density, it is found that the mass must be at least of the order of 10^4 kilograms, or the curvatures cannot be measured with an accuracy equal to the order of magnitude of the terms in the defining equations $G_{ik}=0$. For smaller masses, the curvatures can only be measured with less accuracy and only over large regions of space. Similar limitations apply to alternative laws of gravitation involving higher derivatives of the metric. It is concluded that in any theory which attempts to unite quantum theory with the general theory of relativity, the relation of the metric to the energy momentum tensor, $G_{ik}-g_{ik}=-KT_{ik}$, must appear only in the large and in a statistical sense, i.e., for large regions of space and large numbers of elementary particles.

A4. A Method for Increasing the Safe Power Input of X-Ray Tubes. A. I. BERMAN, *Stanford University* (Introduced by P. H. Kirkpatrick).—A method for cooling x-ray tubes was devised, based on the moving target principle. The tube itself is gyrated without rotation about its axis, so that a point on the target describes a small circle. Simultaneously, the electron beam is deflected by a rotating magnetic field so that the focal spot rotates in synchronism with, but phased 180° from, the mechanical gyration. The strength of the field is adjusted until the circle which the focal spot traces on the target face equals the target circle. Thus the focal spot remains stationary in laboratory space while rotating on the face of the target. The advantages are (1) it is adaptable to most x-ray tubes with target face perpendicular to the tube axis, and target diameter twice that of the longest dimension of the focal spot, without any modification of tube design; (2) it permits anode cooling without the need for vacuum joints, making it especially useful for continuous operation. Tubes, operating continuously at high power for hours at a time at a gyrating frequency of 6 r.p.s., have been cooled successfully by this method without observable shifting of the focal spot in laboratory space.

A5. Betatron Injection. LEVERETT DAVIS, JR. AND R. V. LANGMUIR, *California Institute of Technology.*—The effect of inhomogeneities in the magnetic field on the radial oscillations of an electron in a betatron is considered by treating motion in a magnetic field that is constant in time but has arbitrary small space variations. The conditions that must be imposed in order that the electron not strike the injecting gun are considered and results bearing on the problem of high energy injection into a betatron, synchrotron, or race track are obtained. It is found that for n approximately $\frac{1}{4}$, a one percent variation in B and in n can change the amplitude of oscillation about the equilibrium orbit by as much as 20 percent, the exact magnitude and sign depending on the phase of the inhomogeneities relative to the position of the gun. There is also usually a tendency for the phase to shift quickly to the point where the amplitude increases and to remain there. Thus, in the absence of other effects injection will be difficult. For properly chosen inhomogeneities, and particularly for inhomogeneities that vary with time, a permanent damping that will assist injection can be produced. Similar but less pronounced effects are obtained for other values of n. This work was assisted by the joint program of the Office of Naval Research and the Atomic Energy Commission.

B3. Measurements of Cosmic-Ray Intensity at High Altitudes.* W. C. ROESCH, A. T. BIEHL, AND H. V. NEHER, *California Institute of Technology.*—During May-June of 1948, Geiger counter telescopes similar to those used previously[1] with balloons were flown in a B-29 airplane at 3.1 meters of water equivalent along approximately the 80°W geographic meridian over the geomagnetic latitude range 0° to 64°N. The following measurements were made: (1) the latitude effect in this range, (2) the east-west effect at a zenith angle of 45° in this range, (3) the north-south effect at high and low latitudes, (4) the zenith angle effect at high and low latitudes (the measurements 1–4 were made with 0, 10, and 20 cm of lead absorber), (5) the total intensity was measured with an electroscope, and (6) the latitude effect of wide showers was investigated. At a pressure of 2.35 meters of water equivalent near the geomagnetic equator an azimuth-zenith experiment was made. One of the chief results of these experiments is that there is approximately the same asymmetries in the hard and soft radiations. This makes it unnecessary to assume different primaries for the two components.

* This work was supported in part by the joint program of the ONR and the AEC.

[1] A. T. Biehl, R. A. Montgomery, H. V. Neher, W. H. Pickering, and W. C. Roesch, Rev. Mod. Phys. **20**, 360 (1948).

B4. Latitude Dependence of Cosmic Rays at 33,000 Feet.* A. T. BIEHL, H. V. NEHER, AND W. C. ROESCH, *California Institute of Technology.*—In a series of eight B-29 flights made from Inyokern, California, during the summer of 1948, continuous recordings of the total vertical cosmic-ray intensity were made as a function of latitude. All measurements were made on the 117° West meridian between the borders of Canada and Mexico, and all but one of the flights were made at an altitude of 33,000 feet. The apparatus consisted of two separate Geiger counter telescopes and associated apparatus as previously used by us[1] with slight modifications. The results of these flights indicate that north of about 51° North magnetic latitude the total vertical intensity of cosmic rays is constant. Data from comparable flights made on different days agreed with each other within the probable error at these northern latitudes. However, south of 51° North a definite decrease of from 5 to 6 percent was found to take place within a few degrees of latitude. South of this break, which occurred at latitudes varying from 51° North to 46° North, the vertical intensity was again constant for at least a few degrees. In two cases evidence was obtained for another

step of about the same magnitude at about 41° North. These curves will be presented and discussed.

* This work was supported in part by the joint program of the ONR and the AEC.

[1] A. T. Biehl, R. A. Montgomery, H. V. Neher, W. H. Pickering, and W. C. Roesch, Rev. Mod. Phys. 20, 353 (1948).

B5. Energy of Cosmic-Ray Particles from Ionization Chamber and Counter Telescope Data.* H. V. NEHER, *California Institute of Technology.*—It is well known that the area under the curve of ionization *vs.* depth gives the total energy incident on the top of the atmosphere. Similarly, the area under the curve beyond a given depth, h, gives the energy of all particles at that depth. This ignores energy given to hypothetical particles which never appears in the form of particles that ionize. In a similar way a counter telescope may be used to determine the total energy beyond a given depth provided the average specific ionization is known. Furthermore, the average energy of each ionizing particle may also be determined for any depth. Some of the assumptions and limitations entering into these calculations will be discussed. Application will be made to data taken at the geomagnetic equator and northern latitudes.

* This work was supported in part by the joint program of the ONR and the AEC.

B6. Extensive Penetrating Showers of Cosmic Rays. JOHN ISE, JR., *University of California, Berkeley.**—Experiments have been carried out at 3020 meters on the density spectrum of extensive cosmic-ray showers, both penetrating and non-penetrating, and on the penetrating power of the extensive penetrating showers. Threefold coincidences were observed between three trays of Geiger counters, of variable but equal area, arranged linearly with a separation of 4.8 meters, with various thicknesses of lead, ranging from 0 to 20 cm, over all counter trays. In all the shielded measurements, the lead thickness at sides and ends of the counter trays was 10 cm. The threefold coincidence rate per hour corrected for accidental coincidences is:

Area of counter trays	0 cm Pb	5 cm Pb	10 cm Pb	15 cm Pb	20 cm Pb
400 cm²	48.9±0.8	6.14±0.35	0.55±0.08		0.193±0.015
800 cm²	130 ±5				.588±0.033
1200 cm²	234 ±3	42.1 ±0.8	4.01±0.28	1.56±0.09	1.18 ±0.064

From these observations the frequency of occurrence of Auger showers with an average particle density of σ can be shown to be proportional to $\sigma^{-2.42\pm0.02}$. For extensive penetrating showers through 20 cm of Pb the corresponding relation is $\sigma^{-2.65\pm0.09}$.

* Assisted by the Joint Program of the ONR and the AEC.

B7. The Range Spectrum of Cosmic-Ray Mesotrons. LAWRENCE S. GERMAIN, *University of California, Berkeley.*—A counter-controlled cloud chamber has been used to investigate the differential range spectrum of mesotrons at sea level. The chamber is 16 inches in diameter, has an illuminated region 5 inches deep, and contains eight lead plates each 8 inches wide and ½ inch thick. A lead absorber of variable thickness, up to 27 inches, may be placed above the chamber. The number of mesotrons observed to stop in the chamber per unit time has been found for various thicknesses of absorber above the chamber. A plot of the counting rate of mesotrons which stop *versus* the thickness of absorber above the chamber reveals a broad low peak which has its maximum at a 6-inch thickness of absorber. The counting rate at the peak is 4.60×10^{-5} count/sec./sterad./g/cm² of air. The counting rate with no absorber above the chamber is 4.23×10^{-5} count/sec./sterad./g/cm² of air. The peak is not symmetric, falling off more rapidly on the side towards greater thicknesses of absorber. For large thicknesses of absorber, correction must be made for loss of particles due to scattering.

* Assisted by the Joint Program of the ONR and the AEC.

B8. Theoretical Values of Mass and Life-Time of Mesons. J. BARNÓTHY, *Barat College, Lake Forest, Illinois.*—Theoretical considerations* have led to the conclusion that electrons and protons can exist, beside their stable states, in different unstable states of short lifetime. The particles with lifetimes longer than 10^{-10} sec. are:

Mass in m_0		Lifetime in sec.	
212	(205±20 Powell)	$2.17\cdot10^{-6}$	($2.15\cdot10^{-6}$ Rossi)
3028.6		$(1.40\cdot10^{-8})$	
2726.7		$(6.07\cdot10^{-8})$	
2301.8		$(6.24\cdot10^{-9})$	
1396.2		$4.14\cdot10^{-9}$	
1018.2	(990±100 Leprince-Ringuet)	$1.57\cdot10^{-9}$	
718.5		$2.16\cdot10^{-10}$	
495.3		$4.34\cdot10^{-9}$	
335.7	(336±40 Powell)	$2.20\cdot10^{-8}$	($1.1\cdot10^{-8}$ Richardson)
223.8		$2.31\cdot10^{-10}$	
147.9		$3.33\cdot10^{-10}$	
97.0		$2.43\cdot10^{-10}$	
11.0	(11.4 Cowan)	$0.94\cdot10^{-9}$	

Several of these particles have already been observed experimentally as "mesons." A good agreement with the computed values could be stated in all cases where sufficiently exact determinations have been made.

* J. Barnothy, Zeits. f. Physik 120, 148 (1943); Papers of Terr. Magn. Hungary No. 2 (1947).

B9. Compton-Getting Effect of Cosmic Radiation. M. FORRÓ, *Barat College, Lake Forest, Illinois.*—Sidereal time periodicity of the hard component of cosmic radiation was measured over periods of two years with counter telescopes of small aperture, in different zenith angles and with different lead absorbers. The results furnish for the amplitudes of the Compton-Getting effect values up to one-half percent. The maximum is shifted toward later hours when the thickness of the absorber is increased. (The shift is 8 hours for every 20 cm Pb.) A linear connection can be stated between logarithm of the minimal energy of the radiation and the phase shift of the maximum. With the help of certain assumptions, it was possible to compute from this connection the time of rotation of the Milky Way to 234±10 million years, in agreement with the astronomically determined value.

C1. 10-Mev Magnetic Proton Spectrograph. SYLVAN RUBIN,* *California Institute of Technology.*—A large magnetic spectrograph of the double-focusing type[1] is now under construction. Heavy charged particles will be deflected on a 180° path of 16-in. mean radius in a field decreasing as $r^{-\frac{1}{2}}$. The gap is 2 in. between pole faces and 6 in. wide, containing a brass vacuum chamber, shaped to the contour of the pole faces. It will be connected to the target chamber and particle detector, both located outside the field. The solid angle for detection will be ~0.01 steradian. For maximum magnetic efficiency, the coils will be wound around the C-shaped poles, using $\frac{3}{8}''\times\frac{3}{32}''$ Formvar coated copper strip in 16 layers, water-cooled by 8 interleaved layers of copper tubing. 50,000 ampere turns will be obtained at 120 volts, dissipating 15 kw in the coils, giving a field of 10–11 kilogauss in the gap. The return flux path will be divided between the center and the rim, a 48-in. dia. semicircle. The magnetic field will be measured and calibrated by the same technique used on the present 2-Mev spectrograph[2] with the additional possibility of calibrating with natural alpha-groups.

* Now with Stanford Research Institute.
[1] Svartholm and Siegbahn, Arkiv f. Astro., Math., Fys. **33A**, No. 21 (1946).
[2] Snyder, Lauritsen, Fowler, and Rubin, Phys. Rev. **74**, 1564A (1948).

C2. Automatic Slit-Width Adjuster for an Infra-Red Spectrometer. H. O. MCMAHON, GILBERT W. KING, AND R. M. HAINER, *Arthur D. Little, Inc., Cambridge, Massachusetts.*—A mechanism adjusting slit widths to give the same energy on the detector at all wave numbers allows the actual record to be percent absorption directly in a single-beam instrument. Even if this is accomplished by double beams, or alternating the beam between sample and blank, this slit drive allows constant signal to noise and hence maximum resolution at all wave numbers. The slit width as a function of wave number depends on many variables, such as source temperature, detector sensitivity, which may be changed from time to time. Thus the basic element is a template which can be easily drawn, shaped, and replaced. This template is mounted on a carriage moved on rails by a punched steel tape driven directly from the shaft which rotates the Littrow mirror. The template, a $\frac{1}{4}''$ steel plate cut to shape, drives a rod vertically, whose motion is communicated by a steel tape through a pulley arrangement to the shaft which opens the slit jaws.

For NaCl a range of 18 to 1 in slit width can be achieved, to cover the range 3000 to 700 cm^{-1}. The template can be cut without difficulty to give no irregularities causing spurious noise, and to give a 100 percent curve flat within variations caused by source temperature and drift.

C3. Radiation Accompanying Meson Creation. L. I. SCHIFF, *Stanford University.*—The electromagnetic radiation that is produced during the creation of charged vector mesons in nucleon-nucleon encounters is investigated in order to determine if it can contribute appreciably to the soft component of cosmic radiation. Since there is, at present, no reliable theory of meson creation, the calculation is performed in analogy with the first method used by Knipp and Uhlenbeck[1] for treating the radiation accompanying beta-decay. Radiative transitions from a point-source or extended-source meson state to plane waves are computed with the help of Gunn's formalism.[2] Preliminary results indicate that the probability for emission of hard quanta by relativistic vector mesons is proportional to the product of the fine-structure constant and a power of the ratio of primary meson energy to rest energy; this is in contrast to the electron case, in which the power is replaced by a logarithm. Such radiation may therefore be of significance in cosmic radiation.

[1] J. K. Knipp and G. E. Uhlenbeck, Physica **3**, 425 (1936).
[2] J. C. Gunn, Proc. Roy. Soc. **A193**, 559 (1948).

C4. Decay Time of π-Meson. R. LATTER AND R. F. CHRISTY, *Kellogg Radiation Laboratory, California Institute of Technology.*—The lifetime for $\pi-\mu$-decay was computed assuming the Bethe-Marshak two-meson hypothesis (wherein π and μ are directly coupled) and taking the π a scalar, vector, or pseudoscalar from nuclear force theory, the μ a scalar, pseudoscalar, or spin $\frac{1}{2}$, from burst evidence, and the secondary neutral meson of the same character as the μ. Using all permissible combinations of these fields, using $\mu=212m$, $E_\mu=3.8$ Mev in the $\pi-\mu$-decay, and τ_μ for nuclear capture $\sim 3.3\times10^{-6}$ sec. for $Z=10$, the lifetimes found for a range of m_π from $274m$ to $350m$ are τ(pseudosc.→spin$\frac{1}{2}$)$\sim 0.3-2.1\times10^{-9}$ sec., τ(vector→scalar or pseudosc.)$\sim 1.1-1.4\times10^{-6}$ sec., τ(scalar→scalar or pseudosc.)$\sim 1.5-1.9\times10^{-8}$ sec., τ(vector→spin$\frac{1}{2}$)$\sim 0.3-4.0\times10^{-8}$ sec., and τ(scalar→spin$\frac{1}{2}$)$\sim 0.9-1.6\times10^{-8}$ sec. These numbers may be too high by a factor of 10 or too low by a factor of 3 because of the uncertainty in $g^2/\hbar c$ and by taking the nuclear matrix elements equal to Z. Instead of the Bethe-Marshak hypothesis it is possible to assume that the π and μ are coupled directly to nucleons but not to each other. Divergences in the $\pi-\mu$ decay calculation have prevented quantitative evaluation of this formulation. This work was assisted by the joint program of the Office of Naval Research and the Atomic Energy Commission.

C5. The Spins of the Mesons.* R. SERBER, *University of California, Berkeley.*—The meson mass measurements which show that the third particle involved in $\pi-\mu$ decay has zero mass lead us to seek a description of the phenomena without introducing any new particles. The spins of the mesons are then determined by the capture processes of μ^-- and π^--mesons: (1) $P+\mu^-\rightarrow N+\nu$ (ν=neutrino), (2) $P+\pi^-\rightarrow N$. The lack of stars in μ^- capture shows that a particle is emitted which carries off the energy. Since neither electrons nor γ-rays are emitted, this particle must be a neutrino. Since π^--capture does produce stars, an additional particle cannot be involved in (2). It follows that the μ has spin $\frac{1}{2}$, while the π has spin 0 or 1. The $\pi-\mu$-decay must be (3) $\pi\rightarrow\mu+\nu$. These reactions are not independent; (1) is a consequence of (2) and (3). The μ-decay takes the form (4) $\mu\rightarrow e+2\nu$, and one expects a continuous electron spectrum. Calculation shows that this spectrum is considerably concentrated towards the upper limit, which helps explain the conflicting experiments on this subject.

* The work described was sponsored by the AEC.

C6. A Theorem on Cross Sections. G. C. WICK, *University of California, Berkeley.*—An elementary generaliza-

tion is given of a known theorem connecting the total cross section σ with the imaginary part of the elastically scattered amplitude in the forward direction $ImF(0)$. The derivation holds for the collision between two particles with arbitrary spin interactions. $ImF(0)$ is written as a matrix $B(m,m')$ where $m=(m_1m_2)$ and $m'=(m_1'm_2')$ represent the spin quantum numbers of the colliding particles before and after the collision. The theorem states that: $\sigma=2\lambda\Sigma_m B(m_1m)/W$, where $W=\Sigma_m 1=(2I_1+1)(2I_2+1)$. It follows that the elastic cross section per unit solid angle in the forward direction is $\geq(\sigma/2\lambda)^2$, λ being the (relative) wave-length. A more detailed discussion of special cases will be presented.

C7. Thermodynamic Theory of the Magnetic Transition Curve of Superconductors. OTTO HALPERN, *University of Southern California, Los Angeles, California.*—The problem of the transition curve[1,2] of superconductors in a magnetic field is re-examined. The point of special interest is the small (or vanishing) heat of reaction for zero magnetic field. The difficulties[3] arising from this fact for the thermodynamic interpretation are discussed; it is proposed that the critical field H_c just below the field free transition temperature T_0 be given by the expression:

$$H_c=A(T_0-T)^{1\frac{1}{2}}+B(T_0-T)^{\frac{3}{2}}+\cdots.$$

Here A and B are constants determined by the heat of reaction and the discontinuity in the specific heats at T_0. Our relation is compared with Rutgers[1] formula, and experiment. The discussion is extended to very low temperatures.

[1] A. J. Rutgers, Physica 1, 1055 (1934).
[2] Gorter and Casimir, Physica 1, 306 (1939); Physik. Zeits. 35, 963 (1934).
[3] P. S. Epstein, *Textbook on Thermodynamics* (New York, 1937), pp. 357–359.

C8. Determination of the Rate of Biochemical Reactions.* C. A. TOBIAS, *University of California, Berkeley.*—The turnover of a number of elements in the plant or animal body may be regarded as a series of steady-state reactions. The time distribution of radioactive tracers introduced to the body, however, does not represent a steady state. If certain initial conditions are fulfilled when the tracer is administered, a set of first-order linear differential equations with constant coefficients may be written, describing the turnover of the tracer in the body, assuming n different states, exchange between each pair of states as well as between the states and an external reservoir. The solution may be obtained in terms of a sum of a set of n exponentially varying functions of time, the decay constants being the "eigenvalues" of the problem. In experiment one may actually observe the time dependence of the concentration of the radioactive tracer in each state. By analyzing such data into a sum of n exponential functions, one obtains the eigenvalues, and one may also calculate the turnover rate of the carrier element between all states. The method will be illustrated by examples from human iron metabolism, where such calculations led to the identification of a new intermediary.

* This work was carried out under the auspices of the AEC.

D3. Corona Studies in Nitrogen, Oxygen, and Mixtures.* CHARLES G. MILLER,** *University of California, Berkeley.*—D.c. corona studies have been carried out in concentric cylindrical systems covering the pressure range 715 mm to 27 mm in pure nitrogen, pure oxygen, and in mixtures. Self-sustaining corona discharges in pure nitrogen depend exclusively on γ at the cathode. In positive wire corona this leads to a discharge visible as *anode spots;* in negative wire corona this leads to disruptive currents if the nitrogen is quite pure. Self-sustaining positive corona in pure oxygen gives streamers at high pressures, burst pulses at low pressures, indicating high photon absorption and high photo-ionization in the gas; self-sustaining high current negative corona in oxygen depends on Trichel pulses. It is shown that the Trichel pulse onsets in oxygen and mixtures are not real thresholds set by a second Townsend coefficient. These negative thresholds depend on a preliminary Townsend discharge cleaning up the cathode, giving way to Trichel pulses as a second mode. It is shown that Trichel pulses in oxygen depend on O_3^-, while Trichel pulses in mixtures depend also on negative ions of nitrogen oxides. Comparison of the onset potentials, positive and negative, at various percentages of oxygen are made at various pressures, and throw some light on the relative importance of factors affecting corona thresholds.

* This work was supported in part by the Research Corporation.
** Now at the University of California, Santa Barbara College.

D4. Dust Electrostatics.* WULF KUNKEL, *University of California, Berkeley.*—Previous results with the Hopper-Laby method of analysis of blow electrified dusts indicated these to be groups of large aggregates of the ultimate grains. The unsatisfactory correlation of these aggregates with grain size observed by microscope on collector slides in the chamber led to instrumental refinements in observation of the smaller grains and elimination of minute convection currents. The smallest microscopically observed grains can now reliably be observed. In consequence it appears, as observed by rate of fall, that while the main *bulk by volume* of blown dusts always consists of larger aggregates, these are invariably and distinctly *outnumbered* by the ultimate grains in agreement with microscopic studies of the settled dusts gathered on microscope slides in the chamber. Earlier rate of fall results had been falsified by small upward and downward convection currents which had either eliminated small particles or made them appear larger by increased fall rates. Present data show the small particles to carry relatively smaller charges than previously found on the larger aggregates. The latter have not been restudied since refinement. No sign preference has been detected to date using homogeneous dusts on surfaces of the same material.

* This work is being carried on under an ONR contract.

D5. Purification and Comparison of Some Organic Phosphors for Scintillation Counters.* JOHN W. IRVINE, JR. AND RAYMOND C. SANGSTER, *Massachusetts Institute of Technology.*—Naphthalene, anthracene, phenanthrene, and other aromatic hydrocarbons are purified by passing their hexane or benzene solutions through a heated column of activated alumina. Using an RCA 1P28 at room temperature as a detector and Co^{60} gamma-rays for excitation, the different phosphors are compared under identical conditions. With the test arrangement used a plot of log

counting rate *vs.* discriminator voltage gives a straight line over a 40-volt range. This curve can be described by specifying the ordinate intercept (I) and slope (voltage to reduce counting rate to one-half).

	$I\times10^{-4}$	$V_{\frac{1}{2}}$
Naphthalene (Bakers C.P.)	2.2	1.7
Naphthalene (Al_2O_3 purified)	3.4	2.1
Anthracene (melted in air)	1.0	4.0
Anthracene (melted in N_2)	1.0	6.0
Phenanthrene (Al_2O_3 purified)	1.7	3.0
Stilbene (EKC)	1.9	3.3
1 percent anthracene in naphthalene	3.3	5.3
1 percent phenanthrene in naphthalene	4.5	2.1

The purity of a phosphor has a marked effect on its performance.

* Assisted by the joint program of the ONR and the AEC.

D6. Life Tests on Self-Quenching Geiger-Mueller Tubes with Halogen and Polyatomic Gases as Quenching Agents. F. W. BROWN III, P. J. HARRIS, AND A. L. KLEIN, *Naval Radiological Defense Laboratory.*—Several tubes have been filled with argon as a counting gas, and ethyl alcohol, ethylene,[1] amyl acetate, or 1-butene as the quenching gas. These tubes were counted at a rate of about 3000 counts/second and the plateaus were measured at selected intervals. The lifetimes were 2.2×10^9 for ethyl alcohol, 3×10^9 for ethylene, 1.3×10^{10} for amyl acetate, and 1.4×10^{10} total count for 1-butene. Mass spectrographic analyses have been completed giving the breakdown products of the quenching gases. Tubes have been filled with a mixture of neon and argon as the counting gas, and chlorine[2] as the quenching agent. These tubes have been counted at a rate of 6000 counts/second and are giving good results after having counted 3.5×10^{10} counts. Indications are that their lifetime is limited only by absorption or by chemical removal of the chlorine.

[1] K. H. Morganstern, C. L. Cowan, and A. L. Hughes, Phys. Rev. **74**, 499 (1948).
[2] S. H. Liebson and H. Friedman, Rev. Sci. Inst. **19**, 303 (1948).

D7. Effects of Temperature on Naphthalene and Anthracene Scintillation Counters. G. E. KOCH AND J. D. GRAVES, *Naval Radiological Defense Laboratory.*—The temperature dependence of the particulate gamma-counting efficiency of naphthalene and anthracene scintillation counters has been investigated in the regions between −80°C and +50°C. All pulses occurring above a fixed level determined by the noise level of the 931A photo-multipliers at the maximum temperature encountered (+50°C) were counted directly by a commercial scaler. The time required for a fixed number of counts was observed to be about twofold for naphthalene and fourfold for anthracene. The temperature and counting rate for the end point, and the maxima and minima of the curve for naphthalene and anthracene are shown in the table using arbitrary counting rate scales of 10.

Temperature	Counting rate in naphthalene	Counting rate in anthracene
−80°C	8	4.5
−30°C	4.5 (minimum)	—
+10°C	10 (maximum)	10 (maximum)
+50°C	8.5	2.5

D8. A Laboratory Alpha-Scintillation Counter. J. D. GRAVES AND J. P. DYSON, *Naval Radiological Defense Laboratory.*—A reliable, wide-range alpha-scintillation counter has been developed for use with small samples. It utilizes the 931A photo-multiplier, a commercial ZnS phosphor, and a commercial scaler and power supply. For 4–5 Mev α from a sample up to $\frac{1}{4}$ inch in diameter, 100 percent efficiency is observed with 40 percent geometry. This efficiency remains constant over a wide range of phosphor thickness and temperature. With discrimination at the photo-multiplier noise level, a background count of about 10 counts per hour is observed. The resolving time is less than 1 microsecond. For continuous counting, however, the upper counting rate is limited by fatigue of the tube rather than the resolving time. A light lock is required for sample changing caused by the phosphorescence resulting from the exposure of the phosphor to daylight. The counter is insensitive to changes in humidity and pressure, and tube voltage over a wide range, and is free from microphonic effects.

D9. Optical Method for Improving the Counting Efficiency of Scintillation Counters. R. H. DAVIS AND J. D. GRAVES, *Naval Radiological Defense Laboratory.*—Optical methods of increasing the counting efficiency of scintillation counters by increasing the field of view have been studied. With extended phosphors, the photo-cathode only normally "sees" a small fraction of the scintillations. For truncated Lucite cones, it was found that the detection efficiency increased as the angle of the cone was made smaller. Consequently, various diameters and lengths of cylindrical glass tubing, provided with a reflecting coating, were tested using an extended 5-Mev α *ZnS:Ag* scintillation source. It was found that the maximum counting rate when using the glass tubes was about 20 percent greater than that when using the direct field of view. The dimensions of the glass tube for maximum counting rate occurred when the length was $\frac{1}{2}$″ long and 2″ diameter for a 931A tube. For the direct field of view the greatest counting rate occurred when the position of the phosphor screen was as close as possible to the 931A photo-multiplier. In this position the tube could see a circular area about $\frac{3}{4}$″ in diameter. Consequently, this system gives about a sevenfold increase in area of detection as well as a 20 percent increase in counting efficiency.

D10. The Chi Square Test as a Criterion for Testing Halogen-Filled Geiger Tubes. A. B. WILLOUGHBY, *Naval Radiological Defense Laboratory* (Introduced by Richard I. Condit).—In the past the maximum acceptable plateau slope for organic quenched Geiger tubes has been about five percent. The newly developed halogen quenched tubes have an inherent slope of about six percent or more. Since the latter tubes appear to have an infinite life, it was decided to re-examine the criterion for acceptance of tubes. As a basis for a new criterion, the fact will be used that a good Geiger tube yields an output of counts per unit time that has a Poisson distribution. It is proposed that all tubes be statistically tested using the Chi Square Test to ascertain whether they give this Poisson distribution. If they do, they are accepted. In applying this test at various points along the plateau slope of a number of halogen-quenched tubes, it was found that the tubes passed the

test for quite high values of ρ (at least $\rho=1.5$) where ρ is defined as the ratio of the counting rate at any voltage E to the counting rate at threshold. A Geiger tube which passes the Chi Square Test at the highest operating voltage was found always to pass it at any lower voltage. Thus the proposed criterion for accepting a halogen-quenched Geiger tube reduces to whether or not it passes the Chi Square Test at its highest operating voltage.

E1. Converter Thickness Corrections in Gamma-Ray Spectroscopy.* T. LAURITSEN AND W. F. HORNYAK, *Kellogg Radiation Laboratory, California Institute of Technology.*—The effect of converter thickness on the location of the photo-electron peak for γ-radiation converted in thorium foils has been studied, using a lens-type spectrometer. Spectrometer resolutions of 1.5 percent and 3.0 percent were used, with foils ranging in thickness from 7 to 150 mg/cm^2, and γ-rays ranging in energy from 0.4 to 3.1 Mev. For γ-ray standards the 2.620-Mev radiation from ThD, the 411.1-kev radiation from Au^{198}, and the annihilation radiation from N^{13} were used. The γ-radiations from Co^{60} and the reactions $Be^9(d,n)B^{10*}$ and $C^{12}(d,p)C^{13*}$ were used as auxiliary sources. The F, I, and X internally converted lines from atomic layer deposits of ThB were used as mono-energetic electron sources. For the higher instrument resolution, the high energy extrapolated edge was found to be largely independent of converter thickness at all γ-ray energies. At low energies and for saturation thicknesses, the shift in the location of the photo-line peak is proportional to the absolute resolution, while at high energies and thicknesses small compared to the saturation thickness, the shift is just the most probable collision energy loss in half the converter thickness. A semiempirical expression has been developed to give the shift as a function of γ-ray energy, resolution, and converter thickness.

* This work was assisted by the joint program of the ONR and the AEC.

E2. The Beta-Decay Spectra of B^{12} and Li^8.* W. F. HORNYAK AND T. LAURITSEN, *Kellogg Radiation Laboratory, California Institute of Technology.*—The β-spectrum of Li^8 has been calculated from the Fermi theory of β-decay using as the density of states available in Be^8, the α-particle spectrum resulting from its subsequent break up.[1] A comparison of this predicted spectrum with the experimental one obtained at this laboratory[2] indicates close agreement above an electron kinetic energy of 6.0 Mev and gives a Li^8-2He^4 mass difference of 15.9 ± 0.1 Mev. The deviation of the observed spectrum from the predicted spectrum below 6.0 Mev can be taken to indicate that about 10 percent of the disintegrations go to narrow states in Be^8, at 9.7 ± 0.3 and $\sim$13 Mev, which do not decay by α-particle emission. It is estimated that less than 2 percent of the β-decay is to the ground state of Be^8 and less than 5 percent to the gamma-ray emitting state at 4.8 Mev, the majority of transitions being accounted for by a broad state at $\sim$3 Mev. The Kurie plot of the B^{12} β-spectrum[3] is linear from an electron kinetic energy of 6.0 Mev to the end point. The end point of 13.43 ± 0.06 Mev when combined with the mass of C^{12} gives 12.01827 ± 0.00009 a.m.u. for the mass of B^{12}. If 5 percent of the β-decay is assumed to go to a narrow level in C^{12} at 7.1 ± 0.5 Mev and possibly a broad or composite level at $\sim$11. Mev, the observed non-linearity of the Kurie plot below 6 Mev can be accounted for. A decay of 5 percent or less to the 4.3-Mev level in C^{12} cannot be excluded.

* This work was assisted by the joint program of the ONR and the AEC.
[1] Bonner, Evans, Malich, and Risser, Phys. Rev. 73, 885 (1948).
[2] W. F. Hornyak and T. Lauritsen, Phys. Rev., to be published.
[3] E. R. Cohen and W. F. Hornyak, Phys. Rev. 72, 1127 (1947).

E3. Gamma-Radiation and Nuclear Pairs from $F^{19}+p$.* V. K. RASMUSSEN, W. F. HORNYAK, AND T. LAURITSEN, *Kellogg Radiation Laboratory, California Institute of Technology.*—The reaction $F^{19}(p,\alpha)O^{16*}$ leaves O^{16} in an excited state at about 6 Mev[1] which can decay only by the emission of positron-electron pairs, as well as in two other states yielding gamma-rays of 6.1 and 7.0 Mev, respectively.[2] The radiation from these three states has been studied in some detail, using a magnetic lens spectrometer to measure the energy spectra of the nuclear pairs and of the secondary electrons from the γ-rays. The pair spectrum is found to extend to an upper energy limit of 5.04 ± 0.04 Mev, and the distribution of both positive and negative particles corresponds closely with theoretical expectations above $\sim$2 Mev.** Compton electrons from the γ-rays were examined at bombarding energies of 873, 939, 1352, and 1379 kev corresponding to known resonances, using thin CaF_2 targets and Be converters. A fit to the observed data by shapes calculated from the Klein Nishima formula taking into account the effects of spectrometer geometry and of energy loss in the converter yielded mean values of 6.16 ± 0.04 and 7.06 ± 0.06 for the γ-ray energies, in good agreement with the values 6.13 ± 0.06 and 6.98 ± 0.07 given by Walker and McDaniel.[2] The observed intensity ratios (6 Mev/7 Mev) are 2.5, 3.3, 1, and 4.7, respectively, at the four resonances.

* This work was assisted by the joint program of the ONR and the AEC.
[1] W. F. Hornyak and T. Lauritsen, Rev. Mod. Phys. 20, 191 (1948).
[2] R. L. Walker and B. D. McDaniel, Phys. Rev. 74, 315 (1948).
** We are indebted to Mr. E. R. Cohen for these calculations.

E4. Cross Sections for $C^{12}(p\gamma)$ and $N^{14}(p\gamma)$ Reactions at low Energy.* E. J. WOODBURY, R. N. HALL,** AND W. A. FOWLER, *Kellogg Radiation Laboratory, California Institute of Technology.*—Cross-section measurements for the reaction $C^{12}(p\gamma,\beta^+)C^{13}$ previously reported[1] have been confirmed. Four thick graphite yield determinations at 128-kev bombarding energy gave 7.1 ± 0.6, 7.3 ± 2.7, 8.0 ± 2.4, and 9.2 ± 0.7 positrons per minute per one-hundred microcoulombs with a counting efficiency of 26 percent. The cross section is calculated to be $8.5\pm1\times10^{-10}$ barn. The cross section decreases rapidly with decreasing bombarding energy in a manner consistent with barrier penetration factors and is equal to 10^{-10} barn at 95 kev. A sufficient number of positrons have been counted to give a rough determination of the half-life as 8 ± 2 minutes. The reaction $N^{14}(p\gamma,\beta^+)N^{15}$ has also been studied at 128 kev using a thick target of titanium nitride which showed no appreciable deterioration under extensive bombardment. The cross section was found to be $\sim7\times10^{-10}$ barn but this must be considered to be a lower limit because of the possibility of the escape of O^{15} from the target. These measurements indicate that at stellar temperatures the

nitrogen reaction rate is approximately 1/35 that of the carbon reaction rate giving an abundance ratio $N^{14}:C^{12}$ ~35:1. As this differs from the roughly equal abundances observed for nitrogen and carbon by Aller and Unsöld in hot stars, the problem of the O^{15} escape must be investigated more throughly. However, preliminary yield measurements under somewhat more satisfactory conditions at the first observable nitrogen resonance (277 kev) indicate a radiation width of about 0.01 ev which is only 2 percent of that at the first carbon resonance.

* This work was assisted by the joint program of the ONR and the AEC.
** Now at the General Electric Company, Schenectady, New York.
[1] W. A. Fowler and R. N. Hall, Phys. Rev. 74, 1558A (1948).

E5. The Scattering of Protons by Lithium.* W. A. FOWLER, C. C. LAURITSEN, AND S. RUBIN,** *Kellogg Radiation Laboratory, California Institute of Technology.*—The cross section for the elastic scattering of protons by Li^7 has been measured over the range of bombarding energies from 250 to 1350 kev at angles of 81.1° and 137.8° in laboratory coordinates. Thick layers of natural lithium deposited in vacuum have been employed as targets. A double-focussing magnetic spectrometer was employed to analyze the energy of the scattered particles. In this way it was possible to measure the number of protons scattered from thin layers (~3-kev stopping power) of the target and to separate those scattered by Li^7 from those scattered by Li^6. At both scattering angles the observed cross section agrees approximately with Rutherford scattering except at 440 kev and 1020 kev. The anomaly at 440 kev is associated with the narrow resonance in the $Li^7(p\gamma)$ reaction. The maximum ratios to Rutherford scattering are 2.36 at 137.8° and 1.60 at 81.1°. The anomaly at 1020 kev is associated with a broad resonance in the inelastic scattering of protons by Li^7. The maximum elastic scattering cross sections are 1.41 barns at 81.1° and 1.22 barns at 137.8° while the maximum in the inelastic scattering as measured both by the number of protons and the intensity of the subsequent gamma radiation is 0.07 barn.

* This work was assisted by the joint program of the ONR and the AEC.
** Now at the Stanford Research Institute, Los Angeles, California.

E6. The Disintegration Energy of Be^8.* A. V. TOLLESTRUP, C. C. LAURITSEN, AND W. A. FOWLER, *Kellogg Radiation Laboratory, California Institute of Technology.*—Bombardment of Be^9 by protons leads to the reactions (1) $Be^9(p,d)Be^8$ and (2) $Be^9(p,\alpha)Li^6$. The residual Be^8 is unstable to disintegration into two α-particles. The recoil of the Be^8 nucleus leads to a continuous energy distribution of the resulting α-particles. The Q of the deuteron reaction and the end point of the Be^8 α-spectrum can be measured and thereby the amount of energy by which Be^8 is unstable can be calculated. A double focusing magnetic spectrometer has been used to separate the particles of the above two reactions and to measure accurately their energies. The particles were detected with a scintillation counter essentially of the type described in the references below.[1,2] The residual nucleus Li^6 in the doubly ionized state slightly overlaps in momentum the doubly ionized Be^8 decay alphas, because of energy loss in the beryllium foil. Therefore, it was necessary to supplement magnetic analysis by the use of stopping foils. This was also necessary in the second reaction since the doubly charged Li^6 ions and the accompanying doubly charged α-particles have nearly the same momentum. The results of the analysis are: $Q_1=555\pm3$ kev, $Q_2=2117\pm11$ kev, and Be^8 is unstable by 84.5 ± 10 kev.

* This work was assisted by the joint program of the ONR and the AEC.
[1] Marshall, Coltman, and Bennett, Rev. Sci. Inst. 19, 744 (1948).
[2] A. V. Tollestrup, Phys. Rev. 74, 1561 (1948).

E7. Beryllium-Proton Reactions and Scattering.* R. G. THOMAS, W. A. FOWLER, AND C. C. LAURITSEN, *Kellogg Radiation Laboratory, California Institute of Technology.*—The cross sections of the reactions $Be^9(p,d)Be^8$, $Be^9(p,\alpha)Li^6$, and $Be^9(p,p)Be^9$ have been remeasured[1] at 138° in the range of bombarding energies from 250 to 1300 kev using a high resolution double-focusing magnetic spectrograph[2] for reaction particle analysis. Detection was by means of an ionization chamber, and pulse size discrimination was necessary to discriminate deuterons and alpha-particles at low energies where their curvature in the magnetic field is the same. The proton scattering cross section shows prominent anomalies at 330, 988, and 1077 kev corresponding to $Be^9(p,\gamma)B^{10}$ resonances.[3-5] Over the 988-kev resonance the ratio to Rutherford scattering varies from 0.8 at 920 to 5.1 at 1030 kev. The alpha-particle reaction shows resonance or interference effects at 330 and 988 kev. The deuteron reaction shows resonance or interference effects at 330, 440, and 988 kev. The maximum cross sections for these reactions are 0.3 and 0.4 barn, respectively at 330 kev.

* This work was assisted by the joint program of the ONR and the AEC.
[1] R. G. Thomas, W. A. Fowler, and C. C. Lauritsen, Phys. Rev. 73, 536 (1948).
[2] Snyder, Lauritsen, Fowler, and Rubin, Phys. Rev. 74, 1564 (1948).
[3] C. C. Lauritsen, T. Lauritsen, and W. A. Fowler, Phys. Rev. 72, 739 (1947).
[4] Curran, Dee, and Petrzilka, Proc. Roy. Soc. 169, 269 (1939).
[5] Hole, Holtsmark, and Tangen, Naturwiss. 28, 335 (1940).

E8. Proton Scattering by Li^7 and Be^9.* E. RICHARD COHEN, *California Institute of Technology.*—Proton scattering resonances reported in an accompanying abstract by Lauritsen *et al.*, have been analyzed for the purpose of determining the angular momentum of the compound nucleus and the relative orbital momentum of the protons.

In the reaction $Be^9(p,p)Be^9$ there is a broad resonance at 988 kev which we ascribe to incident s-wave protons forming a compound B^{10} nucleus with $J=2$. With the usual assignment of odd parity to Be^9 and even parity to the ground state of B^{10}, the observed γ-ray is electric dipole (spin of $B^{10}=3$). For an adequate description it has been necessary to include a nuclear potential scattering for the s-waves. Other choices, considering incident s-wave and $J=1$ or incident p-wave and $J=0, \cdots, 3$ have been tried and excluded. The narrow resonance at 1084 kev has been ascribed to incident p-wave and $J=0$.

In Li^7 the well-known 440-kev resonance has been ascribed to incident p-wave forming a compound Be^8 with $J=1$. The resonance at 1020 kev is not inconsistent with an assignment to incident s-waves forming a compound nucleus with $J=1$ but the presence of a broad resonance at higher bombarding energies precludes a detailed agreement.

* This work was assisted by the joint program of the ONR and the AEC.

E9. Angular Distribution of γ-Rays from Lithium.* R. F. CHRISTY, *Kellogg Radiation Laboratory, California Institute of Technology.*—Recent work in this laboratory analyzed by E. R. Cohen[1] suggests that the 440-kev resonance in Li is due to p-wave protons. This, combined with the recent discovery of Devons and Hine[2] that the resonant and non-resonant γ-rays are of different parity requires the non-resonant γ-rays to be due to s-wave protons. Indeed, the intensity of non-resonant γ's is much too great to suppose they are in competition with the p-wave α-reaction. However, the resonant γ-ray going to $J=0$ in Be^8 will then be distributed as $1+0.7\cos^2\theta$. The apparent symmetry of the resonant γ's is then only understandable if the mixture of 17- and 14-Mev γ's results in approximate symmetry which requires that the ground state of Be^8 have $J=2$ and that the 17-Mev γ be an appropriate mixture of electric quadrupole and magnetic dipole. The ratio of 17- to 14-Mev radiation which is 2:1 forward would then be 4:1 at 90°.

* This work was assisted by the joint program of the ONR and the AEC.
[1] See accompanying abstract.
[2] S. Devons and M. G. N. Hine, Phys. Rev. **74**, 976 (1948).

E10. Relative Magnetic Moments of H^1 and H^2. E. C. LEVINTHAL, *Stanford University, Stanford, California.**—A careful re-examination of the relative moments of proton and deuteron has been made. The results lie within the error first reported.[1] While the essence of the method has been unchanged, the technique of observing has been considerably improved. The different line shapes of the proton and deuteron signals has been understood in terms of the relaxation time and spin. Because of these different line shapes it was important that the symmetry of the separate and superimposed signals be carefully determined. The symmetrical signals were obtained by a systematic way of introducing "leakage"[2] of the correct phase. The success of this procedure was verified by careful photographic analysis of the signals. From the separate symmetric signals of proton and deuteron a series of superimposed signals were calculated for a set of values of Δ, the beat frequency of the proton master oscillator and the deuteron transmittor, $(\Delta=\nu_1/6-\nu_2)$. These calculated curves were then compared with the actual photographs of the superimposed curves to give the results.

* Work supported by grants from the ONR and The Research Corporation.
[1] F. Bloch, E. C. Levinthal, and M. E. Packard, Phys. Rev. **72**, 1125–1126 (1947).
[2] F. Bloch, Phys. Rev. **70**, 473 (1946).

F1. Cross Sections for the Reaction $T^3(d,n)He^4$ from 1 to 2.5 Mev and its Use as a Neutron Source. R. F. TASCHEK, A. HEMMENDINGER, AND G. A. JARVIS, *Los Alamos Scientific Laboratory.*—Earlier workers[1,2] accelerating tritons have shown that this reaction has a broad resonance centered near 200-kev triton energy and have made measurements to an equivalent deuteron energy of 600 kev. The present measurements are at deuteron energies of 1.0, 1.5, 2.0, and 2.5 Mev, accelerated onto gaseous tritium targets. The differential cross sections between 45° and 135° were measured by observing the alpha-particles from the reaction. Tentative total cross sections are obtained by integration of a function fitting the observations. The techniques used for handling the small quantities of gas and the small gas target will be described. Experience with the reaction as a strong source of monoergic neutrons of 14 Mev when the target is thick, and as a source of variable energy neutrons from 13 to 18.5 Mev when the target is thin will be discussed. The method used for measuring absolute neutron cross sections in the latter energy range by simultaneous observation of the alphas will be given.

[1] Bretscher and French—LA581 and LA582.
[2] Baker, Holloway, Schreiber, and King—LAMS11.

F2. Excitation Functions for (α,n), (α,2n), (α,3n) Reactions on Indium. G. M. TEMMER,* *University of California, Berkeley.*—Excitation curves have been obtained by means of a magnetic lens beta-ray spectrometer for Sb^{118}, Sb^{117}, and Sb^{116} activities; they were produced by alpha-particle bombardment of stacks of metallic indium foils in the Berkeley 60-inch cyclotron with energies up to 37 Mev. The spectrometer built by R. W. Hayward was used because of the difficulty of resolution of the three periods concerned. The 5.1-hour period previously assigned to Sb^{118} [1] was followed by means of a partially converted gamma-ray of 260 kev. The 2.8-hour activity[1] has definitely been assigned to Sb^{117} by the nature of its excitation and contains a highly converted 156-kev gamma-ray, but apparently no positrons. Finally a 60-minute half-life has been found by Calutron analysis and by chemical separation to belong to a new antimony isotope of mass number 116. The latter is found to emit 1.45-Mev positrons as well as a gamma-ray of about 700 kev. The (α,n) process has a threshold at about 13 Mev and rises to a maximum at around 20 Mev. The $(\alpha,2n)$-process sets in at approximately 18 Mev and reaches its peak at about 28 Mev. The $(\alpha,3n)$ reaction starts in the neighborhood of 27 Mev and still rises at the highest beam energy investigated.

* Atomic Energy Commission Predoctoral Fellow.
[1] K. D. Coleman and M. L. Pool, Phys. Rev. **72**, 1070 (1947).

F3. Radioactive Isotopes of Rh and Pd. D. T. EGGEN AND M. L. POOL, *The Ohio State University.*—Two new isotopes have been found following cyclotron bombardments of Ru. A 32-minute positron activity has been made by Ru p and Ru d bombardments. Gamma-rays and 1.65-Mev positrons were observed. A 5-hour Rh activity has been produced by $Ru(p,n)$ and $Ru(\alpha,p)$ reactions which decays by emitting x-rays, 0.6-Mev positrons, gamma-rays, and some electrons. Ru K x-rays have been photographed with a curved crystal camera during the decay of the 21-hour Rh^{100} activity. The 21-hour activity also decays by emitting a 1.55-Mev gamma-ray and 25 percent of the time by 1.3-Mev positron emission. The 9-hour Pd^{101} has been made by alpha-bombardment of Ru and decays by emitting a 0.53-Mev positron about 10 percent of the time and by K-electron capture to a 4.7-day Rh activity. The 4.7-day activity, also produced by $Ru(p,n)$ and $Ru(\alpha,p)$ reactions, decays by K-electron capture, as seen by x-ray photographs, and the emission of 80- and 130-kev gamma-rays, as determined by electron photographs of the internally converted gammas. Equal bombardments with alpha-particles show that the 2.8-day Ru^{97} is produced from $Mo^{94}O_3$ and $Mo^{95}O_3$* by (α,n) and

$(\alpha,2n)$ reactions, respectively, with a relative cross section of 45:1.

* Supplied by the Y-12 plant, Carbide and Carbon Chemicals Corporation through the Isotope Division, U. S. Atomic Energy Commission, Oak Ridge, Tennessee.

F4. Radioactive Silver Isotopes Produced by Photodisintegration of Cadmium.* R. B. DUFFIELD AND J. D. KNIGHT, *University of Illinois.*—We have observed that several radioactive silver isotopes are produced when cadmium is irradiated with 20-Mev betatron x-rays. Two of these are well-known isotopes, 7.6-day Ag^{111} and 3.2-hour Ag^{112}. In addition we have found that two other periods, 5.3 hours and 20 minutes, are produced in comparable yield. By the use of a sample enriched in Cd^{114} it has been found that the 5.3-hour activity is to be assigned to Ag^{113}. It decays by the emission of 2.0±0.2-Mev beta-rays. Similarly, using a sample enriched in Cd^{116}, the 20-minute period has been assigned to Ag^{115}. It decays by the emission of 3.0±0.2-Mev beta-rays. No gamma-rays have been observed in either case. It has recently been reported that isotopes of similar half-lives and beta-ray energies have been observed among the uranium fission products.[1,2]

* Assisted by the joint program of the ONR and AEC.
[1] W. Seelman-Eggebert and F. Strassman, Zeits. f. Naturforschung **2a**, 80 (1947).
[2] A. Turkevich, Plutonium Project Report ANL-4010 quoted by Seaborg and Perlman in UCRL Report No. 179, dated August 1948.

F5. Angular Distribution of 14-Mev Neutrons Scattered by Deuterons. J. H. COON, R. F. TASCHEK, AND S. G. FORBES, *Los Alamos Scientific Laboratory.*—Monoergic 14-Mev neutrons produced by bombarding a thick tritium target with 220-kev deuterons have been scattered from deuterium in a thin heavy wax radiator and the resulting deuteron recoils counted in double and triple coincidence as a function of scattering angle. Measurements with different gas pressures, counter geometries, and an absorbing foil show that there are no disintegration protons of energies greater than about 3.0 Mev to within about 5 percent of the number of particles observed between 0° and 90° in the laboratory system; the 5 percent observed could be accounted for by ordinary hydrogen contamination recoils. The distribution in number of recoil deuterons per unit solid angle has been measured at seven angles ranging from 0° to 55° in the laboratory system. The laboratory distribution with 7° geometrical resolution shows a rapid drop by a factor of 7 in going from 0° to 30° and a less rapid rise in going from 30° to beyond 55°. A geometrical resolution of 3.5° shows that the factor between 0° and 30° is greater than 7. The center of mass angular distribution will be shown.

F6. Neutron-Proton Scattering.* R. CHRISTIAN AND E. W. HART, *University of California, Berkeley.*—We have calculated the $n-p$ scattering including tensor forces for various potentials. The small angular asymmetry in the 90-Mev experiments[1] indicates that at least 95 percent of the total cross section comes from the S and D states. This necessitates an exchange factor of the form $(1-a+aP_x)$ with a $\sim\frac{1}{2}$. (The more usual "charged" and "symmetrical" dependence are unacceptable.) The best fit is obtained with the meson potential with range 1.25±0.10 $\times10^{-13}$ cm and $a=0.50$–0.55. There is little distinction between the meson, gauss and exponential potentials, all of which overestimate the high energy cross section by 20 percent. The central force square well gives lower cross sections; however, the introduction of tensor forces increases the scattering at 90 degrees to such an extent that the total is also too high. Scattering from the meson potential including tensor forces is only slightly different from that of the corresponding central case. The overall agreement (including the 0–25-Mev experiments) with the meson potential is good considering the experimental uncertainties.

* The work described was sponsored by the AEC.
[1] Brueckner, Hartsough, Hayward, and Powell, Phys. Rev., in press; Hadley, Kelley, Leith, Segrè, Wiegand, and York, Phys. Rev., in press.

F7. Camera for $P-P$ Scattering at 32 Mev.* WOLFGANG K. H. PANOFSKY AND FRANKLIN FILLMORE. *University of California, Berkeley.*—A camera has been constructed for exposing nuclear track emulsion plates to protons scattered in H_2 gas from the 32-Mev beam from the linear accelerator. The camera is arranged such that no exit slits are necessary. The angular range of scattering angles from 10° to 80° is accessible. Since $p-p$ scattering is symmetrical about 45°, this large angular range permits an internal check against the effect of impurities and background. The geometry is such that the number of tracks per unit solid angle interval in the center of mass system is directly proportional to the differential cross section in the center of mass system, without any angular factors. The proton beam is collimated to a diameter of $\frac{1}{16}$", then passed through the camera containing up to twenty 1"×3" Nuclear plates and is then integrated. The plates are arranged symmetrically in order to minimize the required accuracy of the centering of the beam. Background and symmetry studies are in progress and appear satisfactory.

* This work was sponsored by the AEC.

F8. Apparatus for Measuring Proton-Proton Scattering at 32 Mev Using Proportional Counters.* B. CORK, L. JOHNSTON, AND C. RICHMAN. *University of California, Berkeley.*—The linear accelerator is well adapted to proton-proton scattering experiments because of its well-collimated and mono-energetic beam (0.1° angular spread, 0.3 percent energy spread). The scatterer used is hydrogen gas at one atmosphere, the scattering region being roughly a cylinder 0.5 cm in diameter and 2 cm long. Seven proportional counters shaped as annular rings record scattering at 15°, 21°, 27°, 33°, 39°, 45°, 51° (laboratory system) simultaneously, with a possibility of getting a 90° coincidence check between 45°–45° and 39°–51° counters. The annular shape provides a maximum solid angle for the counters. In this way scattering experiments can be done with currents $\sim10^{-11}$ ampere of collimated protons. Scattering from contaminating gases is minimized by continuously flushing pure hydrogen from a palladium tube through the system, the gas entering at the scattering region. A large background was experienced due to energetic neutrons, generated by 32-Mev protons striking the collimating slits; this has been reduced to less than 10 percent of the counting rate by a rearrangement of slits

and absorbing material. The measurements may eventually be extended down to 5°. Some preliminary results will be discussed.

* This work was performed under the auspices of the AEC.

F9. Elastic Scattering of 90-Mev Neutrons. A. BRATENAHL, R. H. HILDEBRAND, C. E. LEITH, AND B. J. MOYER, *University of California, Berkeley.*—An experiment to determine the differential cross sections at various angles for elastic scattering of 90-Mev neutrons by C, Al, Cu, Ag, and Pb nuclei will be described. A comparison will be made between measurements using two types of neutron detectors; pieces of carbon activated by the $C^{12}(n,2n)C^{11}$ reaction (20.5-Mev threshold) and a recoil proton counter (60-Mev threshold). This comparison provides a measure of the error due to detection of inelastically scattered neutrons. Elastic scattering cross sections are obtained by integration of the differential cross sections. These scattering cross sections will be compared to total cross sections determined by attenuation measurements using the same detectors.

* The work described was sponsored by the AEC.

F10. Analysis of Low Energy Proton-Proton Scattering Experiments.* G. F. CHEW AND M. L. GOLDBERGER. *University of California, Berkeley.*—From the proton-proton scattering experiments at Minnesota and Wisconsin[1,2] one finds an "effective range" for the nuclear force of $2.61\pm0.02\times10^{-13}$ cm and a scattering length $7.657\pm0.013\times10^{-13}$ cm. The exact interpretation of these numbers in terms of a particular shape for the potential generally involves extensive numerical calculations. However, the variational formulation of the problem[3] shows that the nuclear phase shift depends only on the wave function in the region of strong nuclear potential. Since the coulomb field is here relatively unimportant, it may be treated as a perturbation. This will be true regardless of the proton energy, and the analysis is greatly simplified since coulomb functions need not be used. The results for square and Yukawa wells, respectively, are: Ranges = 2.61 and 1.16×10^{-13} cm (±1 percent); Depths = 13.27 and 47.94 Mev (±0.2 percent). Similar calculations in connection with experiments at higher energies will also be discussed.

* The work described was sponsored by the AEC.

[1] Blair, Freier, Lampi, Sleator, and Williams, Phys. Rev. **74**, 553 (1948); C. L. Critchfield and D. C. Dodder, Phys. Rev. (to be published).
[2] G. Breit, H. M. Thaxton, and L. Eisenbud, Phys. Rev. **55**, 1018 (1939); Herb, Kerst, Parkinson, and Plain, Phys. Rev. **55**, 998 (1939).
[3] J. Schwinger, Phys. Rev. **72**, 742 B11 (1947); J. M. Blatt, Phys. Rev. **74**, 92 (1948).

G1. The Energy Spectrum of Mesotron Decay Electrons.* ROBERT B. LEIGHTON, CARL D. ANDERSON, AND AARON J. SERIFF, *California Institute of Technology.*—Electrons from the decay of slow mesotrons at sea level are being studied by means of a freely falling cloud chamber of 30-cm inside diameter and 11-cm depth operating in a magnetic field of 7250 gauss. Slow particles are selected by means of a double coincidence counter telescope, the lower counter of which is inside the cloud chamber, and a tray of anticoincidence counters below the cloud chamber. The counter inside the chamber is rectangular in shape and has a flat top and bottom. This counter is also used as an absorber for the determination of the mesotron mass by measurements of the momentum of the mesotron before and after it traverses the known amount of material in the counter. A plate of carbon 1 cm thick in the lower half of the cloud chamber provides an additional absorber for mesotron mass measurements and for the observation of decay electrons. About one in two hundred photographs show decay electrons, corresponding to about one decay electron per day. To date, over fifty decay electrons have been observed, with energies ranging from about 10 Mev to about 50 Mev, with an apparently continuous distribution of intermediate energy values. The correction for instrumental selection is negligible except for electron energies below about 10 Mev.

* This work was supported in part by the joint program of the ONR and the AEC.

G2. The Decay Products and the Mass of the Mesotron.* CARL D. ANDERSON, ROBERT B. LEIGHTON, AND AARON J. SERIFF, *California Institute of Technology.*—The measurements reported in the previous abstract lead to the following conclusions: (1) The decay electron energy spectrum appears continuous in the range 10 Mev to 50 Mev, and cannot correspond either to a unique electron energy or to a set of two discrete "lines" as, e.g., at 25 Mev and 40 Mev. (2) Those cases in which the decay electron energy and the mesotron mass have been measured for the same mesotron show that these quantities do not bear the relationship to one another to be expected on the basis of conservation of momentum and energy if the mesotron decays simply into a single electron and a single particle of low mass (neutrino). Thus the observed spread in energy of the decay electrons is not to be ascribed to a corresponding range of different mass values of the mesotron. (3) The decay electron spectrum is consistent with the assumption that mesotron decay results in the production of one electron and two neutrinos. On this view, the mass of the mesotron computed for the highest energy decay electron so far observed is 210±10 Mev.

* This work was supported in part by the joint program of the ONR and the AEC.

G3. On Nuclear Capture of Negative Mesotrons.* AARON J. SERIFF, ROBERT B. LEIGHTON, AND CARL D. ANDERSON, *California Institute of Technology.*—In the series of photographs made with the 12" freely falling cloud chamber, one case has been observed in which a negative mesotron comes to rest in the gas of the cloud chamber without the production of a decay electron. Several small blobs of ionization which are observed a few mm from the end of the mesotron track are interpreted as tracks of photoelectrons which result from the absorption in the gas of soft x-rays which are produced as the mesotron approaches an argon nucleus prior to its capture by the nucleus. No charged particles are emitted from the nucleus after capture of the mesotron. A blob 1.5 mm long at the end of the mesotron track may represent the recoil of the nucleus after the emission of one or more neutral particles. If a single neutron were emitted, its energy could not have been greater than 25 Mev.

* This work was supported in part by the joint program of the ONR and the AEC.

G4. Secondary Particles from Various Nuclei Bombarded with 90-Mev Neutrons.* HERBERT F. YORK, *University of California, Berkeley.*—The $H\rho$'s and ranges of the secondary particles from C, Cu, and Pb bombarded with neutrons of 90-Mev mean energy have been measured simultaneously by means of a magnetic field and proportional counter telescope arrangement. Both protons and deuterons have been found with energies extending from 25 Mev (the present lower limit of the apparatus) to 100 Mev. In the case of carbon the ratio of deuterons to protons in the forward direction is about 2:3, with both energy distributions showing a broad maximum in the region of 50–60 Mev. All particles are peaked forward—deuterons more so than protons and high energy particles more so than those of low energy. The total cross section of carbon for producing deuterons of more than 25 Mev is surprisingly large, being a few hundredths of a barn. The cross section per proton in the carbon nucleus for this process is thus of the order of one-tenth of the total $n-p$ cross section at 90 Mev. For Cu and Pb the ratio of deuterons to protons in the forward direction is less, being approximately 1:3 and 1:6.

* This work was performed under the auspices of the AEC.

G5. Recoils of Active Fluorine^{18} from 184-in. Cyclotron Bombardment. WARREN EHCKROTTE AND HUGH BRADNER, *University of California, Berkeley.*—F^{19} has been bombarded with high energy neutrons from the 184-in. cyclotron, and an angular distribution and range in Be has been obtained for the resultant F^{18}. The angular distribution shows a pronounced forward maximum:

Angle	Relative activity
0°– 10°	100±15%
5°– 25°	140±15%
20°– 40°	105±15%
35°– 55°	85±15%
80°–100°	10±10%
90°–180°	5

The range, measured by counting the 112-minute activity on a stack of 0.19-mg/cm² Be foils, was 0.8 mg/cm². The interpretation of this distribution with respect to nuclear models will be discussed.

* This work was sponsored by the AEC.

G6. Photographic Plate Confirmation of High Energy Deuterons from 90-Mev Neutrons on Carbon.* H. BRADNER, *University of California, Berkeley.*—In measuring ranges of "protons" knocked out of a carbon target by 90-Mev neutrons, H. York[1] obtained an energy distribution at 10° which had a maximum at 40 to 50 Mev, rather than the 75 Mev predicted theoretically. K. Bruchner and W. Powell[1] re-examined cloud-chamber pictures in which they had obtained $H\rho$ of secondary "protons" from 90-Mev neutrons. Their energy distribution did not agree with theory or with York's experiment. "Proton" energies up to 130 Mev were calculated, but errors from $H\rho$ measurement were large. York pointed out that the two experiments could be reconciled if some of the ions were deuterons of approximately 60 Mev. Further experiments were undertaken with both types of apparatus, and with photographic plates. In the photographic plate experiment, 100 μ emulsion Ilford C-2 plates were set edgewise at 10° to a thin carbon target which was in the neutron beam outside the cyclotron shielding. Grain counts of tracks beginning at the edge of the plates and ending in the emulsion showed definitely that there were high energy deuterons. (Of the 35 tracks counted, 20 were protons, 15 were deuterons.) The measured deuteron energies ranged from 23 Mev to 70 Mev.

* This work was sponsored by the AEC.
[1] Unpublished work.

G7. Inelastic Scattering of Protons.* C. LEVINTHAL, E. A. MARTINELLI, AND A. SILVERMAN, *University of California, Berkeley.*—A photographic method is used to measure the energy distribution of inelastically scattered protons. The 32-Mev linear accelerator is used as a source of protons. Eight plates are exposed simultaneously at fixed polar angle, and the track lengths from 0–200 microns are measured on each plate. With appropriate aluminum absorbers between the target and each plate, the energy distribution from 0–16 Mev or 16–28 Mev can be determined in one run. To determine the energy resolution of the camera, an exposure was made with 16-Mev protons on carbon. The following energy levels of C^{12} were observed: 0; 4.8±.2; 10.0±.4 Mev. This confirms results obtained by Fulbright and Bush.[1] The width of the levels at half-maximum were of the order of 1.0 Mev. The calculated width at half-maximum with the beam stopped down to 16 Mev is 0.7 Mev, considering only straggling in the various absorbers, and the initial spread of the beam. Results obtained by bombarding aluminum with 32-Mev protons will be reported.

* This work was performed under the auspices of the AEC.
[1] H. W. Fulbright and R. R. Bush, Phys. Rev. **74**, 1323 (1948).

G8. On the Injection of Ions in the Bevatron.* R. L. GLUCKSTERN AND LLOYD SMITH, *University of California, Berkeley.*—A serious problem in the operation of a bevatron is to insure that the ions will not strike the injector during the acceleration period. Since the adiabatic damping is negligible during the injection period, it has been proposed to allow the ions to spiral into the center of the chamber before turning on the accelerating voltage. The question is then whether or not the betatron oscillations will enable the ion to clear the injector while the instantaneous circle moves inward. We have investigated the probability of an ion being in the neighborhood of the injector on successive turns for various amplitudes of betatron oscillation and for various shapes of magnetic fields. Our conclusion is that for the proposed machine only $\frac{1}{4}$ of the ions will be lost in this manner. This result was corroborated by tracing some actual ion paths. Apparently, no electromagnetic orbit contracting device will be necessary.

* This paper is based on work done under the auspices of the AEC.

G9. Production Ratio of Positive and Negative Mesons for Various Cyclotron Target Materials.* WALTER H. BARKAS,** *University of California, Berkeley.*—A study has been made to find the relative numbers of positive and negative mesons produced in various target materials by a beam of 380-Mev alpha-particles. Photographic plates to record positive and negative mesons were placed[1] symmetrically on opposite sides of the target in the 184-inch

Berkeley cyclotron. Although the energy range over which mesons are accepted is not well defined, it is the same for both positives and negatives. The area scanned is such that no mesons are counted of energy less than 2 Mev, and few, if any, have energies higher than 5 Mev. The photographic plates used were Ilford types C.2 and C.3, with emulsion thickness 100 microns. Cyclotron targets were $\frac{1}{64}$ inch thick. Observations were made using targets of Be, C, Al, Cu, In, and Pb. The survey indicates: (1) the production of negative mesons in the energy interval studied does not vary rapidly with atomic number, and (2) the ratio of positive to negative mesons, which is about $\frac{1}{3}$ for carbon, falls virtually to zero for heavy elements.

* This paper is based on work performed with the support of the AEC.
** Office of Naval Research, San Francisco, California.
[1] J. Burfening, E. Gardner, and C. M. G. Lattes, Phys. Rev. **75**, (1949).

G10. Meson Mass Measurements. Part I. Experimental Method.* EUGENE GARDNER, *University of California, Berkeley.*—A new determination is being made of the masses of mesons produced by 380-Mev alpha-particles in the 184-inch Berkeley cyclotron. The method, that of bending in the magnetic field and range in emulsion, is similar to that used in an earlier determination,[1] except that several changes have been made in order to increase the accuracy. In addition to improvements associated with more precise positioning of plates and more careful measurement of distances, the following changes have been introduced: (1) the plates used in the present study were exposed in the cyclotron without wrapping. This procedure avoids the energy loss and scattering of the mesons in the black paper or aluminum foil wrapping. (2) Only those mesons which leave the target moving approximately in the direction of the alpha-particle beam are used; the mass value can be determined most accurately for these mesons. The selection is automatically made by means of a "channel" which admits only a narrow angular spread of meson trajectories. (3) The plates are inclined to the meson trajectories in such a way that the mesons enter the emulsion through the top surface. In this way errors associated with the distortion at the edge of the plate are avoided.

* This paper is based on work performed with the support of the AEC
[1] E. Gardner and C. M. G. Lattes, Science **107**, 270 (1948).

G11. Meson Mass Measurements. Part II. Experimental Results.* A. S. BISHOP, *University of California, Berkeley.*—Preliminary values for the meson masses are: heavy negative meson: $285m_e$, heavy positive meson: $286m_e$, light positive meson: $216m_e$, where m_e is the mass of the electron. When this study is completed, it is hoped that the probable error will be as low as 2 percent. The preliminary values given above, however, have an additional uncertainty of one or two percent since several small corrections have not yet been made. The ratio of masses of heavy positive to light positive mesons is 1.32 ± 0.01. This ratio is known to greater accuracy than the masses themselves because the error in the measurement of the magnetic field is largely eliminated. The method of measuring meson masses by $H\rho$ and range is being checked by measuring the proton mass, using the same method. For a range-energy relation in the emulsion (Ilford C.2) we have used a curve obtained by extrapolating to higher energies from the points given by Lattes, Fowler, and Cuer.[1] We hope to verify this curve by means of exposures to protons from the Berkeley linear accelerator.

* This paper is based on work performed with the support of the AEC.
[1] C. M. G. Lattes, P. H. Fowler, and P. Cuer, Proc. Phys. Soc. **59**, 883 (1947).

G12. Meson Mass Measurements. Part III. Discussion of Results.* C. M. G. LATTES,** *University of California, Berkeley.*—The value found in this study for the ratio of masses of heavy and light positive mesons is consistent with the assumption that a light particle (e.g., a neutrino or a gamma-ray) is emitted when a heavy positive meson decays into a light positive one. From studies of negative mesons in which there was a channel between the target and the plates, it is concluded that few, if any, light negative mesons come from the target. From similar studies of positive mesons it is concluded that light positive mesons do originate at the target; their energy spectrum indicates that they come from the decay of heavy positive mesons which stop in the target. By combining the results of the present study with an earlier measurement of the meson mass by grain counting,[1] it is possible to show that the magnitude of the charge on the meson is equal to that on the electron within the accuracy of the measurements. In one group of heavy positive mesons it was observed that 54 out of a total of 59 gave observable secondary mesons. This result indicates that any competing process (such as the decay of the heavy meson into an electron and a neutrino) must have a longer half-life.

* This paper is based on work performed with the support of the AEC.
** On leave of absence from University of São Paulo, Brazil.
[1] W. H. Barkas, E. Gardner, and C. M. G. Lattes, Phys. Rev. **74**, 1558 (1948).

H1. Stars in Photographic Emulsions Initiated by Heavy Negative Mesons.* FRANK L. ADELMAN AND STANLEY B. JONES, *University of California, Berkeley.*—We have tabulated the number of prongs (charged particle tracks) per star for stars initiated by heavy negative mesons in photographic emulsions. The mesons were created in the 184-inch Berkeley cyclotron by bombarding a target with 380-Mev alpha-particles. The mesons used in this study were found to be heavy by the method of $H\rho$ and range. The following table gives the prong distribution for 588 stars.

Number of prongs:	0	1	2	3	4	5	Over 5
Percent of stars:	27.0	23.6	24.0	14.8	8.7	1.9	0

In no case was a heavy negative meson observed to decay into a light negative meson ($\pi-\mu$ decay). Eleven "hammer tracks" were found in a survey of about 3000 stars. These are explained[1] as follows: a Li^8 nucleus, emitted in a nuclear reaction, undergoes β-decay into Be^8, which then splits into two alpha-particles of equal energy.

* This paper is based on work performed with the support of the AEC.
[1] C. Franzinetti and R. M. Payne, Nature **161**, 735 (1948).

H2. Yield of Negative Mesons Produced by High Energy Alpha-Particles as a Function of Alpha-Particle Energy.* STANLEY B. JONES AND R. S. WHITE, *University of California, Berkeley.*—A study is now in progress to find the relative numbers of negative mesons created by alpha-particles of various energies. The various energies are obtained at different radii in the 184-inch Berkeley

cyclotron. The study first included only mesons in a particular energy interval of the order of 2–5 Mev. The intensity of the mesons in this energy interval *versus* the bombarding beam energy is given in the accompanying table. Column 1 gives the energy of the bombarding alpha-particles; column 2, the numbers of mesons actually counted; and column 3, the numbers of mesons relative to the number at 380 Mev, corrected for beam currents, plate thickness, and area scanned.

Beam energy (Mev)	No. of mesons	Corrected relative yield
380	339	100 percent
342	164	33 percent
304	38	7.4 percent
266	7	0.7 percent

The exposures were made with a carbon target and with Ilford type C.2 plates. The plates were scanned over a region estimated to include about 90 percent of the mesons in each plate.

* This paper is based on work performed with the support of the AEC.

H3. Excitation Functions from Deuteron Bombardment of Cu. D. BOCKHOP, A. C. HELMHOLZ, S. D. SOFTKY, J. W. ROSE, AND T. BREAKEY, *University of California, Berkeley.*—Excitation functions have been measured of Zn, Cu, Ni, and Fe from Cu bombarded by 190-Mev deuterons produced by the 184-in. cyclotron. The deuterons are incident on a stack of Cu plates which has Cu foils spaced through it at equal energy intervals, and quantitative chemical separation of the products from the foils gives the relative yield as a function of the energy. The absolute yield at 190 Mev is compared with that of Na^{24} from a thin Al foil[1] at this energy, thus determining cross sections from formation as a function of energy. The yields for Mn^{52}, Mn^{56}, Fe^{59}, and Co^{58} increase with increase of energy, while those of Zn^{62}, Zn^{63}, and Cu^{64} show maxima at low energies and then decrease with energy. Cross sections of the order of that of Na^{24} from Al are obtained for Cu and Zn, but only of the order of one-tenth of that of Na^{24} for Fe and Co. Results obtained to date agree well with previous work done on deuteron bombardment of Cu at this laboratory,[2] and it is indicated[3] that excitation curves may well be obtained for elements even further below Cu.

* The work described was sponsored by the AEC.
[1] H. W. Hubbard, see abstract H7.
[2] D. Bockhop, A. C. Helmholz, and J. M. Peterson, Phys. Rev. 74, 1559 (1948).
[3] D. R. Miller, R. C. Thompson, and B. B. Cunningham, Phys. Rev. 74, 347 (1948).

H4. Radio activities of Ag^{111}, Cd^{111}, and In^{111}.* A. C. HELMHOLZ, R. W. HAYWARD, AND C. L. MCGINNIS, *University of California, Berkeley.*—We have investigated with a magnetic lens spectrograph built by one of us (R.W.H.) the three isobaric activities, Ag^{111}, Cd^{111}, and In^{111}. The second of these is the 48.6±0.3-min. isomer of stable Cd^{111}. It emits a highly converted 149-kev γ-ray and a 247-kev γ-ray of conversion coefficient 0.1. The latter is the same as that observed[1] in the K-capture decay of the 2.84±0.03-*d*. In^{111}. Emitted in coincidence[2] in the In^{111} decay is a 173-kev γ-ray with conversion coefficient 0.18. From these data Cd^{111} has three excited states at 247, 396, and 420 kev. Using the theory of Hebb and Nelson[3] and the K/L ratios, we find the 247-kev γ-ray is magnetic quadrupole, the 173 electric quadrupole, the 149 electric 2^4 pole. The β^--spectrum of the 7.5-*d*. Ag^{111} was analyzed according to the Fermi theory. It appears to be of simple form with an upper limit of 1.06±0.03 Mev. This is a once forbidden transition according to Konopinski's classification. Difficulties in the formulation of a level scheme point out the need of accurate theoretical conversion coefficients for $Z\sim 50$.

* The work described was sponsored by the AEC.
[1] J. H. Lawson and J. M. Cork, Phys. Rev. 57, 982 (1940).
[2] H. Bradt, *et al.*, Helv. Phys. Acta 19, 77 (1945).
[3] M. H. Hebb and E. Nelson, Phys. Rev. 58, 486 (1940).

H5. Study of Cd^{115} Isomers.* R. W. HAYWARD** AND A. C. HELMHOLZ, *University of California, Berkeley.*—Using a magnetic lens spectrograph of the type constructed by Siegbahn,[1] we have investigated the β-spectrum of the 43-d Cd^{115}, in a sample of Cd obtained from Oak Ridge. The spectrum has an end point at 1.67 Mev and seems to be simple. The 86 kev converted γ-ray of Cd^{109} is also observed. A separate investigation of the other isomer of Cd^{115}, the 2.3-d activity, gave agreement with the work of Lawson and Cork.[2] The spectrum is complex, and has an end point of 1.10 Mev. It shows γ-rays of 337 kev and 520 kev and conversion lines of the 337-kev γ-ray which is due to the 4.5-hr. In^{115} in equilibrium. Thus the 43-d isomer must be the upper state by 0.2 Mev. Since no evidence of such a γ-ray has been found, the γ-transition must correspond to at least a 2^5 and probably a 2^6 pole transition. Possible spin and parity assignments to the levels assuming the ground state of In^{115} is 9/2 and even might be: In (4.5 hr.) 1/2 odd; Cd (2.3 d) 1/2 even; Cd (43 d) 13/2 even. A discussion of possible level schemes will be given.

* The work described was sponsored by the AEC.
** AEC Predoctoral Fellow.
[1] K. Siegbahn, Phil. Mag. 37, 162 (1946).
[2] J. H. Lawson and J. M. Cork, Phys. Rev. 57, 982 (1940).

H6. Absolute Cross Section for Production of Heavy Negative Mesons by 380-Mev Alpha-Particles.* VINCENT PETERSON, *University of California, Berkeley.*—The absolute cross section per atom of target material for production of heavy negative mesons by 380-Mev alpha-particles has been measured for carbon and several other elements of widely different Z. Photographic plates were used to detect the mesons, and the flux of alpha-particles was determined by measuring the C^{11} radioactivity produced in a thin polystyrene foil covering the face of the target. The absolute cross section for the reaction $C^{12}(\alpha,\alpha_n)C^{11}$ was also measured to relate C^{11} activity to alpha-current. The solid angle of meson radiation accepted by the photographic plate was calculated from either: (a) emulsion thickness, for edge-on exposure, or (b) tilt angle, for plates inclined slightly to the horizontal. Only mesons entering the plate within ±45° from the normal were counted. Assuming the angular distribution to be spherically symmetric, and a theoretical energy distribution $dN(E)=f(E)(E_m-E)^4E^4dE$, where $E_m=45$ Mev and $f(E)$ is the Coulomb factor, the absolute cross section for carbon has been calculated to be $(1.8\pm.3)\times10^{-29}$ cm². Correction for decay in flight has been made. The plates accept mesons of energies from 2–5 Mev (normal incidence).

* This work was done under the auspices of the AEC.

H7. $Al^{27}(d,\alpha p)Na^{24}$ Cross Section.* H. W. HUBBARD, *University of California, Berkeley* (introduced by A. C. Helmholz).—The cross section for the reaction $Al^{27}\times(d,\alpha p)Na^{24}$ was measured for incident 194-Mev deuterons by means of the deflected deuteron beam from the 184-inch cyclotron at Berkeley. An aluminum foil was bombarded for about one hour, the beam current being measured by means of a Faraday cage system of known capacitance. The number of Na^{24} atoms was then measured by means of beta-gamma coincidences, which is possible since Na^{24} emits two γ-rays in coincidence with each electron.[1] The results obtained in this way agreed closely with those obtained by comparing the active foils with a uranium β-standard. The best result from four independent measurements gives a value for the cross section at 194 Mev of 0.048 barn, the result probably being accurate to 15 percent.

* The work described was sponsored by the AEC.
[1] M. L. Wiedenbeck, Phys. Rev. 72, 429 (1947).

H8. Nuclear Cross Sections for 90-Mev Neutrons.* N. KNABLE, J. DE JUREN, AND B. J. MOYER, *University of California, Berkeley.*—Using bismuth fission chambers (threshold about 50 Mev) to monitor and detect high energy neutrons produced in the 184-in. cyclotron, total cross sections for twelve different elements were measured. The mean detection energy is estimated at 95 Mev. The hydrogen cross section result was 0.073 ± 0.002 barn, and the deuterium-hydrogen difference was determined to be 0.031 ± 0.002 barn. An arrangement giving simultaneous measurements of neutron attenuation with both good and poor geometry has given values for the ratios of inelastic to total cross sections for various elements lying between 0.4 and 0.5. An absolute measure of the elastic scattering cross section in the case of carbon was in good agreement with that deduced from the total and inelastic values. A plot of inelastic collision radius *vs.* $A^{\frac{1}{3}}$ shows the same slope as the plot of total collision radius in the region of high atomic number where transparency effects become unimportant.

* This work was done under the auspices of the AEC.

H9. High Energy Gamma-Radiation from 184-Cyclotron Target.* B. J. MOYER, H. F. YORK, AND R. BJORKLUND, *University of California, Berkeley.*—An electron pair counter has been assembled, utilizing a magnetic field to separate the pairs, and coincidence counting to detect them. A radiator of thin Ta serves to materialize the photons. This is exposed to the cyclotron target from outside the shielding, through the neutron beam defining hole. The direction of rotation of the deuteron beam is reversed to minimize the background counting due to effects from neutrons. In any of the targets used (Be, Cu, Pb) photons were observed in distributions extending to at least 70 Mev. An energy distribution for Be will be shown, corrected for variation in pair production probability, variation in energy breadth detected, and effects due to scattering of the pair electrons. For a mean detection energy of 50 Mev the integrated cross section for production of photons in the energy breadth detected (approximately 40–60 Mev) is about 10^{-30} cm². This value and the distribution with respect to energy are reasonably consistent with a bremsstrahlung origin for the photons.

* This work was done under the auspices of the AEC.

H10. Detection of Very High Energy Protons by Means of Anthracene Scintillation Counters.* L. WOUTERS, *University of California, Berkeley.*—Because of the low ionization density of very high energy protons (as generated in synchro-cyclotrons), the pulses produced in proportional gas counters are all but lost in the competing beta-background. Anthracene scintillation counters can be arranged so that an amount of usefully detectable energy, large compared to the energy of the competing radiation, is abstracted from the protons; no difficulty then exists in sorting these out. The equipment used at the Radiation Laboratory for experimental work at the 184″ site will be described. The most expeditious way of determining the usefulness of the apparatus was to perform an $n-p$ scattering experiment for which reliable results had been established by more orthodox methods; agreement well within the range of the best data of these other methods was obtained. The unique degree of energy discrimination appeared as a broad counting plateau between the proton and the background pulse levels. The percentage of non-coincidence pulses from the individual counters was then relatively small; together with the short radiation time of anthracene, enormously faster counting rates are made permissible, in comparison with gas counters.

* The work described was sponsored by the AEC.

H11. Radiation Field of the 184-Cyclotron.* W. K. BENSON, JR., R. L. MATHER, B. J. MOYER, AND JOSEPH YATER, *University of California, Berkeley.*—The distribution and intensity of the radiation field outside the shielding of the 184″ cyclotron have been studied with various types of detectors. Three-dimensional surveys were made with proton recoil counter, calibrated slow neutron counter, and an ion chamber so constructed as to read approximately the "roentgen equivalent physical" dosage rate. Average values at normal areas of habitation are: 60 slow neutrons cm^{-2} $sec.^{-1}$, 0.5 milli-rep/hr., and a fast neutron flux about an order of magnitude below tolerance. Determination of the actual value for fast neutron flux depends upon energy distribution assumed. Studies of this are in progress. Calibrated indium foil measurements of slow neutron flux as a function of depth in the 10-ft. concrete shielding indicate, apart from transition and boundary effects, an attenuation with a half-value thickness of 7 to 8 inches, and a value at the outside surface in agreement with that mentioned above.

* This work was done under the auspices of the AEC.

H12. Kinetic Energy Release in Fission Induced by High Energy Neutrons.* J. JUNGERMAN AND S. C. WRIGHT, *University of California, Berkeley.*—The ionization produced by single fission fragments was observed in an ionization chamber using electron collection. Fission was induced in bismuth and other substances by 90-Mev neutrons. The distribution of fragment energy *versus* number of fragments has a single peak. This is in contrast to the double peaked curve obtained with thermal neutron fission of U^{235}. For bismuth the most probable single fragment energy is 74 Mev, and the mean fragment energy is 71 Mev.

* The work described was done under the auspices of the AEC.

SUPPLEMENTARY PROGRAMME

SP1. Inelastic Scattering of Protons from Li^7.* W. A. FOWLER, C. C. LAURITSEN, AND S. RUBIN, *Kellogg Radiation Laboratory, California Institute of Technology.*—The energy of the lowest excited state of Li^7 has been redetermined[1] with a double-focusing magnetic spectrograph[2] by measuring the energy of the protons inelastically scattered at angles of 81.1° and 137.8° from lithium bombarded by 1233.5-kev protons. The spectrograph was calibrated by the elastic scattering of protons of the same energy by copper. The scattering angles were carefully measured and checked by elastic scattering in lithium, beryllium, carbon, and oxygen. The bombarding proton energy is stabilized to better than 1 kev by an electrostatic analyzer calibrated at 440 kev with the γ-ray resonance in $Li^7(p\gamma)$. Careful attention was given to loss of energy of the incident and scattered protons in surface layers ($\sim$100 atoms) of carbon and oxygen on the various targets. The scattering observed from these layers indicated a thickness corresponding to an 0.5-kev energy loss for 1-Mev protons incident normally. The final result of this determination is 477.4 ± 2.0 Mev for the excited state in Li^7 and is to be compared with the value 476.8 ± 1.0 found by measurement of the gamma-ray[3] emitted by Li^{7*}. If the gamma-ray measurement is accepted the resonance in $Li^7(p\gamma)$ is located at 439.5 ± 2.3 kev, and the first strong resonance in $F^{19}(p\alpha,\gamma)$ is located at 869.9 ± 4.6 kev.

* This work was assisted by the joint program of the ONR and the AEC.
[1] Rubin, Snyder, Lauritsen, and Fowler, Phys. Rev. **74**, 1564A (1948).
[2] Snyder, Lauritsen, Fowler, and Rubin, Phys. Rev. **74**, 1564A (1948).
[3] W. F. Hornyak and T. Lauritsen (unpublished).

SP2. Comets and the Reciprocal Force. F. W. WARBURTON, *University of Redlands.*—Verification of relative electrodynamics may possibly be found in the behavior of comets. Electrical equilibrium of a body receiving ions from the sun[1] and re-emitting ions at the same rate is similar to temperature equilibrium of a body receiving and re-emitting radiation. An increase in the reception of negative ions from the sun as the comet approaches perihelion is believed to augment the normal radiation excitation of atoms and so be related to the rapid variation in brightness of the comet. The relative reciprocal force is a function of the speed of the emitting charge e', and rapid increase in average electron speed in the comet should result in negative ion emission and account for the explosive ejection of matter which forms the comet's envelope and tail. Also radiation pressure can be augmented by the negative ion emission from the sun acting on the ejected matter which forms the tail.

The shift in balance of electrical charge emission in the comet should affect the force of the sun on the comet itself. It is evidently related to the shortening of the period which is so prominent in Encke's comet.

[1] See Abstract No. A2.

SP3. Report of Initial Performance of the Berkeley Synchrotron. E. MCMILLAN, *Radiation Laboratory, University of California, Berkeley.*

SP4. Acceleration of Protons in the 184-inch Berkeley Cyclotron. K. M. MCKENZIE, *Radiation Laboratory, University of California, Berkeley.*

SP5. Neutron Diffraction in Liquid Elements. OWEN CHAMBERLAIN, *University of Chicago.*

Author Index to Contributed Papers Presented at the Berkeley Meeting

Adelman, Frank L. and Stanley B. Jones—No. H1
Anderson, Carl D., Robert B. Leighton, and Aaron J. Seriff—No. G2
Barkas, Walter H.—No. G9
Barnóthy, J.—No. B8
Bedell, F.—No. C9
Beeck, Otto—No. A6
Benson, W. K., Jr., R. L. Mather, B. J. Moyer, and Joseph Yater—No. H11
Berman, A. I.—No. A4
Biehl, A. T., H. V. Neher, and W. C. Roesch—No. B4
Bishop, A. S.—No. G11
Bockhop, D., A. C. Helmholz, S. D. Softky, J. W. Rose, and T. Breakey—No. H3
Bradner, Hugh—No. G6
—— and Warren Ehckrotte—No. G5
Bratenahl, A., R. H. Hildebrand, C. E. Leith, and B. J. Moyer—No. F9
Brattain, R.—No. A7
Brown, F. W., III, P. J. Harris, and A. L. Klein—No. D6
Chamberlain, Owen—No. SP5
Chew, G. F. and M. L. Goldberger—No. F10, B1
Christian, R. and E. Hart—No. F6
Christy, R. F.—No. E9
Cohen, E. Richard—No. E8
Coon, J. H., R. F. Taschek, and S. G. Forbes—No. F5
Cork, B., L. Johnston, and C. Richman—No. F8
Davis, Leverett, Jr. and R. V. Langmuir—No. A5
Davis, R. H. and J. D. Graves—No. D9
Donoghue, J. J., E. Gerjuoy, and R. E. Vollrath—No. A1
Duffield, R. B. and J. D. Knight—No. F4
Eggen, D. T. and M. L. Pool—No. F3
Forró, M.—No. B9
Fowler, W. A., C. C. Lauritsen, and S. Rubin—No. E5, SP1
Gardner, Eugene—No. G10
Germain, Lawrence S.—No. B7
Gluckstern, R. L. and Lloyd Smith—No. G8
Graves, J. D. and J. P. Dyson—No. D8
Halpern, Otto—No. C7

Hayward, R. W. and A. C. Helmholz—No. H5
Helmholz, A. C., R. W. Hayward, and C. L. McGinnis—No. H4
Hornyak, W. F. and T. Lauritsen—No. E2
Hubbard, H. W.—No. H7
Irvine, John W., Jr. and Raymond C. Sangster—No. D5
Ise, John, Jr.—No. B6
Jones, Stanley B. and R. S. White—No. H2
Jungerman, J. and S. C. Wright—H12
Knabel, N., J. De Juren, and B. J. Moyer—No. H8
Koch, G. E. and J. D. Graves—No. D7
Kunkel, Wulf—No. D4
Latter, R. and R. F. Christy—No. C4
Lattes, C. M. G.—No. G12
Lauritsen, T. and W. F. Hornyak—No. E1
Leighton, Robert B., Carl D. Anderson, and Aaron J. Seriff—No. G1
Levinthal, C., E. A. Martinelli, and A. Silverman—No. G7
Levinthal, E. C.—No. E10
Loeb, L. B.—No. D2
McKenzie, K. M.—No. SP4
McMahon, H. O., Gilbert W. King, and R. M. Hainer—No. C2
McMillan, E.—No. SP3
Miller, Charles G.—No. D3
Moyer, B. J., H. F. York, and R. Bjorklund—No. H9
Neher, H. V.—No. B5
Osborne, M. F. M.—No. A3
Panofsky, Wolfgang K. H. and Franklin Fillmore—No. F7
Peterson, Vincent—No. H6
Powell, Wilson M.—No. B2
Rasmussen, V. K., W. F. Hornyak, and T. Lauritsen—No. E3
Roesch, W. C., A. T. Biehl, and H. V. Neher—No. B3
Rubin, Sylvan—No. C1
Schiff, L. I.—No. C3
Serber, R.—No. C5
Seriff, Aaron J., Robert B. Leighton, and Carl D. Anderson—No. G3
Taschek, R. F., A. Hemmendinger, and G. A. Jarvis—No. F1
Temmer, G. M.—No. F2
Thomas, R. G., W. A. Fowler, and C. C. Lauritsen—No. E7
Thornton, R.—No. D1
Tobias, C. A.—No. C8
Tollestrup, A. V., C. C. Lauritsen, and W. A. Fowler—No. E6
Warburton, F. W.—Nos. A2 and SP2
Wick, G. C.—No. C6
Willoughby, A. B.—No. D10
Woodbury, E. J., R. N. Hall, and W. A. Fowler—No. E4
Wouters, L.—No. H10
York, Herbert F.—No. G4

THE AMERICAN INSTITUTE OF PHYSICS

INCORPORATED

57 East 55 Street New York 22, N.Y.

MEMBER SOCIETIES:

American Physical Society
KARL K. DARROW, *Secretary*, Columbia University, New York 27, New York.

Optical Society of America
ARTHUR C. HARDY, *Secretary*, Massachusetts Institute of Technology, Cambridge 39, Massachusetts.

Acoustical Society of America
WALLACE WATERFALL, *Secretary*, 57 East 55th Street, New York 22, New York.

Society of Rheology
EARL K. FISCHER, *Secretary*, Institute of Textile Technology, Charlottesville, Virginia.

American Association of Physics Teachers
R. F. PATON, *Secretary*, University of Illinois, Urbana, Illinois.

AFFILIATED SOCIETIES:

American Society for X-Ray and Electron Diffraction
Electron Microscope Society of America
Physical Society of Pittsburgh
Physics Club of Chicago
Physics Club of Philadelphia
Cleveland Physics Society
Physics Club of the Lehigh Valley

ASSOCIATES:

Over seventy-five leading industrial enterprises and other institutions which contribute to the support of the Institute.

JOURNALS:

The Physical Review
JOHN T. TATE, *Editor*, University of Minnesota, Minneapolis, Minnesota.

Reviews of Modern Physics
J. W. BUCHTA, *Editor*, University of Minnesota, Minneapolis, Minnesota.

Journal of the Optical Society of America
GEORGE R. HARRISON, *Editor*, Massachusetts Institute of Technology, Cambridge, Massachusetts.

The Journal of the Acoustical Society of America
FLOYD A. FIRESTONE, *Editor*, 3312 Fessenden Street, N.W., Washington, D. C.

American Journal of Physics
THOMAS H. OSGOOD, *Editor*, Michigan State College, East Lansing, Michigan.

The Review of Scientific Instruments
GAYLORD P. HARNWELL, *Editor*, Randal Morgan Laboratory of Physics, University of Pennsylvania, Philadelphia, Pennsylvania.

The Journal of Chemical Physics
JOSEPH E. MAYER, *Editor*, Kent Chemical Laboratory, University of Chicago, Chicago 37, Illinois.

Journal of Applied Physics
ELMER HUTCHISSON, *Editor*, Case Institute of Technology, Cleveland 6, Ohio.

Physics Today
DAVID A. KAUCHER, *Editor*, American Institute of Physics, 57 East 55 Street, New York 22, New York.

OFFICERS

GEORGE R. HARRISON, *Chairman*
Massachusetts Institute of Technology

WALLACE WATERFALL, *Secretary*
The Celotex Corporation

GEORGE B. PEGRAM, *Treasurer*
Columbia University

JOHN T. TATE,
Adviser on Publications
University of Minnesota

GOVERNING BOARD

LUIS W. ALVAREZ
I. W. BUCHTA
WALLACE R. BRODE
E. U. CONDON
W. F. FAIR, JR.
HARVEY FLETCHER
GEORGE R. HARRISON
W. V. HOUSTON
PAUL KIRKPATRICK
PAUL E. KLOPSTEG
F. W. LOOMIS
PHILIP M. MORSE
J. R. OPPENHEIMER
GEORGE B. PEGRAM
HAROLD K. SCHILLING
JOHN T. TATE
WALLACE WATERFALL
M. W. WHITE
A. G. WORTHING

Consultant on Printing
MELVIN LOOS

ADMINISTRATIVE STAFF

HENRY A. BARTON, *Director*

THEODORE VORBURGER,
Business Manager

RUTH F. BRYANS,
Publication Manager

EDITH HOFSTADTER, *Office Manager*

EILEEN B. NEUBERGER,
Circulation Manager

THE American Institute of Physics was founded in 1931 as a federation of leading societies in the field of Physics. It combines into one operating agency those functions on behalf of physics which can best be done by the Societies jointly. Its purpose is the advancement and diffusion of physics and its applications to human welfare. To this end it publishes for itself or the Societies the nine journals listed on this page; promotes unity and effectiveness of effort among all who are interested in physics; renders numerous direct services to physicists and to the public; and cooperates with government agencies, national associations, educational institutions, technical industries, and others in such manner as to realize the opportunities and fulfill the responsibilities of physics as an important and constructive human activity.

CONTENTS

THE PHYSICAL REVIEW SECOND SERIES, VOL. 75, NO. 9 MAY 1, 1949

Alpha-Particles from Fission as Recorded by Photographic Emulsions . . . . . L. MARSHALL 1389
Angular Distribution of 1- to 2.5-Mev Protons Scattered by He . . . . . GEORGE FREIER, EUGENIE LAMPI, W. SLEATOR, AND J. H. WILLIAMS 1398
Neutron Diffraction Study of the Structure of Ice . . . . . E. O. WOLLAN, W. L. DAVIDSON, AND C. G. SHULL 1348
Scattering of High Energy Neutrons by Nuclei . . . . . S. FERNBACH, R. SERBER, AND T. B. TAYLOR 1352
He^3 Isotopic Abundance . . . . . J. H. COOK 1363
Disintegration of He^3 and N^{14} by Thermal Neutrons . . . . . J. H. COOK AND R. A. NOBLES 1358
Study of the Interaction of Protons with Tritium . . . . . R. F. TASCHEK, G. A. JARVIS, A. HEMMENDINGER, G. G. EVERHART, AND H. T. GITTINGS 1361
Total Cross Section of the He_2 Nucleus for Slow Neutrons . . . . . L. D. P. KING AND LOUIS GOLDSTEIN 1365
Radioactive Isotopes of the Rare Earths. I. Experimental Techniques and Thulium Isotopes . . . . . GEOFFREY WILKINSON AND HARRY G. HICKS 1370
Effects of Nuclear Stability on the Formation of the Chemical Elements . . . . . J. S. SMART 1379
Tensor Forces and the Triton Binding Energy . . . . . HERMAN FESHBACH AND WILLIAM RARITA 1385
S-Wave Proton-Proton Scattering from 6.2 to 40 Mev for the Yukawa and Gauss Exter Potentials . . . . . R. D. HATCHER, G. R. ARFKEN, AND G. BREIT 1389
Accurate Determination of the Threshold for the Nuclear Reaction $C^{12}(d,n)N^{13}$ . . . . . T. W. BONNER, J. E. EVANS, AND J. E. HILL 1398
Neutrons and Gamma-Rays from the Disintegration of C^{12} by Deuterons . . . . . T. W. BONNER, J. E. EVANS, J. C. HARRIS, AND G. C. PHILLIPS 1401
Measurements of the Absolute Intensity of Cosmic Radiation at Sea Level . . . . . R. A. MONTGOMERY 1407
Paramagnetic Absorption in Single Crystals of Copper Sulfate Pentahydrate . . . . . JOHN WHEATLEY AND DAVID HALLIDAY 1412
Second Viscosity of Liquids . . . . . L. N. LIEBERMANN 1415
On the Theory of Diffraction by an Aperture in an Infinite Plane Screen. II . . . . . HAROLD LEVINE AND JULIAN SCHWINGER 1423
Energy Spectrum of the Decay Particles and the Mass and Spin of the Mesotron . . . . . ROBERT B. LEIGHTON, CARL D. ANDERSON, AND AARON J. SERIFF 1432

Letters to the Editor:

Some Possible Rare Stable Isotopes . . . . . HENRY E. DUCKWORTH 1436
New Stable Isotope of Platinum . . . . . HENRY E. DUCKWORTH, ROBERT F. BLACK, AND RICHARD F. WOODCOCK 1436
Decay of Scintillations in Calcium Fluoride Crystals . . . . . W. J. MACINTYRE 1439
Anomalous Behavior of the Dielectric Constant of a Ferromagnetic Ferrite at the Magnetic Curie Point . . . . . FRANK G. BROCKMAN, P. H. DOWLING, AND WALTER G. STEINECK 1440
Divergences in Field Theory . . . . . K. M. CASE 1442
On Meteor Speed Measurements by the Radio Doppler Method at Low Frequencies . . . . . D. D. CHERRY AND C. S. SEYMAN 1443
Beta-Ray Spectrum of S^{35} . . . . . DAVID E. ALBURGER 1443
Microwave Magnetic Resonance Absorption in a Nickel Salt Near 1.25 Cm . . . . . A. N. HOLDEN, C. KITTEL, AND W. A. YAGER 1443
Decay of Co^{60} . . . . . MARTIN DEUTSCH AND ARNE HEDGRAN 1443
Electron-Neutrino Correlation in Heavy Elements . . . . . M. E. ROSE 1444
Possible Experimental Verification of the Statistics of He^3 . . . . . D. TER HAAR 1444
Determination of the Potential from the Asymptotic Phase . . . . . NORMAN LEVINSON 1445
On the Beta-Particle Spectrum from the Decay of Radium *E* . . . . . ARTHUR WALTNER AND F. T. ROGERS, JR. 1445
Measurement of Particle Energies with Scintillation Counters . . . . . G. F. J. GARLICK AND R. A. FATEMALLY 1446
Beta-Decay Spectrum of Ag^{110} . . . . . WERNER S. EMMERICH AND J. D. KURBATOV 1446
Hyperfine Structure of the Ground Term of Hydrogen . . . . . G. BREIT AND R. E. MEYEROTT 1447
On the Decay of K^{40} . . . . . E. L. FIREMAN 1447
On the Maximum β-Energy Release in Tritium . . . L. SLACK, G. E. OWEN, AND H. PERLMAN 1448
Neutron and Proton Binding Energies in the Region of Lead . . . . . KATHARINE WAY 1448
Erratum: On the Applicability of Heisenberg's Theory of *S*-Matrix to the Problems of Resonance Scattering and Reactions in Nuclear Physics . . . . . NING HU 1449
Erratum: Second-Order Stark Effect of Methyl Chloride . . . . . ROBERT KARPLUS AND A. HARRY SHARBAUGH 1449
Hydrogen Sulfide Bands at 16300 Cm^{-1} . . . . . HAROLD R. GRADY, PAUL C. CROSS, AND GILBERT W. KING 1450
On the Anomalous Line Shapes in the Ammonia Inversion Spectrum at High Pressures . . . . . P. W. ANDERSON 1450
Interaction Hamiltonian for Photon, Meson, and Nucleon Fields . . . . . GEORGE J. YEVICK 1450
Erratum and Addendum: Domain Interactions in the Theory of Ferromagnetic Resonance . . . . . GEORGE T. RADO 1451
Cosmic-Ray Induced Nuclear Stars at High Altitudes . . . . . P. FREIER, E. P. NEY, AND F. OPPENHEIMER 1451
On the Intuitive Approach to the Spectrum of a Wave Equation . . . . . PHILIP HARTMAN AND AUREL WINTNER 1452
Nuclear Quadrupole Effects in the Microwave Spectrum of the Asymmetric Top Molecule, Vinyl Chloride . . . . . J. H. GOLDSTEIN AND J. K. BRAGG 1453
On the Decay of Isotropic Turbulence . . . . . S. CHANDRASEKHAR 1458

Proceedings of the American Physical Society:

Minutes of the Meeting at Berkeley, California, February 3–5, 1949 1456

LANCASTER PRESS, INC., LANCASTER, PA.